EFFECT OF POLYMER STRUCTURE AND COMPOSITION ON PHOTOVOLTAIC PERFORMANCE OF ORGANIC CONJUGATED POLYMER BULK HETEROJUNCTION SOLAR CELLS

GETACHEW ADAM

A Thesis Submitted to the Department of Chemistry

Presented in Fulfillment of the Requirements for the Degree of Doctor of Philosophy (Physical Chemistry)

ADDIS ABABA UNIVERSITY

ADDIS ABABA, ETHIOPIA

May 2012

Addis Ababa University

School of Graduate Studies

This is to certify that the thesis prepared by Getachew Adam Workneh entitled: *Effect of Polymer Structure and Composition on Photovoltaic Performance of Organic Conjugated Polymer Bulkheterojunction Solar Cells* and submitted in partial fulfillment of the requirements for the Degree of Doctor of Philosophy (Physical Chemistry) complies with the regulations of the University and meets the accepted standards with respect to originality and quality.

Signed by the Examining Committee

Name	Signature	Date
Prof. Yongfang Li External Examiner		12 June 2012
Prof. Theodros Solomon Examiner		12 June 2012
Dr. Ahmed Mustefa Examiner		12 June 2012
Dr. Mesfin Redi Examiner		12 June 2012
Dr. Shimelis Admassie Examiner		12 June 2012
Prof. Teketel Yohannes Advisor		12 June 2012

Chair of Department or Graduate Program Coordinator

Abstract

Effect of polymer structure and composition on photovoltaic performance of organic conjugated polymer bulk heterojunction solar cells

Getachew Adam

Addis Ababa University, 2012

In this thesis solar energy to electrical energy conversion using organic conjugated polymer based bulk heterojunction solar cells has been studied by aiming at the effect of polymer structure and composition on minimizing the limitations such as lower charge carrier mobility, narrow absorption spectrum, poor nanomorphology of these solar cells which improves the photovoltaic performance in such a way that:

a) By random distribution of segments of *linear* octyloxy side chains, inducing *ordering*, and of *branched* 2-ethylhexyloxy side chain, inducing *disorder* on the backbone of anthracene containing poly(phenylene-ethynylene)-*alt*-poly (phenylene-vinylene) (PPE-PPV) a side chain based statistical copolymer, denoted **AnE-PV*stat***, has proven to be very effective in terms of field independent higher intrinsic charge carrier mobility $\mu = 5.43 \times 10^{-4}$ cm^2/Vs demonstrated by CELIV that might be due to its highest π-π-stacking distance of $d_{\pi\pi} = 0.393$ nm and conformationally balanced morphology as compared to the well-defined congeners. The random combination of the underlying constitutional units seems to promote the side chain geared *order* and *disorder* enabling effective tuning of the nanoscale morphology of photoactive layer. Power conversion efficiency up to 3.77% in a bulk heterojunction photovoltaic system and a significant device performance in solid state photoelectrochemical solar cells made using **AnE-PV*stat:*** PCBM as a photoactive active layer in an open air showing an open-

circuit voltage of 320 mV is the present state-of-art value for PPV based materials.

b) A 1:1 mixture of two thiophene based poly(*p*-phenylene-ethynylene)-*alt*-poly(*p*-phenylene-vinylene)s denoted DO-PThE_1-PPV_2 (**D1**) and MEH-PThE_1-PPV_2 (**D2**), consisting of the same conjugated backbone but different types and volume fraction of alkoxy side chains on the phenylene-ethynylene unit, has lead to enhanced charge carrier mobility as compared to the individual polymers. The resulting ternary blend with PCBM showed better photovoltaic performance as compared to binary blends. This is due to improved active layer nanomorphology in the ternary system as revealed by AFM studies.

c) By varying one moiety with thiophene, bithiophene or 3,4-ethylenedioxy thiophene at the **X** position in the thiophene containing poly(p-phenylene-ethynylene)-alt-poly(p-phenylene-vinylene)s (PPE-PPV) copolymers with a general structural design (Ph-C≡C-**X**-C≡C-Ph-CH=CH-Ph-CH=CH-) bearing identical side chains at the phenylene rings were synthesized. The effect of this structural alteration on the properties such as photophysics, electrical, charge carrier mobility and morphology of the materials and its impact on their photovoltaic performance were studied. The copolymer with a single thiophene ring at the X positions showed the highest V_{OC} of 930 mV and the copolymer with a bithiophene unit at X position showed the highest short-circuit current density and charge carrier mobility. Where as the copolymer with 3,4-ethylenedioxy thiophene showed the lowest photovoltaic performance.

d) To change the structure of the polymer by doping, a 1:1 ratio of Poly(3-hexylthiophene) (P3HT) to [6,6]-phenyl-C_{61}-butyric acid methyl ester (PCBM) was dissolved in chlorobenzene containg four different molar concentrations of

the dopant ferric chloride. The photophysical properties in solution as well as in their films were characterized using Uv-Vis absorption and bulk hetrojunction solar cell devices were fabricated from each solution were characterized. It was found that with increasing the dopant concentration, monochromatic photocurrent spectra and IPCE of the devices showed a red shift which is consistent with the optical absorptions and the instu spectroelectrochemical behavior of P3HT. By doping the short circuit current of the devices increased due to an increase in charge carrier mobiliy. It was also observed that the best photovoltaic performance was achieved at lower concentration of $FeCl_3$ as compared to undoped devices used in this experiment.

e) A ternary blend of two polymers poly(3-hexylthiophene) and poly[4,4-bis(2-ethylhexyl)-4*H*-cyclopenta[2,1-*b*:3,4-*b*2]dithiophene-2,6-diyl-*alt*-4,7-bis(2-thienyl)-2,1,3-benzothiadia-zole-5',5''-diyl] (PCPDTTBTT) with complementary absorption and an acceptor [6,6]-phenyl C_{61}-butyric acid methyl ester (PCBM) were used to fabricate the bulk hetrojunction type solar cells inorder to increase (broadening) the absoprption in the visible spectrum. It was found that the ternary blend showed better absorption spectrum as evidenced from the optical absorption, photocurrent spectra and IPCE curves of the blend. Due to this increased absorption of light the ternary blend has shown improved short circuit current and open circuit voltage due to n-type behaviour of PCPDTTBTT as compared to the binary blends of each polymer with PCBM.

Acknowledgements

I would like to express my sincere gratitude to my advisor Prof. Teketel Yohannes for his encouragement, constant guidance and valuable suggestions in all stages until the completion of this work. I thank him for giving me the oppourtuity to do my PhD on this interesting topic.

My special gratitude goes to my research collaborator Dr. Daniel Ayuk Mbi Egbe at Linz institute for organic solar cells (LIOS), Linz, Austria for fascinating collaboration by providing me polylmers and teach me how to synthesize polymers for photovoltaic devices. I also thank him for giving me five months research scholarship in his DFG (Deutsche Forschungs gemeinschaft) project to extend my research stay in LIOS. Many of the results presented in this thesis would become possible because of knowledge and advice I experienced from him. For me, it was a pleasure to work alongside him and learn from such an extraordinary person.

My word of many thanks goes to Prof. Niyazi Serdar Sariciftci for giving me the opportunity to do part of my research work in his laboratory at LIOS. Thank you for your unreserved encouragement and best scientific experiences I got in your institute. I thank all of the group members in LIOS for their friendship and cooperation especially Dr. Helmut Neugebauer, Mr. Manfred Lipp, Mrs. Gerda Kalab and Mrs. Birgit Paulik. The Austrian Academic Exchange Service (ÖEAD) is highly acknowledged for giving me a one year scholarship for part of my PhD research work in LIOS.

I would like to thank, Dr. Alberto Montaigne Ramil, Dr. Matthew White, Dr. Mateusz Benorz, Dr. Ercan Avci, Dr. Pavel Troshin for their, cooperation, valuable comments,

suggestions and long scientific discussions we had while I was in LIOS. Let me take this oppourtunity to express my deepest gratitude to Dr. Christoph Ulbricht, I really appreciate his help for all kinds of questions I asked him during my stay with him in LIOS.

I would like to express my thanks to the staff members of chemistry department of Addis Ababa University; Dr. Shimelis Admassie who was always encouraging me, Dr. Mesfin Redi, Prof. Theodros Solomon, Prof. Wondimagegn Mammo, Dr. Ahmed Mustefa, Dr. Merid Tessema, Ato Solomon Mehretie, laboratory assistants, secretaries and the store keeper Ato Sahliemichel Demie.

I am deeply indebted to Dr. Almantas Pivrikas who shared me all his experiances in the area of organic solar cells and charge transport studies. I have no words to express his professional encouragement and care to the extreme of visiting my home land Ethiopia and my families in Bichena.

I would like to thank my friends Sisay Tadesse, Siraye Esubalew, (PhD candidates), Dr.Tesfaye Atsbaha, Dr. Belina Terfasa, Mr. Endale Tsegaye, Mr. Bekele hayilegnaw, and Mr. Eyob Daniel for their care and support by sharing their ideas and views during our stay at Addis Ababa University.

My heartfelt word of thanks goes to my beloved mother W/o Yewubdar Gebeyehu and my father Ato Adam Workneh for the material and moral support starting from my elementary school up to this level. It is my pleasure to express my gratitude to my sisters and brothers Ato Yibeltal Adam, W/o Tiruwork Tsegaye, W/o Belay Adam, Ato Yesgat Negusie, W/ro Ayichlushem Adam, Ato Mekuriew Teferie, W/ro Elelie Adam, Ato Awoke Talema, Ato Habtam Adam, W/ro Ajebush Moseye, W/t Tigest Adam, Ato Habtamu Ayitenaw and Ato Abebe Kegne for their moral support and

encouragement which contributed much to my success. Without the love and support of my family, this would have been a very hard journey. My love for them is eternal.

Words cannot express the gratitude I owe to my lovely wife Hana Tesfaye for her unwavering love and care that always strengthen me. I dare not even imagine how it would have been without you. My affection also goes to my little son Yishak Getachew who brings me the happiness I have never felt before in my life.

Finally I would like to thank Dilla university for sponsoring my education and the Chemistry Department of Addis Ababa university for providing me with laboratory and other facilities needed for the accomplishment of this work. The DFG (Deutsche Forschungsgemeinschaft) is highly acknowledged for giving me a five months research funding to stay in LIOS and letting me to participate in summer school at Kripen in Dresden, Germany.

It is impossible to remember all who, in one way or another, helped me to reach this stage in my life; I apologize to anyone that I have inadvertently overlooked. Lastly, I thank them all.

TABLE OF CONTENTS Page

List of Figures Page

List of Tables Page

CHAPTER ONE: INTRODUCTION

1.1. The need for solar energy

The global demand for energy is growing in an alarming rate due to the increasing population and technological advances in the world. This demand is projected to more than double by 2050 which is around 10 - 20 Tera watt (TW) power and to more than triple by the end of this century [1, 2]. Particularly in Africa the lose of forests which were used as the main source of energy for cooking aggravates the problem to each house hold level. Incremental improvements in existing energy networks (Nuclear, wind, hydroelectric, fossil fuel, etc) will not be adequate to supply this demand in a sustainable way.

The non renewable fossil fuels which are still the major sources of this limited supply of energy release gases during their combustion which are the main causes of environmental pollution and global warming and their cost as well is constantly increasing. The only existing carbon free non renewable technology that can scale up to 10 TW or greater level is nuclear fission. Given the limits that we can handle the heat and radiation flux in a fission reactor and make it viable commercially where safe reactor designs are rated at 1 GW of electricity output. So we would need to build a new nuclear power plant every other day for the next 50 straight years to satisfy the global demand. But the proven reserves and the resource base of all terrestrial uranium (nuclear reactor fuel) would be enough to provide only 10 years of operation for the 10,000 necessary nuclear power plants under once through operations. So Nuclear power is not a long term solution because of its non renewable nature and its waste disposal and radiation risks [2].

In order to fulfill the world's energy needs and sustain further technological development, it is important to develop renewable, none polluting, and low cost energy production techniques. A report on the total potential of clean and renewable energy sources existing in our world shows [2, 3];

a. The amount of technically feasible ***hydroelectric power*** globally has been estimated to be about 1.5 TW, from this the economically feasible amount is only about 0.9 TW, and 0.6 TW capacities of that has already been installed. Though hydroelectricity is an attractive renewable resource that should continue to be exploited wherever possible, it will not make a significant contribution toward our 10 – 20 TW global carbon free energy requirements in the mid 21st century.
b. The amount of sustainable global ***geothermal*** heat energy that can be used is equal to 11.6 TW. Since the second law of thermodynamics prevents us from getting 100% efficient heat engines at a low temperature difference, practically we extract much less than a few terawatts sustainably.
c. In terms of ***oceanic and tidal*** energy, all the energy in all the currents, all the tides, and all the waves on our planet combined is about 10 – 20 TW though the technology to do this is very expensive.
d. On a global scale wind mills could produce a total of 2 – 4 TW of electricity. Producing 2 TW of ***wind*** power would require the operation of 2 million state of the art wind turbines. Wind energy could be a good alternative providing perhaps approximately 10% of our total energy needs, if used exhaustively on suitable land around the globe.
e. Using photosynthesis plants store less than 1% of the total incident energy they receive from sunlight. 30% of the total land on earth would have to be covered with energy farms devoted solely to produce ***biomass*** to meet the carbon neutral

energy demand requirements. Assuming that all of the rain fed cultivatable land not required for food was functioning as an energy farm with no need for any energy coming in or going out the result would be about 5 TW of power. Biomass could be a significant contributor to the overall carbon neutral power requirements, but we cannot rely on it alone to meet the estimated demand.

f. The sun is the champion of all energy sources which provides earth with 120,000 TW power. More energy from sunlight strikes the earth in one hour (4.3×10^{20} J) than all the energy consumed on the planet in a year (4.1×10^{20} J) [1]. In fact, ***solar energy*** is the only clean and renewable resource that has enough terrestrial energy potential to satisfy alone, with room to spare, the 10 – 20 TW carbon free supply constraint in 2050. It is abundant, readily available, and secured from geopolitical tension. The amount of land that would be required for a solar energy "farm" operating at 10% efficiency, to supply 3 TW of power would cover 1.7% of U.S. land which is so small area as compared to the land devoted to the nation's numbered highways. Therefore, it is important to develop low cost and efficient technologies for solar energy conversion.

Solar energy can be converted into electricity by photovoltaic effect using devices called solar cells (also known as photovoltaics). It can also be used in combination with other sources like wind, geothermal, hydro power, etc. to produce electrical energy. Unique properties of photovoltaic are;

a) It directly generates electricity without the need of generators.
b) It is an outstanding flexible technology, supplying electrical power in form of portable modules in the milliwatt scale up to entire power plants with peak capacities in the multiple megawatt regimes.
c) It is the only renewable energy which can be customized by individuals.

1.2. History of photovoltaics

The history of photovoltaic dates back to 1839 when French experimental physicist Alexandre-Edmond Becquerel detected a photo voltage when sunlight was allowed to shine one of two electrodes he had placed in an electrolytic solution [4, 5, 6]. Then in 1954, researchers at the Bell telephone laboratories demonstrated the first practical conversion of solar radiation into electric energy based on crystalline silicon *via* use of a *p-n* junction where p-type silicon that contains positively charged holes and n-type silicon that contains excess electrons come in contact and formed a solar cell. In this type of silicon solar cells, absorption of light generates electron-hole pairs that diffuse to the junction. The photogenerated electron-hole pairs are driven efficiently in opposite directions by an electric field existing at the boundary (p-n junction). This directs the electric current to flow in only one direction through an external circuit and to produce electrical current. A power conversion efficiency of 6% was achieved at the beginning using this devices [7], then these research progresses more to acquire the needs for energy source has boosted inorganic photovoltaic cells investigations and reached the efficiency of 24.4% for the first generation crystalline Si (first generation photovoltaics) with energy intensive processing techniques [8].

Thin film photovoltaic technologies, referred to as second generation photovoltaics, are based on inorganic semiconductor materials that absorb light more than crystalline silicon and can be processed directly onto large area substrates. Such semiconductors include amorphous silicon, semiconductors such as CdS, CdTe, and chalcogenides such as Cupper Indium diselenide $CuInSe_2$ (CIS) or Cupper Indium gallium diselenide $CuInGaSe_2$ (CIGS) [9]. The laboratory demonstration of these cells with controlled manufacturing showed high efficiencies up to 19.9% for CIGS [10, 11] and

16% for CdTe [12]. Eventhough these traditional inorganic semiconductor technologies enable us to manufacture high efficiency solar cells, their price is still rather high for these solar panels to enter the market on a large scale.

The organic based approaches and those that do not rely on conventional single p–n junctions are often referred to as third generation technologies. They include: (i) the dye-sensitized solar cells ii) hybrid solar cells iii) Organic photoelectrochemical and iv) all organic solid state approaches.

The dye-sensitized solar cells (also named as Graetzel type solar cells for his discovery) which consist of nanoporous TiO_2 semiconductor coated on a transparent working electrode, ruthenium bipyridial based dye /or other dyes for absorption of light and an electrolyte containing a redox couple like Iodide /Triiodide (I^-/I_3^-) in acetonitrile or ethylene/propylene carbonate containing and a counter electrode. The process involves the excitation of the dye from its neutral ground state to an excited state by the absorption of a light, followed by relaxation through electron transfer to the semiconductor substrate. The dye is left as a surface adsorbed cation where it is neutralized by reaction with a redox species in the contacting electrolyte, which in turn recovers an electron from a counter electrode, thereby constituting a closed regenerative cycle for the conversion of incident light into an electric current. These cells showed an efficiency of 10 - 11% [13 -17]. Although dye sensitized photoelectrochemical cells show high power conversion efficiency, their commercial application has been limited due to problems in stability and in the large module production using a liquid electrolyte. Lots of attempts have been made to substitute the liquid electrolyte solutions with molecular [18], polymeric hole conductors [19,

20] and polymer or gel electrolytes containing redox couples to produce all solid state photoelectrochemical cells [21, 22].

A major step in the development of hybrid polymer solar cells was achieved in 2002 by Huynh *et.al* when they made a blend CdSe nanoparticles with regioregular poly(3-hexylthiophene) (P3HT). In this hybrid solar cell P3HT is used as a hole transporting material and CdSe as an electron transporting material giving a power conversion efficiency of 1.7% under Air Mass 1.5 global solar condition [23]. These type hybrid approaches in which inorganic nanoparticles/rods and quantum dots of ZnO, CdSe, CdS, PbS, and $CuInS_2$ [24-28] are doped into a semiconducting polymer matrix or by combining nanostructured inorganic semiconductors such as TiO_2 with organic materials [29] are still under investigation and concern of many researchers in the field.

1.3. Organic conjugated polymer bulk heterojunction solar cells

The great potential of organic polymers for photovoltaic devices attracts the scientific community for the development of low cost renewable electrical energy source which addresses growing global energy needs [30 - 34]. Since the first reports on molecular thin film devices more than 30 years ago, their power conversion efficiencies have increased considerably from 0.001% in 1975 [35] to 1% in 1986 [36], to 4 – 6% in the poly(3-hexylthiphene) (P3HT)/[6,6]-phenyl-C_{61}-butyric acid methyl ester (PCBM) system in 2009 [37-39], and more recently to 7 -10% in 2012 [40, 41]. The progresses in efficiency will possibly make them a competitive alternative to inorganic solar cells in the near future.

There are several reasons and peculiar advantages to use organic materials for photovoltaic solar cell applications;

a) They can be processed easily using spin coating or doctor blade techniques (wet-possessing) or evaporation through a mask (dry-processing) [42].
b) In contrast, solar cells based on the inorganic crystalline silicon and polycrystalline semiconductors $Cu(In,Ga)Se_2$ which need few micron thick active layer for good absorption, organic semiconductors exhibit very high absorption coefficients above 10^5 cm^{-1} with 100 - 300 nm active layer thickness [30, 43, 44]. Consequently the amounts of organic materials are relatively small (100 nm thick films) and large scale production (chemistry) is easier than for inorganic materials (growth processes) which shows that it is a low cost technology
c) They can be tuned chemically in order to adjust their band gap, charge transport, as well as solubility and several other structural properties [45].
d) Flexability of organic conjugated polymer films which can be coated on plastic substrates.
e) The vast variety of possible chemical structures and functionalities of organic materials (polymers, oligomers, dendrimers, organo minerals, dyes, pigments, liquid crystals, etc) favors an active research for alternative competitive materials with the desired photovoltaic properties.

In organic solar cells the π electrons of conjugated polymers, oligomers or molecules allow light absorption to form excitons in solar cells made from these conjugated organic materials. As the exciton binding energy in organic semiconductors is generally large (0.1 – 1 eV) compared to silicon [46], the built-in electric fields (on the order of 10^6 – 10^7 V/m) are usually not high enough to dissociate the excitons directly. Hence, a system has to be introduced that efficiently separates the bound

electron-hole pairs. This is possible at the sharp drop of potential at donor–acceptor (D-A) as well as semiconductor–metal interfaces. Different solar cell device architectures have been used for this efficient charge separation these are;

a) The first organic solar cells were based on single thermally evaporated molecular organic layers sandwiched between two metal electrodes of different work functions. Because the exciton diffusion length for most organic solar cell materials is below 20 nm, only those excitons generated in a small region within 20 nm from the contacts contribute to the photocurrent. Due to the high series resistances, these devices show a low fill factor (FF) and a field-dependent charge carrier collection [47].

b) The second type of cells were bilayer devices, where a donor and an acceptor material are stacked together with a planar interface where the charge separation occurs which is mediated by a large potential drop between donor and acceptor [48, 49]. The bilayer is sandwiched between two electrodes matching the donor highest occupied molecular orbital (HOMO) and the acceptor lowest unoccupied orbital (LUMO) for efficient extraction of the corresponding charge carriers. The charge transfer in bilayer heterojunction between donor and acceptor materials is due to the differences in the ionization potential and electron affinity of the adjacent materials. A big advantage over the single layer device was achieved because after the excitons are dissociated at the materials interface, the electrons travel within the *n*-type acceptor, and the holes travel within the *p*-type donor material. But due to the long distance of the donor–acceptor interface only those excitons in limit of the exciton diffusion length are dissociated in this device. Power conversion efficiencies of about 3.6% under one sun AM 1.5 solar illumination with this geometry were reported with an evaporated bilayer device

using copper phthalocyanine and C_{60} [50, 51, 30].

c) In an attempt to solve the problem of "long diffusion distance to the interface" in the bilayer devices a new concept was introduced called bulk heterojunction (BHJ). The essence of the bulk heterojunction is to intimately mix the donor and acceptor components in a bulk volume so that each donor–acceptor interface is within a distance less than the exciton diffusion length of each absorbing site. The bulk device is similar to the bilayer device with respect to the donor acceptor concept, but it exhibits a largely increased interfacial area where charge separation occurs. Due to the interface being dispersed throughout the bulk, no loss due to too small exciton diffusion lengths is expected, because ideally all excitons will be dissociated within their lifetime. This concept involves nano scale self assembly of heterojunctions by spontaneous phase separation of the donor polymer and the acceptor which leads to charge-separating heterojunctions throughout the bulk resulted in transport of charges to opposite electrodes *via* percolating pathways to provide a photocurrent. Recombination is reduced to a large extent and the photocurrent increases as compared to the bilayer heterojunction [30]. The history of bilayer as well as bulk heterojunction (BHJ) polymer solar cells dates back to 1992 when a fast photoinduced electron transfer from a conjugated polymer (MEH-PPV) to the buckminsterfullerene (C_{60}) was discovered by Niyazi Serdar Saricifitci *et.al* [34]. The realization of improved performance of the first solar cell of this kind from poly(2-methoxy-5-(2-ethyl-hexyloxy)-1,4-phenylene vinylene) (MDMO-PPV): [6,6]-phenyl C_{61}-butyric acid methyl ester ($PC_{61}BM$) as compared to the pure polymer was reported in 1995 [52].

BHJ solar cell based on conjugated polymer/PCBM blends which is much more sensitive to the nanoscale morphology has been the subject of increasing interests of

synthetic and device scientists. To increase the power conversion efficiency of such devics synthesis designs of novel conjugated polymer donors such as derivatives of polythiophene, polycarbazole, polyfluorene, poly(para-phenylenevinylene) (PPV), poly(para-phenylene ethynylene) (PPE), Anthracene / thiophene containing PPE-PPV [44-58], and acceptors partcularly fullerene derivative and n-type conjugated polymers [59] have been undergoing and well developed.

1.3.1. Limitations of organic conjugated polymer bulk heterojunction solar cells

Although chemical design and synthesis offers almost unlimited possibility of using new materials and material combinations, the development of efficient bulk heterojunction solar cells still requires more investigation to minimize the limitations. This limitations are

a. Eventhough Organic semiconductors often exhibit very high absorption coefficients above 10^5 cm^{-1} [30, 43, 44] at a very low thicknesses between 100 – 300 nm which is sufficient for a good absorption yield, many organic materials have rather narrow absorption width which typically cover the visible optical spectrum width of few hundred nm which can generate only 20% of the maximum available photocurrent as compared to silicon and $Cu(In,Ga)Se_2$ solar cells achieve up to 60% [60]. So synthesis approaches towards polymers with wider absorption bands or combining polymers and coplolymers in multiple blends are very important.

b. The dissociation of excitons is ultrafast and of almost 100% efficient, if and only if the diffusion length is sufficient to reach the interface [61, 62]. Nevertheless, the generation of a polaron pair from an exciton is only possible when energy can be gained for the charge carriers. The fill factor and the short circuit current are both

influenced by this process. Also, the energy of the charge transfer state determines the maximum open circuit voltage, which is reduced to its experimental value by recombination. So novel organic materials with higher dielectric constant to reduce the exciton binding energy [63] and advanced device configurations for an optimum phase separation and/or nanocrystallinity of the donor–acceptor domains [64] are the potential approachs for improvement.

c. The charge carrier mobility limits the power conversion efficiency in bulk heterojunction solar cells to a certain degree [65]. As the recombination rate at short circuit current is rather low, the extraction depth is sufficient, but limited for devices further beyond 200 nm thickness. At voltages approaching the open circuit voltage, charge recombination is also critical, limiting the maximum open circuit voltage. Novel materials with higher charge carrier mobility for improved transport is the potential approach to minimize this limitation.

The above limitations show that a comprehensive research is needed on the fundamental processes governing energy conversion by organic bulk hetrojunction solar cells in order to find the most promising optimisations. This research work is based on finding better ways/routes to improve the performance of organic solarcells by organic polymer structural variation during synthesis or by blending different polymers with varied structures and by inducing new structural properties through chemical reactions.

1.4. Objectives of the study

General Objective:

The general objective of this thesis is to study the effect of varying structures and compositions of organic conjugated polymers on ***photophysical, morphology***, ***electrochemical***, ***charge transport*** properties, and ***photovoltaic*** performance of bulk heterojunction type organic solar cells made from such conjugated organic polymers/ polymer blends with acceptor PCBM.

Specific objectives:

1. To show the effect of randomly distributed linear and branched side chains of anthracene containing PPV-PPE polymers on photophysical properties, morphology, and charge carrier mobilities of the polymer as compared to polymers with side chains at fixed positions and its impact on the photovoltaic performance of bulk heterojunction solar cells.
2. To describe the effect of mixing polymers having the same backbone with different side chains on morphology and charge carrier mobility compared to the individual polymers and its impact on photovoltaic performance.
3. To investigate the effect of varying one moiety in the backbone of thiophene containing PPV-PPE polymer with the same side chains on photophysics, charge carrier mobility, electronic energy levels of the polymers and its correlation with their photovoltaic performance in bulk heterojunction solar cell.
4. To investigate the effect of chemical doping that alters the electronic structure of polymers on photovoltaic performance of organic conjugated polymer bulk

heterojunction solar cells and to show the consistencies of electrochemical and chemical doping on the photophysical properties of polymers.

5. To show the effect of using ternary blends with complementary absorption on the optical absorption spectrum and photocurrent spectra, and describe its effect on photovoltaic performance of bulk heterojunction solar cells as compared to binary blends.

CHAPTER TWO: FUNDEMENTALS

2.1. Organic conjugated polymers

2.1.1. Electronic structure of organic conjugated polymers

In conventional polymers like polyethylene $(CH_2)_n$, every carbon atom in the backbone is σ-bonded to four atoms in the sp^3 hybridized configuration. The energy separation between molecular bonding *(σ)* and antibonding *(σ∗)* orbitals joining -CH_2- groups due to the considerable axial overlapping of these orbitals as permitted by the polymer geometry display forbidden bands at energy levels ≥ 5 eV situated well outside the optical spectrum as a result they are dielectric materials [66]. The difference with a conjugated polymer is that three of the four electrons in the outer shell of carbon occupy sp^2 hybridized states, creating the σ bonds that form the strong structural backbone of the polymer. The remaining free electron occuping the p_z orbital overlap with the equivalent p_z orbitals from neighboring carbon atoms and form the so-called π electron system, which in principle extends over the full length of the polymer backbone [62]. To lower the total energy, the polymer forms an *alternating structure of single and double bonds* of π orbitals which gain an electronic energy and creates an opening of an energy gap of about 1.5 to 3.5 eV between the the highest occupied molecular orbital (HOMO) states and the lowest unoccupied molecular orbital (LUMO) states. It is this lower energy gap that makes the polymer a semiconducting and responsible for a discrete optical transition that exists between HOMO and LUMO [67, 68].

In reality the electronic picture on a microscopic scale of a conjugated polymer sample would look like that each polymer chain consist of a number of separated

conjugated segments because of the presence of twists, kinks, or impurities that disrupt the π-conjugation of the same physical chain. The term "conjugation length" is used to describe the mean length of these conjugated segments. As a result of these twists and kinks the chains cannot be aligned over their whole length and that is why these polymers show only a partial crystallinity. The typical size of these crystalline regions is 10 - 50 nm and these regions are always interconnected by amorphous regions [69]. The energies of the conjugated segments are modified by their different local arrangement, which gives rise to locally varying polarizabilities and dipole interactions between neighboring chains, as well as by the distribution of the conjugation lengths [70]. All these effects together will cause the charge carriers to be localized. In order to have transport of these localized charge carriers, their motion will be "hopping-like" from one chain to another chain in order to move through the system [71]. This transport mechanism is different from the "band-like" transport, present in inorganic semiconductor crystals like silicon or germanium.

2.2.Doping in organic conjugated polymers

Doping organic conjugated polymers was first discovered by MacDiarmid, Shirakawa, and Heeger [72] when they observed that chemical doping of polyacetylene resulted in an increase in electronic conductivity over several orders of magnitude. During the process, an organic polymer, either an insulator or semiconductor having a small conductivity, typically in the range 10^{-10} - 10^{-5} S/cm, is converted to a conducting regime up to 10^{5} S/cm due to the formation of new conduction bands [73]. This transformation is done when electrons are added (or removed) to (or from) the backbone resulting in anions or cations respectively which act as charge carriers. Hopping type charge transport from one site/chain to another

along the π-bonded highway under the influence of an electrical field increases conductivity [74]. Doping is reversible process that we can get back the original neutral polymer with little or no degradation of the backbone. With doping, the electrochemical potential (the Fermi level) is moved in to a region of energy where there is a high density of electronic states [75, 76]. Charge neutrality is maintained by the introduction of counter ions. Since every repeat unit is a potential redox site, conjugated polymers can be doped *n* type (reduced) or *p* type (oxidized) to a relatively high density of charge carriers [77, 78]. The attraction of an electron in one repeat unit to the nuclei in the neighboring units leads to carrier delocalization along the polymer chain and to charge-carrier mobility extended into three dimensions through interchain electron transfer [76]. Doping can be accomplished by different techniques such as chemical, electrochemical, charge injection, photodoping and non redox doping [73,76].

2.2.1. Chemical doping

Chemical doping is a charge transfer redox reaction between the dopant and the polymer (Equation 2.1 and 2.2). Depending on the nature of the dopant, the polymer undergoes *p*-doping or *n*-doping by partial oxidation or reduction of the π-backbone of the polymer respectively. *Trans* polyacetylene showed a dramatic increase in conductivity from ~ 10^{-5} to ~ 10^{3} S/cm when it is oxidized (p-doped) with iodine [73,76].

p- doping, $[poly]_n + \frac{3}{2}nyI_2 \rightarrow [poly^{+y}(I_3^-)_y]_n$ .....(2.1)

n-doping, $[poly]_n + [Na^+(Naphtalide)^-]_y \rightarrow [poly^{-y}(Na^+)_y]_n + Naphtalide$ .....(2.2)

2.2.2. Electrochemical doping

Electrochemical doping takes place in an electrolytic cell where the working electrode supplies the redox charge to the conducting polymer deposited on its surface, while ions from the electrolyte solution diffuse into (or out of) the polymer structure for electroneutrality. Control on the doping processes like the doping level is possible by controlling electrochemical parameters such as electrochemical charge and electrode potential applied. The *p*-doping can be accomplished by electrochemical anodic oxidation and *n*-doping can also be carried out by electrochemical cathodic reduction by reversing the polarity of the electrodes (Equation 2.3 and 2.4) [73, 76].

p-doping, $[Poly]_n + (ClO_4^-)_{solution} \rightarrow [Poly^{+y}(ClO_4^-)_y]_n + ye^-$ .....(2.3)

n- doping, $[Poly]_n + ye^- + (Li^+)_{solution} \rightarrow [Poly^{y-}(Li^+)_y]_n$ .....(2.4)

2.2.3. Photo-doping

Irradiating organic conducting polymer with light of energy greater than the band-gap of polymers ($h\nu \geq E_{\pi-\pi*}$) promots electrons across the band gap and the polymer undergo 'photo-doping'. These excited electron enable the semiconducting polymer locally oxidized and (nearby) reduced to form charged states which might disappear rapidly due to recombination of electrons and holes when irradiation is discontinued. If a potential is applied during irradiation, then the electrons and holes separate and photoconductivity is observed over the broad spectral range from the near infrared to the ultraviolet. This observation is in full a greement with the photoinduced electron transfer phenomenon which leaves metastable positive polarons on the polymer backbone by photo-doping as confirmed by ESR signal [73, 76, 79].

2.2.4. Charg injection doping

Charge-injection doping is most conveniently carried out using a metal/semiconductor /metal (M_1SM_2) configuration where a conducting polymer is sandwiched between two metals with appropriate work functions. By applying an external voltage the fermi levels of the metals are adjusted in such a way that one electrode injects electrons into the $\pi*$ band and the other extracts electrons from the π band (injecting holes into this band) which give rise to the formation of charged states in the polymer without any associated dopant ion [73, 76, 80].

2.2.5. Non redox doping

Protonation induces an insulator-to-conductor transition (doping), while the number of electrons in the polymer backbone does not change during doping process. A typical example is treating emeraldine base with aqueous protonic acids [73,76, 81, 82]. Upon protonation of the emeraldine base to the emeraldine salt, the proton induced spin unpairing mechanism leads to a structural change with one unpaired spin per repeat unit, but with no change in the number of electrons and an increase in conductivity by 9 - 10 order of magnitude [73,76, 83] (Scheme 2.1).

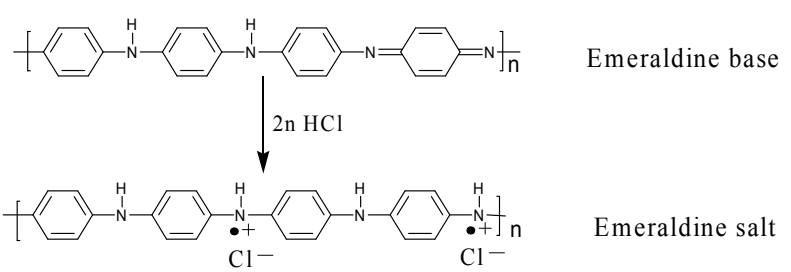

Scheme 2. 1: Non redox doping in polyanline**.**

2.3. Solitons, polarons, and bipolarons in conducting polymers

In polyacetylene (PA) the alternate single and double bonds keep the carbon atoms in their positions. Double bonds are stronger and shorter than single bonds (although not twice). If one part of a doublebond is cleaved, it will be weakened by its transformation in to a single bond. As a result the lattice is distorted due to lengthening of respective inter atomic distance which is called peierls distortion [84].

The thermodynamically stable *trans* configuration of PA which is a dimerized pattern of alternating single and double bonds forms two structures having different bond order with ground states are degenerate. These two structures I and II are formed by interchanging the single and double bonds (Figure 2.1). As a consequence of these degenerate ground states excitations exist in the form of a topologigical soliton or moving domain wall separating I and II domains [85]. A soliton in PA are domain walls between regions of the two possible ground state dimerization. A soliton distorts the electronic state of the polymer resulting in the formation of a new localized energy level in the middle of the band gap that is occupied by the unpaired electron [86]. Such defects, in the form of an unpaired electron has a charge of zero and spin ½. This unpaired electron is accompanied by bond length distortions in a region over about 14 carbon atoms [87]. There are also positively charged and negatively charged solitons with zero spin as shown in Figure 2.1.

Soliton is a topological defect that separates two inequivalent but degenerate regions of the polymer chain. Because of this degeneracy the position of the soliton does not matter energetically. For *cis*-polyacetylene and for the other polymers like polyphenylene or polythiophene the two regions that are separated by this defect are no longer degenerate. The soliton separates a low-energy region (benzenoid) from a

high-energy region (quinonoid) in this case. The soliton or single defect is of course driven to the chain end, changing the high-energy quinoidal rings into low-energy aromatic rings as it moves. However, defect pairs or double defects are calculated to be stable defects when charged, either singly to form a polaron, or doubly to form a bipolaron [88**].**

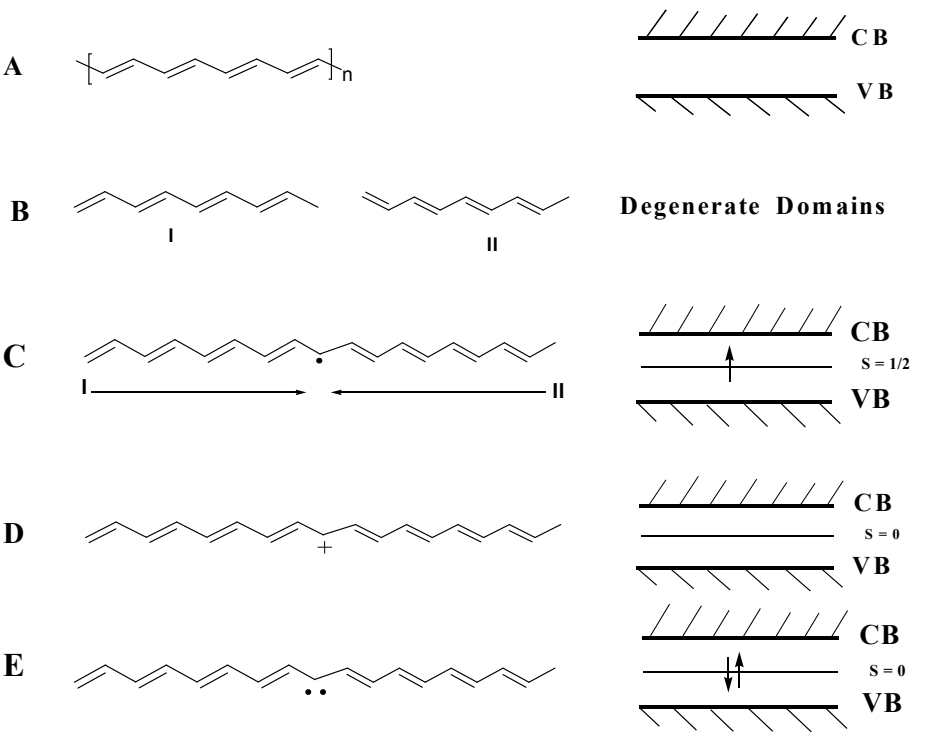

Figure 2.1: *a) Trans-polyacetylene, b) the two degenerate structures in trans-polyacetylene c) neutral soliton, d) positive soliton, e) negative soliton*.

The optical signature of a soliton is the midgap state where as polaron is characterized by two states in the gap. The emergence of two states can be rationalized to occur through interaction between the mid gap states belonging to the soliton components of the polaron. Depending on the occupancy, the defect is either neutral or charged [84].

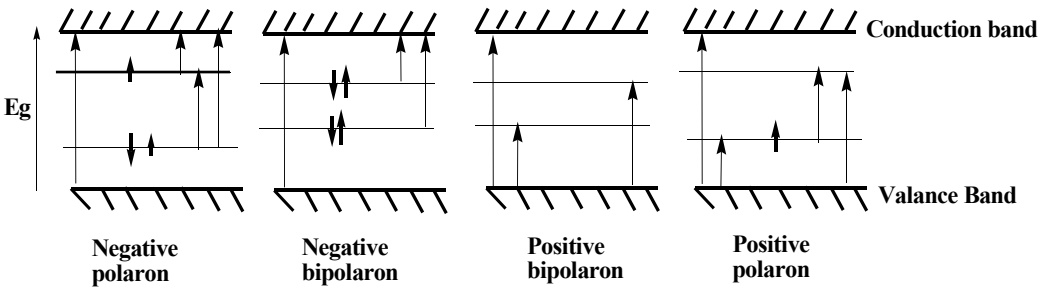

Figure 2.2*: Energy band diagrams of polaron and bipolaron states in the non-degenerate polymer. The arrows represent the possible optical transitions.*

A polaron is a radical cation (one unpaired electron), which is locally associated with a structural distortion in the conducting polymer. A hole polaron, created upon *p*-doping of the polymer has a charge of +1 and a spin of ½. The lower level of the in-gap states is half occupied and the upper level is empty as diplayed in Figure 2.2 [89, 90].

At higher doping levels, removal of electrons preferably forms a bipolaron (two positive charges) (Figure.2.2) rather than two polarons [91]. The stability of the bipolaron, despite the coulombic repulsion between the two positive charges, is considered to arise from electron-phonon coupling [92]. Bipolarons are mobile which can propagate along the conducting polymer chain (delocalized over some 6 to 8 monomer units) (Scheme 2.2) giving rise to the high conductivity under the application of an electric field. As one progresses further to very high doping levels, the individual bipolaron states coalesce into bipolaron bands. At maximum doping levels, the bipolaron bands of conjugated polymers with low band gaps (~ 2 eV), such as polythiophenes, can merge with the valence and conduction bands, producing metal-like conduction stemming from the lower, half-filled valence/ bipolaron band. [89, 90].

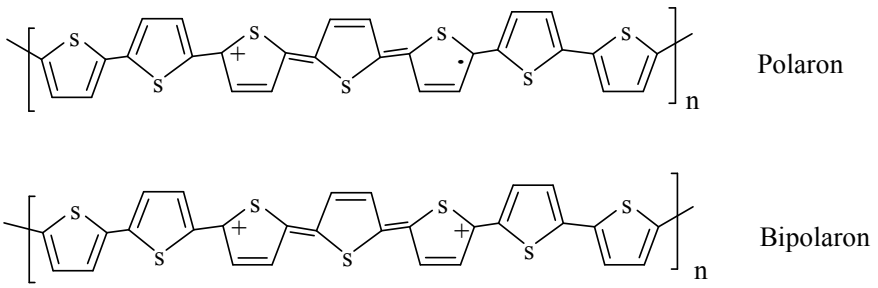

Scheme 2. 2: Actual structures of polarons and bipolarons in polythiophenes.

2.4. Electrochemistry of conjugated organic polymers

Most of the classical conducting polymers, like those based on heterocycles (polypyrrole, polythiophene, polyaniline) can be synthesized by electrochemical polymerization [93, 94]. The polymerization process starts with oxidation of the neutral monomer to form delocalized radical cations. Since the electron transfer reaction is much faster than the diffusion of the monomer from the bulk solution, a high concentration of radicals are continuously maintained at the electrode/solution interface. It is followed by the combination of two radical cations to form a dimer and then loses two protons to become electrically neutral. This dimer, which is more easily oxidized than the monomer, is further oxidized to a radical cation, and reacts with other radical cations. Chain growth proceeds between the radical cations of the monomer and those of the continuously forming oligomers. The cation radical formation leads to a very rapid dimerization step. The greater stability of the double charged dimer prevents its dissociation to the same radicals during the reduction scan [93, 95]. The polymer growth during electrochemical polymerization can be monitored and followed by a cyclic voltammetry (CV), by scanning up to the oxidation potential of the monomer and then down to the reduction potential of the polymer formed. Therefore the growth of the conducting polymer clearly appears as

an increasing reversible peak on each incoming CV, at lower potential than the monomer one [96].

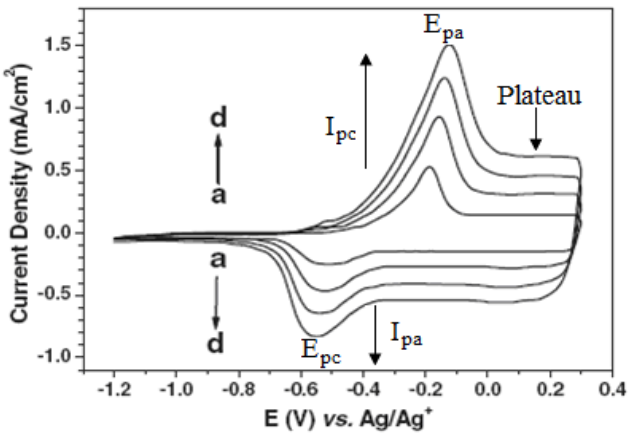

Figure 2. 3: *CV of P(BEDOT-MEBH) in 0.1 M $LiClO_4$ / PC monomer free solution at a Pt working electrode at scan rates of a) 50 mV/s, b) 100 mV/s, c) 150 mV/s, d) 200 mV/s [96].*

Charging and discharging process of conducting polymers as shown in Figure 2.3 for poly(1,4-bis(2-(3',4'-ethylenedioxy)thienyl)-2-methoxy-5-2"'-ethylhexyloxybenzene) P(BEDOT-MEBH) is a steep anodic wave followed by a broad flat plateau as the potential increases. It has been suggested that the plateau is related to capacitive charging of double layers of the system. In the reverse scan a potential shifted cathodic wave appears at the low potential end of the plateau with a peak height of about half the value of the anodic peak which is different from the ideal symmetrical waves for a material adsorbed on electrode with identical cathodic and anodic peaks. This is because of the fact that there is an interaction between charged sites and there are differences between the neutral and doped state regarding conformation as well as transport properties [95 - 97].

At low scan rate, peak currents vary linearly with the scan rate, which is characteristic of the behavior of a thin layer material deposited on the electrode as shown in Figure 2.3. Conversely, at higher scan rates, linear variation with the square root of the scan rate is frequently observed, corresponding to diffusion limited currents, arising either from charge transfer process (hopping mechanism) or from an ionic contribution (diffusion of counterions) [98]. The characteristic conductivity vs. potential curves of conducting polymers exhibited a three-step variation; a threshold followed by linear variation and a plateau. The same features can be observed on conductivity vs. charge (i.e.*vs*. doping level) curves. The threshold is related to percolation phenomenon, while the plateau indicates that a nearly constant density of states is reached at high doping levels. Interestingly, the conductivity profile changes with the natures of dopant and electrically conducting polymer [99, 100]. Sometimes conductivity may decreases at high doping levels, in contrast to the predictions of the bipolaron model because of over oxidation phenomena leading to the polymer chemical degradation, and due to the stabilization of bipolaronic state through H-bonding.

2.4.1. Electrochemical band gap determination of conducting polymers

Device performance of organic polymer bulk heterojunction solar cells has been correlated to the frontier orbital energies of the individual donor and acceptor components [101]. Unlike smaller molecules, the addition or removal of an electron from polymer films carries several implications. The reverse reaction of the doping process cannot be equated to the de-doping reaction, since conformational reorganization and variations of the energy levels are promoted by the addition or removal of an electron [102]. Therefore, the oxidation and reduction potentials are

estimated by the *onset* potential [103], defined as the potential at which the initial injection of holes or electrons to the HOMO and LUMO respectively [102].

Research carried out on organic compounds showed a correlation between the energy required to add one electron to a molecule, the standard reduction potential, and the energy of the LUMO. The energy of the LUMO can be approximated by the electron affinity, which is the energy required to add an electron to an atom or molecule in the gas phase. In a similar fashion, correlations have been found for organic molecules between the standard oxidation potentials and the ionization energies [104]. The latter is the minimum energy required to remove an electron from an atom or molecule in the gas phase related to the energy of the HOMO. Based on these observations, it is clear that a great deal of approximation arises from the fact that the HOMO/LUMO energies are scaled in vacuum, while the reduction/oxidation potentials are measured in solution.

In organic photovoltaic literature inconsistent use of redox standards (values used for standard electrode potentials) and Fermi energy scale values have been observed. Thus, comparing HOMO/LUMO levels of conjugated polymers prepared and investigated by different research groups in the expectation of predicting possible performance may be misleading. There are several Fermi energy scale values that have been correlated to the formal potential of the normal hydrogen reference electrode (NHE) [104]. In order to evaluate the frontier energy orbitals of materials, these correlations have been applied in conjunction with electrochemical formal potentials. The precision of these correlations is not fully understood as it is difficult to incorporate corrections for the gas phase ionization potentials, and thus make a direct link to the vacuum scale [102]. Consequently, caution should be exerted when

the HOMO/ LUMO energy levels of conducting polymers are evaluated with electrode Fermi energy scales. Cyclic voltammetry cannot provide only the *formal potentials* of these species but the measurements are done in solution and not in the gas phase. A range of work function values from 4.4 eV to 4.85 eV were reported for standard hydrogen electrode which inturn leads to a variation in the work function of the standard ferrocene/ferrocenium (Fc/Fc^+) redox couple from 4.8 eV to 5.4 eV [104]. Therefore, orbital energies obtained with different scales cannot be directly compared and researchers should state in their experimental procedures what parameters and assumptions are included in their calculations.

A number of reports rely on a scale − 4.8 eV for 0.0 V versus Fc^+/ Fc [105 - 109]. This value is based on the calculations obtained by Pommerehne et al. [110]. Their estimate begins with the premise that the standard electrode potential for the NHE was about − 4.6 eV, which was given in the first edition of Bard and Faulkner's book [111]. Then, a value of 0.2 V vs. NHE was given for the Fc^+/Fc in 0.1 M $(C_4H_9)_4NPF_6/CH_3CN$ solution [104].

Bandgap of conducting polymers can be determined electrochemically through cyclic voltammetry experiments. This band gap value can be compared with the one deduced from absorption wavelengths. The onset potentials of the *n*-doping (E_{red}) and *p*-doping (E_{ox}) can be used to determine the LUMO and HOMO energy levels of conducting polymers, respectively and the potential difference, $\Delta E = E_{ox} - E_{red}$, can be used to estimate the energy gap of the polymer $E_g = e\,(\Delta E)$, (e is the elementary charge). The energy levels in electron volts, eV corresponding to the electrochemical potentials vs. the reference standard calomel electrode (SCE) for example can be obtained by adding a correction 4.4 V, to vacuum level. Thus, $E_{LUMO} = (E_{red} + 4.4)$

(eV) and E_{HUMO} = (E_{ox} + 4.4) (eV) [112, 113]. But the electrochemical oxidation/reduction reaction of most organic conducting polymers takes place in nonaqueous solvents which is difficult to find a standard reference electrode, instead a *quasi reference electrode* (QRE) that does not contaminate the test solution with undesirable species is often employed [114]. This is usually just a metal wire, Ag , Pt, or Ag wire coated with AgCl are used. It is unacceptable to report potentials *vs.* an uncalibrated quasi reference electrode [115], so the actual potential of the quasi reference electrode *vs.* a true reference electrode must be calibrated. Typically the calibration is achieved by measuring the standard potential vs. the QRE of a redox couple whose standard or formal potential is already known *vs.* a true reference under the same conditions. The ferrocene/ferrocenium (Fc/Fc^+) couple is recommended as a calibrating redox couple, since both forms are soluble and stable in many solvents and usually shows nernstian behavior [116]. The values of HOMO and LUMO can be estimated from the onset oxidation and reduction potentials respectively on the basis of the reference energy level of ferrocene (4.8 eV below the vacuum level) [117, 118] according to Equation 2.5 where *q* refers to quasi [119 - 121].

$$E_{HOMO} / E_{HOMO}\ (eV) = [-e\ (E_{onset\ \ (vs\ qAg/AgCl)} - E_{onset\ \ (Fc/Fc^{+}vs\ qAg/AgCl)}] - 4.8 \quad \text{..... (2.5)}$$

2.5. Spectroelectrochemistry of conjugated organic polymers

Spectroelectrochemistry is the simultaneous characterization of materials using spectroscopic techniques while the materials are undergoing electrochemical processes. So in spectroelectrochemical studies spectral changes induced by electrochemical processes occurring at polymer film deposited at the electrode surface are registered. Various spectroscopic techniques such as Uv-visible-near infrared (UV-Vis-NIR), foruier transform infrared (FTIR), electron spin resonance (ESR), and

Raman have employed in combination with electrochemical techniques like cyclic voltammetry.

Using *insitu* UV-Vis-NIR spectroelectrochemistry, we can follow the changes in the electronic properties of the polymer film upon oxidation/reduction. The new electronic levels polaron/bipolaron formed by the electrochemical doping of the polymer provide intermediate channels to the promotion of electrons from the valence band (VB) to the conduction band (CB), decreasing the energy required for the electronic transition and leading to a red shift in the UV–Vis spectrum. So that the emergence of new optical transitions at longer wavelength NIR region are observed in the UV-Vis-NIR spectrum of conducting polymers [99, 122]. Other pathways to study polymer redox spectroscopically is to follow the structural changes that accompany the doping (oxidation/reduction) process. Vibrational techniques, including FTIR [89, 123 - 125] and Raman scattering [126, 127], provide molecular-level information that is highly sensitive to conformation changes. The occurrence or disappearance of paramagnetic species like radicals and triplet states during redox processes can also be observed by the *insitu* electron spin resonance spectroscopy (ESR) [128].

As shown in Figure 2.4 for the absorption spectroelectrochemical series of poly (2,2'-dimethyl-3,4-propylenedioxythiophene) (PProDOT-Me_2) [99], the neutral polymer is characterized by an absorption maximum centered at 550 nm with a bandgap of 1.7 eV. As the potential applied to the polymer film is increased to more positive values, an absorption begins to emerge between 700 and 1100 nm while the $\pi - \pi^*$ absorption begins to decrease in intensity. At slightly higher oxidation levels, an even lower energy absorption band begins to emerge above 1250 nm. When the polymer approaches full oxidation, the bipolaron band absorption begins to dominate at the

expense of the polaron and $\pi - \pi^*$ transitions.

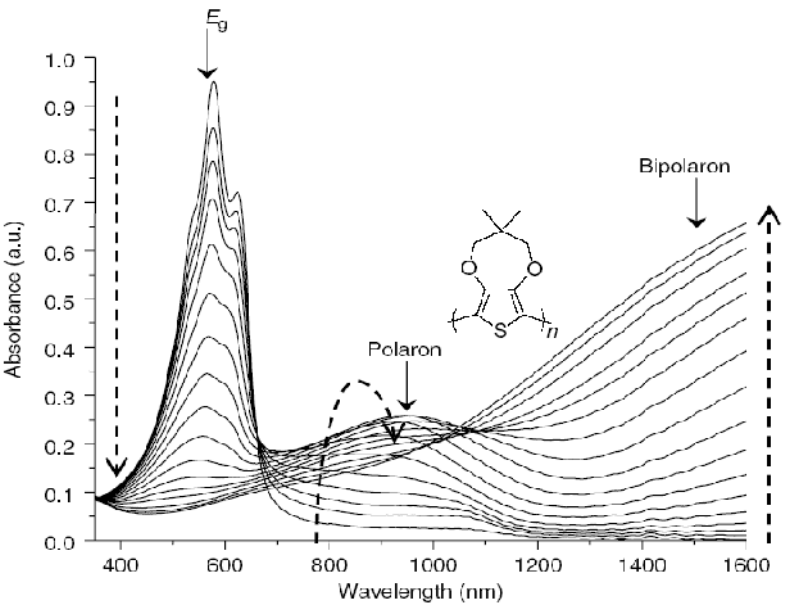

Figure 2. 4: *Spectroelectrochemistry of PProDOT-(Me)$_2$ showing electronic transitions for the bandgap (E_g), polaron, and bipolaron. Dashed arrows show direction of spectral growth or recession* [99].

2.6. Photophysics of conducting polymers

Up on absorption of photon of energy higher than the absorption edge of a conducting polymer an electron from the ground state (M) is raised to the conduction band and hole is left behind in the valance band to form an excited state analog of the ground state [129]. Usually the photogenerated electron-hole pair remain in the same chain with their coloumbic attraction to form excitons which are singlets in nature ($^1M^*$) because of electron and hole are created in opposite spins [130]

There are many possible fates or routes of deactivation of excitons as shown in Figure 2.5. The rate of deactivation determines the inherent life time of the excited state.

Fluorescent transitions which are radiative decay of the excitons occur following excitation between states of the same multiplicity ($\tau = 10^{-12} - 10^{-8}$ s), while a phosphorescent transition occurs ($\tau = 10^{-6} - 10^{-2}$ s) between states of different multiplicity, non radiative transitions of internal conversion (IC) and inter-system crossing (ISC) compete with radiative processes. IC is relatively fast ($\tau = 10^{-12}$ s) and occurs *via* vibronic coupling between an upper excited state to the lowest excited or ground state. ISC is a spin-forbidden radiationless transion ($\tau = 10^{-11} - 10^{-6}$ s) by which triplet states are usually populated [130 - 132].

When local density of chromophores is high such as in case of π-conjugated polymers interaction can exist between the excited species and its nearest ground state neighbours. When this interaction occurs with in the life time of the excited state, bimolecular mechanisms dominate deactivation process. Quenching (Figure 2.5 paths 1 and 4), migrative energy transfer (paths 2 and 5) and annihilation (path 3) are bimolecular processes [131, 132]. Annihilation is rare for singlet states but can occur with triplets to yield a delayed fluorescence. Alternatively an excited singlet state can interact with ground state molecules of the same species to yield an excimer [133], characterized by a broad structureless fluorescence which is red shifted with respect to the monomer fluorescence. Many excimers have very low quantum yields of luminescence. Their emission has lower frequency than the excited molecule alone [130, 131]. The ground state dimmer (D) is unstable and readily dissociates. Complex formation between the excited state species and ground state of different molecules give rise to an exciplex [131].

The non radiative deactivations are very important in the sense that the donation of excitation energy or the transfer of charge from one molecule to another, can serve to

funnel excitation energy into a reactive center [131]. It is based on this photo induced charge transfer from the donor organic conjugated polymer to the acceptor molecules like fullerene that polymer solar cells work [134].

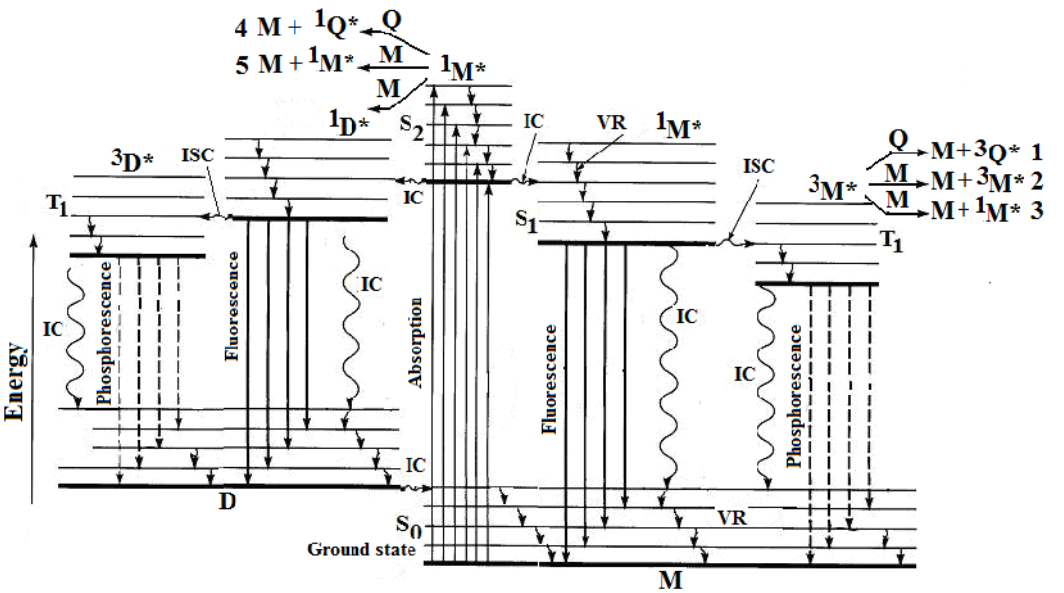

Figure 2. 5: *Photophysical processes in conducting polymers [131].*

Oxygen is an efficient quencher of both singlet and triplet excited states, forming singlet oxygen ($^1O_2$) in the process by increasing the photoconductivity but singlet oxygen has a sufficiently reactive to initate reactions with most unsaturated hydrocarbon and destroy polymers like polyparaphenylene vinylene (PPV) [131,135].

If the electron and hole separate sufficiently so that they do not interact to form an exciton a polaron is formed. This might happen by the electron and hole within femto second time of creation and separating into different chains. When there is an isolated electron and hole on a chain, the chain proceeds to relax or deform with in the next 100 femto second time so as to decrease the energy of the carrier and the resulting deformation is called a polaron (negative or positive depending on the charge).

A bipolaron consists of the same charges in opposite spins in the same chain. Polaron pair is an electron and a hole in a nonparallel nearest neighbour chain. Polaron pairs are intermediate state between electronic molecular excitations and free charge carriers. These excitation may also called charge transfer excitons. Movable polarons can hope from the next neighbouring chain sites to further chain sites still belonging to the pair which is now called distant polaron pair. Distant polaron pair conserves the main property of the pair to have recombination rate within the pair competing with the dissociation which determined the life time of the pair [130, 136]

The recombination of trapped polaron pairs $p_t^+ p_t^-$, generated by a visible excitation is now widely believed to be almost entirely non radiative (Equation 2.6).

$$p_t^+ + p_t^- \rightarrow S_0 + phonons \quad \text{.....(2.6)}$$

Where S_0 is the ground state. Note that this process is spin dependant, and will be much faster if the spins of the trapped polarons are anti parallel than if they are parallel. These trapped polaron pairs which are interchain or interconjugation-segement in nature are essentially charge transfer states generated by doping. They are apparently efficient non radiative singlet exciton S_1^* quenching centers (Equation 2.7).

$$\begin{matrix} S_1^* + p_t^+ \rightarrow S_0 + p_t^+ + phonons \\ S_1^* + p_t^- \rightarrow S_0 + p_t^- + phonons \end{matrix} \quad \text{.....(2.7)}$$

In any scenario, however, the excited singlet state which undergo radiative decay must originate from the free polarons to which the injected electrons and holes immidately relax (Equation 2.8).

$$p_t^+ + p_t^- \rightarrow S_1^* \rightarrow 1B_u \rightarrow S_0 + h\upsilon + phonons \quad \text{.....(2.8)}$$

Where $1B_u$ is the lowest state in singlet manifold of luminescing polymers. Note that similar to Equation 2.6 and unlike Equation 2.7 this process is spin dependant and will essentially require an antiparallel configuration of polaron spins. The parallel configuration may fuse to triplet excitons (T_1^*) [137]. Primary singlet exciton can produce triplet intrachain excitons by intersystem crossing or transfer of electron to the neighbouring chain. The latter process forms charge transfer (CT) interchain or interconjugation excitons or polaron pairs. Triplates in general are more bound than singlets and have longer life time (Equation 2.9).

$$p_t^+ + p_t^- \rightarrow T_1^* \quad \text{.....(2.9)}$$

Many classes of polymers fluoresce because of delocalized π-conjugated system. Photo excitation results in the formation of an exciton. There is a tendency for this excitation to become self trapped and confined to the polymer chain because of the quasi one dimensional nature of the chain [138]. Dissociation of the excited state results in photoconductivity and a non radiative decay where as recombination can yield luminescence. Variations exist in the colour of emission, radiative life time, and quantum efficiency of luminescence due to differences in molecular architecture of which determines the band gap $\pi - \pi^*$ transition energies which decrease as the extent of conjugation increases [139]. The change in conformation of the polymer where the polymer takes up a rod like in the solid state which imparts a red shift to the fluorescence compared to the coil like conformation adopted in solution form [126].

Similarly the presence of large bulky substituent attached to the conjugated backbone prevents the polymer from achieving a planner configuration and increase the $\pi - \pi^*$ transition energy. Noticeably both the absorption and emission spectra are broad due to the conformational statistics of the polymer coil which segementalizes π-

conjugated lengths in to a range of persistence lengths. Stokes shift are usually due to relaxation of the structure in the excited state. Structural homogenity of the polymer chain is of similar importance. In substituted conjugated polymers the electronic structure depends on the type of substituent distribution along the conjugated backbone, but for a given type of distribution pattern, it is strongly influenced by the regiospecificity of the system [140].

There is a significant increase in the emission intensity when the solvent is changed from a chlorinated to a non-chlorinated solvent due to fluorescence quenching by the heavy atom effect. Both absorption and photoluminescence are greatly influenced by solvent polarity, perturbing the fundamental and excited state of the polymer. An excited state with a high polar character will interact with solvents of high polarity (high dielectric constants) stabilizing the excited state on a lower energy level hence causing a red-shift of the emission. A blue shift is expected for solvents of lower polarity [141, 142]. The fluorescence quantum yield (Φ) is the ratio of photons absorbed to photons emitted through fluorescence. In other words the quantum yield gives the probability of the excited state being deactivated by fluorescence rather than by another non-radiative mechanism. The most reliable method for recording fluorescence quantum yield is the comparative method which involves the use of well characterized standard samples (references) with known Φ values. Essentially, solutions of the reference and test samples with identical absorbance at the same excitation wavelength can be assumed to be absorbing the same number of photons. Hence, a simple ratio of the integrated fluorescence intensities of the two solutions (recorded under identical conditions) will yield the ratio of the quantum yield values. So fluorescence quantum yield (Φ) of a material is given by Equation 2.10.

$$\Phi = \Phi_R \frac{IA_R n^2}{I_R A n_R^2} \quad \text{.....(2.10)}$$

where I is integrated intensity of fluorescence, A is absorption (optical density) and n is the refractive index and R stands for the reference fluorophore of known quantum yield [142,143].

2.7. Charge transport and conductivity in conjugated polymers

Semiconducting nature of organic conjugated polymers can be changed to conducting by the introduction of mobile charge carriers in π-electronic system by doping. At low and intermediate doping level these charge carriers self localize and form nonlinear configurations of solitons, polarons, and bipolarons. At high doping level a shift of the fermi level to the effective transport degenerate fermi sea (solitonc or bipolaronic band) where the $\pi - \pi^*$ gap will vanish to a metallic state is observed [138, 144, 145]. Studies showed that charge is stored in the mid-gap states of these doping-induced charged solitons, polarons, and bipolarons. These charged sites/defects are either mobile to take part directly in the transport, or they are pinned with electrons moving through the mid-gap band of levels through variable range of hopping [146, 147].

Electronic conductivity resulted from charge transport in a polymer is also related to charge carriers mobility, both along the polymer chain and between adjacent chains by *hopping* across chains due to interchain interaction or *tunneling* between conducting segements that are separated by less conducting regions. The first one is related to the actual conjugation length which depends upon the orbital overlap between repeating units and the defects number, the second one is related to the orbital overlap between adjacent chains that can occur either by stacking or simply by the presence of dopant ions acting as bridges for electronic coupling [148].

Conductivity (σ) of conducting polymers is defined as $\sigma = n\mu e$, where the mobility μ and the charge carrier concentration (density of charge carriers) *n* are two separate and independent quantities and *e* is the charge of electron. The charge carrier concentration can easily be manipulated and controlled by injection, photogeneration, or doping. The mobility is a quantity which involves material properties such as structure, morphology, and disorder. The mobility also depends on temperature, electric field strengths and charge carrier concentration in a way specific for the material. To optimize the conductivity one wants to achieve the highest carrier density and these carriers to have high mobility. The mobility can be expressed in terms of the average directional velocity or the drift velocity, v, electric field strength *E,* and diffusion/drift length *l* as shown in Equation 2.11.

$$\mu = \frac{v}{E} \Rightarrow l_{\text{drift}} = \mu \tau E \quad \text{.....(2.11)}$$

In the absence of an electric field, the motion of the charges is of diffusive character in which the momentum is transferred to the carrier from the surrounding medium. The Einstein Smoluchowski relation gives the following expression for the mobility in the field free limit with charge carrier diffusion coeficient D, the temperature, T , and the Boltzmann's constant, k_B [149, 150] (Equation 2.12).

$$\mu = \frac{De}{k_B T} \Rightarrow l_{\text{diff}} = \sqrt{\mu \tau k_B T / e} \quad \text{.....(2.12)}$$

The total mobility can be expressed to a good approximation as a sum of two contributions: $\mu_{Total} = \mu_{Tunneling} + \mu_{Hopping}$, where $\mu_{tunneling}$ dominates transport at low temperatures and $\mu_{Hopping}$ dominants at higher temperatures as phonons assist the upward hopping. The relative contributions of each mechanism depend however, on the actual values of the microscopic parameters (electron-phonon coupling, electronic

and phonon band widths, and phonon energy) [151, 74]. As phonons freeze due to low temperature the electron has to look further and further to find an energetically accessible state. Consequently, the average hopping distance decreases. Because the tunneling probability decreases exponentially with distance, the conductivity also decreases. In the moderately doped sample of a polymer the conductivity vanishes at absolute zero but the most highly doped samples behave like very dirty metals or disordered alloys, in which the conductivity is nearly temperature independent [152]. As it can be seen from Equations 2.11 and 2.12, in both cases the $\mu\tau$ product will determine the average distance the charge carrier can travel before recombination. The mobility lifetime product $\mu\tau$ is therefore an important parameter in determining whether or not the power conversion efficiency of the photovoltaic devices is limited by the charge transport and recombination.

Charge transport in polymers depends on the molecular weight (MW). It is clear that intergrain transport is severely limited in the low MW films due to the poor connectivity between grains and the large number of insulating grain boundaries. In the case of the high-MW films, there are no well defined grain boundaries. Since the molecules are much longer than the size of the ordered domains, individual molecules are expected to be part of several domains. These bridging molecules limit the amount of misorientation between neighboring domains and provide a possible pathway for charges to go between neighboring domains. A trend of increasing mobility with increasing MW was still observed. The large variation in mobility of the low MW films with processing suggests that the low MW mobility is limited by morphology [153].

Free charge carrier generation, charge transport to the opposite electrodes and extraction by the electrodes or carrier recombinations are among the main important processes which might limit the power conversion efficiency of organic bulk heterojunction photovoltaics. The important parameters here are the exciton diffusion length and the distance between the donor and acceptor phases. Excitons can be split into free electrons and holes if the carrier dissipation distance is larger than the coulomb radius. To fulfill this condition the coulomb field must be screened or charge carrier hopping distance must be larger than the coulomb radius [154]. Mobile charge carriers can be transported to the contacts either by carrier diffusion or electric field induced drift. In order to have unity quantum efficiency for charge extraction, one needs to fulfill the condition that the charge carrier transit time t_{tr} is much smaller than the carrier lifetime τ ($t_{tr} \ll \tau$). The carrier transit time $t_{tr} = d/\mu E$ is determined by the charge carrier mobility, μ, sample thickness *d*, and the electric field, *E,* inside the film.

Transport properties are highly affected by recombination of charge carriers. In low mobility materials such as π-conjugated polymers diffusion controlled bimolecular recombination or the so-called Langevin recombination is dominating [155]. In Langevin recombination oppositely charged carriers are within the coulomb radius and are attracted to each other by their mutual coulomb field. Since the hopping distance in low mobility materials is usually much smaller than coulomb radius, the carriers will have a lower probability to escape recombination and will eventually find each other and recombine either radiatively or nonradiatively. The magnitude of Langevin bimolecular recombination coefficient β_L can then be calculated using Equation 3.13 [156, 157].

$$\beta_L = e(\mu_p + \mu_n)/\varepsilon\varepsilon_0 \quad \text{.....(2.13)}$$

where μ_p and μ_n are the mobility of holes and electrons, respectively.

If one type of carriers is much faster than the other usually holes for organic conjugated polymers, then Langevin recombination coefficient will be determined by the faster carriers. At high light intensities Langevin recombination causes limitation on the maximum charge that can be extracted from the sample leading to the fact that only space charge perturbed current transients can be observed. This shows that if Langevin recombination is present, then it might eventually set an upper limit on the efficiency of photovoltaic cells. But studies showed that Langevin recombination constant for recombination in polymer/fullerene solar cells is not dominated by the fastest charge carrier. It is rather determined by the slowest one as a consequence of the confinement of the respective carriers to different materials. Measurements of the recombination rate in a conjugated polymer/PCBM blend quantitatively confirm this reduction of Langevin recombination constant [158].

In organic solar cells the mobility simultaneously controls both the carrier extraction and the losses *via* carrier recombination. It was proposed that the spatial average of the electron and hole mobilities should be used, in order to compensate for the eventual mobility differences of carriers in the different components of the blend. For such intimately mixed blends, only a few weight percent of the electron acceptor is sufficient to quench virtually all excitations. For efficient photovoltaic devices, however, the created charge carriers need to be transported to the corresponding electrodes within their respective lifetimes, which depend on the charge carrier mobility of the materials. It has been shown that the slowest carrier mainly governs the recombination process in the blend. Since the fastest carrier cannot cross the

interface due to the energy offset between the donor and the acceptor, it must wait for the slowest carrier in order to recombine. As a result, solar cells made of organic semiconductors are special in the sense that the two competing processes, extraction and recombination of charge carriers, are both governed by the mobility of the charge carriers [158]. In low mobility disordered polymer/fullerene blends, there is also a possibility that the photogenerated electron–hole pairs would finally recombine geminately without a possibility to escape each others coulomb attraction [159, 155].

An increase in carrier mobility would have a positive effect on transport, facilitating carrier extraction, but on the other hand it will increase the bimolecular recombination strength as well. At low mobility there is a buildup of charge carriers in the solar cells not only increases recombination, but also many of the photogenerated bound electron-hole pairs will not dissociate into free carriers and recombine to their ground state. These indicate that relatively high charge mobility is beneficial for the performance of an organic solar cell but extremely high mobility give rise to an efficient extraction that will lead to a depletion of charge carriers in the solar cell. Thus, sweeping carriers efficiently out of the device will lead to low quasi-Fermi levels for electrons and holes that leads to the reduction of the Voc and a decrease in the solar cell performance. The maximum attainable efficiency is then a trade off between the polaron pair dissociation, which enhanced by a high carrier mobility results in high short circuit currents, and the efficient charge extraction at high carrier mobilities, which lead to low carrier concentrations, thus limiting the open circuit voltage [160].

As a consequence of disorder in organic conjugated polymers charge carriers will relax within the inhomogeneously broadened Gaussian distribution of localized states

towards the statistically defined transport level and reach dynamic equilibrium [161]. If dynamic equilibrium is not reached before the carriers have been extracted, then the carrier transients will be featureless [162, 163] and the transients will depend on the measurement conditions. On the other hand, if dynamic equilibrium is achieved the carrier transients will typically show a clear plateau with a drop in the current level as the carriers reach the opposite electrode from which the charge carrier transit time t_{tr} is estimated and the mobility can be calculated using $\mu = d^2 / t_{tr} U_0$, where d is the thickness of the film and U_0 is the applied voltage. Hence, in order to obtain true material specific parameters it is important for the charge carriers to reach dynamic equilibrium. This can be achieved by having thick enough films of several μm so that the relaxation time is much smaller than the transit time [164].

2.7.1. Measuring charge carrier mobility using CELIV technique

For better performance of organic photovoltaic and other optoelectronic devices, a polymer with reasonably high charge carrier mobility is one of the requirements. So understanding the charge carrier transport (charge carrier mobility) in these materials is one of the scientific inputs in the field [155, 151]. Since semiconducting organic polymers are low mobility materials with low quantum photogeneration efficiency in their pristine phase [165], bulk heterojunction concept is introduced for an efficient charge generation and for a long carrier lifetime [166 - 168]. Charge extraction by linearly increasing voltage (CELIV) technique is one of the several techniques like the field effect transistor configuration (FET), the impedence technique [169], and the time of flight (TOF) [170], to study equilibrium charge transport and recombination in disordered π-conjugated polymers and inorganic semiconductors. Simultanous determination of the charge carrier mobitity and the life time of carriers is possible

using this technique [65, 171- 177]. Time-of-Flight (TOF) technique is usually used to measure the charge carrier mobility in the bulk of the film [178], however in disordered films with dispersive transport TOF is not well applicable.

A comparative study between CELIV and TOF showed a good agreement between charge carrier mobility values [175]. CELIV allows a direct measurement of the dispersive (time-dependent) charge carrier transport and recombination in films with energetically and structural disorders, where other time-resolved techniques like TOF are not applicable [65, 179]. In CELIV, the charge carrier mobility is directly estimated from the current or photocurrent transients without a need for assumptions, which are necessary when applying other methods with integral-nature like current-voltage characterization [155]. In this method charge carriers are extracted by a linearly increasing (triangle-shaped) voltage pulse. If the semiconductor under investigation is intrinsically pure (undoped) and contains no significant amount of mobile charge carriers, a laser light pulse is used to photogenerate the charge carriers which are further extracted from the film by increasing voltage after some delay time t_{del}. The voltage rise speed (A) applied to the sample is the rate of applied voltage $U(t)$ with time $A = U(t)/t$. Initial current step seen at time t = 0 and the negative current at the end of applied pulse represents the capacitor charging and discharging (displacement) currents, whereas further extraction current shows movement of the mobile charge carriers. Transients increase at larger applied voltages due to higher displacement currents.

Photo-CELIV is based on the comparison of the extraction current transients of equilibrium (dark transient) and photogenerated charge carriers [171, 177]. The time-dependent relaxation of photogenerated charge carriers within Density-of-States

distribution in disordered media is studied [180, 181]. CELIV can also measure non-equilibrium charge carrier mobility as opposed to steady state mobility techniques such as space charge limited current (SCLC) or field effect transistor (FET) measurements [65, 182, 183].

The sample is of sandwich type with non-injecting contacts (e.g. reverse bias). The initial current step j_0 is expressed by Equation 2.14.

$$j_0 = \frac{\varepsilon\varepsilon_0 A}{d} \quad \text{.....(2.14)}$$

(where d is the interelectrode distance) is caused by the geometric capacitance of the sample. This equation can be used for estimation of either the dielectric constant or the thickness of the active material by assuming the dielectric constant of conjugated poymers to be approximalty equal to 3. The rise speed of the current following j_0 is caused by the bulk or photogenerated conductivity of the sample. Low-conductivity materials do not exhibit any extraction current transient in the dark, but after photoexcitation of charge carriers a clear transient can be observed as shown in Figure 2.6. The conductivity, σ, can be estimated according to Equation 2.15.

$$\sigma = \frac{3\varepsilon\varepsilon_0 \Delta j}{2t_{\max} j(0)} \quad \text{.....(2.15)}$$

The time to reach the extraction current maximum $t_{\max}$ is also used to estimate the drift mobility of the charge carriers, when the carriers are generated in the bulk. Equations 2.16 -18 are used for calculating mobility depening on the conductivity of the material [171, 172, 173].

For low conductivity where $j_0 \gg \Delta j$

$$\mu = K\frac{d^2}{At_{\max}^2} \quad \text{.....(2.16)}$$

where $K = 2/3$ for volume and $K = 2$ for surface photogeneration.

For high conductivity materials where $j_0 \ll \Delta j$,

$$\mu = \frac{d^2 j_0}{A t_{max}^2 \Delta j} \quad \text{.....(2.17)}$$

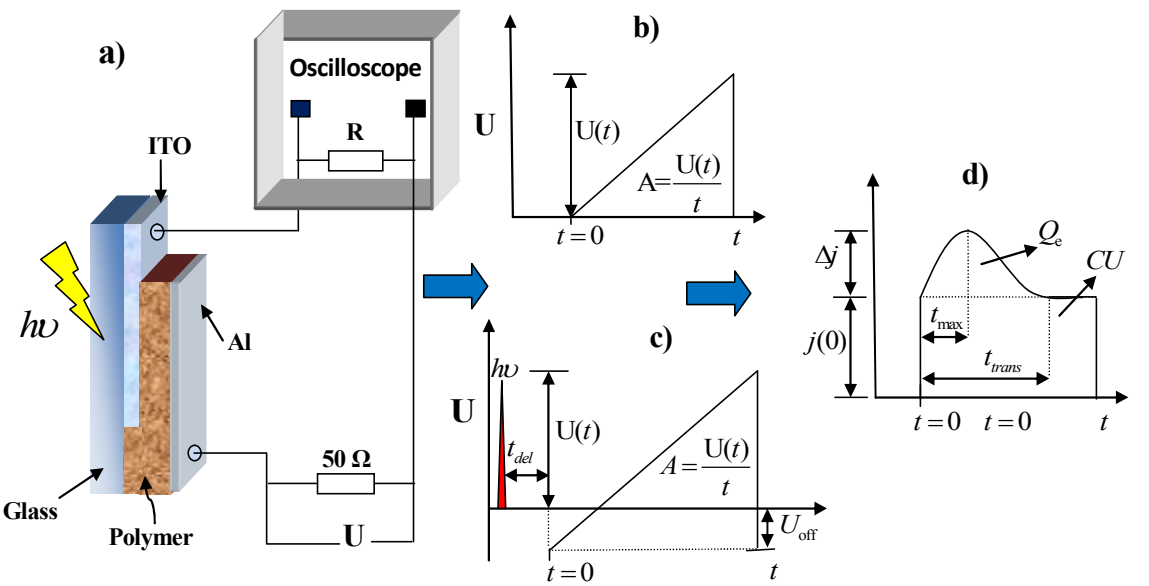

Figure 2. 6: *Illustration of the CELIV method a) the experimental setup b) Voltage input for CELIV, c) the voltage input for photo-CELIV d) the current output.*

and for moderately conductive, where $j_0 = \Delta j$

$$\mu = \frac{d^2}{A t_{max}^2 (1 + 0.36\Delta j / j(0))} \quad \text{.....(2.18)}$$

where $1 + 0.36\Delta j / j(0)$ is numerically calculated correction factor.

The main extraction occurs at the moment t_{max} when the field is strongest. Therefore, the mobility calculated and conductivity roughly correspond to the values at an electric field E (Equation.2.19) .

$$E = \frac{At_{max}}{d} \quad \text{.....(2.19)}$$

To independently estimate the time dependent charge carrier density one has to use very long voltage pulses. The ideal voltage pulse would be linearly increasing at first to level out at a constant voltage at long times in order to minimize RC effects.

2.8. Designing organic conjugated polymers for photovoltaics

The general trend in synthesis of conjugated polymers lies essentially in the efficient carbon-carbon single bond formation between two unsaturated carbons. In addition to electrochemical [184] or chemical [185] oxidative polymerizations, transition-metal-catalyzed cross-coupling reactions are used for carbon - carbon (C-C) bond formation with sp^2 - sp^2 *or* sp - sp^2 unsaturation. The reaction, in general, involves a transition-metal-catalyzed oxidative addition reaction across the C-X bond of an electrophile and then trans metalation with a main group organometallic nucleophile, followed by a reductive elimination step leading to the C-C bond formation where the active catalyst is regenerated.

The most commonly employed transition metal catalysts are palladium or nickel based complexes, although other metals have also been used. The organometallic nucleophiles can be Grignard reagents [45, 186] ,stannyl (Stille coupling), [45, 186, 187] boron reagents (Suzuki-Miyaura) [45,186,188] or A combination of palladium and Cu(I) effects coupling of terminal alkynes with vinyl or arylhalides (Sonogashira reaction) [45, 186, 189, 190]. Thus, conjugation lengths can be extended through consecutive transformations in the catalytic cycle. These reaction conditions are generally mild and can tolerate many functional groups. On the other hand, nickel-mediated Yamamoto dehalogenation coupling reactions also provide an alternative

pathway for carrying out self-polymerizaiton of single monomers. Traditional reactions such as the Horner–Wadsworth–Emmons and Knoevenagel condensation are particularly useful in the synthesis of vinylene-containing conjugated polymers *via* the carbon-carbon double bond formation between two respective monomers [56].

Initial conjugated polymers were intractable due to the lack of side chains. The addition of side chains lowers the melting temperature and increases the solubility by separating the conjugated backbones and reducing the rigidity of the backbone. When designing functional organic conjugated polymers for the purpose of photovoltaic device, combination of the intrinsic properties of the conjugated polymer backbone such as electroactivity, conductivity, photophysical properties with the changes related to the additional moiety solubility, the band gap tunnning, the morphology, efficient charge transport, etc is very important.

It is highly desirable to develop conjugated polymers with broader absorptions through narrowing their optical band gap and high overall extinction coefficients of the polymers to efficiently absorb light. In general an attachment of electron donating moieties to the main conjugated back bone raise the HOMO energy by decreasing the ionization potential, while electron withdrawing groups lower the LUMO energy by increasing the electronic affinity through inductive or mesomeric effects, resulting in a decreased bandgap. In poly[3,4- ethylenedioxythiophene] with direct attachment of electron donating alkoxy groups has a band gap of 1.5 eV, which is about 0.5 eV lower than that of the parent polythiophene [45, 191].

There is also a dual effects of electron donating amino groups and electron withdrawing nitro groups on the neighboring thiophene units resulting in a dramatically reduced bandgap due to its high degree of zwitterionic and quinoid

character [192]. A more powerful strategy in designing low bandgap conjugated polymers is to alternate a conjugated electron rich donor (D) unit and a conjugated electron deficient acceptor (A) unit in the same polymer backbone. Through the introduction of push-pull driving forces to facilitate electron delocalization and the formation of quinoid mesomeric structures over the conjugated main chain. Photoinduced intramolecular charge transfer (ICT) correlated with HOMO of the donor unit and LUMO of the acceptor unit can also account for the reduced optical band gap [193, 194].

The grafted alkyl and/or alkoxy side groups do not only fulfill the function of solubilising agents and enabling the processability of the polymers into thin films but also lead to dramatic changes in the optical, electronic, intermolecular ordering, and transport properties. [195 - 197]. The separation of the backbones by the side chains reduces the intermolecular overlap, and thus slow down hopping of charges between molecules. Since the packing associated with crystalline aggregates decreases the power efficiency due to excimers such polymers typically have asymmetric, bulky side chains that cause the molecules to twist. The twisted molecules cannot pack efficiently. Conjugated polymers that crystallize tend to be more rigid and planar [198].

The molecular weight (MW) of a rigid rod polymer like P3HT would be expected to affect the morphology. Molecules in low-MW polymer films should be able to crystallize into a structure more like that obtained with high-mobility small molecules like pentacene. Molecules in high-MW films would be expected to be kinetically limited from forming large crystalline domains. Conventional theory on charge transport in organic semiconductors would predict that the more ordered, low-MW

films should have higher charge carrier mobility than their less-ordered, high-MW counterparts. But in reality the opposite is true. This is because of intergrain transport is severely limited in the low-MW films due to the poor connectivity between grains and the large number of insulating grain boundaries. In the case of the high-MW films, there are no well-defined grain boundaries. Since the molecules are much longer than the size of the ordered domains, individual molecules are expected to be part of several domains. These bridging molecules limit the amount of misorientation between neighboring domains and provide a possible pathway for charges to go between neighboring domains [198].

Since the discovery of an ultrafast (femto second) photoinduced charge transfer from alkoxy-substituted poly[2-methoxy, 5-(2-ethylhexyloxy)p-phenylene-vinylene] MEH-PPV to the buckminsterfullerene by Sariciftci *et al* [34], great attention was given to PPV derivative polymers. As compared to PPVs the dehydrogenated analogues poly(p-phenylene-ethynylene)s (PPEs) have comparatively low lying LUMO due to enhanced electron affinity, which is ascribed to the electron withdrawing nature of triple bonds (–C≡C–). PPEs moreover exhibit a highly rigid conjugated system with differences in polarization, molar extinction coefficients, and especially higher fluorescence quantum yields in non-aggregated states. In solution but very low fluorescence quantum yield in aggregated states due to very strong π-π interchain interactions creating multifarious radiationless deactivation pathways [56]. The coplanar and rigid nature of the acetylene moiety in the polymer chain may have the potential to obtain a higher degree of packing and thus improve the photovoltaic performance of such devices. The synthesis of these group of polymers is *via* the Horner-Emmons reaction of the dialdehyde and p-xylylenebis (diethyphosphonate) monomers in the presence of t-BuOK as the base [53]. Having coplanar electron rich

anthracene units and triple bond bridges, exhibits broader absorption, a lower HOMO level, and a smaller optical band gap of 1.9 eV, compared to MDMO-PPV.

By inserting thiophene units which has lower aromaticity than benzene within PPE-PPV backbones , copolymers are expected to have optical bandgap energies of ~2.0 eV, due to the electron rich thiophene moieties. A reduction in aromaticity of the aromatic units in the conjugated main chain allows a greater tendency to adopt the quinoid form through π-electron delocalization. Moreover, thiophene unit is known to induce planarity in polymeric backbone, which is related to the very small torsion angle that it forms with its neighbors [191, 194, 198]. This aspect is of great significance for enhanced intermolecular packing (π-stackings) and ordering, which is relevant for charge transport ability and better morphology in the bulk and resulting an increased short circuit current, I_{SC}, in solar cells made by these copolymers [57]. Nowadays numerous types of organic conjugated polymers with varying backbones and sidechains are being produced and tested for organic photovoltaic in different corners of the globe.

2.9. Organic bulk heterojunction polymer solar cell devices and characteristics

The organic photovoltaic effect is generally based on light absorption by the organic polymer which induces electron hole pair (exciton) formation followed by charge separation with the help of junction to produce photocurrent. The dark characteristics of such a junction structure correspond to a standard diode [199 - 201]. The strongly bound excitons could not undergo direct electron–hole dissociation as a consequence of the low dielectric constants in organic components, which are insufficient to creat this effect, as it is found in high dielectric inorganic counterparts [46, 202]. So in organic solar cells, exciton dissociation occurs almost exclusively at the interface

between two materials of high ionization potentials and high electron affinities, which corresponds to the electron donor and the electron acceptor materials, respectively [43, 203, 204].To generate photocurrent effectively, appropriate donor–acceptor pair and device architecture of bulk heterojunction (BHJ) devices was found to be very important [31, 52]. BHJ devices, most closely conform the ultimate vision of organic solar cells as low-cost, light weight, and flexible devices. The other advantage of BHJ devices is the ability to process the composite active layer from solution in a single step, by using a variety of techniques that range from inkjet printing to spin coating, and roller casting [42]. The high electron affinity and superior ability to transport charge makes fullerene and its derivaives as the best acceptor molecules for this kind of devices [34]. The state of art in BHJ solar cells with polymer: [6,6]-phenyl-C_{61}-butyric acid methyl ester (PCBM) blend currently reached certified efficiencies above 7 - 10% [40, 41].

The device structure of bulk heterojunction organic cell consists of at least four distinct layers, on a substrate, which may be glass or some flexible transparent plastic material as shown in Figure 2.7a .

1) On top of the substrate is the transparent anode where light can inter through it. Indium doped tin oxide (ITO) is a popular anodic material due to its transparency as a result glass substrates coated with ITO are commercially available.
2) A layer of hole conductive polymer (PEDOT/PSS), poly(3,4-ethylenedioxy-thiophene) /poly(styrenesulfonate) may be applied between the anode and the active layer. The PEDOT/PSS layer serves several functions. Not only does it serve as a hole transporter and exciton blocker, but it also smoothens out the ITO surface, seals the active layer from oxygen, and keeps the anode material from diffusing into the active layer, which can lead to unwanted trap sites [205].

3) Next, on top of the PEDOT/PSS, the active layer (s) is deposited. This layer is responsible for light absorption, exciton generation/dissociation, and charge carrier diffusion. The active layer in a heterojunction device is made up of two materials: a donor (which is usually a conjugated organic polymer or mixture of polymers) and an acceptor (fullerene and its derivatives like PCBM).

4) On top of the active layer is a metal electrode typically Al (cathode) ~ 100 nm thick is deposited by vacuum evaporation.

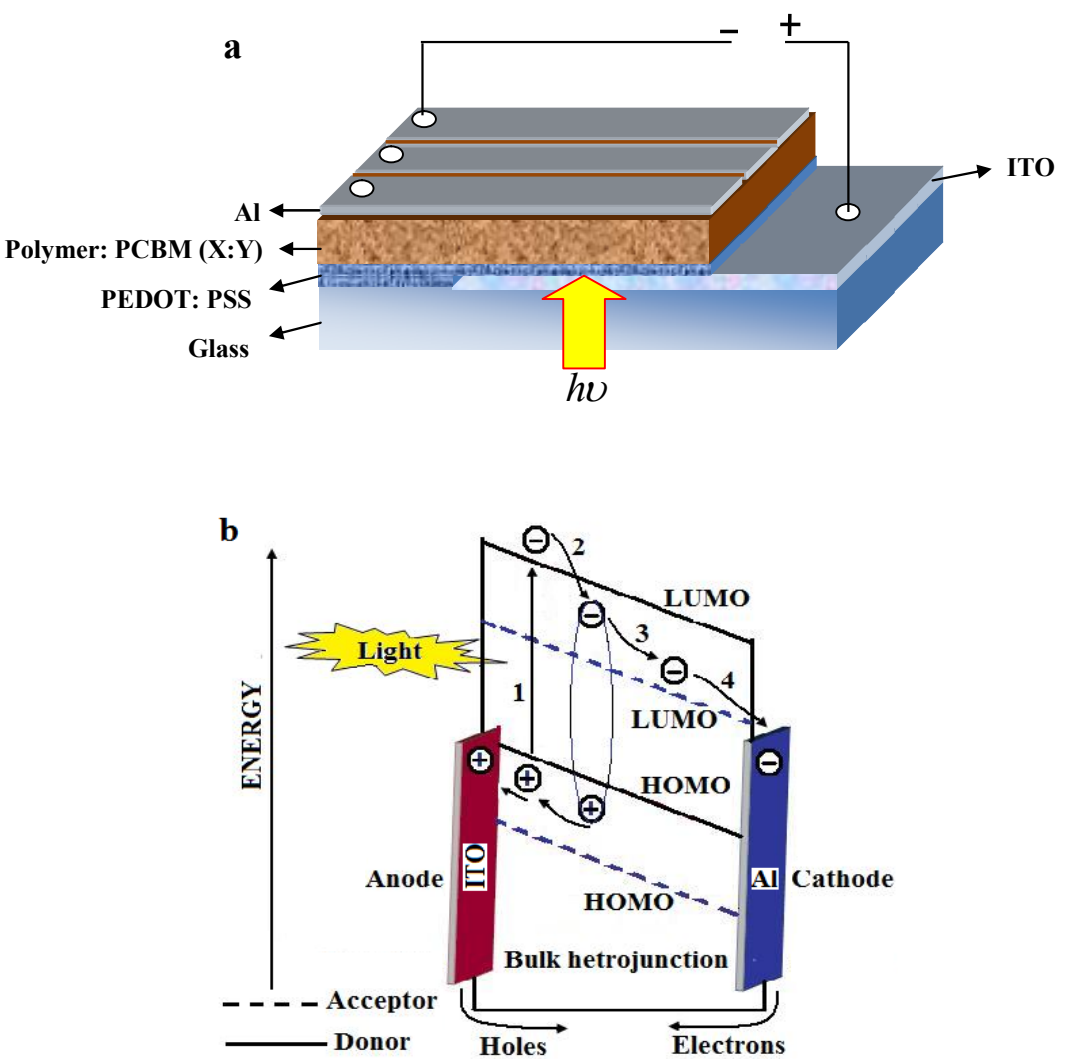

Figure 2. 7: *Bulk heterojunction solar cell a) Device architecture b) photon to current conversion mechanism.*

Figure 2.7 b shows a schematic representation of the mechanism of energy conversion in a typical BHJ solar cell, illustrating the components involved in the mechanistic steps. The energy conversion process has four fundamental steps in the commonly accepted mechanism (1) Absorption of light and generation of excitons, (2) Diffusion of the excitons, (3) Dissociation of the still coulomb bound electron hole pair by subsequent electron transfer to the acceptor at the interface and (4) Charge transport and charge collection to the respective electrodes (photocurrent generation) [206 - 208].

(1) Absorption of light and generation of excitons

Light absorption and generation of excitons is the first step in the mechanism of photocurrent generation in BHJ soalr cells. Light is absorbed by the donor material which is usually conjugated polymer. One of the limitations in organic conjugated polymer solar cells is their poor absorption because of their large bandgap leading to a mismatch to the terrestrial solar spectrum. For example, polyparaphenylene vinylenes (PPVs), polyphenylene ethylene (PPE), polythiophenes, (PT) and their alkyl and alkoxy substituted derivatives have bandgaps in the range of 1.85 to 2.2 eV. The bandgap of 1.85 eV with absorption edge of 670 nm only allowed 46% of irradiated photon to be harvested. A bandgap of 1.1 eV (Si) allowed more than 90% of photon to be harvested. There is always an optical loss due to polymer bandgap mismatched with the solar spectrum. In order to exceed the power conversion efficiency (PCE) over 10% from single bulk hetrojunction polymer solar cells, the bandgap of donor polymers should be 1.7 eV and the LUMO of this donor polymers should be 0.4 eV less than the LUMO level of PCBM if it is used as the electron acceptor [209, 210].

The most effective way to improve the J_{SC} is to enlarge absorption. In the standard solar spectrum (AM 1.5G), the maximum irradiance energy is at 500 nm, the maximum photon flux is at 670 nm as shown in Figure 2.8a. Therefore, polymer solar cells materials need not only to absorb the photons at the maximum irradiance but also to have a broad absorption spectrum and high absorption coefficient [111, 212]. Semiconducting polymers have higher extinction coefficient than that of inorganic semiconductors. About 300 nm film is thick enough to absorb the most incident light. But due to the low carrier mobility, the optimized thickness for most polymer solar cells is less than 100 nm [113, 214]. When a photon was absorbed by an electron donor, the electron was excited to an exciton energy state which was inside the energy gap. Once the exciton is generated, the electron and hole remain localized on a few polymer repeated units and they are bound to each other by the electrostatic attraction. Indeed before singlet exciton dissociation at the donor–acceptor interface take place, the neutral exciton has to diffuse towards this interface.

(2) Diffusion of the excitons

Once excitons are created still there is an electrostatic (coulomb attraction) force that binds electron with the hole with a binding energy of ~ 0.4 eV, and this quasi-particle will diffuse in its lifetime until it is recombined and/or separated. The fraction of excitons that reach the donor acceptor interface is determined by the exciton diffusion length and the location at which an exciton is created with respect to the nearest dissociation center and the charge carrier mobility of the material. The typical exciton diffusion length in semiconducting polymers is less than 20 nm so that the donor acceptor phase separation should be in the limit of the diffusion length to reduce recombination [113, 214].

(3) Dissociation of excitons

Semiconducting polymers have lower dielectric constant (ε) than that of inorganic semiconductors. The electrostatic (coulombic) attractive force between the holes and the electrons is proportional to $1/\varepsilon$, where $\varepsilon = 3$ (typical values for semiconducting polymers) [76]. The coulomb attraction in inorganic semiconductors with a larger dielectric constant can be neglected. In contrary, semiconducting polymers require a force more than 0.4 eV [215] to separate the exciton once created by absorption. If the exciton does not separate in time, it will recombine to a photon, or decay *via* thermalization. If the exciton reaches the donor/acceptor interface the electron can then be transferred to the material with lower lying LUMO of the acceptor if $I_D - E_A -$ Coulomb < 0, where I_D is the ionization potential of the excited donor, E_A the electron affinity of the acceptor, and coulomb summarizes all the electrostatic interactions including the exciton binding energy and all polarizations. It will be separated in the time scale of femto-second (~ 50 fs) [216]. This process is much faster than other competing processes like photoluminescence (ns) and charge recombination (ms) which is approximately 100% efficient. But geminate polaron pairs are photo-induced instead of exciton, which are not separated at the interface between the donor and the acceptor.

(4) Charge transport and charge collection

Following excitons dissociation, charges need to travel through the materials towards the respective electrodes. Due to the lack of long-range order and random oriented domains of solution processed organic semiconductors, the electrical transport mostly takes place by hopping from one localized state to the next, instead of band transport found in crystalline semiconductors which can greatly reduce the cell efficiency not

providing the necessary conductivity that charges require in the last step of the operating sequence. Because of this intrinsic characteristic of polymer molecules, high traps density, dead end in the transport net and so on, the mobility is low and unbalanced [217]. Therefore, the charge transport efficiency in polymer solar cells is not unity. Due to an ohmic contact between active layer and the electrodes and an enlarged build-in electric field, a better charge collection condition was created, as a result, charge transport efficiency was compromised [218, 219]. The resulting photocurrent is thus generated by the extracted charges: the holes leave the device through the anode, the electrons are extracted from the cathode. For devices with a bad contact with the corresponding electrodes surface recombination at the metal/organic interface, which influences the carrier concentration at the interface might happen and reduce the charge collection efficiency [206].

Air Mass (AM)

To characterize quantitatively the performance of solar cells for terrestrial applications, standardized illumination conditions are used in which the spectrum of the source simulates the solar spectrum AM 1.5. AM is measure of how much atmosphere sunlight must travel through to reach the earth's surface. It is denoted as AM **x**, where **x** is the inverse of the cosine of the zenith angle of the sun as shown in Figure 2.8a. Air Mass (AM) was standardized by both the international organization for standardization and the American society for testing and materials [220].

The total energy emitted by the sun is equal to 1353 W/m^2 in free space outside the atmosphere which corresponds to AM 0 spectrum. AM 1 spectrum corresponds to sunlight in the earths surface when the sun is overhead at the Zenith. AM 1.5 G corresponds to an angle of about 48.2^0 for inclination of the sun from the Zenith

(Figure 2.8a). G stands for global and refers to a small contribution of diffuse light to the direct incident ligh. The corresponding spectral irradiance of AM 1.5G spectrum is shown in Figure 2.8b and the standarized integrated photon flux has been corrected to 100 mW/cm^2 [211, 212].

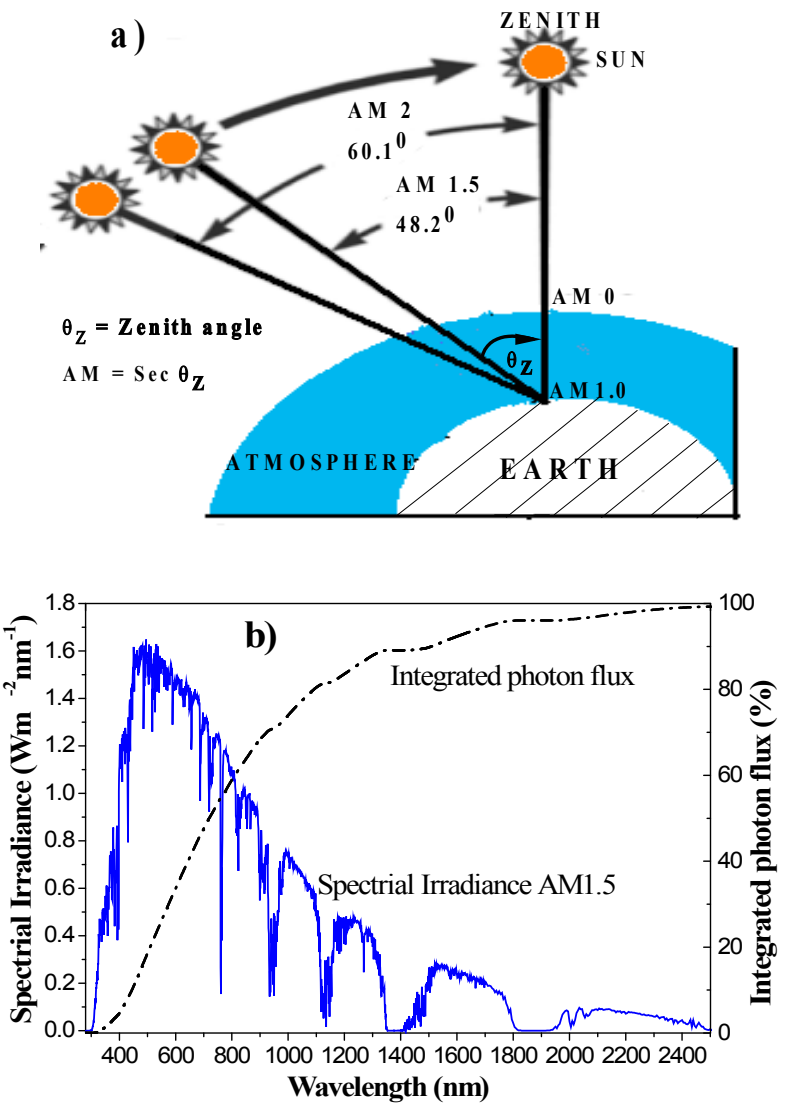

Figure 2. 8: *a) AM 1.5 b) Solar irradiance and integrated photon flux.*

2.9.1. Current–voltage (I-V) characteristics of bulk heterojunction solar cells

Typical I-V characteristics of bulk heterojunction devices in dark and during illuination are presented in Figure 2.9a. In the case of no illumination where there is no photocurrent the parallel resistance (R_p) is much greater than serial resistance (R_s) , $R_p \gg R_s$, the electrical response of the solar cell is expected to consist of three distinctive regimes [199].

i. A linear regime at negative voltages and low positive voltages where the current is limited by R_p,

ii. An exponential behavior at intermediate positive voltages where the current is controlled by the diode, and

iii. A second linear regime at high voltages where the current is limited by the serial resistance.

The three regimes can be easily identified. The linearity of this I-V regime in the semilogarithmic representation indicates an exponential correlation between the current density and the voltage. Upon illumination of the bulk heterojunction device a light dependent current is generated. When no current is flowing out of the device, i.e., open circuit condition, then the current produced by the current source recombines internally *via* R_p and the diode. Since R_p is rather high, the exponential behavior dominates several orders of magnitude in the current density, and the open circuit voltage is mainly determined by the properties of the diode. Together with the common positive slope that is displayed by the devices in region 2, the electrical response of the solar cell is dominated by the exponential regime at intermediate voltages. Solving for the simple circuit in Figure 2.9a provides the analytical

expression for the current voltage characteristics (Equation 2.20) which is called the Shockley equation [199,207,221-223].

$$J = \frac{1}{1 + R_S / R_P}\left[J_0 \left\{ \exp\left(\frac{V - JR_S A}{nkT / e} \right) - 1 \right\} - \left(J_{Ph} - \frac{V}{R_P A} \right) \right] \quad \text{.....(2.20)}$$

Where e is the elemental charge, kT is the thermal energy, and A is the device area.

Open-Circuit Voltage (V_{OC}): is the maximum possible voltage across a photovoltaic cell when the cell is exposed to light and when no current is flowing (Figure 2.9b). Solving Equation 2.20 at open circuit condition will give the expression for V_{OC} (Equation 2.21) where n is an ideality factor [193].

$$V_{OC} = n\frac{kT}{e}\ln\left\{ 1 + \frac{J_{Ph}}{J_0}\left(1 - \frac{V_{OC}}{J_{Ph} R_P A} \right) \right\} \approx n\frac{kT}{e}\ln\left\{ 1 + \frac{J_{Ph}}{J_0} \right\} \quad \text{.....(2.21)}$$

The resulting open circuit voltage of bulk heterojunction solar cells is directly related to the energy difference between the highest occupied molecular orbital (HOMO) level of the electron donors and the LUMO level of the electron acceptors and its value is limited between this range as it is empirically described in Equation 2.22 [209, 221].

$$eV_{OC} = (\left| E_{HOMO}^{Donor} \right| - \left| E_{LUMO}^{Acceptor} \right|) - 0.3 \quad \text{.....(2.22)}$$

Short-Circuit Current (Isc): The short-circuit current is directly related to the number of photons that are absorbed from the light source to form excitons, the conversion of excitons into electrons and holes, the efficiency of charge transport, and charge collection at the electrodes. It is the current that flows through an illuminated solar cell when there is no external resistance (i.e., when the electrodes are simply connected or short circuited) and at zero voltage (Figure 2.9b). It is the maximum

current that a device is able to produce. Under an external load, the current will always be less than I_{SC} [211]. The short-circuit current density J_{SC} can also be derived from Equation 1.20 above to give Equation 2.23.

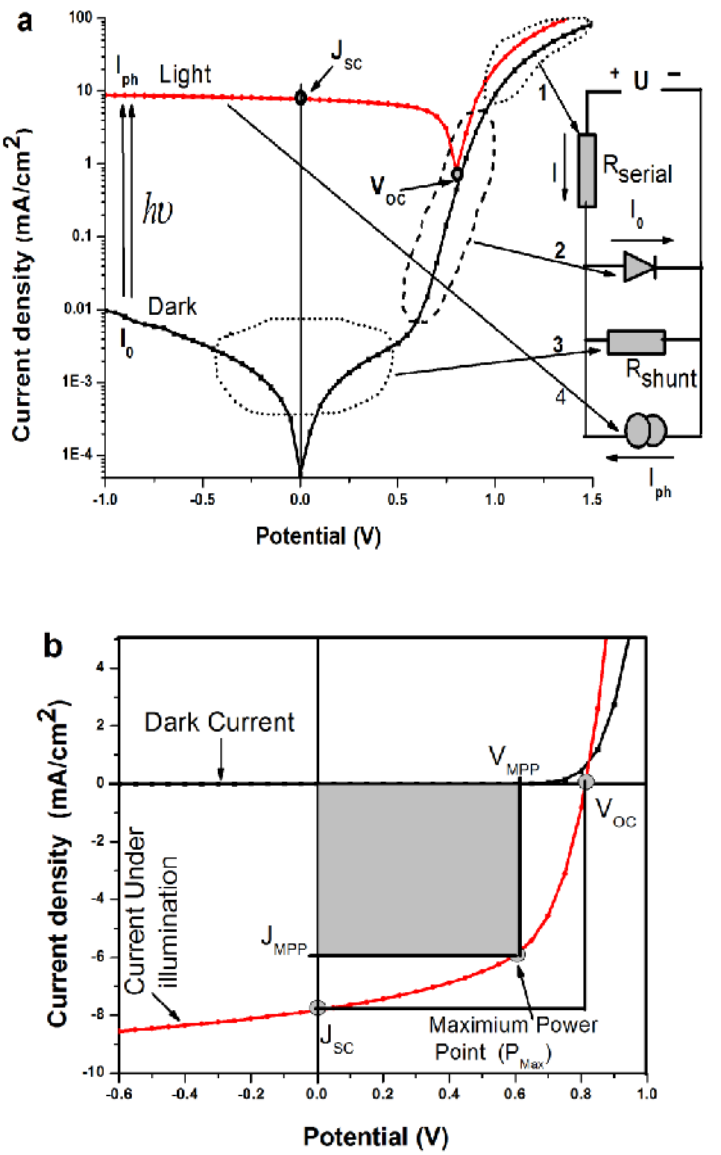

Figure 2. 9: *Current–voltage (I-V) characteristics of bulk heterojunction solar cells (a) semi- logarithmic with the equilvalent circuit diagram where numbers 1, 2, 3, and 4 showed the characteristic of the device in dark and under illumination. (b) Linear representation of the IV curve and defining primary quantities.*

$$J_{SC} = \frac{1}{1 + R_S / R_P}\left\{ J_{Ph} - J_0 \left(\exp\left(\frac{|J_{SC}| R_S A}{nkT / e} \right) - 1 \right) \right\} \approx J_{Ph} \quad \text{.....(2.23)}$$

Maximum Power Point: is the point (I_{mpp},V_{mpp}) on the I–V curves where the maximum power is produced. Power (P) is the product of current and voltage (P = IV) and is illustrated in the Figure 2.9b as the area of the rectangle formed between a point on the I–V curve and the axes. The maximum power point is the point on the I–V curve where the area of the resulting rectangle is the largest.

Fill Factor (FF): The ratio of a photovoltaic cell's actual maximum power output to its theo- retical power output if both current and voltage were at their maxima, Isc and Voc, respectively. This is a key quantity used to measure cell performance. It is a measure of the squareness of the I–V curve. Fill factor of the device strongly depend on the quality of the inteface between the active layer and the cathode [43] and markedly dependenant on recombination strength [153]. FF is a measure of the shape of the current-voltage characteristic of a photovoltaic device. The formula for FF in terms of the above quantities is shown in Equation 2.24 [211, 212].

$$FF = \frac{I_{mpp} V_{mpp}}{I_{SC} V_{OC}} \quad \text{.....(2.24)}$$

Power conversion efficiency (PCE): The ratio of power output to power input. In other words, PCE measures the amount of power produced by a solar cell relative to the power available in the incident solar radiation (P_{in}). P_{in} here is the sum over all wavelengths and is generally fixed at 100 mW/cm^2 when solar simulators are used. This is the most general way to define efficiency. The formula for PCE, in terms of quantities defined above is indicated in Equation 2.25 [211, 212]

$$\eta = \frac{I_{mpp} V_{mpp}}{P_{in}} = \frac{FF\ J_{SC} V_{OC}}{P_{in}} \quad \text{.....(2. 25)}$$

Quantum Efficiency (**QE**) is the efficiency of a device as a function of the energy or wavelength of the incident radiation. For a particular wavelength, it specifically relates the number of charge carriers collected to the number of photons shining on the device. QE can be reported in two ways as internal QE and external QE.

Internal Quantum Efficiency (**IQE**): This quantum efficiency factors out losses due to reflection and transmission of photons such that it considers processes only involving absorbed photons.

External Quantum Efficiency (**EQE**): This type of quantum efficiency includes losses by reflection and transmission. External quantum efficiency is also called IPCE (Incident photon to collected electron efficiency) (IPCE) is simply the number of electrons collected under short circuit conditions, divided by the number of incident photons. IPCE is calculated using the Equation 2.26 [211, 212].

$$IPCE = \frac{hc\ J_{SC}}{e\lambda P_{in}} = \frac{1240 J_{SC}}{\lambda P_{in}} \quad \text{.....(2.26)}$$

Where h is planks constant (6.63×10^{-34} J.s), c is the speed of light (3×10^{8} m/s), e charge of an electron (1.6×10^{-19} C), λ (nm) is the incident photon wavelength, J_{SC} (mA/cm^2) is the photocurrent density of the device, and P_{in} is incident power power at each wavelength. The short circuit current density can be calculted by integrating the IPCE using the equation 2.27 [222].

$$J_{sc} = \frac{hc}{q} \int_{\lambda_1}^{\lambda_2} \frac{P_{AM1.5G(\lambda).IPCE(\lambda).d\lambda}}{\lambda} \quad \text{.....(2.27)}$$

Serial resistance and shunt resistance

From the drawing of the current voltage characteristics of a photovoltaic cell under illumination in Figure 2.9a the slopes at the short circuit current and at the open circuit voltage are the inverse values of the shunt resistance, R_{sh}, and the series resistance, R_s, of the equivalent circuit scheme of a solar cell, respectively. Series resistance, R_s, in series with the ideal diode was included to describe contact resistances such as injection barriers and sheet resistances. In contrast, the parallel resistance or shunt resistance (R_{Sh}) covers the influence of local shunts between the two electrodes, i.e. additional current paths circumventing the diode.

The main effect of a small R_{Sh} value, i.e. diode with leaks and shorts, is decrease in V_{OC}. An increase in R_S decreases I_{SC} and FF [208, 223, 224]. An increase in R_{Sh} enhances charge transport of carriers which increases both the fill factor and V_{OC} to ensure maximum efficiency [208, 224, 225]. R_{Sh} increases with decreasing thickness [223], increasing temperature, and decreasing light intensity [225].

2.10. Towards a controllable morphology

Conjugated polymers are thought of semicrystalline films with small ordered domains and large amounts of amorphous materials. Morphology analysis shows that the structure and molecular weight of the polymer affects the nature of the film that dictates the photophysics and the charge transport properties which play an important role in photovoltaic conversion of polymer solar cells [153, 226].

In conjugated polymer bulk hetrojunction solar cell devices the nanostructure of the active layer plays a large role in determining photovoltaic properties of the solar cells. Since the exciton diffusion lengths in these cells are small and the dissociation

process only occurs at the donor/acceptor interface, controlling the structure of the active layer is very important in constructing efficient devices. Proper morphology provides not only enough interfaces with high separating force for exciton dissociation, but also a bicontinous interpenetrating networks with in the blend for effective transportation of electrons and holes. Therefore the need for finely phase separated donor/acceptor blends should be in the limit of the respective exciton diffusion lengths of the two components. Typical distances that these photo-excitations can travel within a pristine material are around 10 –20 nm [227]. The precondition for getting such optimized morphology is the good miscibility which is the inherent character of the materials and also dependent on the solvent and processing steps. Particularly the chemical structures determine to a large extent the solubility in common organic solvents and the miscibility between the donor and acceptor or the third material if ternary blends are used [227, 153]. Morphology effects are really critical even in a given film/blend where large variations in current from domain to domain can be observed [228].

Because the photoactive layer is deposited from solutions mainly *via* spin coating, one important parameters determining morphology could be the thermodynamic aspects that arise due to the constituents involved, the ratio between the constituents, and the interaction or solubility of these constituents in the solvent. The thermodynamic parameters reflect the nature or fundamental properties of the solution composed of the constituents and solvent applied for thin film deposition. The other parameter is related to kinetic effects that mainly play their roles during the thin-film formation process, which includes solvent evaporation rate, crystallization behavior, and post treatments. Both thermodynamic and kinetic parameters show comparable

significance in determining the morphology of the photoactive layer obtained eventually [229].

Intensive morphology studies have been performed on polymer/PCBM systems. One is by varying the solvent and solvent mixtures that are used to dissolve the active layer components where significant differences were observed [230 - 232]. An approach of adding a small amount of high boiling solvent to the host solvent which selectively dissolve the acceptor to change the kinetics of film formation showed an improved morphology photovoltaic performance enahancement [232 - 235]. Beside solvent used and evaporation rate applied, the overall compound concentration and the ratio between the two compounds in the solution are important parameters controlling morphology formation; high compound concentrations induce large-scale phase segregation up on film formation [236].

Another common tool to influence the morphology of the active layer of polymer solar cells is application of a controlled thermal post-treatment (annealing). The purpose of such treatment is twofold: on the one hand, reorganization of the film morphology is forced, in particular when one or all constituents of the bulk heterojunction have the ability to crystallize. On the other hand a better phase separation between the donor and acceptor materials can be obtained. High efficiency values of P3HT:PCBM bulk heterojunction solar cells were obtained by annealing the device [38, 237].

CHAPTER THREE: EXPERIMENTAL

In this chapter materials used in the experiments are described together with their chemical structures. Device or sample preparation procedures and structures are also discussed in detail. The experimental procedures and equipments used in the measurements are explained.

3.1. Materials

3.1.1. Donor semiconducting conjugated organic polymers

a) Poly-{1,4-[2,5-dioctyloxy-or-di(2-ethylhexyloxy)]phenylene-ethynylene-9,10-anthracenylene-ethynylene-1,4-[2,5-dioctyloxy-or-di(2-ethylhexyloxy)] phenylene -vinylene-1,4-[2,5-dioctyloxy-or-di(2-ethylhexyloxy)]phenylene-vinylene}**AnE-Pv*ab*, AnE-PV*ba*, AnE-PV*bb*, and AnE-PV*stat*** .

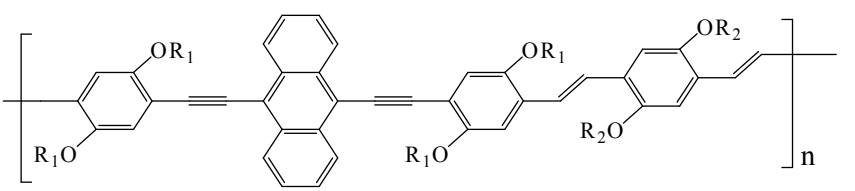

AnE-PV*ab*: R_1 = octyl, R_2 = 2-ethylhexyl **AnE-PV*bb*:** R_1= R_2 = 2-ethylhexyl

AnE-PV*ba* : R_1 = 2-ethylhexyl, R_2 = octyl

AnE-PVstat: R_1= 2-ethylhexyl/ octyl **and** R_2 = 2-ethylhexyl/ octyl randomly

b) Poly{1,4-(2,5-dioctyloxy)-phenylene-ethynylene-2,5-thiophenylene-vinylene-1,4-[(5-(2-ethylhexyl)oxy)-2-methyloxy]-phenylene-vinylene}(DO-PThE_1-PPV_2) (**D1**) and poly{1,4-(5-[(2-ethylhexyl)oxy]-2-methoxy)-phenylene-ethynylene-2,5-thiophenylene-vinylene-1,4-[(5-(2-ethylhexyl)oxy)-2-methyloxy]-phenylene vinylene} (MEH-PThE_1-PPV_2) (**D2**)

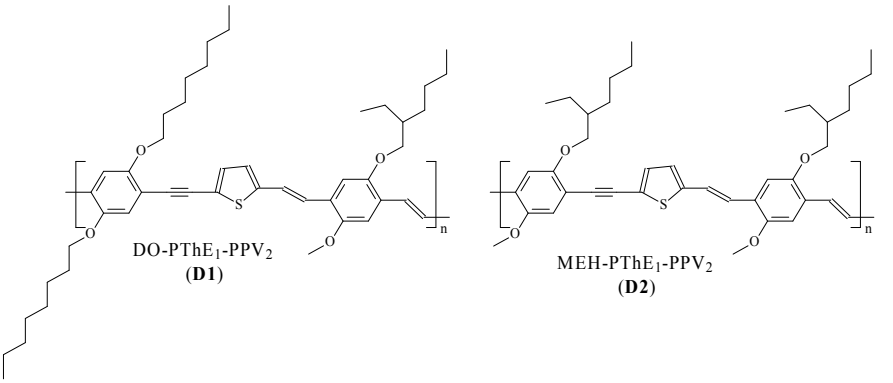

c) *Poly{1,4-(2,5-dioctyloxy)phenylene-ethynylene-2,5-(thiophene or bithiophene or 3,4 ethylenedioxythiophene)-ethylene-1,4-(2,5-dioctyloxyphenylene)vinylene-1,4-[2,5-bis-(2-ethyl)hexyloxy]phenylene-vinylene}(**GP1,GP2** and **GP3**)*

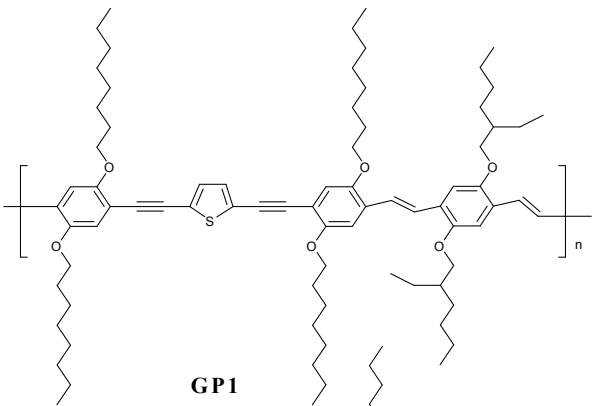

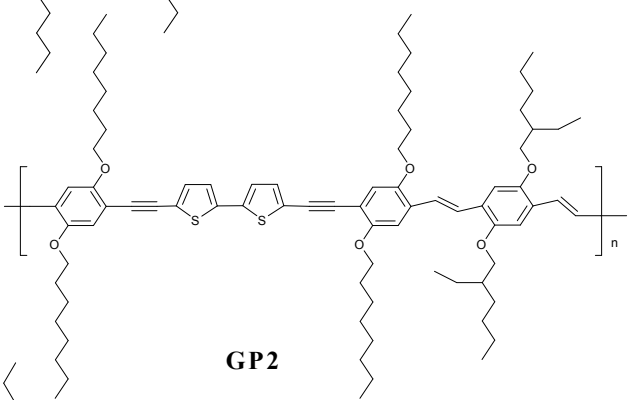

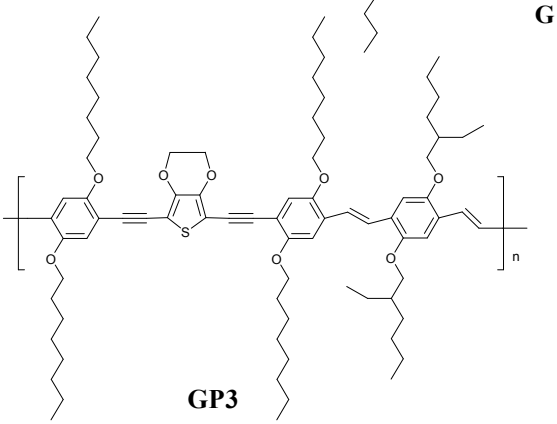

d) RR-poly(3-hexylthiophene) (P3HT) (purchased from Rekie) and Poly [4,4-bis(2-ethylhexyl)-4H-cyclopenta[2,1-b:3,4-b2]dithiophene-2,6-diyl-alt-4,7-bis(2-thienyl)-2,1,3-benzothiadiazole-5',5''-diyl] (PCPDTTBTT)

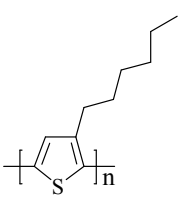

RR-P3HT

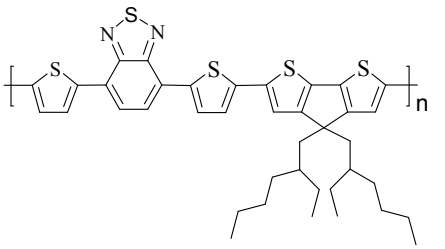

PCPDTTBTT

Figure 3.1. 1: *a) – d) Organic conjugated electron donor polymers used as light absorbing active layer in the bulk heterojunction solar cell devices prepared.*

Conjugated organic polymers listed from a) to d) were used as photoactive (light absorbing) and electron donor materials in the bulk heterojunction solar cells studied**.** Particularly polymers listed under c) are synthesized in this work where as the others were received from collaborating groups.

3.1.2. PEDOT:PSS and PCBM

Poly(3,4-ethylenedioxythiophene)/poly(styrenesulfonate) (PEDOT/PSS) (Baytron PH) is used as a hole conducting material in the bulk hetrojunction solar cells studied. Electrochemically polymerized PEDOT without doping with poly(styrenesulfonate) (PSS) was used as a catalyst for charge transfer between ITO and the I_3^-/I^- redox couple in the photoelectrochemical solar cell device (Figure 3.1.2a).

[6,6]-phenyl-C_{61}-butyric acid methyl ester (PCBM) (from SOLENE) (Figure 3.1.2b) was used as an acceptor in the bulk heterojunction solar cell devices studied. After the first observation of fast photoinduced electron transfer from conjugated polymers to

buckminsterfullerene (C_{60}) [34], C60 was used as an electon acceptor which later on modified to PCBM by introducing side chains just for improving its solubility and its miscibility with organic polymers.

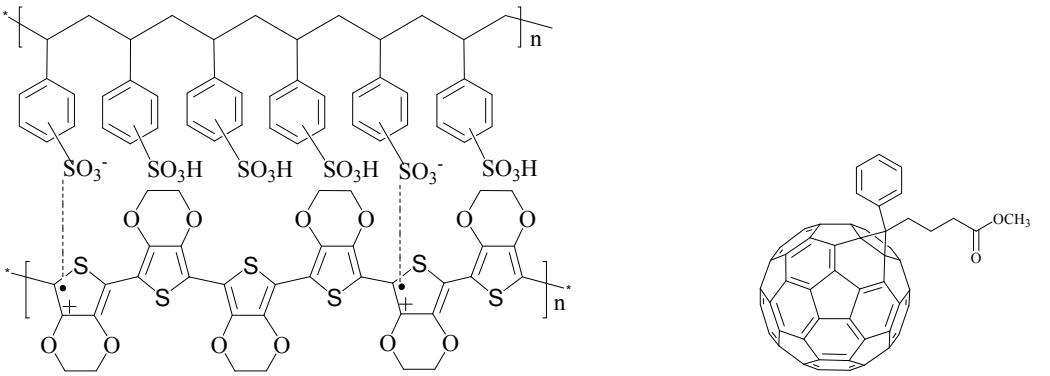

a) PEDOT:PSS *b)* PCBM

Figure 3.1. 2*: Chemical structures of a) PEDOT:PSS b) PCBM*

3.1.3. Other inorganic materials and solvents

a) Ferric chloride ($FeCl_3$) was used as a chemical dopant for RR-P3HT.

b) Aluminium metal and Indium doped tin oxide (ITO) coated glass were used as a cathode and anode, respectively in the bulk heterojunction solar cell devices and CELIV measurements.

c) Standard solvents such as deionized water, ethanol, acetone, isoprpanol, chloroform including the deuterated one, and chlorobenzene were used.

3.2. Sample preparations

For absorption and luminescence experiments either dilute solution or thin films prepared by spin coating on glass slides were used. These thin film samples were also used for Atomic force microscopy (AFM) surface morphology studies.

For CELIV measurements, sandwich-type samples were fabricated as follows: Polymers were dissolved in chlorobenzene with a concentration of 10 mg/ml filtered and deposited by drop casting on top of the pre-patterned ITO covered glass substrates. 30 nm aluminum top electrodes with typical dimensions of 8 - 10 mm^2 were evaporated on top of the film in vacuum under 10^{-6} mbar. The samples were prepared in air, but after the deposition of top contact films were kept in the nitrogen atmosphere for measurement. The experimental setup is already shown in Figure 2.6. The sample structure is similar to the solar cell device in Figure 3.1.2 but in this case no PEDOT:PSS is used and the active layer is only the conjugated polymer with out the acceptor PCBM and illumination is also possible from the aluminium side since it is vey thin (30 nm) which is transparent.

For the fabrication of bulk heterojunction type solar cells, solutions were prepared with appropriate mixture ratios of polymer or polymer/polymer mixtures to the acceptor [6,6]-phenyl-C_{61}-butyric acid methyl ester (PCBM) in chlorobenzene with a appropriate concentration, stirred overnight. The indium tin oxide (ITO) coated glass substrate was first cleaned by ultra-sonication successively with glass cleaning detergent, acetone, isopropanol, and deionized water and dried by purging with air. PEDOT/PSS (Baytron PH) stirred overnight and filtered was spin coated from aqueous solution on top of ITO with 2000 - 3000 rpm to get a film of 50 - 80 nm thickness and dried overnight in open air. The active layer (polymer: PCBM) solution was then filtered and spin-coated on top of PEDOT:PSS film with 800 - 1000 rpm. Then the sample was kept in the glove box dried for 24 h/or (dried in air for experiments in air). It is this sample which was also used for surface morphology studies. The top electrode aluminum metal (100 nm) deposition was done by thermal evaporation in vacuum of about 4×10^{-6} mbar. The schematic structure of the cell is

depicted in Figure 3.1.3. (Particular parameters like polymer: acceptor ratio, concentration of polymer: acceptor, and other parameters specific to a particular experiment are mentioned in each particular experiment result and discussion section)

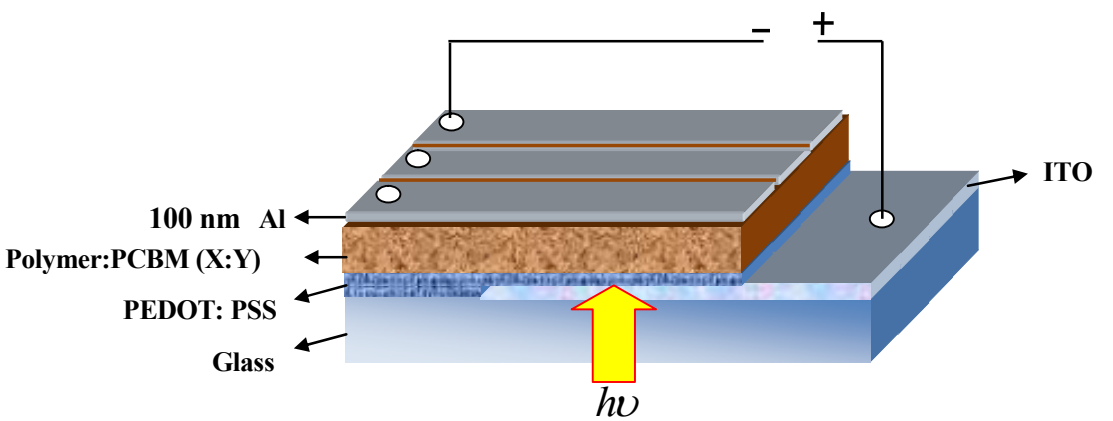

Figure 3.1. 3: *Schematic architecture of the solar cells constracted.*

For preparation of photoelectrochemical solar cells, cleaned ITO coated transparent glass was used as a substrate for the photoactive materials and counter electrode. The bulk heterojunction blend of **AnE-PVstat**:2PCBM was used as a photoactive layer by drop casting from its (3% Wt) solution in chlorobenzene on ITO-coated glass. A thin polymer film of PEDOT for the catalytic purpose was deposited on the counter electrode ITO by electrochemical polymerization of 0.1 M 3,4-ethylenedioxy thiophene (EDOT) in 0.1 M $LiClO_4$ acetonitrile solution carried out potentiostatically at +1.8 V *vs* quasi Ag/AgCl using Pt sheet counter electrode. The polymer electrolyte was prepared by dissolving 309 mg of amorphous poly(oxymethylene-oligo-oxyethylene) (POMOE), with a repeating unit of $CH_2O(CH_2CH_2O)_9$, in 25 mL of methanol. The redox couple I_3^-/I^- was prepared by dissolving 48.13 mg KI and 7.36 mg I_2 separately in 25 mL of methanol. Then, equal volume of each of the above three solutions were mixed to produce the polymer electrolyte complexed with a redox

couple. Finally, a thin film of polymer electrolyte complexed with I_3^-/I^- was drop casted on top of **AnE-PVstat**:2PCBM precoated on ITO-glass and allowed to dry in an open air atmosphere and the device fabrication was completed by bringing the two electrodes and pressing against PEDOT coated ITO/glass counter electrode

3.3. Mesurements and Instruments

1H NMR and 13C NMR spectra were measured in deuterated chloroform using a Bruker DRX 500 and a Bruker AC 250. Elemental analysis was performed on a CHNS-932 Automat Leco. Differential scanning calorimetry (DSC) measurements were carried out on a Mettler DSC 30 with a cell purged with nitrogen. Gel permeation chromatography (GPC) was performed on a set of Knauer using THF as eluent and polystyrene as standard. Infrared spectroscopy was recorded on a Nicolet Impact 400. The absorption spectra were recorded using Cary (3G) UV-Vis and GENESYS 2PC Uv–Vis spectrometers. Emission spectra were measured HORIBA JOBIN YVON fluorescence spectrometer. The solution photoluminescence quantum yields were calculated either according to Demas and Crosby against quinine sulfate in 0.1 N sulfuric acid as a standard (Φf = 55%) or in ethanol against rhodamine 6G standard (Φf = 95%).

Cyclic voltammetry (CV) experiments were performed using an electrochemical analyzer (CHI instruments) in three-electrode cell. Platinum (Pt) wire electrodes were used both as working and counter electrodes, and a quasi Ag/AgCl electrode (Ag wire coated with AgCl) was used as the reference electrode. CV measurements were made in solutions of 0.1 M tetrabutylammoniumhexafluorophosphate $(C_4H_9)_4NPF_6$) in acetonitrile under nitrogen atmosphere. The surface morphology of pure polymer thin films as well as solar cell blends spin-coated from their chlorobenzene solution were

studied with atomic force microscopy (AFM) Dimension 3100 system (Digital instruments Santa Barbara CA) in taping mode.

CELIV experiments were measured in the cryostat (Oxford Optistat DNV) under vacuum. A variable pulse generator (Agilent 33250A) and the oscilloscope (Tektronix TDS 754C) were used to record the extraction current transients. To control the delay time between voltage and light pulses, an arbitrary pulse (Agilent AG33250A) and a delay function generator (Stanford DG535) were employed. Nd:YAG laser (Coherent Infinity 40 - 100), with a light pulse width of 5 ns, wavelength 355 nm, energy of less than 1 mJ per pulse, was used for the charge carriers photogeneration.

Current-voltage (I–V) characteristics of the devices in the glove box were measured using a Keithley 236 source measurement unit under 100 $mWcm^{-2}$ AM 1.5 white light illumination of the solar cell. Incident photon to current conversion efficiency (IPCE) or external quantum efficiency (EQE) measurements were taken using an optical fiber light source from 90 W Xenon lamp, which is connected to a ACTON Spectra Pro150 monochromator and EG & G 7260 DSP Lock in amplifier to measure the current.

For experiments in open air (section 4.5) current-voltage (I–V) characteristics were measured using Hp4140-PA meter/DC voltage source measurement unit under a solar simulator of 80 $mWcm^{-2}$ white light illumination. For the photoelectrochemical solar cells I-V characteristics of (section 4.1) a CHI630A electrochemical analyzer by illumination of white light 100 mW/cm^2 from a 250 W tungsten–halogen lamp by an Oriel power supply (Model 68830) were used. For IPCE a grating monochromator (Model 77250) placed into the light path was used to select a wavelength between 300 and 800 nm was used in open air. The photocurrent spectra responses of the lamp were corrected using a standard silicon photodiode (Hamamatsu, Model S1336-8BK).

CHAPTER FOUR: RESULTS AND DISCUSSIONS

4.1. Improvement in photovoltaic performance and charge carrier mobility through random distribution of segments of linear and branched side chains

4.1.1. Background

The great potential of organic conjugated compounds for the design of efficient, flexible, low cost and light weight organic photovoltaic (OPV) devices as energy source is a well established fact [31, 34, 37, 38, 45, 238 - 242]. Intensive interdisciplinary research in this area is presently going on worldwide, so that a rapid enhancement of the state-of-art power conversion efficiency is noted. Certified efficiency (η) values of 7 - 10% have been reported for small molecules as well as polymer based organic photovoltaics (OPVs) [40, 41, 243, 244]. First products based on OPV are now marketed [245]. The bulk heterojunction concept consisting of an intermixing of the active layer donor and acceptor components has proven to be the most efficient way to design high performance devices. The way both components intermix is crucial in the overall performance of the solar cells. Different approaches have been provided in literature on how to favorably tune the nanoscale morphology of the donor and acceptor blend [64, 246 - 248]. The combination of hydrophobic nature and variation of the volume fraction of solubilizing alkoxy side chains is an approach to tune the active layer phase separation of PPE-PPV/PCBM bulk heterojunction solar cells [56, 57, 249]. It was also furthermore demonstrated that the nature (linear and/or branched) of alkoxy side groups can be used to tune the π-π-stacking of anthracene-containing PPE-PPV, which subsequently affects their solar

cell active layer phase separation and the resulting photovoltaic performance [250, 251]. For instance, the grafting of solely linear octyl side chains as in **AnE-PV*aa***, leads to a π-π-stacking distance, $d_{\pi\pi}$, of 0.380 nm (Figure 3.1.1, Table 4.1.1). The grafting of bulky 2-ethylhexyl at R_2, as in **AnE-PV*ab***, showed $d_{\pi\pi}$ of 0.386 nm and an efficiency of ~ 3% at AM1.5 white light illumination [251]. In contrast, no π-π-stacking peak was observed in the X-ray diffractogramms of the extruded fibers of **AnE-PV*ba*** and **AnE-PV*bb***, bearing branched 2-ethylhexyl close to the anthracenylene-ethynylene unit [252]. Solar cell efficiencies achieved with both materials were around 1%, despite the fact that they exhibited the highest charge carrier mobility among the polymers [250 - 252]. The low solar cell efficiencies of both amorphous materials was explained by too intimate mixing of the active layer components resulting in hampered percolating path of the photogenerated charges.

In an attempt to combine the tendency to stack (*ordering*) as found in **AnE-PV*aa***, **AnE-PV*ab*** and the strong amorphous nature of **AnE-PV*ba***, **AnE-PV*bb*** (*disorder*) with the aim to efficiently tune the resulting solar active layer morphology and charge carrier mobility, we have synthesized a side chain based statistical conjugated copolymer, **AnE-PV*stat***, by using the starting materials leading to **AnE-PV*aa***, **AnE-PV*ab***, **AnE-PV*ba,*** and **AnE-PV*bb***. A more conformationally and supramolecularly balanced material results from this combination of "*order*" and "*disorder*", in such a way that high efficiency solar cells are designed with even little amount of the acceptor component, as shown below. To our knowledge, a solely alkoxy side chain based statistical conjugated copolymer, purposely designed for solar cell active layer morphology control is not known. The literature describes mostly side chain based statistical conjugated copolymers, where side groups of different nature and

functionalities are present, most of which are purposely designed for sensory applications [253].

In this work, we describe photophysical, electrochemical, morphology, charge carrier mobility properties and photovoltaic performance of **AnE-PV*stat*** and compare them with those of the well defined homologues **AnE-PV*aa***, **AnE-PV*ab***, **AnE-PV*ba.*** and **AnE-PV*bb***. Their structures are shown in Figure 3.1.1a of the experimental section. The detail of the synthesis part of this polymer is shown in appendex A. Charge carrier mobility was also measured using CELIV (Charge Extraction by Linearly Increasing Voltage) technique. It was shown that this side chain distribution enhances the $d_{\pi\pi}$ value to 0.393 nm, from 0.380 nm (**AnE-PV*aa***) through 0.386 nm (**AnE-PV*ab***) [252]. In addition, the highest hole mobility of 5.43×10^{-4} cm^2/Vs and as well as solar cell efficiency up to 3.77% were obtained for this compound which is the best performance for PPV based materials.

4.1.2. Results and Discussion

The side chain based statistical copolymer was obtained from the reaction of equimolar ratio of two dialdehydes **1a** ($R_1 = C_8H_{17}$ = octyl) and **1b** ($R_1 = C_8H_{17}$ = 2-ethylhexyl) with two bisphosphonate esters **2a** ($R_2 = C_8H_{17}$ = octyl) and **2b** ($R_2 = C_8H_{17}$ = 2-ethylhexyl) as illustrated in Scheme 4.1.1.

89% yield was obtained after extraction of the crude product with a hot mixture of methanol and diethyl ether. The chemical structure was elucidated by NMR, IR, and elemental analysis. No aldehyde or phosphonate end groups were detectable in NMR, indicating the high molecular weight of the compound. The use of diethyl ether in the extraction process was a crucial step to obtain a monomodal Gauss curve [254],

whose peak was found at M_p = 49700 g/mol and M_p = 50700 g/mol using a UV detector and an IR detector respectively, during the GPC molecular weight determination.

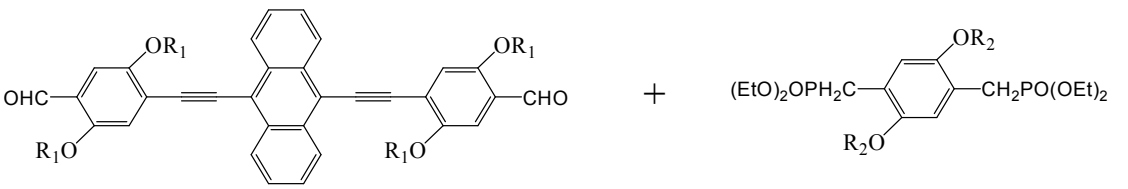

1a (R_1 = Octyl) : 1b (R_1= 2-ethylhexyl) **2a (R_2 = Octyl) : 2b (R_2= 2-ethylhexyl)**

(1:1) **(1:1)**

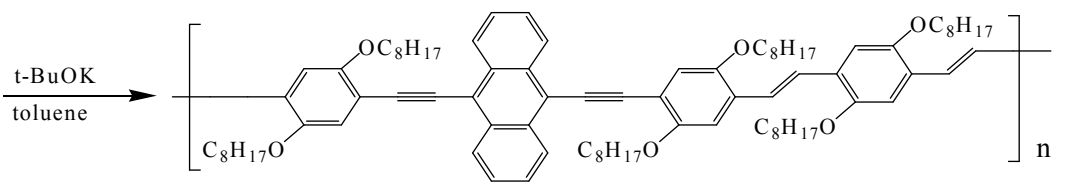

AnE-PV*stat*

Scheme 4.1. 1: *Synthesis of side chain based statistical copolymer AnE-PVstat , by distribution of sequences of octyl (C_8H_{17}) and 2-ethylhexyl (C_8H_{17}) at R_1 and R_2 positions.*

Both detection methods revealed a PDI (polydispersity index) of 2.0 and a P_n (degree of polymerization) of 22. **AnE-PV*stat*** incorporates the repeating units of polymers **AnE-PV*aa***, **AnE-PV*ab***, **AnE-PV*ba,*** and **AnE-PV*bb***, whose chemical structures are shown in Figure 3.1.1a (experimental section). Their data from GPC, TGA, DSC and X-ray together with those of **AnE-PV*stat*** are summarized in Table 4.1.1 for purpose of comparison [251,252]. **AnE-PV*aa***, bearing solely octyl side chains, is insoluble due to strong intermolecular interaction. X-ray scattering measurements on extruded

fibers reveal clear ππ-stacking peaks for polymers bearing octyl side chains in the vicinity of the PPE-segment, while those bearing bulky branched 2-ethylhexyl, **AnE-PV*ba*** and **AnE-PV*bb*** remained amorphous, even after extrusion [252]. **AnE-PV*stat*** combines the "*ordered nature*" as in **AnE-PV*aa***, **AnE-PV*ab,*** and the "*disordered nature*" as in **AnE-PV*ba***, **AnE-PV*bb***, which is reflected by the highest $d_{\pi\pi}$ value of 0.393 nm (Table 4.1.1) [252]. From the reported $d_{\pi\pi}$ values, it is possible to establish a correlation between $d_{\pi\pi}$ and the solar cell energy conversion efficiency. From the comparison we found the solar cells efficiency increases with increasing $d_{\pi\pi}$ of the polymers as confirmed by the results shown in Table 4.1.1 [251, 252] and from the efficiency of **AnE-PV*stat*** in this work.

Table 4.1. 1: *GPC (THF as eluent, polystyrene standards), TGA, DSC, and X-ray data of polymers AnE-PVi: M_n = number-average molecular weight, PDI = polydispersity index, DP = degree of polymerization, $T_{5\%,10\%}$ = decomposition temperatures at 5% and 10 % weight loss, respectively, DSC transitions temperatures, T^1_{DSC} and T^2_{DSC}, respectively, and $d_{\pi\pi}$ = ππ-stacking distance* [251, 252].

Polymer **AnE-PV*i***	M_n (g/mol)	PDI	DP	$T_{5\%}$ (°C)	$T_{10\%}$ (°C)	T^1_{DSC} (°C)	T^2_{DSC} (°C)	$d_{\pi\text{-}\pi}$ (nm)
aa	-	-	-	326	343	61/130	213	0.380 ± 0.002
ab	40 000	3.54	32	330	351	58	212	0.386 ± 0.002
ba	25 500	3.05	20	327	348	67	-	-
bb	15 800	2.98	13	325	346	53	-	-
stat	27 000	2.04	22	312	322	62	-	0.393± 0.002

4.1.2.1. Surface morphology

When the morphology of **AnE-PV*stat*** is compared with the corresponding non statistical polymers **AnE-PV*ab*,** **AnE-PV*ba*,** and **AnE-PV*bb*** in Figure 4.1.1, it can be seen that the **AnE-PV*bb*** is relatively smooth while **AnE-PV*ba*** is rough though both of them show featureless images. Images of **AnE-PV*ab*** and **AnE-PV*stat*** showed better features indicating some orientations of grains. Generally the features in the images and the calculated roughness, height and peak parameters of the four images indicated in Table 4.1.2 shows that the statistical copolymer **AnE-PV*stat*** have an intermediate morphology which confirms that the number and positions of side chains in this copolymer are distributed in a balanced way since equimolar amounts were used during synthesis.

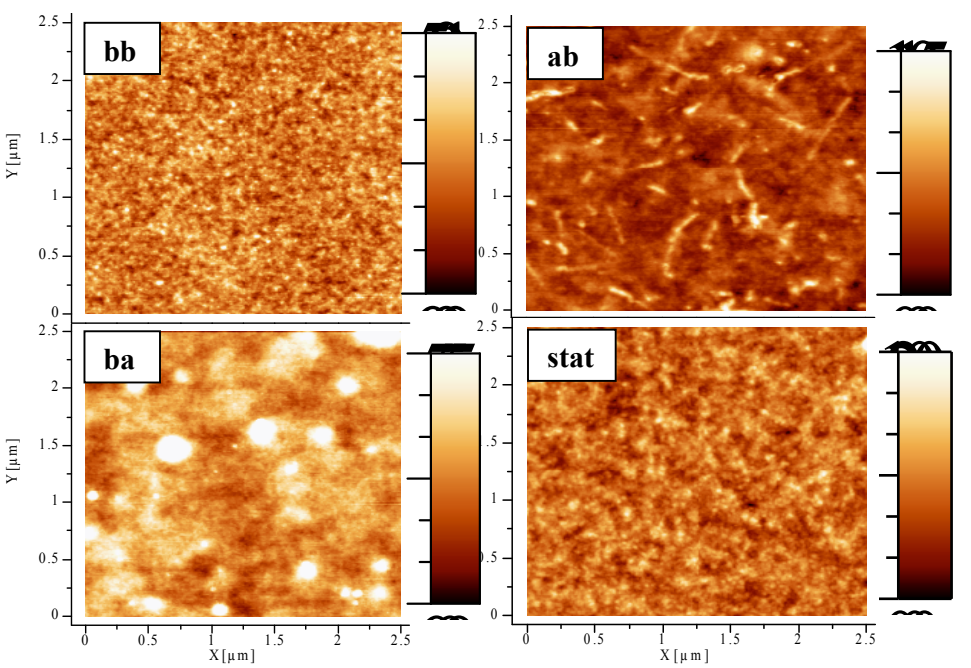

Figure 4.1. 1*: AFM images of* ***AnE-PVi, (i = ab, ba, bb,*** *or* ***stat)*** *thin films spin coated from chlorobenzene solution.*

Table 4.1. 2: *Height and roughness parameters of the AFM images of* **AnE-PV*ab*,** **AnE-PV*ba*, AnE-PV*bb*,** and **AnE-PV*stat*** *thin films in Figure 4.1.1.*

AFM parameter	AnE-PVab	AnE-PVba	AnE-PVbb	AnE-PVstat
RMS roughness (nm)	1.4521	3.2537	0.9641	1.3126
Peak to peak (nm)	17.2926	56.191	12.8401	19.9963
Roughness average (nm)	1.1302	1.3847	1.0683	1.0378
Average height (nm)	6.4365	14.1574	5.677	5.0453

The surface morphology of pure **AnE-PV*stat*** thin films spin-coated from chlorobenzene was also studied to see its stability during temperature changes. These group of polymers showed side chain melting at around 100^0C and backbone melting of 210^0C [251]. In this experiment a temperature 110^0C for 5 minutes was choosen for annealing to make sure that all the side chains melt.

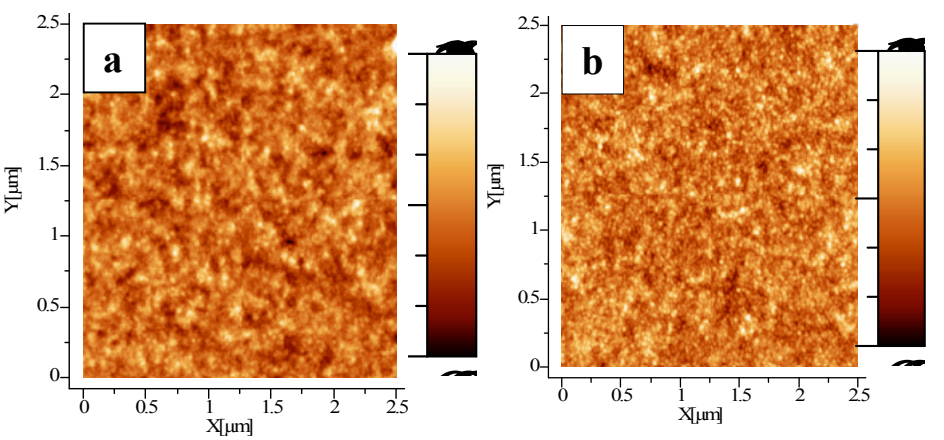

Figure 4.1. 2: *AFM images of* ***AnE-PVstat*** *film spin coated from chlorobenzene solution before (a) and after (b) annealing in inert atmosphere at 110 ^{0}C for 5 minutes.*

As shown from the images in Figure 4.1.2 with the corresponding AFM height and roughness parameters in Table 4.1.3, the change in RMS roughness as well as the average height of **AnE-PV*stat*** was insignificant upon annealing. But the peak to peak height is significantly reduced since annealing at this temperature leads to high degree of ordering as confirmed from wide angle X-ray scattering experiments [251] which might redues the peak to peak heights on the surface. This confirms the conformationally and supramolecularly balanced and stabilized nature of the statistical copolymer under the mentioned experimental conditions.

Table 4.1. 3: *AFM image parameters of* **AnE-PV*stat*** *thin film before and after annealing at 110 ^{0}C*

AFM parameter	AnE-PVstat Before annealing	AnE-PVstat Annealed at 110 ^{0}C
RMS roughness (nm)	1.3126	1.3343
Peak to peak (nm)	19.9963	12.1987
Roughness average (nm)	1.0378	1.0567
Average Height (nm)	5.0453	5.0537

4.1.2.2. Photophysics

Figure 4.1.3a depicts the absorption and emission spectra in dilute chlorobenzene solution of **AnE-PV*ab***, **AnE-PV*ba***, **AnE-PV*bb***, and **AnE-PV*stat***, and their corresponding thin film absorption and emission spectra are shown in Figure 4.1.3b. In solution, there are differences in the absorption shapes between the amorphous polymers **AnE-PV*ba***, **AnE-PV*bb***, and **AnE-PV*ab***, **AnE-PV*stat*** polymers showing stacking/ordering behaviour. The first group is characterized by a structureless main

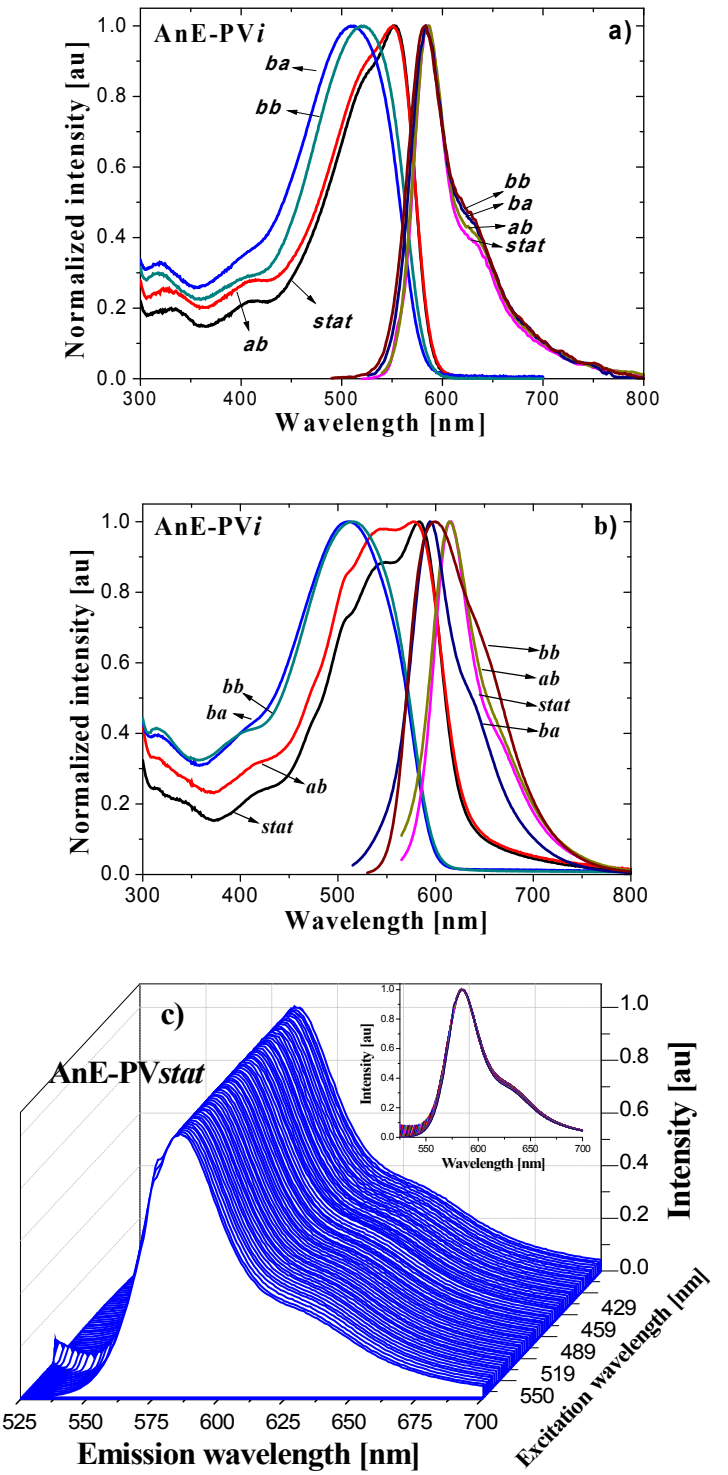

Figure 4.1. 3: *Normalized absorption and emission spectra of a) solutions b) thin films spin coated from chlorobenzene solution of* **AnE-PV*i*, (*i* = *ba, ab, bb* and *stat)** *c) two dimensional emission spectra of* ***AnE-PVstat*** *solution in the range of*

excitation wavelengths, the inset is emission intensity vs wavelength of the same spectra.

absorption band peaked at 510 nm and 522 nm, respectively where as the second group exhibits structured and red-shifted main absorption bands, which consist of a peak around 555 nm and a higher energy shoulder around 520 nm.This difference becomes even more clearer in thin film (Figure 4.1.3b), whereby **AnE-PV*ab*** and **AnE-PV*stat*** exhibit two well defined peaks around 543 nm and 582 nm due to enhanced planarization of the conjugated backbones and ordering as it goes from the solution form to the compact bulk materials, while **AnE-PV*ab*, AnE-PV*bb*** remain structureless.

All four polymers show similar solution fluorescence spectra with maximium peak around 583 nm. In contrast, the thin film emission spectra of both **AnE-PV*ab*** and **AnE-PV*stat*** are red-shifted and demonstrate more pronounced features due to enhanced order by interlayer stacking as compared to the amorphous polymers counterparts (Table 4.1.4, Figure 4.1.3a, b). Typical two dimensional emission spectra in the range of excitation wavelengths of **AnE-PV*stat*** are revealed in Figure 4.1.3c showing similar emission spectra with scanning in the range of excitation wavelengths. The inset in Figure 4.1.3c shows all specra have the same maxima with insignificant shifts, which are strong evidences of only one or (very similar) emitting species (chromophores) in the polymer.

Photophysical data of **AnE-PV*stat*** in comparison with those of **AnE-PV*ab***, **AnE-PV*ba*** , and **AnE-PV*bb*** using their dilute solution in chlorobenzene and thin films are provided in Tables 4.1.4, namely the absorption maximum $\lambda_{a,10\%}$, of the absorption maximum from the lower energy edge, $\lambda_{a10\%}$, the optical band gap energy E_g^{opt}

calculated using $1240/\lambda_{a10\%}$, the emission maximum λ_f, Stokes shift, $\Delta\nu_{af}$, the fluorescence quantum yield Φ_f (relative to rhodamine G6 in solution, the fluorescence lifetime, τ, the fluorescence rate constant k_f, and the rate constant, k_{nr} of radiationless deactivation (assuming the absence of phosphorescence) [250, 251].

Table 4.1. 4: *Photophysical data of **AnE-PVi** in dilute chlorobenzene solution [s] and in thin film spin coated from chlorobenzene [f] [250].*

AnE-PV*i*	$\lambda_{a\ max}$ (nm)	$\lambda_{10\%}$ (nm)	E_g^{opt} (eV)	$\lambda_{f\ max}$ (nm)	$\Delta\nu_{af}$ (cm^{-1})	Φ_f (%)	τ (ns)	k_f (ns^{-1})	k_{nr} (ns^{-1})
AnE-PV*ab* [s]	553	590	2.10	585	990	57	0.94	0.61	0.46
AnE-PV*ab* [f]	583	687	1.80	624	1100	-	-	-	-
AnE-PV*ba* [s]	510	578	2.15	583	2500	29	0.72	0.40	0.99
AnE-PV*ba* [f]	504	636	1.95	605	3300	-	-	-	-
AnE-PV*bb* [s]	522	582	2.13	583	3200	48	0.85	0.56	0.61
AnE-PV*bb* [f]	527	613	2.02	600	2300	-	-	-	-
AnE-PV*stat* [s]	555	590	2.10	585	920	52	0.87	0.60	0.55
AnE-PV*stat* [f]	582	652	1.90	620	1050	-	-	-	-

The slightly higher solution fluorescence quantum yields for both **AnE-PV*ab*** (57%) and **AnE-PV*stat*** (52%) and lower Stokes shifts, $\Delta\nu_{af}$, as compared to the amorphous polymers suggest a more plannarized ground state. Moreover, **AnE-PV*stat*** shows the smallest Stokes shift both in solution and in thin film, which is an indication of comparatively less conformational changes from the ground to the first excited state. From fluorescence kinetics measurements a fluorescence lifetime τ = 0.87 ns was obtained for **AnE-PV*stat***, which led to a fluorescence rate constant, k_f, of 0.60 ns^{-1}

and a radiationless deactivation constant, k_{nr}, of 0.55 ns^{-1}. These values are similar to those of its well-defined homologues **AnE-PV*ab***, **AnE-PV*ba***, and **AnE-PV*bb***.

4.1.2.3. Electrochemistry

Thin film of **AnE-PV*stat*** from chlorobenzene solution dip coated on Pt sheet working electrode was used for electrochemical characterization using 0.1 M teterabutyl ammonium hexa florophosphate in acetonitrile solution. The electrochemical characterizations of the non statistical polymers were already given in ref [251]. Cyclic voltammogram (CV) of **AnE-PV*stat*** at scan rate of 50 mVs^{-1} is displayed in Figure 4.1.4.

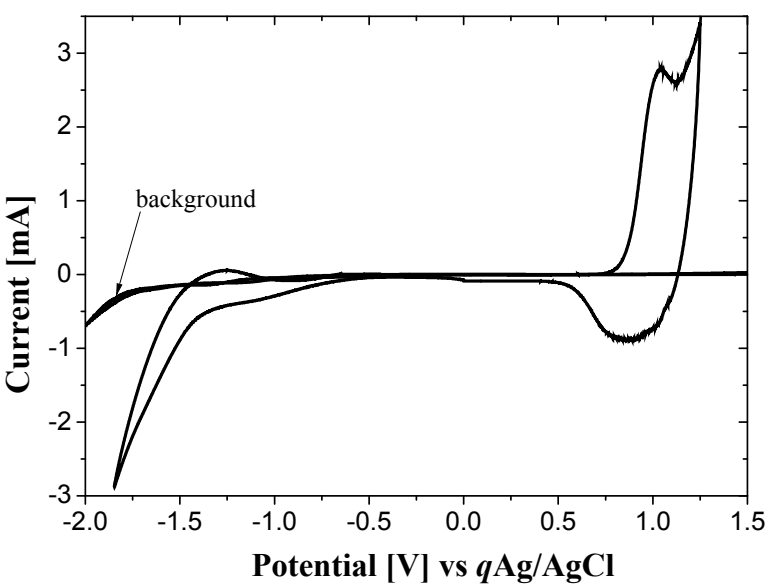

Figure 4.1. 4: C*yclic voltammogram of* **AnE-PV***stat film coated on Pt sheet working electrode in 0.1 M* $(C_4H_9)_4NPF_6$ */*CH_3CN *at the scan rate of 50 mV/s.*

The CV shows both oxidation peak (*p*-doping) and indication of *n*-doping peaks. The oxidation peak was located at 0.84 V where as the reduction peak is located -1.08 V vs. quasi Ag/AgCl. The ionization potential, E_{IP}, (HOMO level), and electron affinity,

$E_{A,}$ (LUMO level), were estimated from the onset potentials E_{onset} on the basis of the reference energy level of ferrocene (4.8 eV below the vacuum level) using the equation E_{IP} (E_A) = – (E_{onset} – E_{ferr}) – 4.8 eV, where E_{ferr} is the value for ferrocene vs. the quasi Ag/AgCl electrode [119]. E_{onset} (Fc/Fc^+) Vs (quasi Ag/AgCl) in this experiment was 400 mV. Ionization potential (HOMO level), E_{IP} = 5.24 eV and the electron affinity (LUMO level), E_A = 3.25 eV were estimated from the onsets of oxidation and reduction potentials which leds to the electrochemical band gap value of 1.99 eV. This value is in a good agreement with the optical band gap, E_g^{opt}, of 2.10 eV and 1.90 eV evaluated from the absorption edge of solution and thin film spectra, respectively [255, 256].

4.1.2.4. Charge transport studies

The current extraction transients from CELIV experiment for all four polymers are diplayed in Figure 4.1.5. As can be seen from the Figure **AnE-PV*stat*** show extraction maxima even in the dark current transients indicating the presence of non-negligible thermally generated equilibrium charge carriers concentration in the film due to intrinsic doping therefore carrier photogeneration using laser was not necessary for **AnE-PV*stat*** [257]. In case of other non statistical polymers **AnE-PV*ab*, AnE-PV*ba***, and **AnE-PV*bb*,** the thermally generated charge carriers which are shown as dark current are negligible (much lower level of doping) as can be seen from flat dark current transients compared to the photogenerated ones (Figure 4.1.5). As a result the charge carriers were photogenerated with laser pulse. After 100 ns delay time the applied triangle-shaped rising voltage pulse extracts the photogenerated charge carriers towards back electrode and the carrier mobility is directly estimated from the extraction maxima. This is one of the typical properties of **AnE-PV*stat*** that makes it different from the non statistical ones. From the extraction maximum the mobilities of

dark thermally generated charge carriers in case of **AnE-PV*stat*** and photogenerated charge carriers in case of the non statistical polymers were calculated using Equation 2.16 and shown with their corresponding electric field applied in Table 4.1.5. **AnE-PV*stat*** showed the highest charge carrier mobility (~ hole mobility if the electron mobility is assumed insignificant in p type polymers).

In all polymers a typical shift of an extraction maximum towards shorter times is seen when the applied voltage is increased as shown in Figure 4.1.6a for **AnE-PV*stat*** where the voltage ranges from 2 V to 30 V. This, as expected, demonstrates faster carrier extraction at higher applied electric fields from which carrier mobility is calculated.

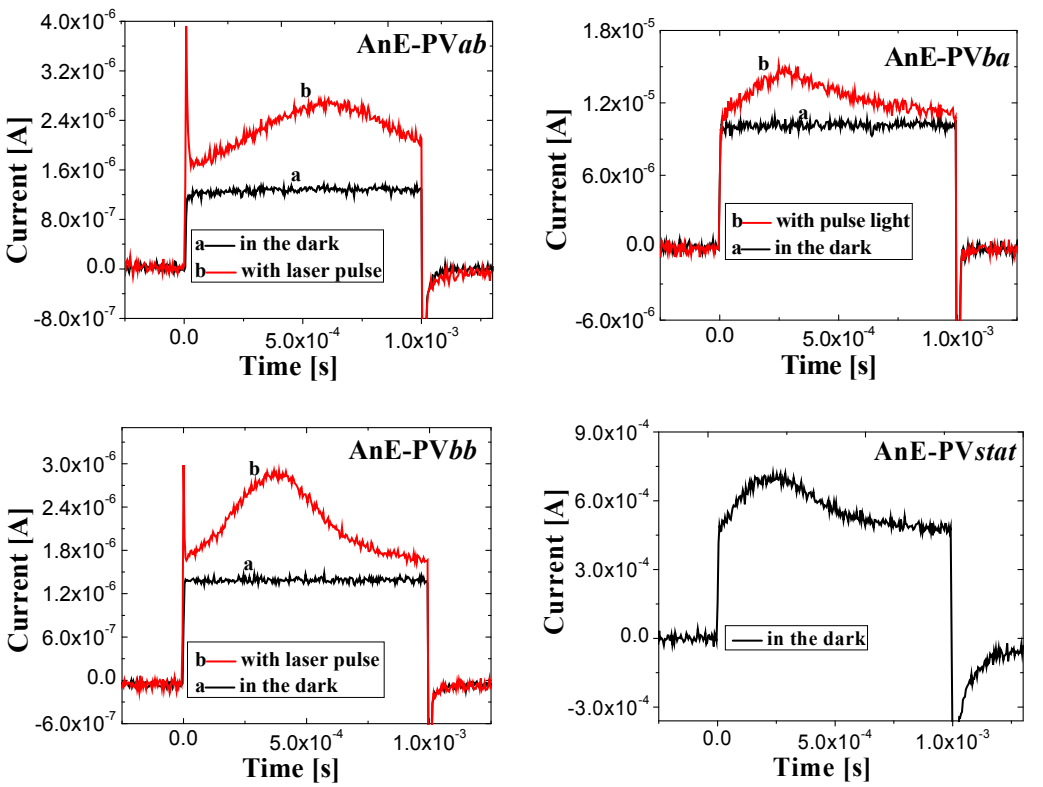

Figure 4.1. 5: *CELIV current extraction transients of* **AnE-PV*ab*,** **AnE-PV*ba*,** **AnE-PV*bb*,** and **AnE-PV*stat*** *in dark and with a laser pulse.*

Table 4.1. 5: *Mobility (μ), of the polymers calculated in increasing order.*

Code	μ (cm^2/Vs)	Electric field (V/cm)
AnE-PV*ab*	2.57×10^{-5}	27870
AnE-PV*ba*	4.52×10^{-4}	28235
AnE-PV*bb*	1.53×10^{-4}	16604
AnE-PV*stat*	5.43×10^{-4}	10721

Current transient were measured at different applied voltages and a maximum for each current transient as shown in Figure 4.1.6a for **AnE-PV*stat*** were taken and the equilibrium carrier mobility at different applied electric fields were calculated using Equation 2.16 [177, 258] and plotted in Figure 4.1.6b.

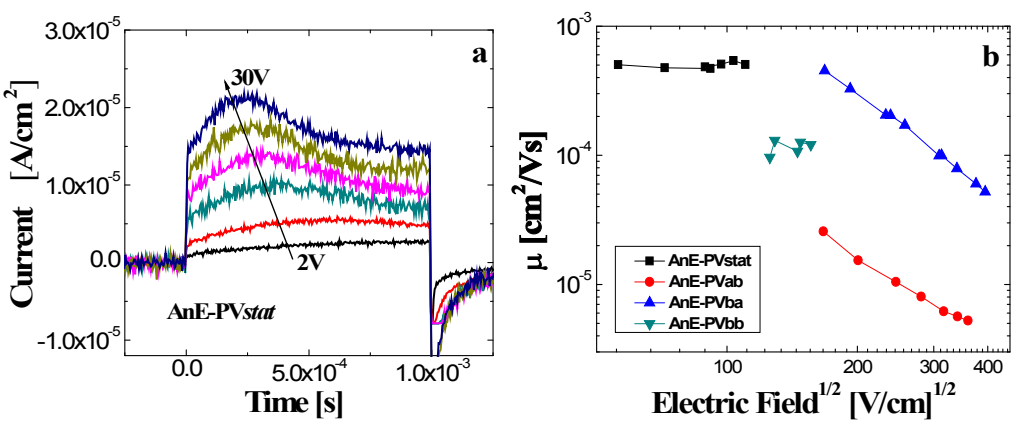

Figure 4.1. 6: *a) Current transients of* **AnE-PV*stat*** *at different applied voltage showing shift of extraction maxima at higher voltages b) Mobility vs electric field for* ***AnE*-PV*stat***, **AnE-PV*ab***, **AnE-PV*ba***, and **AnE-PV*bb***.

As shown in Figure 4.1.6b **AnE-PV*stat*** and ***AnE-PVbb*** showed electric field independence mobility where as **AnE-PV*ab*** and **AnE-PV*ba*** showed a negative dependence with electric field. The electric field independent high carrier mobility of

AnE-PV*stat* indicates that relatively less activation energy is required to reach higher mobility values. This provides a hint for the existence of optimal Density-of-States (DOS) for charge carrier transport in the studied **AnE-PV*stat*** polymer [259]. It was shown before that the charge carrier mobility can demonstrate even the negative electric field dependence at low fields in high mobility poly(3-hexylthiophene) (P3HT) films [179] which confirms the observed negative electric field dependence result of **AnE-PV*ab*** and **AnE-PV*ba***.

Intrinsic film conductivity of $\sigma = 2.6 \times 10^{-8}$ S/cm was directly estimated from the dark current extraction transients using Equation 2.15 [171]. So for **AnE-PV*stat*** it was found that the conductivity was almost independent on the applied voltage in the measurement range. Doping level giving the concentration of thermally generated charge carriers $n = 4 \times 10^{14}$ cm^{-3} was estimated from the conductivity relation $\sigma = en\mu$, where e is the elementary charge, n is the carrier concentration, and μ is the carrier mobility.

Obtained mobility values are the highest compared to the whole family group of anthracene based **AnE-PV*i*** as well as poly[2-methoxy-5-(3,7-dimethyloctyloxy)-phenylene vinylene] (**MDMO-PPV**) polymers studied in the past (Table 4.1.4) [251, 174]. The observed electric field and concentration independent carrier mobility suggest the suitability of **AnE-PV*stat*** for applications as a hole transporting material or for use in high power conversion efficiency organic solar cells.

4.1.2.5. Bulk heterojunction Photovoltaic studies

For the fabrication of bulk heterojunction type solar cells, solutions were prepared with three mixture ratios (1:1, 1:2, and 1:3) of **AnE-PV*stat*** to the acceptor [6,6]-

phenyl-C_{61}-butyric acid methyl ester (PCBM) in chlorobenzene with a concentration of (30 mg **AnE-PV*stat***: PCBM)/ml stirred overnight. The **AnE-PV*stat***:PCBM solution was then filtered and spin coated on top of PEDOT/PSS film with 1000 rpm. Both I-V and IPCE measurements were done before and after annealing of the solar cells at 110^0C for 5 minutes in glove box. The nanomorphology of the pristine film and of the various blends was also investigated before and after annealing. The measured active layer thickness of **AnE-PV*stat***: PCBM was ~190 - 195 nm for 1:1, ~245 - 250 nm for both 1: 2 and 1:3 ratios. PEDOT:PSS layer was about ~50 - 55 nm.

The emission spectra of the blends show significant fluorescence quenching of **AnE-PV*stat*** emission upon blending **AnE-PV*stat*** with PCBM at three different ratios as shown in Figure 4.1.7. This is evidence of effective photoinduced electron transfer from **AnE-PV*stat*** to PCBM even at a ratio of 1:1 which is our motivation for the fabrication of bulk heterojunction solar cells using **AnE-PV*stat*** with PCBM [260]. The inset in Figure 4.1.7 shows the effect of the concentration of PCBM in the blend. With increasing the amount of PCBM the degree of quenching increases. As the ratio changes from 1:1 to 1:2 the difference is higher as compared to the change observed from 1:2 to 1:3 ratio which indicates the limit of PCBM required. From the electrochemical calculation of the LUMO level of **AnE-PV*stat*** shown above, the energy difference between the electron affinity of the polymer and the LUMO of PCBM is ~ 0.45 eV, which is sufficient to resist the exciton binding energy, a prerequisite for efficient electron transfer that resulted an efficient fluorescence quenching of **AnE-PV*stat*** [261].

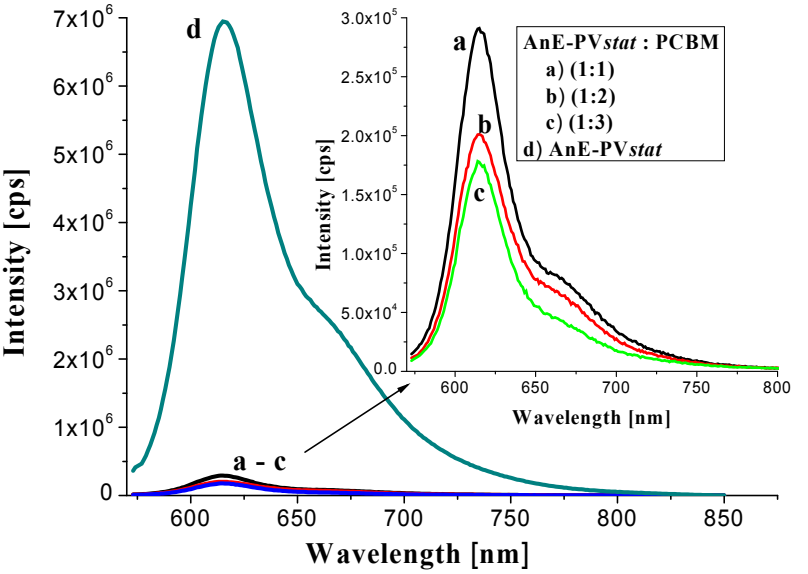

Figure 4.1. 7: *Fluorescence spectra of* **AnE-PV*stat***: *PCBM blends at different ratios (a-c) and the pure film (d).The inset shows enlarged curves of (a-c) as indicated.*

Figure 4.1.8 and Table 4.1.6 depicts the IV-curves of the solar cell devices from 1:1, 1:2, and 1:3 **AnE-PV*stat***:PCBM blend ratios, respectively. It is ascertained from these curves that in dark condition the solar cells show very high rectification with rectification ratio of approximately 10^4 at ± 2V, an indication of efficient polarization of the device in the forward direction where electrons are injected from a low work function electrode (Al) to the LUMO of the blend while holes are injected from high work function electrode to the HOMO of the blend. This is evidence of a good forward biased diode [262].

Under illumination of 100 mW/cm^2 AM 1.5 white light a high reversed biased photocurrent is observed with three order of magnitude increase (Figure 4.1.8 semilogarithm curves) as compared to the dark current which shows an efficient photo polarization of the device in the reversed direction where electrons are extracted from LUMO of acceptor PCBM to a low work function electrode (Al) of the blend while

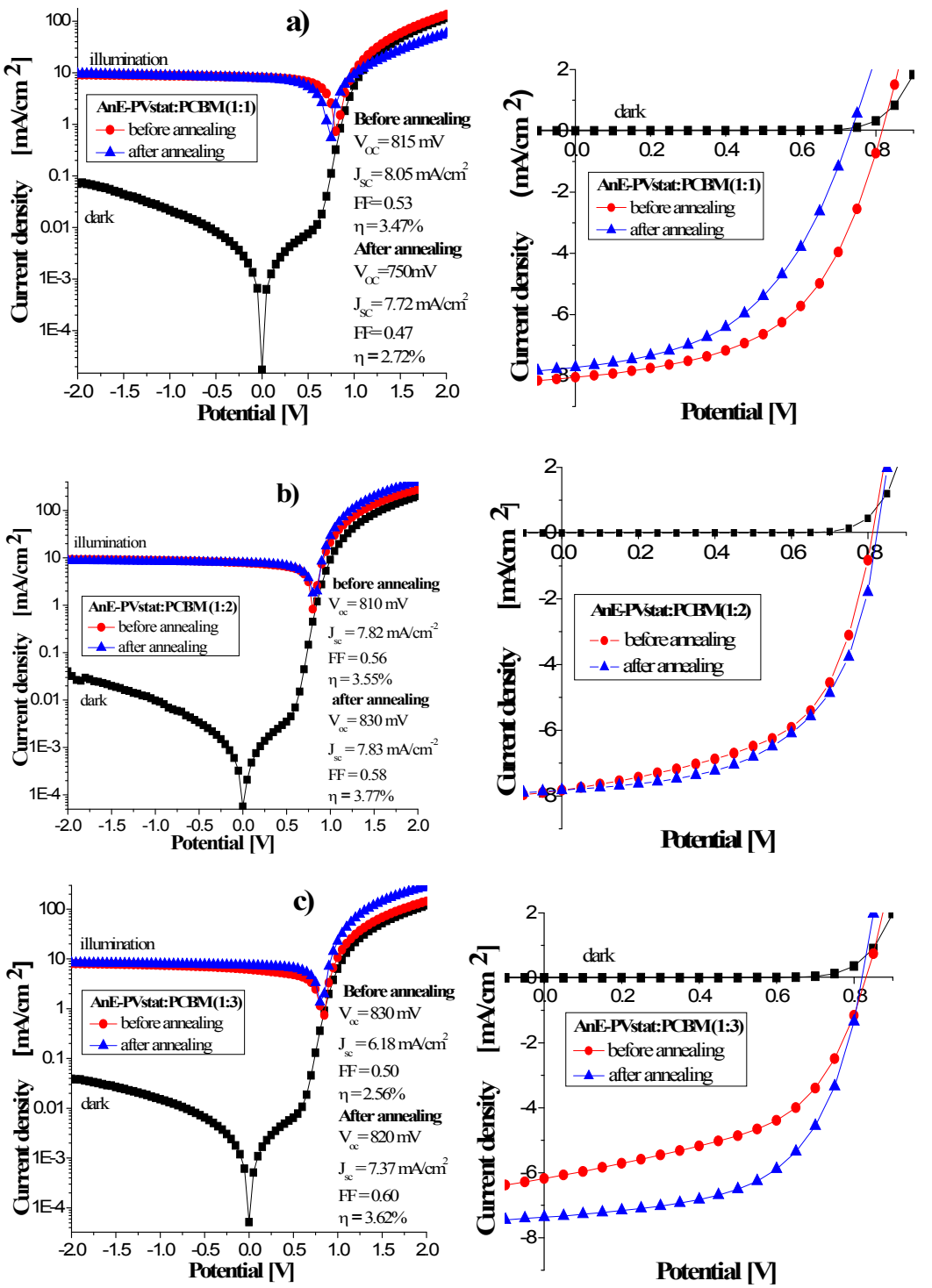

Figure 4.1. 8: *Semilogarithm (left side) and linear (right side) I-V characteristic of the best solar cells made at different ratios of AnE-PVstat: PCBM a) 1:1 ratio b) 1:2 ratio c) 1:3 ratio of blend before and after annealing at 110°C for 5 minutes.*

holes are injected from HOMO of the donor polymer AnE-PVstat to high work function electrode ITO *via* a hole conducting layer PEDOT:PSS. Irrespective of **AnE-PV*stat***:PCBM blend ratio, the solar cells showed reproducible open circuit voltage V_{OC} values between 800 and 840 mV, which is a function of the HOMO of the polymer and that of the LUMO of the acceptor independent of the blend ratio [31, 45, 221, 238, 239].

Table 4.1. 6: *Photovoltaic parameters from solar cells with different blend ratios before and after annealing at 110 °C for 5 minutes.*

Polymer to PCBM ratio	Sample No	V_{OC} (mV)		J_{SC} (mA/cm^2)		FF		η (%)	
		before	after	before	after	before	after	before	after
1:1	1	800	750	8.01	7.62	0.50	0.49	3.20	2.80
	2	815	750	7.58	7.32	0.52	0.45	3.21	2.47
	3	815	750	8.05	7.72	0.53	0.47	3.47	2.72
1:2	1	810	830	7.82	7.83	0.56	0.58	3.55	3.77
	2	820	820	6.14	7.13	0.47	0.59	2.36	3.45
	3	800	820	6.12	7.11	0.49	0.59	2.40	3.43
1:3	1	830	830	5.58	6.1	0.57	0.56	2.63	2.83
	2	840	820	5.51	6.43	0.52	0.58	2.40	3.05
	3	830	820	6.18	7.37	0.50	0.60	2.56	3.62

The short circuit current density, J_{SC} , and fill factor, FF, values were found to be dependent on both polymer:PCBM ratio and thermal treatment. As can be seen in

Figure 4.1.8a, b, and c as well as Table 4.1.6, the short circuit current density decreases with increasing PCBM proportion prior to annealing. After annealing at 110 ^{0}C J_{SC} decreases in the case of 1:1 blend ratio, remain almost the same in the 1:2 blend ratio and increases in the 1:3 blend ratio. There is an increase in the fill factor with increasing PCBM concentration going from 1:1 to 1:2 ratio prior to annealing. Further increase to 1:3 ratio brings virtually no changes as compared to 1:2 ratios. The annealing process led to a decrease in the FF in 1:1 ratio, but an increase in case of 1:2 and 1:3 ratios. The trend in the J_{SC} and FF in these devices showed that with low PCBM concentration, the solar cells perform better before annealing, but with higher PCBM concentration better performance is achieved after annealing. The best performance was achieved with 1:2 blend ratios where V_{OC}, J_{SC}, and FF values are relatively higher and stable even after annealing of the solar cells.

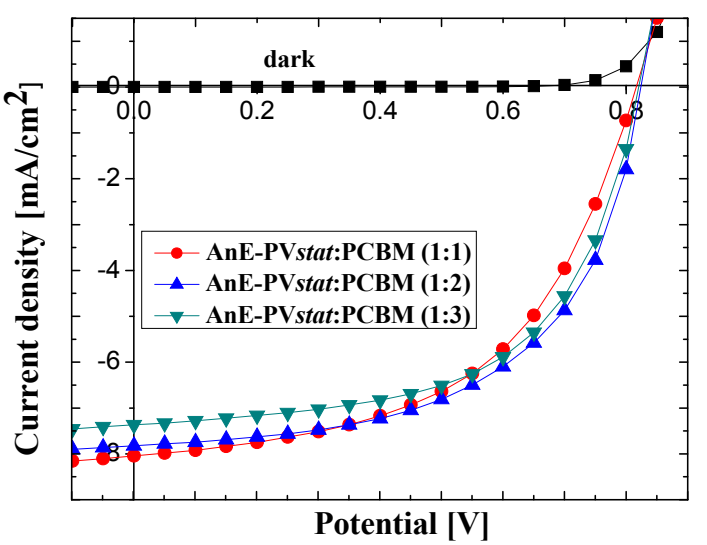

Figure 4.1. 9: *Overlay plot of I-V curves of the best solar cells from AnE-PVstat: PCBM (1:1) before annealing, AnE-PVstat:PCBM (1:2) and AnE-PVstat:PCBM (1:3) after annealing at 110 °C for 5 minutes.*

Overlay plot in Figure 4.1.9 shows the clear difference among the three blend ratios of **AnEPV*stat*:**PCBM interms of all I-V characteristic values. Table 4.1.6 displays the consistency and reproducibility of the device made with three **AnEPV*stat*:**PCBM ratios before and after annealing.

As can be seen from the IPCE curves in Figure 4.1.10a, b, and c, a contribution to photocurrent from the absorption of PCBM is observed at a peak around 390 nm and a kink around 710 nm. This is evidenced from the intense optical absorption peak of the blend at around 390 nm, but not in the pure polymer film. The intensity of the IPCE peaks at 390 nm and 710 increased with increasing PCBM concentration. The IPCE of the solar cells increases from 1:1 to 1:2 polymer:PCBM blend ratio because the charge transport becomes more efficient with increasing PCBM amount [263], but the IPCE decreases as the amount of PCBM further increases in the 1:3 ratio. This is associated with the less contribution of PCBM to the total absorption in the visible spectral range leading to a decrease of the fraction of photons absorbed by the solar cell [236]. With annealing the device at 110^0C for 5 minutes, the change in IPCE is consistent with the change observed in short circuit current density where 1:1 ratio showed a decrease in IPCE where as 1:2 and 1:3 ratios showed an increase in IPCE after annealing. The closeness of the change in the characteristic I-V and IPCE values of **AnE-PV*stat*: PCBM** (1:2) before and after annealing showed that this ratio is the optimium as compared to the other two ratios.

As shown in Figure 4.1.11 the IPCE curves of best devices made from each ratio are consistent with the corresponding optical absorption of the pristine polymer and its blend with PCBM. Integrating the IPCE data of the best cell measured after annealing in this experiment with **AnE-PV*stat***: PCBM 1:2 gives an estimate for J_{sc} under

AM1.5 conditions of 7.82 mA/cm^2 which is consistent with the J_{sc} value of 7.83 mA/cm^2 obtained during I-V measurement. The slight difference observed in the non annealed case between the calculated current from the IPCE (7.77 mA/cm^2) and the experimental value from the I-V measurement (7.82 mA/cm^2) lies within the range of error.

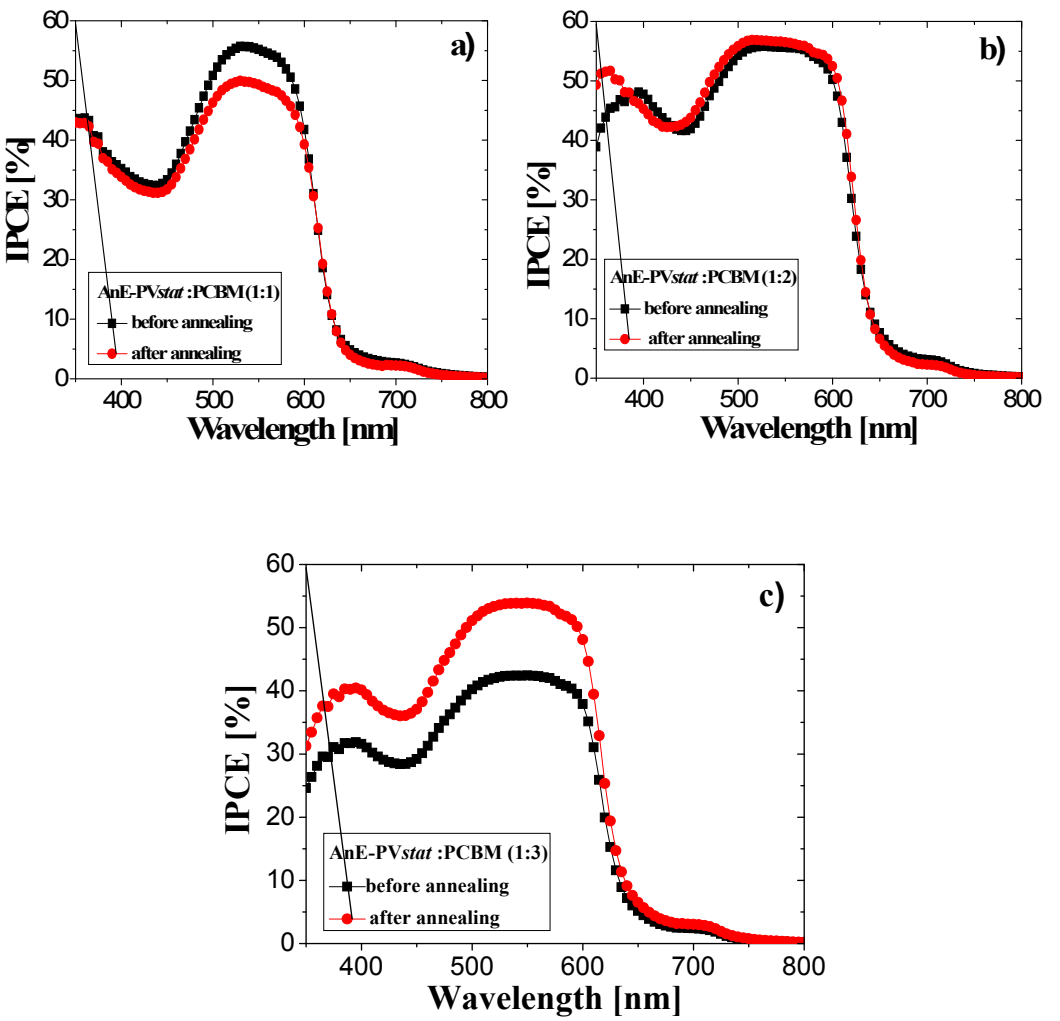

Figure 4.1. 10: *IPCE curves of the solar cells with different ratio of* **AnE-PV*stat*** *:PCBM.*

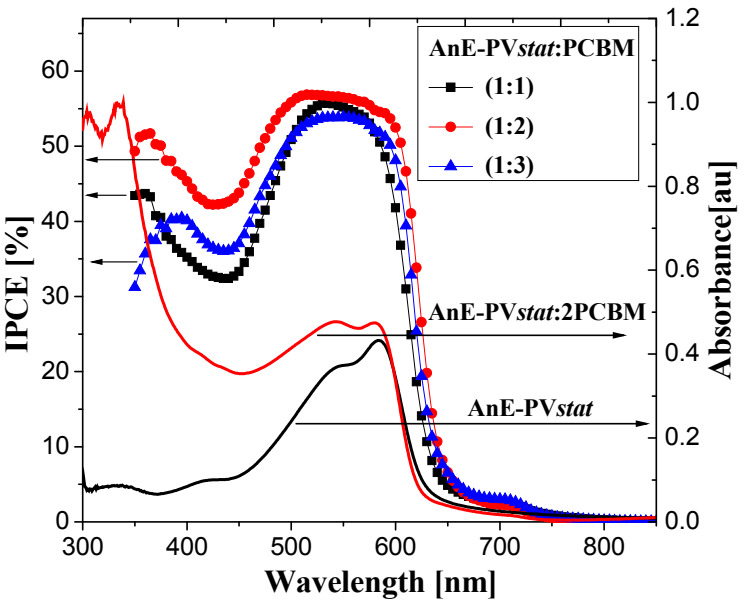

Figure 4.1. 11: *Overlay plot of IPCE curves of the best solar cells from AnE-PVstat: PCBM at three ratios (1:1) before annealing for (1:2) and (1:3) after annealing at 110 °C for 5 minutes as well as the corresponding optical absorptions of the pristine polymer and the blend.*

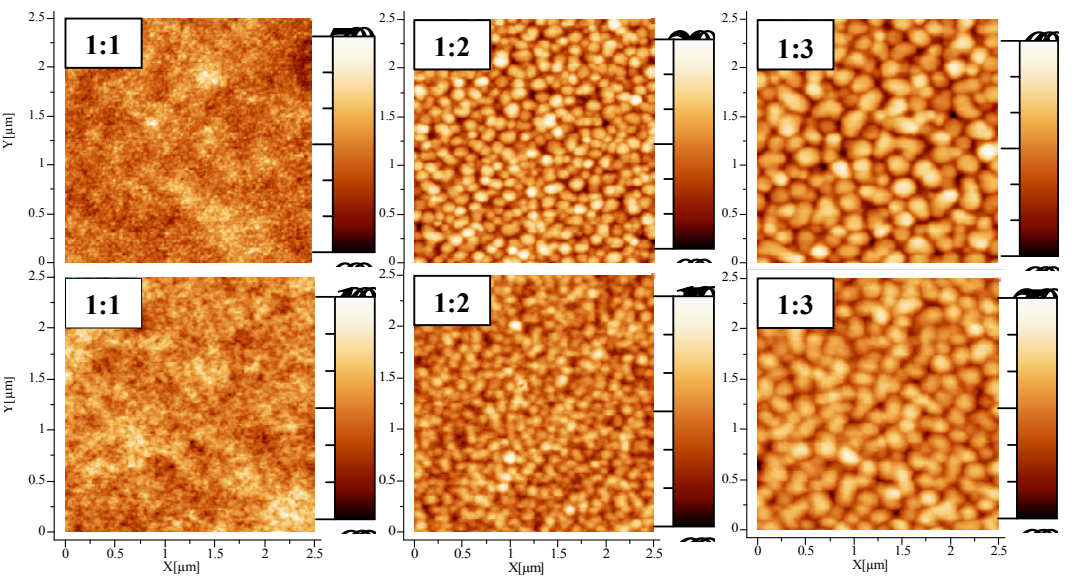

Figure 4.1. 12: *AFM images of* AnE-PV*stat:PCBM solar cells for three different blend ratios, 1:1, 1:2, and 1:3 before annealing (top) and after annealing (bottom).*

The atomic force microscopy (AFM) surface morphology images of **AnE-PV*stat***:PCBM solar cells made with three different **AnE-PV*stat*** to **PCBM** ratios are presented in Figure 4.1.12 and the AFM image parameters measured for all the images are shown in Table 4.1.7. Generally as we go from devices with 1:1 ratio to 1:3 ratio the phase separation and domain size of the images increased as confirmed from the significant increase in both roughness and height of the surface. This is because as PCBM concentration increases it separates out as oval domains (clusters) as shown in the images. With 1:1 blend ratio of **AnE-PV*stat***:PCBM the solar cell films are relatively smooth and almost featureless surfaces with a slight increase of the roughness and height after annealing the device. Phase separated domains are not clearly observed which indicates high miscibility of the acceptor PCBM with the donor **AnE-PV*stat*** at this ratio**.** The slight increase in roughness and height parameters is an indication of induced phase separation which resulted, a decrease short circuit current and fill factor of the devices. This shows that in this ratio the device has better phase separation and percolation path before annealing as compared to the annealed devices. In case of devices made by 1:2 and 1:3 ratios of **AnE-PV*stat*** to PCBM, well defined grain morphology is observed showing a clear phase separation where the PCBM domains are clearly seen in the images. With annealing these devices the images become more compact as the roughness and height parameters decreased in both cases unlike devices with 1:1 ratio. This decrease in roughness and height is an indication of reduction of free spaces in the film as the big domains of PCBM come together and improved percolation of the donor material as it melts and coalesce. Because of this changes annealing improved both the short circuit current density and fill factor of solar cell devices fabricated from 1:2 and 1:3 ratios of AnE-PVstat to PCBM. When we compare the photovoltaic performances of the

devices before and after annealing (Table 4.1.6) with the corresponding morphology characteristic changes (Table 4.1.7) at the three ratios relatively **AnE-PV*stat*** to PCBM with 1:2 ratio is the optimum blend ratio though the other two ratios showed significant performance.

Table 4.1. 7: *AFM image parameters of **AnE-PVstat**:PCBM solar cells before and after annealing at 110 ^{0}C.*

AFM parameter (nm)	**AnE-PVstat to PCBM ratio**					
	1:1		**1:2**		**1:3**	
	Before annealing	Annealed	Before annealing	Annealed	Before anneling	Annealed
RMS roughness	0.6699	0.9966	3.7087	1.8321	6.0326	3.0638
Peak to peak	6.007	9.1276	23.6033	14.8447	34.9781	21.5705
Roughness average	0.5314	0.7917	3.0159	1.4783	4.9457	2.4756
Average height	2.5108	5.2216	12.1071	6.5695	19.4988	11.7471

As compared to the photovoltaic performance of non statistical polymers optimized in reference [251], high performance solar cells are obtained with **AnE-PV*stat*** even at low PCBM content. In all three blending ratios efficiencies above 3% were achieved, whereby the best cell with AnE-PVstat:PCBM (1:2) showed a V_{OC} of 830 mV, J_{sc} of 7.83 mA, a fill factor of 58% and an energy conversion efficiency of 3.77%. Table 4.1.6 shows the reproducibility of the PV parameters measured in various devices.

4.1.2.6. Solid state photoelectrochemical solar cell studies

A Photoelectrochemical solar cell is just electrochemical cell (battery) with two electrode system and an electrolyte with a redox couple. The photoactive semiconductor is acting as a photosensitizer of the other working electrode semiconductor like TiO_2 or directly used as both absorber and an electrode to generate current by absorbing light. Dye sensitized solar cells are typical photoelectrochemical solar cell based on liquid electrolytes. The sensitizer can be an organic dye or a polymer which is another approach in the area of organic solar cells which have reached efficiency as high as 10% under AM 1.5 (100 mW/m^2) [14,264].

The main problem is that, liquid electrolytes limit device stability because the liquid may evaporate when the cell is imperfectly sealed, and more generally, permeation of water or oxygen molecules and their reaction with the electrolytes may worsen cell performance. Liquid electrolytes also makes the manufacture of multi-cell modules difficult because cells must be connected electrically yet separated chemically, preferably on a single substrate [265, 266].

Many attempts have been made to solve the above problems by the replacement of liquid electrolyte with solid or quasi solid-state hole conductors [267 - 269]. A typical example is an amorphous polymer electrolyte, poly(oxymethylene-oligo(oxyethylene) with a repeating unit of $CH_2O(CH_2CH_2O)_9$ (POMOE), which has a melting point below room temperature and a glass transition temperature of 209 K. It will not crystallize or form crystalline polymer-salt complexes with moderate salt concentrations at room temperature [15, 270].

Another approach that has been done is using an organic polymer semiconductor both as light absorber and an electrode into the solid electrolyte system which showed a significant photocurrent [271, 272]. Due to high recombination rate of the electron hole pairs in pure organic conjugated polymer, a better result was obtained by combining the polymer with high electron affininty molecules like fullerene and its derivatives in a bulk heterjunction form. This phenomena was observed in poly(3-hexylthiophene) when it is alone and blended with fullerene (C_{60}) or 1-(3-methoxycarbonyl)propyl-1-phenyl[6,6]C_{61}, (PCBM) in a bulk heterojunction blend [273, 274].

The mechanism of photocurrent generation is different from the usual BHJ photovoltaic because of the presence of additional solid (gel) electrolyte junction to the semiconductor where it follows the semiconductor/electrolyte (conductor) junction (Schottky junction) [275]. Illumination of the semiconductor generates an exciton that dissociates in electrons and holes at the semiconductor/electrolyte interface where the minority carriers (electrons for *p*-type) migrate towards the interface and reduce the redox couple that will oxidized back at the counter electrode to produce the photocurrent at the load [5].

In the case of the bulkhetrojunction active layer a fast photoinduced electron transfer from the polymer semiconductor to C_{60} or PCBM occurred and then these electrons transported to the bulk heterojunction/redox couple containing solid polymer electrolyte interface to reduce the redox couple which later on catalytically oxidized back at the counter electrode and regenerated as shown in Figure 4.1.13. The electrochemically oxidized PEDOT is used as a catalyst for charge transfer between

ITO and I_3^-/I^- redox couple [22]. It is known that I_3^-/I^- is irreversible on bare ITO [276].

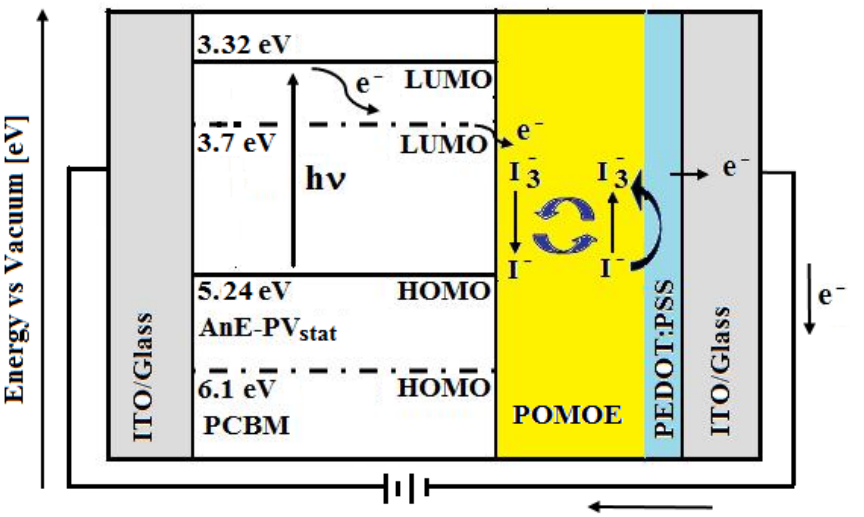

Figure 4.1. 13: *Photocurrent generation in photoelectrochemical solar cell with a bulk heterojunction blend active layer of* ***AnE-PVstat****:2PCBM.*

Unlike the bulk heterojunction photovoltaics these solid state photo electrochemical approach using bulk heterojunction blend as an active layer used just two conducting glass electrodes like (ITO) without any expensive vacuum based thermal evaporation of metal electrodes and other instruments like spin coater are not necessary since films are prepared by drop casting . So it is a very cost effective procedure to fabricate the device in any laboratory. This is the real advantage of these type of cells as compared to the traditional bulk heterojunction photovoltaic fabrication procedures and cost. In this study AnE-PVstat:2PCBM bulk heterojunction which was already characterized and optimized in section 4.1.2.5 above in the bulk heterojunction photovoltaic system was used as an active layer in the solid state photoelectrochemical solar cell and characterized.

As explained in detail in the experimental section the polymer electrolyte was prepared by dissolving POMOE in methanol and the redox couple I_3^-/I^- was prepared by dissolving KI and I_2 separately in methanol and finally equal volume of each of the above three solutions were mixed to produce the polymer electrolyte complexed with a redox couple [273]. The mole ratio of oxygen to potassium is calculated by taking into account both the oxymethylene and oxyethylene oxygen atoms was 25 and the mole ratio of KI to I_2 was 10, i.e. the concentration of I_2 is one-tenth the concentration of KI since the kinetics of the two reversible reactions and mobility of the two ions are different [277]. The ionic conductivity of POMOE is known to be high at room temperature when the oxygen to cation (potassium) mole ratio is 25 [278]. Finally, a thin film of polymer electrolyte complexed with I_3^-/I^- was drop casted on top of **AnE-PVstat**:2PCBM precoated on ITO-glass and allowed to dry in an open air atmosphere. The photoelectrochemical device fabrication was completed by bringing the two electrodes and pressing against PEDOT coated ITO/glass counter electrode (Figure 4.1.14).

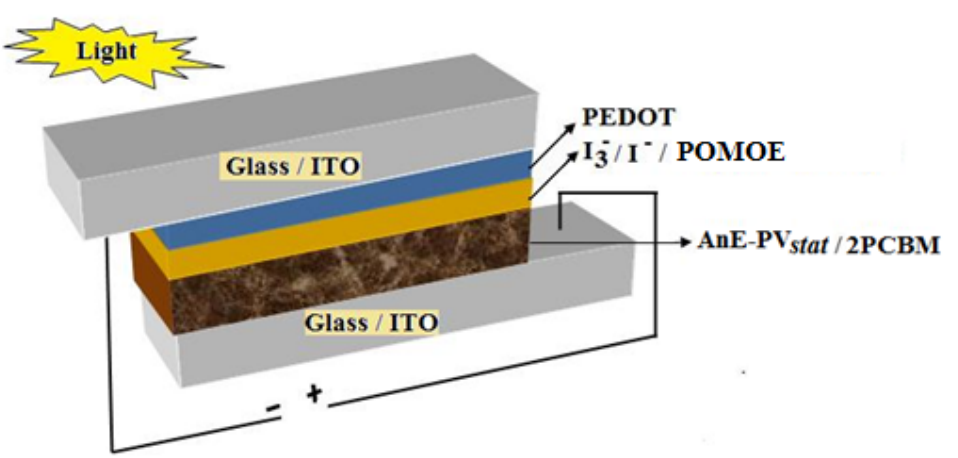

Figure 4.1.14: *Device structure of the photoelectrochemical solar cells fabricated*.

Results and discussion

As displayed in Figure 4.1.15, the time dependent measurement of open circuit voltage of the device in the dark showed a zero voltage. Under illumination of white light (100 mW/cm^2) from the side of ITO/PEDOT photogenerated open circuit voltage value of 315 mV stable with the measurement time was observed. Illumination from the ITO/ polymer/PCBM side doesn't show significant voltage because the thickness of the **AnE-PVstat**:2PCBM is in the order of micrometer which makes the junction on this side very bad. Though this bulk heterojunction blend of **AnE-PVstat**:2BCMB showed a V_{OC} of 870 mV wth the bulk heterojunction photovoltaic system, the V_{OC} of 315 mV with this simple and cheap processing system is significant as compared to the well known polymer P3HT:PCBM which showed a V_{OC} of 140 mV using similar system [273]. The time dependent photocurrent measurement of the device showed no photocurrent in the dark and a cathodic (reduction) photocurrent density of 14 μA/cm^2 was observed with illumination of the device as dipicted in Figure 4.1.16.

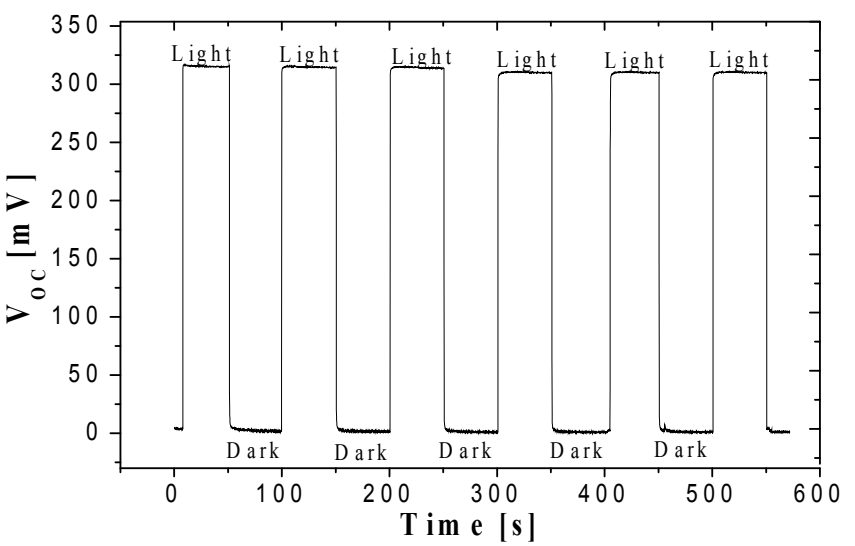

Figure 4.1. 15: *Time dependent measurement of open circuit voltage of the device*.

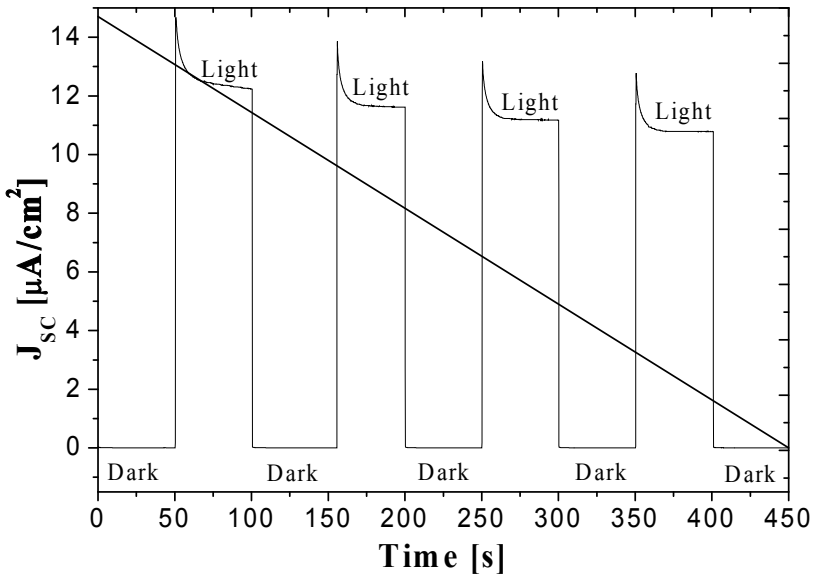

Figure 4.1. 16: *Time dependent measurement of short circuit current of the device.*

Since the whole processs is made in an open air enviroment some degradation of the photocurrent of the device is seen as due to strong interaction of oxygen with PPV conjugation [131, 135]. This cathodic photocurrent indicates that electrons are transferred from the LUMO of **AnE-PVstat** to LUMO of PCBM then to the electrolyte there by reducing I_3^- to I^- and holes are transferred to the back contact and then to the external circuit where they oxidize I^- to I_3^- at the counter electrode by the catalytic effect of PEDOT. Therefore the polymer electrolyte junction leads to electron flow from the LUMO of the polymer to the electrolyte solution as expected for a *p*-type semiconductor /electrolyte junction.

The current voltage characteristic of the device displayed in Figure 4.1.17, shows that the open circuit voltage of ~320 mV and a short circuit current of 14 μA/cm^2 which is consistent with time dependent measurements of V_{OC} and I_{SC}. Though the device showed a significant photocurrent and open circuit voltage the fill factor of the device is very poor since the thickness of the device is very large which increases the serial

resistance and the current path is crossing different junctions until it goes out as a photocurrent.

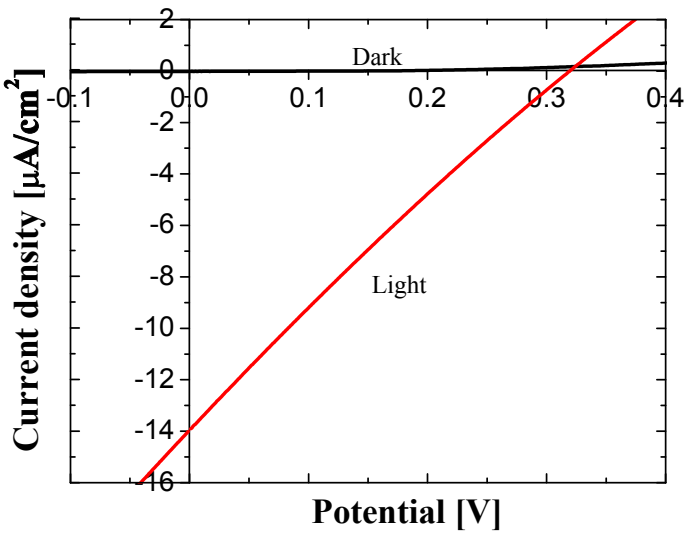

Figure 4.1. 17: *The current density -voltage (I-V) characteristics of the device.*

The photocurrent spectra of the device shown in Figure 4.1.18a confirms that the device photocurrent generation is consistent with the absorption spectra of the active layer **AnE-PV*stat***:2PCBM film. This consistency of optical absorption spectrum and the spectral photoresponse is commonly used to identify the active junction responsible for the photoelectrochemical phenomena. If illumination is made from the side close to the junction where charge separation takes place, the spectral response corresponds to the absorption spectrum and a maximum current is observed because of a more effective charge collection [272].

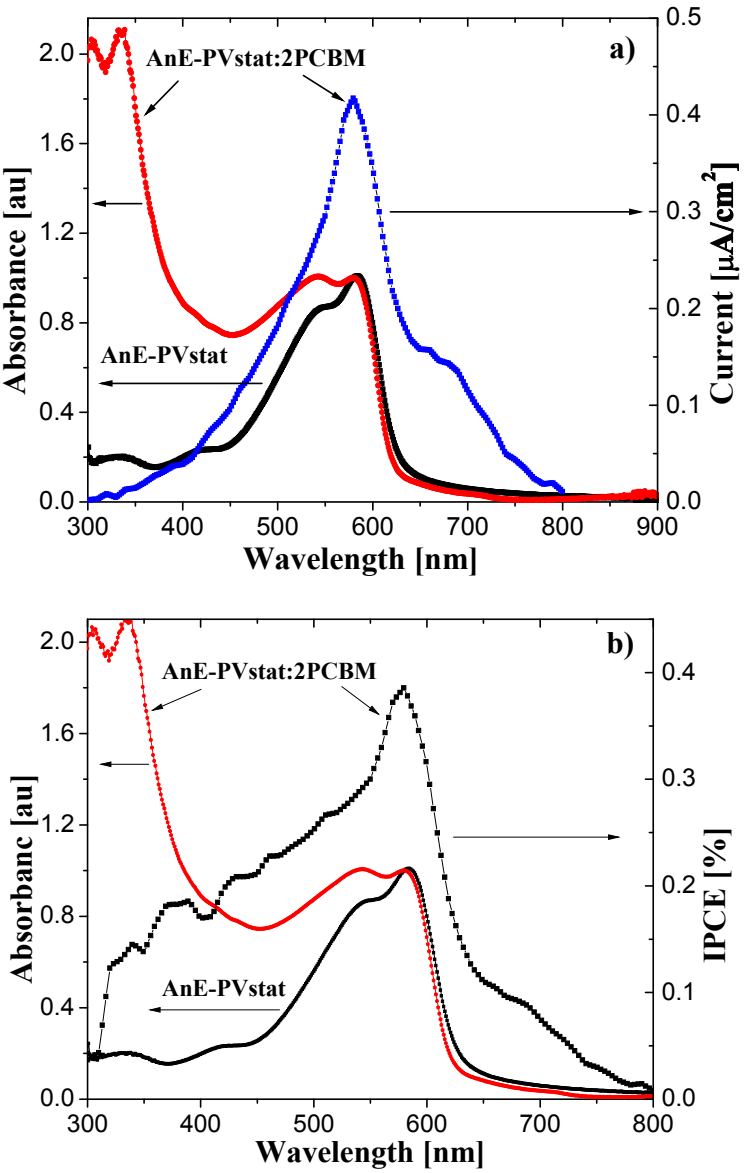

Figure 4.1. 18: *a) Photocurrent action spectra b) IPCE of the photoelectrochemical solar cells from **AnE-PVstat**:2PCBM with the corresponding optical absorptions.*

The absorption spectra of **AnE-PV*stat*** as well as the blend **AnE-PV*stat***:2PCBM films exactly fit the photocurrent action spectra of the solar cell illuminated from the side glass/ITO/PEDOT which is consistent with open circuit voltage observed by illumination of the same side where the active junction is located. The calculated incident photon to collected electron (IPCE) spectra depicted in Figure 4.1.18b

showed a maximum value of 0.38% at 580 nm which is exactly the absorption maximium of the polymer **AnE-PV*stat*** as well as the blend.

4.1.3. Conclusion

By random distribution of segments of *linear* octyloxy side chains, inducing *ordering*, and of *branched* 2-ethylhexyloxy side chain, inducing *disorder* on the backbone of anthracene containing poly(phenylene-ethynylene)-*alt*-poly(phenylene-vinylene) (PPE-PPV) a side chain based statistical copolymer, denoted AnE-PV*stat*, has been synthesized. The polymer proven to be very effective in terms of field independent higher intrinsic charge carrier mobility $\mu = 5.43\times10^{-4}$ cm^2/Vs demonstrated by CELIV that might be due to its highest π-π-stacking distance of $d_{\pi\pi}$ = 0.393 nm and conformationally balanced morphology as compared to the well-defined congeners. The random combination of the underlying constitutional units seems to promote the side chain geared *order* and *disorder* enabling effective tuning of the nanoscale morphology of photoactive layer. Photocurrent conversion efficiency up to 3.77 % in a bulk heterojunction photovoltaic system and a significant device performance in solid state photoelectrochemical solar cells made using AnE-PV*stat:* PCBM as a photoactive layer in an open air showing an open circuit voltage of 320 mV is the present state-of-art value for PPV based materials.

4.2. Mobility and Photovoltaic Performance of Conjugated Polymer Blends: Effects of Side Chains Volume Fraction

4.2.1. Background

Photovoltaic devices based on organic polymers have the potential for low cost renewable energy sources to address the growing global energy needs [30 - 33]. Among the various solar cell device architectures, the bulk heterojunction concept has proven to be the most efficient [31, 213]. This concept is based on ultrafast photoinduced electron transfer from poly[(2-methoxy-5-(2-ethyl-hexyloxy)-1,4-phenylene-vinylene] (MEH-PPV) to buckminster- fullerene (C_{60}) [34] and the realization of improved performance of the first solar cell of this kind from poly(2-methoxy-5-(3,7-dimethyloctyloxy)-1,4-phenylene-vinylene) (MDMO-PPV):C_{60} blend [52]. The concept involves nanoscale self-assembly of heterojunctions by spontaneous phase separation of the donor polymer and the acceptor, which leads to charge-separating heterojunctions throughout the bulk. The resulting photogenerated holes and electrons are then transported to the corresponding electrodes *via* percolating pathways to provide a photocurrent. The high interest for polymer:fullerene based solar cells has triggered the design of a large number of novel conjugated polymeric donor materials such as derivatives of polythiophene, polycarbazole, poly(*p*-phenylenevinylene) (PPV), poly(*p*-phenyleneethynylene) (PPE), and combinations thereof [53 - 58, 279] as well as fullerene derivatives as acceptor materials [45, 59, 280].

To improve the power conversion efficiency donor polymers should have low energy band gap so as to harvest light from most of the solar spectrum which leads to higher short-circuit current density (Jsc) and better overall performance [30,209,221]. In

addition to the required bandgap and a match of the energy levels of the donor and of the acceptor components, a better nanostructural ordering to get optimized phase separation of both components and an efficient percolation of the photogenerated charges are crucial to improve the power conversion efficiency of organic solar cells [229, 281, 282]. Most studied approaches to improve the nanoscale morphology of the active layer are 1) thermal annealing [64, 197, 227, 283 - 286], 2) solvent variation [37, 230, 287 - 293] and 3) using additives like alkyldithioles [64, 285, 257, 294 - 296] and diiodoalkanes [40, 244], in the bulk heterojunction solution. A set of other approaches to efficiently control the active-layer morphology has been reported in the literature, such as doping of the polymer with small molecules like triphenylamine [297], blending the active layer with ionic solid electrolyte (such as polyethylene oxide and $LiCF_3SO_3$) [298], and ternary blends [299].

For instance, by using ternary thienothiophene copolymers as a nucleating agent, an enhancement of the degree of crystallization of P3HT in P3HT:PCBM system was observed. This increases the charge carrier transport properties and enlarges the active layer absorption spectrum [299]. Electron transporting polymer, poly(9,9-dioctylfluorene-*co*-benzolthiadiazole (F8BT), mixed with PCBM blended with P3HT showed improved efficiency due to enhanced optical absorption, better charge collection, and improved charge carrier mobility [300, 301]. Heeger *et al*. reported a highly efficient tandem cell achieving efficiency over 6% by utilizing two p-type conjugated polymers in the two independent active layers to effectively harvest the solar photons [243]. A ternary blend bulk heterojunction consisting of two electron donor polymers, MDMO-PPV and P3HT, and PCBM as an acceptor showed an improvement of the V_{OC} at a minimum expense of the J_{SC} [302]. In a recent report two donor conjugated polymers poly[2,6-(4,4-bis(2-ethylhexyl)-4H-cyclopenta[2,1-*b*;3,4-

b']dithiophene)-*alt*-4,7-(2,1,3-benzothiadiazole)] (PCPDTBT) and a dithiophene-*alt*-benzothiadiazole based polymer, which are capable of absorbing light complementarily in the spectral region covering 400 to 900 nm, were used together with $PC_{71}BM$ to form a ternary blend system. This resulted in an improved photovoltaic performance as compared to the individual polymer:$PC_{71}BM$ blends [303].

Here we report on photovoltaic device from ternary blend by mixing $PC_{61}BM$ with two thiophene containing PPE-PPV based donor polymers having the same conjugated backbone but different alkoxy side chains grafted on the phenyleneethynylene (PE) segment of poly{1,4-(2,5-dioctyloxy)-phenylene-ethynylene-2,5-thiophenylene-vinylene-1,4-[(5-(2-ethylhexyl)oxy)-2-methyloxy]-phenylene vinylene}(DO-$PThE_1$-PPV_2) (**D1**) and poly{1,4-(5-[(2-ethyl hexyl)oxy]-2-methoxy)-phenylene-ethynylene-2,5-thiophenylene-vinylene-1,4-[(5-(2-ethylhexyl)oxy)-2-methyloxy]-phenylenevinylene} (MEH-$PThE_1$-PPV_2) (**D2**). Their chemical structures are displayed in the experimental section (Figure 3.1.1). The synthesis, electrochemical, and photophysical characterizations of **D1** and **D2** are reported elsewhere [57, 254, 304].

Systematic variation of the nature (*linear* or *branched*), *density, length,* and *position* of alkoxy side chains has been used to tune the supramolecular ordering, the photophysical, photoconductive, electrochemical, electroluminescent, and photovoltaic properties of PPE-PPV based materials [175, 251, 305 - 310]. For instance, the lower side chain volume fraction in **D2** than in **D1** leads to higher miscibility between **D2** and PCBM (1:3 ratio) than between **D1** and PCBM. This, on the one hand, increases the donor/acceptor interfacial area, resulting in higher density

of photogenerated charges, and on the other hand, fosters the recombination of the photogenerated charges that at the same time hampers the percolation paths to the electrodes, which lowers both the expected J_{SC} and the FF [57, 254, 304]. The mixing of **D1**, **D2**, and PCBM in a ternary system as described in this work resulted in a different active layer nanomorphology than in the individual **D1**:PCBM or **D2**:PCBM binary system. Thus higher photovoltaic performance was obtained from the ternary blend system than from the individual binary systems.

4.2.2. Results and discussion

Photophysics

For photophysical measurements, pure polymers (**D1**, **D2**), their 1:1 mixture films and their corresponding blend films with PCBM in a 1:3 ratio were prepared from their solution (10 mg/ml) polyme in chlorobenzene by spin coating on glass. After the films were allowed to dry in the glove box for 24 h, optical absorption and photoluminescence measurements were carried out. From thin film absorption and photoluminescence (PL) spectra of **D1**, **D2**, and their 1:1 blends in Figure 4.2.1, it can be seen that all three entities exhibit almost the same optical features, which is consistent with the previous reports [57, 254, 304]. The absorption contribution of PCBM in the binary and ternary blends is viewed by the strong absorption band in the range of 325 - 390 nm and a kink at 710 nm. It is possible to correlate the intensity of the absorption bands with the volume fraction of the alkoxy side chains which are acting as *diluting agents* of the photoactive species. The concentration of the photoactive species increases from **D1**:PCBM blend over **D1**:**D2**:PCBM blend to **D2**:PCBM. This is consistent with the higher quantum efficiency 60% value of **D2** as compared to 40% for **D1** [57, 254]. The highest photoexcited interaction in the blends

of **D2** with PCBM (i.e. highest miscibility) resulting in the highest photoluminescence quenching in **D2**: PCBM blend, followed by **D1**:**D2**:PCBM blend, then **D1**:PCBM blend as shown in Figure 4.2.1b. So by mixing the two polymers in a ternary blend with PCBM an intermediate photoexcited interaction was observed.

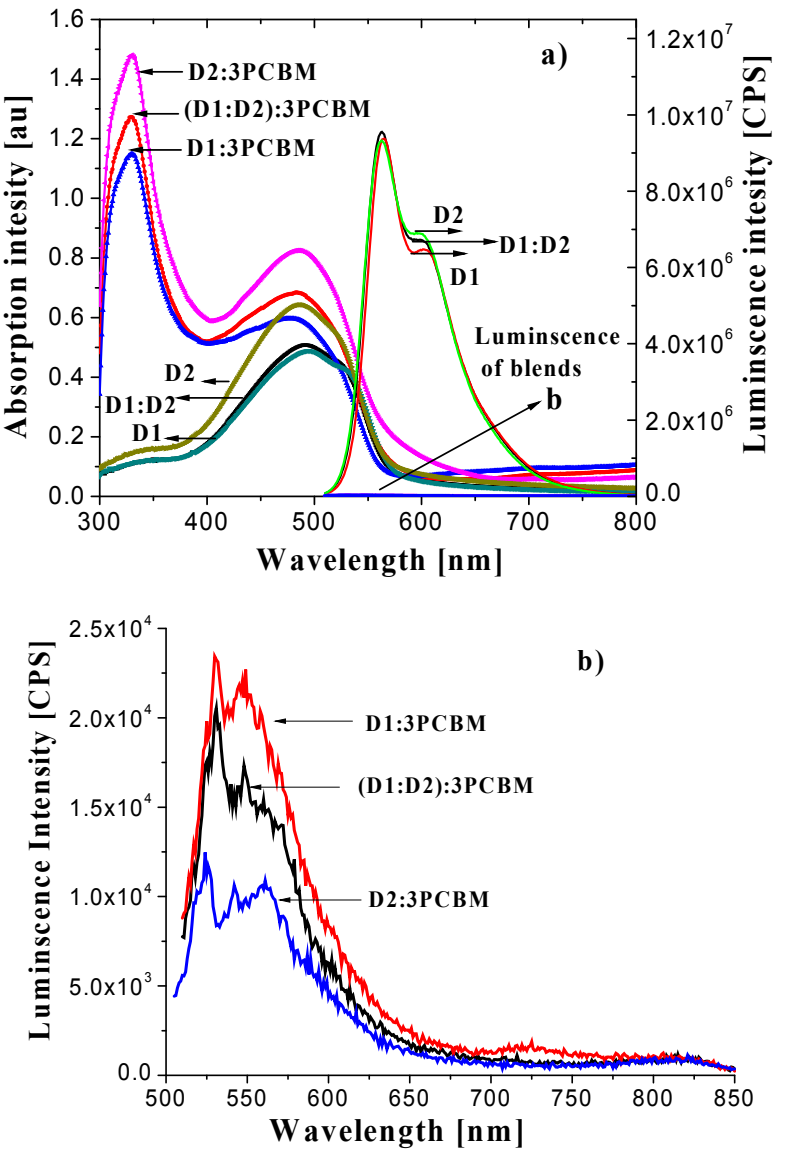

Figure 4.2. 1: *a) Thin film absorption and emission spectra of **D1**, **D2** and **D1:D2** (1:1) as well as their blend with PCBM in a 1:3 ratio. b) Enlarged photoluminescence spectra of the blends.*

For the fabrication of bulk heterojunction solar cells, solutions were prepared according to the previous literature [254, 304] with mixing ratio of 1:3 polymer to the acceptor [6,6]-phenyl-C_{61}-butyric acid methyl ester (PCBM) in chlorobenzene (99%) (ACROS ORGANICS) with a concentration of (40 mg/ml) polymer:PCBM stirred overnight. Poly(3,4-ethylenedioxy thiophene) /poly(styrenesulfonate) (PEDOT/PSS) (Baytron PH) stirred overnight and filtered was spin coated from aqueous solution on top of ITO with 2000 rpm to get a film of 80 nm thickness and dried overnight in open air. The polymer:PCBM solutions were then filtered and spin coated on top of PEDOT:PSS film.

The current-voltage (I-V) characteristics of the solar cells are given in Figure 4.2.2. Statistical studies were also made in order to ensure the reproducibility of results and their characteristic average values of these solar cells made is shown in Table 4.2.1. The I-V characteristics of the solar cells in Figure 4.2.2 reveal a dark rectification ratio of approximately 10^3 at ± 2V. The solar cells made from **D2**:PCBM (1:3) showed average open circuit voltage (V_{OC}) value of 735 mV and that of **D1**:PCBM (1:3) showed 842 mV. This difference in V_{OC} is consistent with the relatively lower HOMO level of **D2** as compared to that of **D1** though their band gap is similar [57, 254]. The average V_{OC} of the ternary blend of 860 mV in contrast is higher than that of the respective binary systems. It is reported that V_{OC} is a function of the HOMO of the polymer and that of the LUMO of the acceptor [31, 209, 221]. So this result shows by mixing two polymers of the same backbone but with different side chains volume fraction, the open circuit voltage can be improved in the limit of either of the HOMO levels of the donors and the LUMO level of the acceptor [177].

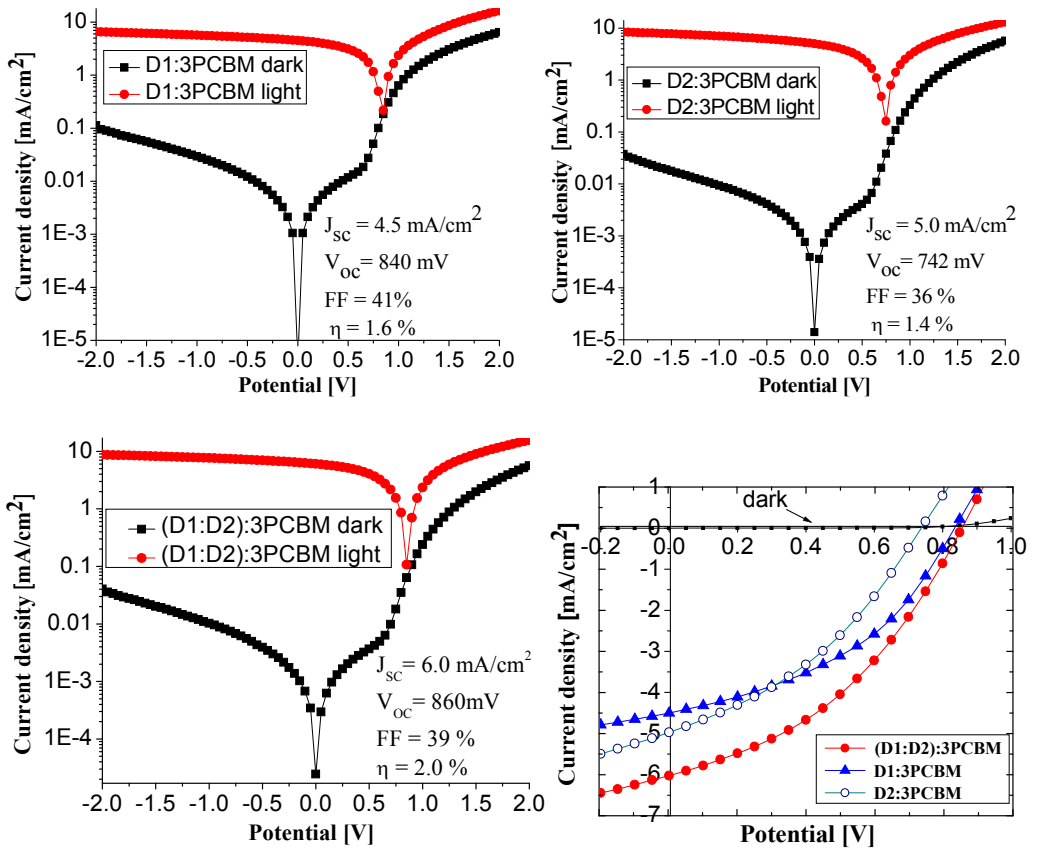

Figure 4.2. 2: *I-V characteristics of the solar cells made from the binary blends* ***D1****:3PCBM and* ***D2****:3PCBM as well as ternary blend (****D1:D2****):3PCBM.*

When we compare the solar cells made from the individual polymers with PCBM, **D2**:3PCBM showed an average short circuit current density (J_{SC}) of 4.9 mA/cm^2 which is higher than that of **D1**: 3PCBM which showed an average J_{SC} of 4.5 mA/cm^2. This trend is consistent with the photoluminescence (PL) spectra of the blends where **D2**:3PCBM showed the strongest PL quenching due to more efficient photo-induced electron transfer to the acceptor PCBM as compared to **D1**:3PCBM. The highest average J_{sc} of 5.7 mA/cm^2 obtained for the ternary blend is due to its better active layer nanomorphology than the binary blends. The fill factor FF values

observed for the ternary blend (40%) is very close to the highest average value of 41% obtained for **D1**: 3PCBM binary system.

Table 4.2. 1: *I-V characteristic results of solar cells made along with the average values.*

Blend	Sample No.	Electrode	V_{OC} (mV)	J_{SC} (mA/cm^2)	FF(%)	η (%)	Blend	Sample No.	Electrode	V_{OC} (mV)	J_{SC} (mA/cm^2)	FF (%)	η (%)
D1:PCBM (1:3)	1	1	840	4.85	42	1.71	**D2**:PCBM (1:3)	1	1	745	4.97	38	1.42
		2	830	4.30	40	1.49			2	730	5.18	36	1.40
		3	825	4.30	42	1.47			3	710	5.12	37	1.35
	2	1	850	4.35	43	1.61		2	1	740	5.06	37	1.41
		2	855	4.03	43	1.48			2	740	4.97	36	1.35
		3	836	4.36	41	1.53			3	740	5.04	35	1.35
	3	1	850	5.06	41	1.74		3	1	736	4.77	36	1.29
		2	850	4.61	42	1.67			2	725	4.66	36	1.20
		3	840	4.50	41	1.58			3	725	4.48	36	1.14
(**D1**:**D2**): PCBM (1:3)	1	1	885	5.6	41	1.95	***Summary***	**Average Values**			**Blend**		
		2	865	5.34	40	1.85					**D1**:3PCBM	(**D1**:**D2**): 3PCBM	**D2**: 3PCBM
		3	855	5.45	39	1.81							
	2	1	870	5.59	42	2.04							
		2	855	5.57	40	1.91							
		3	865	5.52	42	1.79		V_{OC} (mV)			842	860	735
	3	1	860	6.02	39	2.02		J_{SC} (mA/cm^2)			4.5	5.7	4.9
		2	850	5.94	38	1.95		FF (%)			41	40	36
		3	830	6.10	37	1.90		η (%)			1.6	2.0	1.3

As can be seen from the incident photon to collected electron efficiency (IPCE) curves in Figure 4.2.3, the IPCE for the ternary blend is the highest (52% at its

maximium) and covers the largest area as compared to the binary blends. At their maximum point **D1**:3PCBM and **D2**:3PCBM showed IPCE values of 40% and 41% respectively. Eventhough the optical absorption of the two polymers are almost the same a difference in the position of the onsets of the IPCE curves were observed. **D2**:3PCBM blend absorbs strongly at longer wavelengths compared to **D1**:3PCBM blend. The IPCE onset of the ternary blend starts at the longest wavelength as compared to the binary blends. The difference in the IPCE values between the binary blends and the ternary blend is consistent with their difference in short circuit current values. This clearly shows that by mixing the two polymers a new nanomorphology with improved properties was obtained.

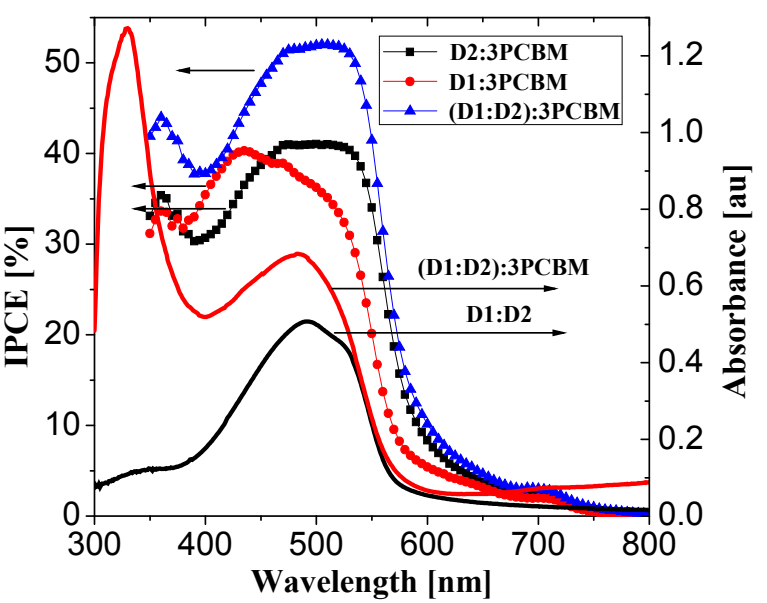

Figure 4.2. 3: *IPCE of the solar cells from the binary and ternary blend systems together with the absorption spectra of **D1**:**D2** (1:1) mixture.*

The AFM images in Figure 4.2.4 show the nanomorphological differences between the two polymer films **D1** and **D2** and their 1:1 mixture from their 1% solution in chlorobenzene spin coated on glass. The calculated AFM parameters from the image

are shown in Table 4.2.2. Based on these values **D1** has higher roughness around 0.8 nm than that of **D2** which is 0.3 nm, whereas their 1:1 mixture shows an intermediate roughness of 0.4 nm. The same trend was observed in their average height where an average value of 2.6 nm was obtained for **D1**, 1.2 nm for **D2**, and 1.6 nm for the mixture. As expected, a clear phase separation is observed from AFM picture of **D1**:3PCBM blend with a roughness of 4.0 nm and an average height of 10.7 nm, the blend **D2**:3PCBM showed a very flat film with a roughness of 0.3 nm and average height of 1.4 nm due to higher miscibility between **D2** and PCBM. The ternary blend thin film has a roughness 0.5 nm and a height of 2.1 nm height which is still flat as compared to **D1**:3PCBM but relatively rough as compared to **D2**:3PCBM. The increase in J_{SC} and concomitant overall performance of the ternary blend is proposed to be due to optimized phase separation of the ternary blend as compared to the two binary blends. i.e highest phase separation in **D1**:3PCBM blend and the highest miscibility in **D2**:3PCBM blend.

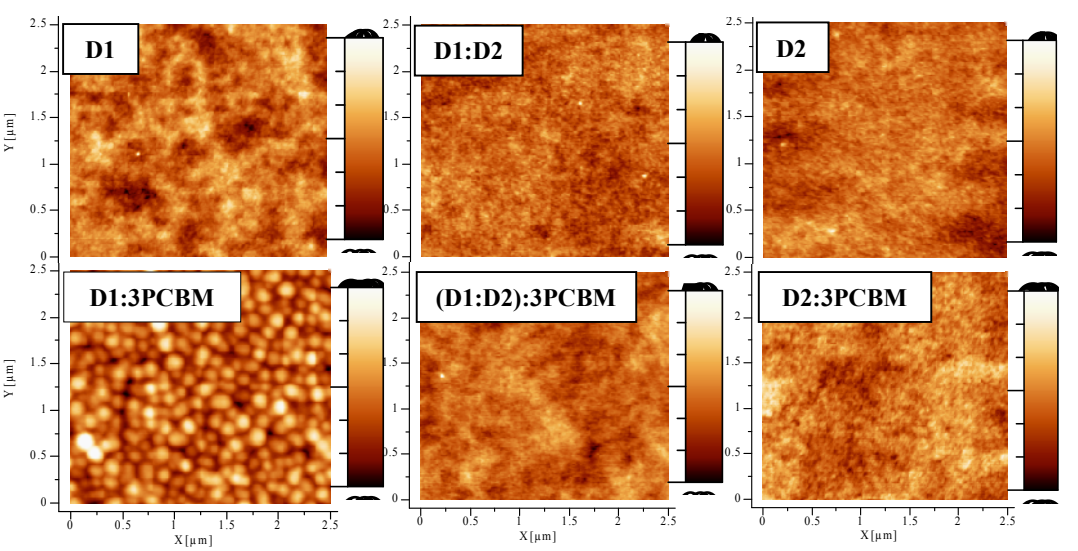

Figure 4.2. 4: *AFM images of the two polymers and their 1:1 mixture films and their corresponding blends with PCBM in 1:3 polymer:PCBM ratio.*

Table 4.2. 2 *AFM image height and roughness parameters of **D1**, **D2**, **D1:D2**, and their blends with 3PCBM.*

AFM Parameter (nm)	**D1**	**D1:D2**	**D2**	**D1:** 3PCBM	**(D1:D2):** 3PCBM	**D2:** 3PCBM
RMS roughness	0.7515	0.3736	0.3954	3.98353	0.46450	0.34082
Average height	2.6359	1.6310	1.2181	10.6891	2.11605	1.41878

The current extraction transients from CELIV experiment for **D1** and **D2** and their 1:1 blend are shown in Figure 4.2.5. Vertical bar marks the extraction maximum from which carrier mobility is calculated. A typical CELIV current transient response presents several important features. The very initial current step *j(0)* (displacement current) observed in the figures is caused by the geometrical capacity of the sample and it is used to estimate the sample thickness. The following increasing extraction current is caused by the photoconductivity of the sample when the mobile charge carriers are being extracted from the film. As the triangle voltage pulse continues to increase, the majority of charge carriers reach the electrode and the current starts to decrease forming a characteristic extraction maximum from which carrier mobility (μ) is calculated [177].

$$\mu = K \frac{d^2}{At_{\max}^2},$$

where $K = 2/3$ for volume (for thin films) and $K = 2$ for surface photogeneration (for thick films), d is the film thickness, A is the slope of applied rising triangle-shaped voltage pulse. The charge carriers are photogenerated with laser pulse of 355 nm since films are undoped with negligible amount of thermally generated charge carriers in the dark.

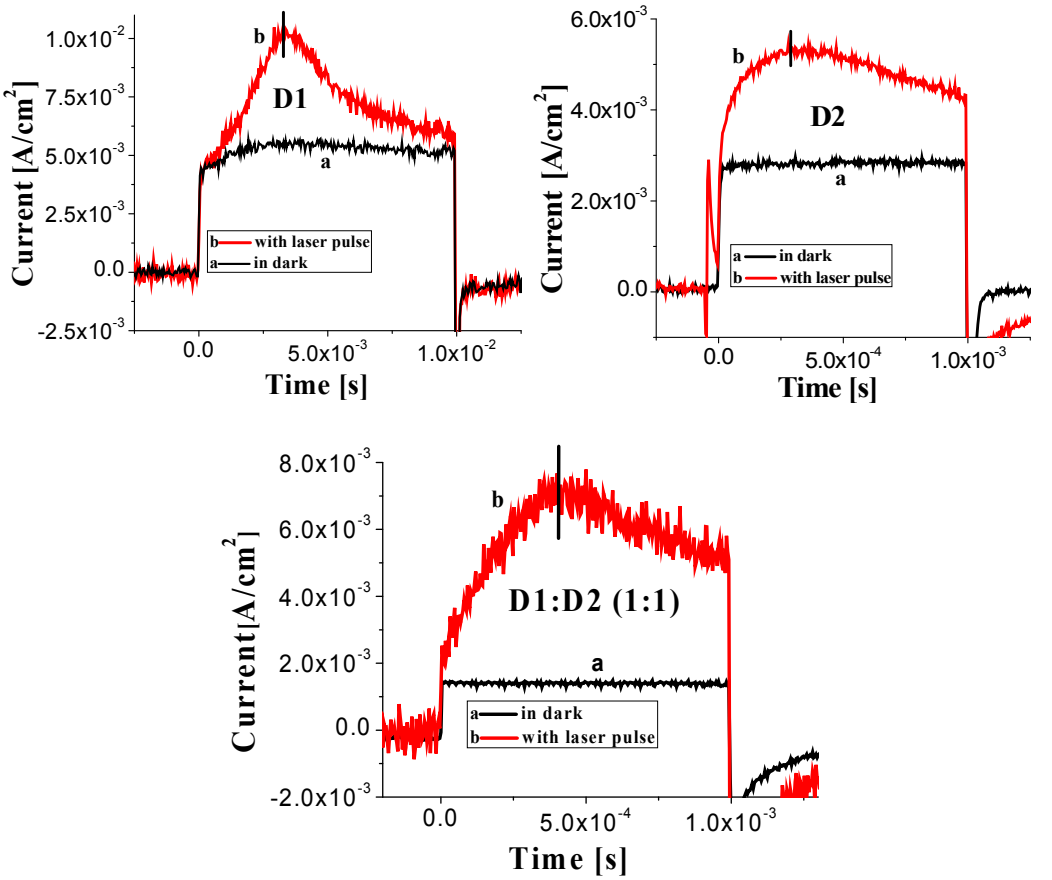

Figure 4.2. 5: *CELIV extraction current transients for **D1**, **D2,** and **D1**: **D2** (1:1) in the dark (a) and with laser pulse (b).*

Usually the mobility of fast charge carriers is measured in the blends using time-resolved methods since it dominates the transient photocurrent. However, the photovoltaic performance of solar cells is limited by the slower carrier mobility which is the hole transport in bulk heterojunction solar cells. We have intentionally measured carrier mobility in pristine polymers and their 1:1 mixture but not in their blends with PCBM in order to find the relation between carrier mobility and photovoltaic performances. Typical photo-CELIV extraction transients with initial capacitive current step and further extraction maximum are seen in both polymers (**D1**, **D2**) and their 1:1 mixture. From the extraction maximum in Figure 4.2.5 the unequilibrated mobility of photogenerated charge carriers is calculated. Hole mobility

(assuming electron mobility is negligible in p type polymers) for **D1** is $\mu = 1.8 \times 10^{-5}$ cm^2/ Vs (at electric field ≈ 18000 V/cm), for **D2** $\mu = 2 \times 10^{-6}$ cm^2 / Vs (at electric field ≈ 9400 V/cm) and for 1:1 mixing ratio of **D1** and **D2** an enhanced charge carrier mobility of $\mu = 2.6 \times 10^{-4}$ cm^2/Vs (at electric field ≈ 9600 V/cm) is obtained as compared to the single polymers **D1** and **D2**.

The dependence of carrier mobility with electric field was also studied as showen in Figure 4.2.6. Since Poole-Frenkel type dependence of carrier mobility on electric field is usually seen in disordered films [65], the charge carrier mobility is non-constant as a function of electric field and the electric field values, at which carrier mobility is measured, must be specified [312]. Figure 4.2.6 displays the elelctric field dependant mobility of **D1**, **D2**, and the **D1:D2** (1:1). It is observed that the mobility of **D1** increases with electric field while that of **D2** decreases at lower fields and become stable with increasing the field. The mobility of the mixture also looks relatively stable with change in electric field and the extraction was observed at very low electric fields. In photo CELIV the time gap between the application of laser and the applied voltage for the charge extraction matters in measuring the mobility. In Figure 4.2.6b the delay time dependence of the mobilities of the individual polymers and their mixtures show that the mobility of **D2** goes down with increasing delay time which shows that the generated carriers recombine faster as compared to **D1** and the mixture (**D1:D2**) which showed almost constant mobility with the time range shown.

So the CELIV result shows that when the two polymers are mixed they form a new intermolecular arrangement which is favorable to higher charge carrier mobility as compared to the individual polymers. The binary mixture also showed relatively stable carrier mobility with change in electric field and the delay time. This correlates

well with the better photovoltaic performance of the ternary blend as compared to the individual binary blends.

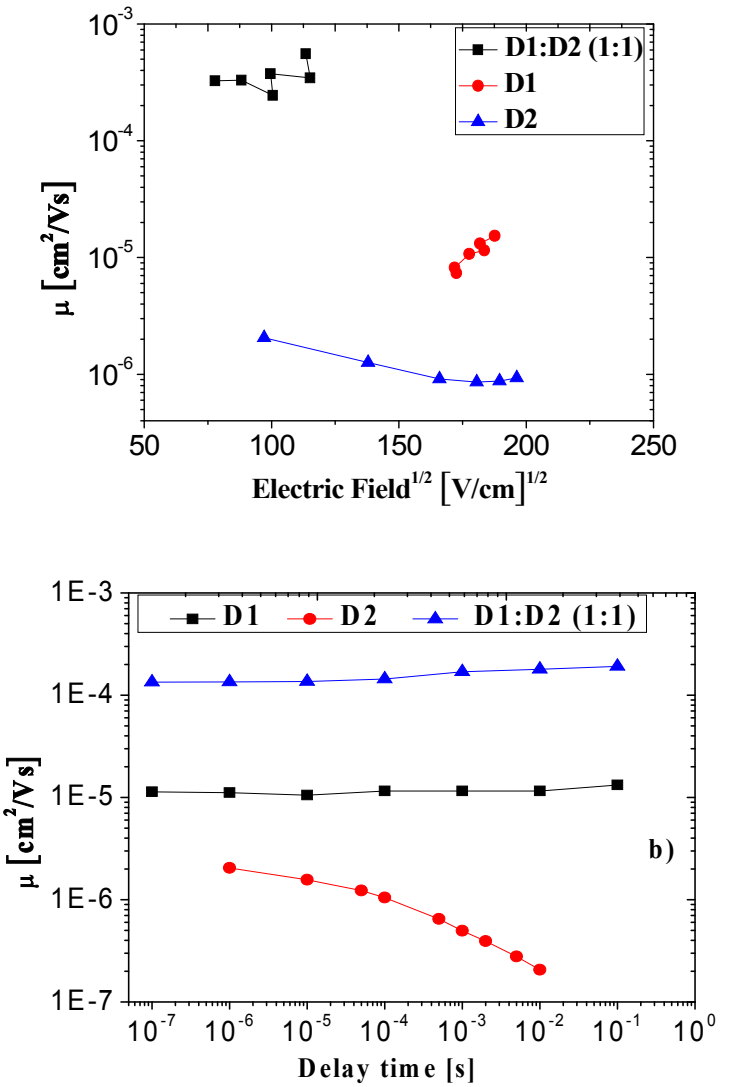

Figure 4.2. 6: *(a) Electric field dependance and (b) delay time dependence of charge carrier mobility for **D1**, **D2**, and their 1:1 mixture.*

In general, charge carrier transport is determined by the relation between material's chemical structure and film morphology. Surface roughness of polymer films shown in Figure 4.2.4 and Table 4.2.2 indicates very little difference. However, the delicate differences in film structure and level of disorder might not be visible from AFM

studies of film surface. In the past it has been observed that in contrast to polythiophenes, PPE-PPV structures demonstrate higher charge carrier mobility in the films with less degree of chain stacking [251]. Similarly, mixing of two polymers might disturb the chain stacking (since the polymer phase separate when mixed) and result in higher carrier mobilities. Another possible explanations for improved carrier mobility in the blends could be the change in film conductivity or polarizability, for which further studies are required.

4.2.3. Conclusion

Blending of two thiophene-based PPE-PPV polymers having identical conjugated backbone decorated with different volume fraction of hydrophobic alkoxy side chains, has lead to enhanced well stable charge carrier mobility and improved photovoltaic performance. This is proposed to be due to favourable nanoscale intermolecular arrangement of the blend while the two polymers are mixed as revealed by AFM images of the pure polymers, their mixtures and their corresponding blend nanomorphologies with PCBM.

4.3. Effect of varying one moiety in the backbone of thiophene containing PPE-PPV conjugated copolymers on charge carrier mobility and photovoltaic performance

4.3.1. Background

There is a growing interest in design, synthesis, and characterization of π-conjugated organic polymers since the discovery of conductivity in polyacetylene [72, 73, 76, 313] by aiming at the application of these polymers in the areas of photonic devices and plastic electronics [314, 315]. More attention has been given to them because of their attractive properties such as high absorption coefficient, light weight, solution processability, easy and cheap chemical/electrochemical synthesis methods as compared to the traditional inorganic semiconductors. Particularly the various routes in chemical synthesis which gives the possibility to tune the photophysical, electrochemical, and charge transport properties of polymers by varying the side chains [308, 309, 316] as well as the back bones of polymers and copolymers attract researchers in the area.

Among the known π-conjugated organic polymers polyphenylene vinylenes (PPVs) have been most widely investigated since the discovery of electroluminescence [317] and fast photoinduced electron transfer from its derivative poly[(2-methoxy-,5-(2'-ethyl-hexloxy)-p-phenylene vinylene)] (MEH-PPV) to fullerene (C_{60}) molecule [34] as organic photovoltaic devices [52, 293, 305, 318, 319]. PPV and its derivatives exhibit rather low oxidation potential (low lying HOMO) and low reduction potentials (high lying LUMO) which has a great impact on their oxidative degradation in the presence of small amount of water or oxygen [320, 321]. But derivatives of

polyphenyleneethynylene (PPE), in which backbone double bond in PPV has been replaced by the triple bond possess relatively high reduction potentials (low lying LUMO) [322] due to enhanced electron affinity of the polymer as a result of an electron withdrawing effect of the C≡C moiety [56, 323]. Moreover PPEs exhibit a highly rigid conjugated system with differences in polarization, molar extinction coefficients, and especially higher fluorescence quantum yields in non aggregated states, but very low fluorescence quantum yield in aggregated states due to very strong interchain interactions creating multifarious radiationless deactivation pathways [190, 324].

The attachment of electron donating alkoxy side chains to a PPV or PPE backbone supports solubility agents and enabling the processability of the polymers into thin films for various applications, and also lead to remarkable changes in the optical, electronic, and transport properties of solid state [308, 309].

The combination of PPE and PPV elements with the corresponding alkoxy side chains yields copolymers (PPE-PPVs) with better HOMO-LUMO values and optimized rigidty as compared to pure PPV polymers. Compared with PPEs, they exhibit red-shifted absorption and emission spectra and enhanced solid state photoluminescence quantum yield, due to reduced π-π interchain interactions and excimers formation caused by the presence of the PPV segments with lower aggregation tendency. Their enhanced electron affinity with respect to PPVs is reflected by higher absorption coefficients, lower lying HOMO levels, lower turn on voltages in light emitting diodes as well as higher open circuit voltages from fabricated organic solar cells [56].

Polythiophenes and their derivatives are good candidates for organic photovoltaic. In particular poly(3-hexylthiophene) (P3HT) has been extensively investigated as an

efficient donor materials for photovoltaic devices with high short circuit current density, above 10 mA/cm^2 and a power conversion efficiencies of above 5% [38, 197, 325]. The open circuit voltage (V_{OC}) of such devices generally does not exceed 650 mV [197,325] whereas poly(aryleneethynylene)-alt-poly(arylenevinylene) (PAE-PAV) based solar cell devices have shown higher V_{OC} up to 900 mV [53, 326].

Seeking for materials with a better photovoltaic performance (high V_{OC} and I_{SC} values) PAE-PAV copolymers were synthesized featuring thiophene moiety in the backbone the copolymers prepared showed higher V_{OC} values and good I_{SC} values in the range of 2 - 5 mA/cm^2 [57,327]. Varying the side chains as well as the backbone composition lead to significant differences in the photophysical, electrical properties and the morphology of the obtained copolymers which showed to affect their photovoltaic performance [304, 328, 329].

In this report the synthesis and characterization of three thiophene containing poly(p-phenylene-ethynylene)-alt-poly(p-phenylene-vinylene)s (PPE-PPV) copolymers with a general structural design of (Ph-C≡C-**X**-C≡C-Ph-CH=CH-Ph-CH=CH-) is described (Appendex B). Copolymers bearing identical alkoxy side chains at the phenylene rings but by possessing various moieties at the **X** position with thiophene, bithiophene or 3,4-ethylenedioxythiophene as shown in Figure 3.1.1c and Appendex B were prepared to study the effect of this structural alteration on the properties such as photophysics, electrical, charge carrier mobility, and morphology of the materials and its impact on their photovoltaic performance. In the ^{1}H NMR spectra of the polymers no aldehyde or phosphonate signals are visible indicating the full consumption of the monomers during polymerization process. Furthermore, the present siginals are broad and featureless which is another indication for the formation of high molecular

polymeric material. The absence of a carbonyl carbon signal in the ^{13}C NMR spectra of the polymers indicates the formation of polymer by Horner–Wadsworth–Emmons olefination reaction as well [332].

Due to the functionalization with octyloxy and 2-ethylhexyloxy side chains these polymers are well soluble in common organic solvents such as chloroform, chlorobenze and dichlorobenzene. The copolymer with a single thiophene ring at the X positions showed the highest V_{OC} and the copolymer with a bithiophene unit at X position showed the highest short-circuit current density and charge carrier mobility. Where as the copolymer with 3,4-ethylenedioxythiophene showed the lowest photovoltaic performance.

4.3.2. Results and discussion

4.3.2.1. Photophysics

The spectroscopic properties of the monomers **GD1, GD2**, and **GD3** as well as the polymers **GP1**, **GP2** and **GP3** have been studied in dilute chloroform and chlorobenzene solutions and in thin solid films spin coated from chlorobenzene solutions. Optical absorption of films of dialdehydes and the resulting polymer films and polymer films photoluminescence are shown in Figure 4.3.1. The photophysical data of the monomers (dialdehdes) and the polymers are summarized in Table 4.3.1, in a similar fashion with Table 4.1.4. Comparing the absorption spectra of the dialdehydes and their corresponding polymers a broadening, red shifted, and loss of structure were observed confirming the increase in conjugation length and molecular weight as the copolymers are formed [139]. The smooth nature of the absorption curves indicates that the polymers are amorphous with less π-π stacking nature [251].

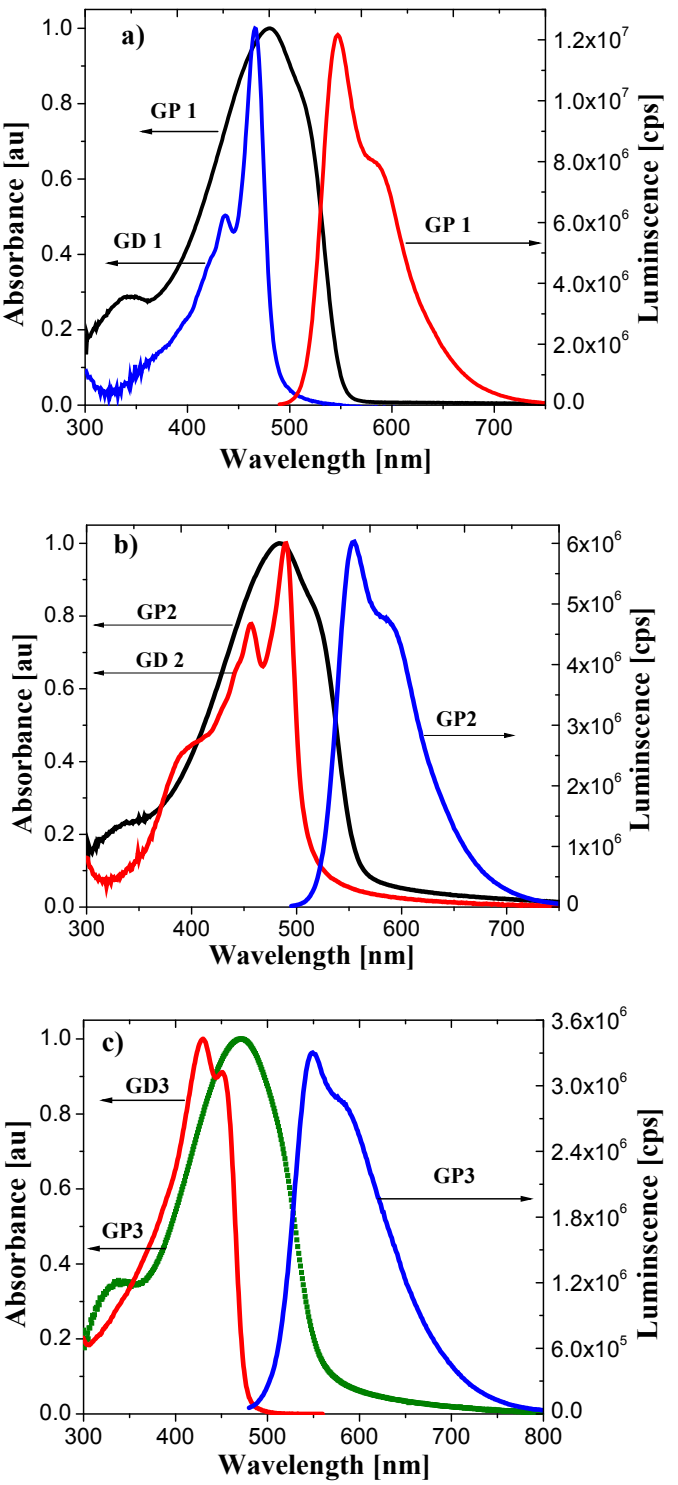

Figure 4.3. 1: *Optical absorption of solutions of dialdehydes and resulting polymer films, and polymer films photoluminescence a)* ***GD1*** *and* ***GP1*** *b)* ***GD2*** *and* ***GP2*** *c)* ***GD3****, and* ***GP3****.*

As shown in Figure 4.3.1. The photoluminescence spectra of all three polymers are structured with shoulders due to the 0 – 1 and 0 – 2 vibronic transitions. Particularly 0–1 vibronic transition is more pronounced due to thiophene which enhances the planarization in the S1-state [56, 57, 328].

The determined optical bandgaps using solutions as well as films spin coated from chlorobenzene solution (E_g opt) of the polymers are rather very close to each other 2.21 eV for **GP1**, 2.22 eV for **GP2**, and 2.18 eV for **GP3** as shown in Table 4.3.1. A blue shift in absorption of all the three polymers were observed as the solvent changed from chlorobenzene to chloroform. These E_g opt values for all polymers are consistent with the corresponding electrochemicaly determined (E_g elec), (Table 4.3.1 and Table 4.3.2). The copolymers show solvatochromism. A slight bathochromic shift in the absorption as well as photoluminescence were observed by changing the solvent from chloroform to chlorobenzene. This might be caused by the higher polarity of chlorobenzene which seems to cause differential stabilization excited states by solvation and charge transfer and thus, decrease in the energy gap [142, 333]. Thin film of the copolymers (spin coated from chlorobenzene) show a red shift in their absorption compared to the dilute solutions in the same solvent which is attributed to enhanced planarization of the conjugated backbones and ordering from the solutions to the compact bulk materials.

The fluorescence lifetime and quantum efficiencies of polymers in solutions were also found to be dependent on the nature of the applied solvent (see Table 4.3.1). In the less polar solvent, chloroform higher values were found for both parameters. Polymer **GP3** showed by far the lowest quantum efficiency of the three polymers which might be due to higher interchain interactions which favors excimer formation and non

radative decay that decreases the light emitting power efficiency [153]. Generally these polymers show rather low fluorescence quantum efficiency which was further confirmed by kinetic experiments. The fluorescence rate constants (k_f) of the polymers were found to be lower than the rate constant of the non radiative deactivation ($k_{nr} = (1-\Phi_f)/\tau$) in both solvents which might be associated with the heavy atom effect of sulphur in thiophene [56, 142].

Table 4.3. 1: *Photophysical data of* **GP1**, **GP2**, *and* **GP3** *polymers in solution* [s] *and film* [f].

Polymer	Solvent	$\lambda_{a(max)}$ (nm)	$\lambda_{f(max)}$ (nm)	$\Delta\nu_{af}$ (cm^{-1})	Φ_f (%)	τ (ns)	k_f (ns^{-1})	k_{nr} (ns^{-1})	E_g opt. (eV)	E_g elec. (eV)
GP1	$CHCl_3$ [s]	472	527	2210	48	0.72	0.67	0.72	2.41	2.35
	C_6H_5Cl [s]	479	533	2120	43	0.66	0.56	0.95	2.34	
	C_6H_5Cl [f]	481	547	2552	-	-	-	-	2.21	
GP2	$CHCl_3$ [s]	475	530	2180	60	0.75	0.80	0.53	2.40	2.31
	C_6H_5Cl [s]	479	536	2220	56	0.69	0.51	0.94	2.32	
	C_6H_5Cl [f]	484	554	2653	-	-	-	-	2.22	
GP3	$CHCl_3$ [s]	466	537	2840	27	0.81	0.21	1.02	2.36	2.34
	C_6H_5Cl [s]	471	540	2710	35	0.67	0.52	0.97	2.28	
	C_6H_5Cl [f]	476	543	2592	-	-	-	-	2.18	

4.3.2.2. Morphology

In order to investigate the morphology of the polymer films atomic force microscopy (AFM) measurements were conducted. The AFM images in Figure 4.3.2 show that films of **GP1** and **GP2** are rather rough with RMS roughness of 0.92 and 0.77 nm

and an average height of 3.86 nm and 3.631 nm, respectively while **GP3** forms a very smooth film with RMS roughness of 0.49 nm and average height of 2.66 nm. **GP1** and **GP2** are relatively rough as compared to **GP3** which has a very smooth and flat morphology. The highest rate constant of radiationless deactivation (Table 4.3. 1) for **GP3** might also be associated with this nature where there is intrachain and interchain communication in the entire structure for radiationless relaxation. In case of **GP1** and **GP2** the surfaces are relatively rough with grains due to the separation of the backbones by alkoxy side chains [153].

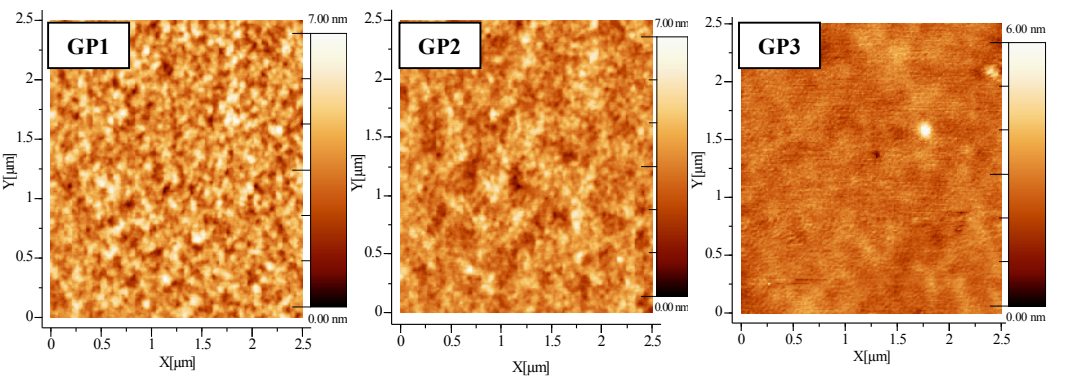

Figure 4.3. 2: *AFM images of spin coated films of polymers **GP1**, **GP2**, **GP3** on glass.*

4.3.2.3. Electrochemistry

For determining the redox potentials, the redox couple ferrocene/ferrocenium (Fc/Fc^{+}) was used as a standard. The corresponding HOMO and LUMO values were determined using the empirical relation $E^{HOMO/LUMO}$ = - [e (E_{onset} vs (quasi Ag/AgCl) - E_{onset} (Fc/Fc^{+}) Vs (quasi Ag/AgCl)] - 4.8 eV [118, 121]. - 4.8 eV is the ferroceene value with respect to vacuum which is equal to zero. E_{onset} (Fc/Fc^{+}) Vs (qusi Ag/AgCl) in this experiment was 400 mV. The CV curves of the three polymers are shown in Figure 4.3.3. The redox potentials from the CV and the calculated HOMO, LUMO, and the derived bandgap (E_g elec) values given in Table 4.3.2. **GP1** and **GP3**

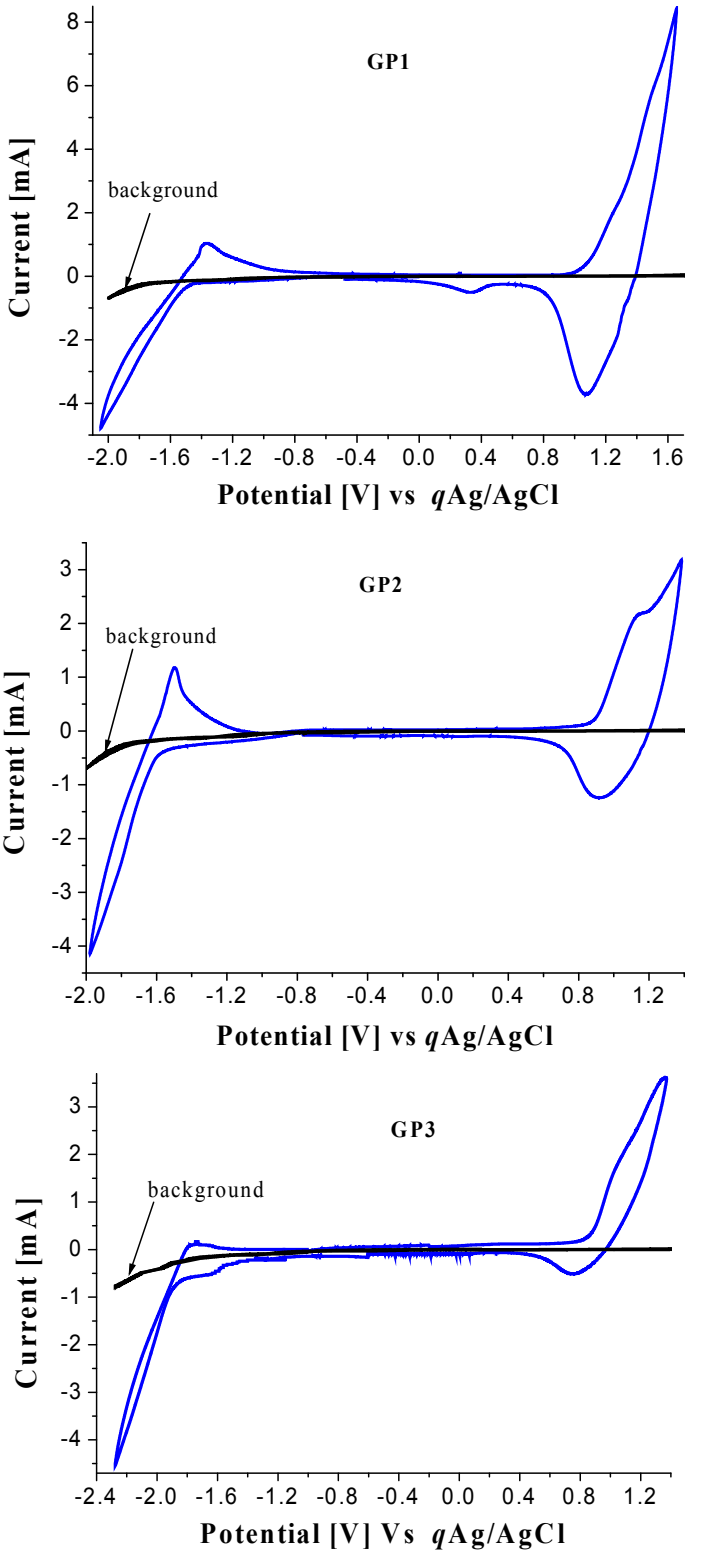

Figure 4.3. 3: *Cyclic voltammograms of* ***GP1***, **GP2**, *and* **GP3** *at Pt sheet working in 0.1 M* $(C_4H_9)_4NPF_6$/ CH_3CN *solution and quasi (q) Ag/AgCl reference electrode.*

show similar electrochemical bandgaps (2.35 eV) and a lower value was found for **GP2** (2.31 eV). **GP1** possesses the highest oxidation potential (0.95 V) as copmpared to the the two polymers **GP2** (0.86 V) and **GP3** (0. 84 V).

Table 4.3. 2: *Summary of the electrochemical results of **GP1**, **GP2**, and **GP3** with the corresponding Mw and PDI values.*

Polymer	Mw g/mol	PDI	E^{ox} onset (V)	E^{red} onset (V)	HOMO (eV)	LUMO (eV)	Eg (eV)
GP1	54534	2.98	0.95	-1.41	5.35	3.0	2.35
GP2	33700	4.2	0.86	-1.45	5.26	2.95	2.31
GP3	84250	6.74	0.84	-1.50	5.24	2.90	2.34

4.3.2.4. Charge transport study

The current extraction transients from the CELIV experiment for **GP1**, **GP2**, and **GP3** are shown in Figure 4.3.4. The very initial current step *j(0)* (displacement current) was observed in each sample caused by the geometrical capacity of the sample and it is used to estimate the sample thickness. The following increasing extraction current is caused by the photoconductivity of the sample when the mobile charge carriers are being extracted from the film.

From the extraction maximum the unequilibrated mobility of photogenerated charge carriers is calculated $\mu = 1.32 \times 10^{-4}$ cm^2/Vs (at an electric field of 21810 V/cm) for **GP1**, $\mu = 1.53 \times 10^{-4}$ cm^2/Vs (at an electric field of 12070 V/cm) for **GP2**, and $\mu = 8.61 \times 10^{-5}$ cm^2/Vs (at an electric field of 21810 V/cm) for **GP3**.

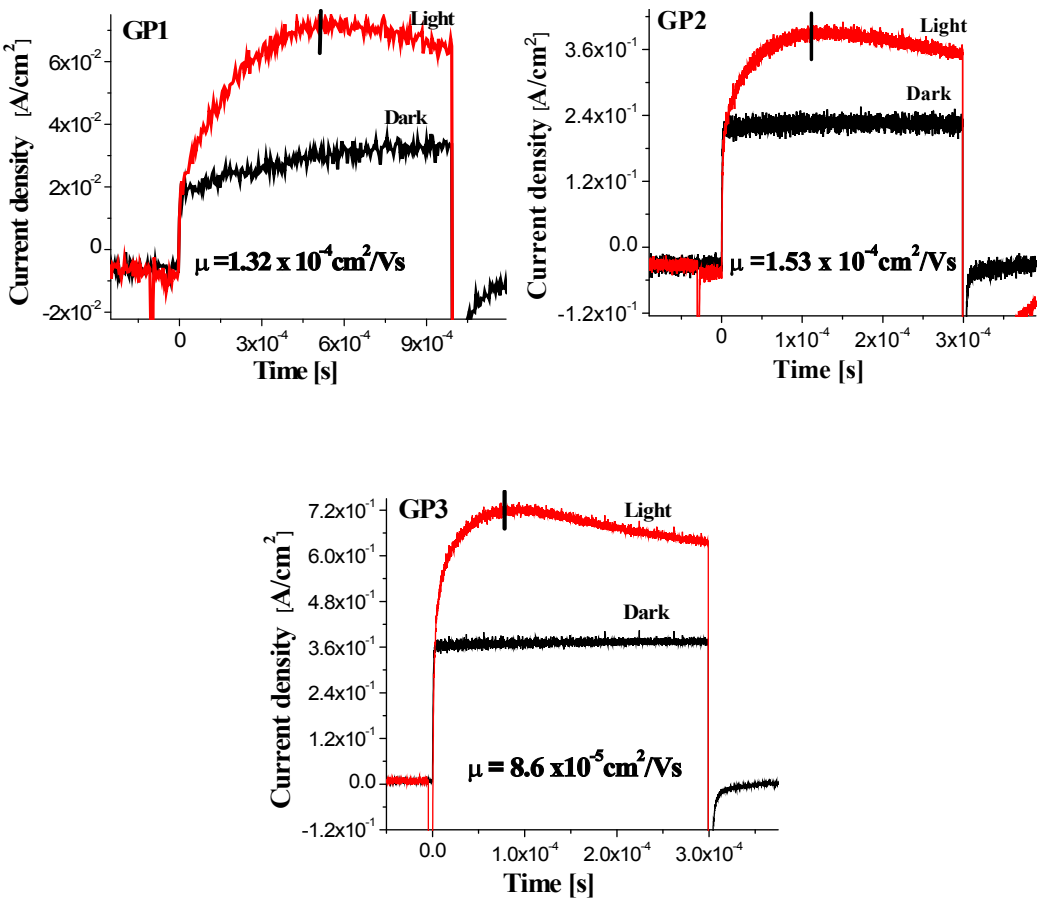

Figure 4.3. 4: *Photo CELIV extraction current transients for **GP1**, **GP2**, and **GP3**.*

Based on these results the charge carrier mobility of polymer **GP3** is lower than that of other two polymers **GP1** and **GP2** which might be due to its extremely high PDI value as shown in Table 4.3.2 which is a function of irregularity of the chains that impede the transport [153], where as **GP2** showed relatively higher charge carrier mobility which might be due to better plannarity of the polymer as a result of the bithiophene moity compared to the single thiophene in case of **GP1**.

4.3.2.5. Bulk heterojunction photovoltaic performance

For the fabrication of bulk heterojunction solar cells, solutions were prepared with polymer/acceptor ratios of 1:1, 1:2, and 1: 3 (30 mg per milliliter of chlorobenzene). [6,6]-phenyl-C_{61}-butyric acid methyl ester (PCBM) was used as an acceptor.

Poly(3,4-ethylene dioxythiophene)/poly(styrenesulfonate) (PEDOT:PSS) (Baytron PH) stirred overnight and filtered was spin coated on top of ITO with 2000 rpm to yield a film of 80 nm thickness after drying (overnight in open air). The polymer:PCBM solutions (filtered through 0.45 μm filters) were spin coated on top of PEDOT:PSS films at 1000 rpm.

Figure 4.3.13 shows the current voltage (IV) characteristics of the solar cells fabricated from **GP1**. As can be seen from Figure 4.3.5a the degree of rectification gets improved going from 1:1 to 1:2 and from 1:2 to 1:3 **GP1**:PCBM ratio which indicates that the acceptor play a role on the nature of the diode. There is a significant photocurrent generated from the devices. As it is shown in the overlay plot in Figure 4.3.5b, increasing the amount of PCBM ratio from 1:1 to 1:3 improves the V_{OC} from 750 mV to 930 mV as well as the J_{SC} which increases significantly from 1.28 mA/cm^2 (at 1:1 ratio) to 1.95 mA/cm^2 (1:3 ratio). Eventhough the V_{OC} is a function of the HOMO of the donor and LUMO of the acceptor [31, 209, 221] it is also highly dependant on the parallel (shunt) resistance which is the influence of local shunts between the two electrodes that creates additional current paths circumventing the diode. So the increase in the amount of PCBM which showed an improvement in the rectification of the diode in the dark as well as an increase in V_{OC} is due to better percolated paths to the electrodes resulted from better phase separations as shown in the AFM images (Figure 4.3.8) and increased shunt resistance [200, 208, 223, 224]. With the **GP1**:PCBM (1:3 ratio) the highest J_{SC} (1.95 mA/cm^2) and the highest V_{OC} (930 mV) were observed (see also Table 4.3.3) which is consistent to its highest HOMO level compared to **GP2** and **GP3**. The fill factor values of 42% and 40% in the devices with 1:2 and 1:3 ratios, respectively are also relatively best values in these groups of polymers.

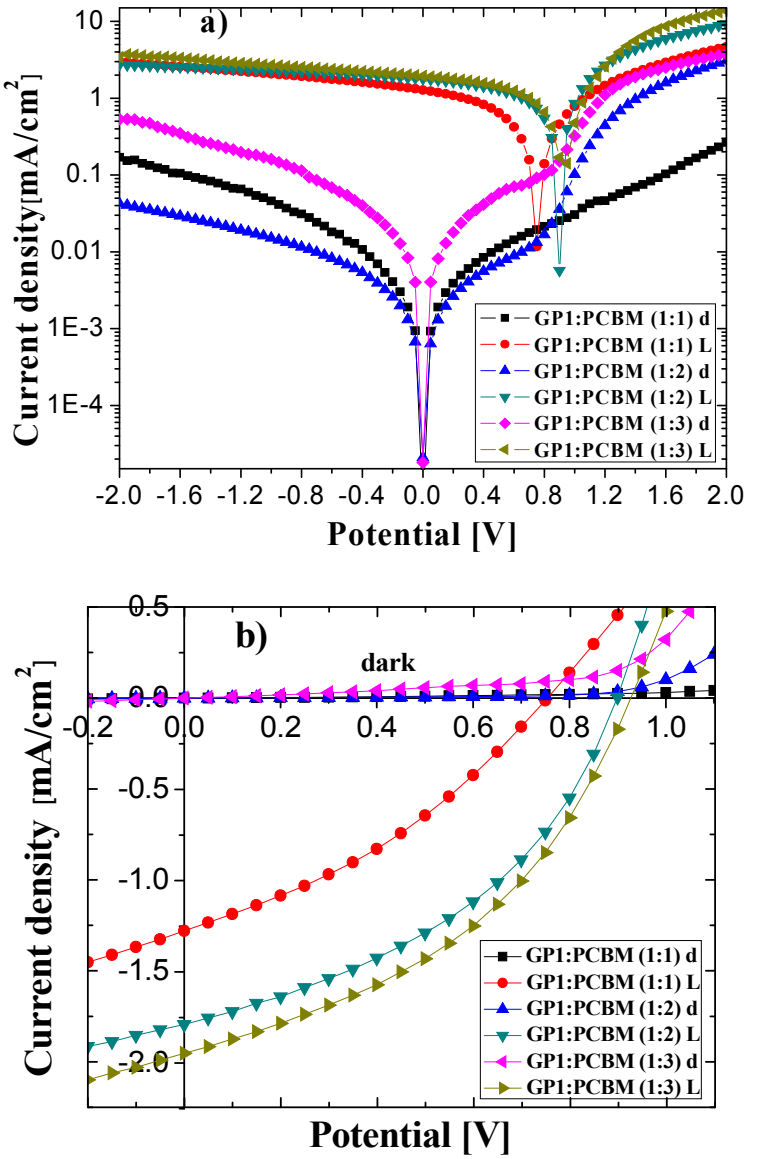

Figure 4.3. 5: *I-V curves of photovoltaic devices in dark (d) and under illumination (L) with different* **GP1***: PCBM ratios a) logarithmic scale b) linear scale.*

The photoluminescence spectra of the solar cells made in Figure 4.3.6, showed quenching of fluorescence of the polymer which is an indication of an efficient photoinduced electron transfer from the polymer to the acceptor PCBM [34]. With increasing the PCBM ratio the degree of quenching increases as shown in the Figure 4.3.6 inset.

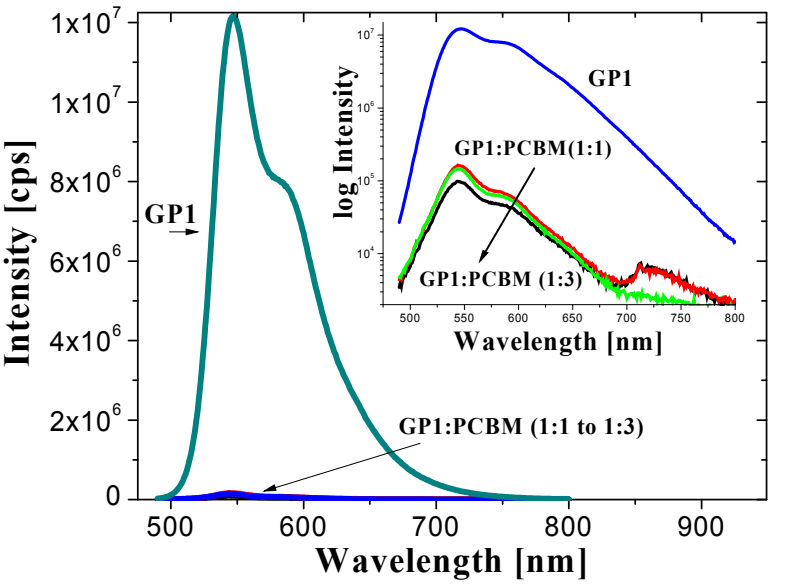

Figure 4.3. 6: *Photoluminescence spectra of the solar cells prepared from varying ratios of **GP1**:PCBM and pure **GP1** films, inset is the logarithmic scale.*

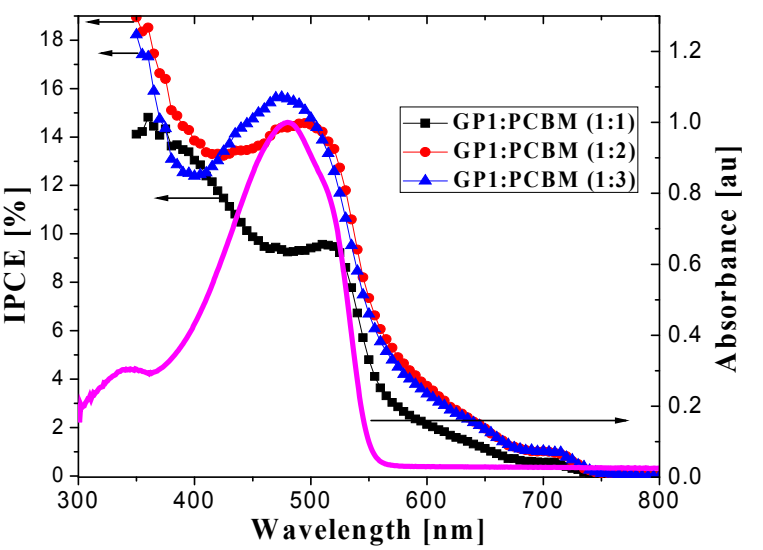

Figure 4.3. 7: *Overlay plot of the IPCE of devices with 1:1, 1:2, 1:3, **GP1**:PCBM ratios and absorption specra of **GP1** thin film.*

As dipicted in Figure 4.3.7, the incident photon to current conversion efficiency (IPCE) of the devices showed maximum value (~ 15%) with (1:3) **GP1**: PCBM ratio at the absorption maximum which is consistent with the highest J_{SC} at this ratio. All

the IPCE curves correlate well with the absorption spectrum of **GP1**. The contribution of the acceptor to produce photocurrent by itself as a semiconductor is also clearly reflected in the IPCE curve from 350 - 400 nm and a hump at 710 nm.

The morphology of the solar cell devices were investigated using AFM (Figure 4.3.8). There is a significant difference in the surface morphology of the devices depending on the PCBM concentration. As shown in the AFM images the device with 1:1 **GP1**:PCBM ratio exhibits very smooth surface with no distinct phase separation (RMS roughness 1.48 nm, average height 4.92 nm). Significant phase separation were found for devices with 1:2 and 1:3 polymer:PCBM ratios (Figure 4.3.8) which is accompanied with an increased in RMS roughness and average height 19.89 and 55.17nm for 1:2 ratio, 27.93 and 78.16 nm for 1:3 ratio respectively. The increased J_{SC} and V_{OC} values with 1:2 and 1:3 ratios as compared to 1:1 ratio might be associated with a better phase separation as PCBM coalesce in larger domain as clearly shown (Fig 4.3.8) which creates better paths. The best performance with an open circuit voltage of 930 mV and fill factor of 40% in this group of polymer:PCBM blends was obtained for the system with **GP1**:PCBM at ratio of 1:3.

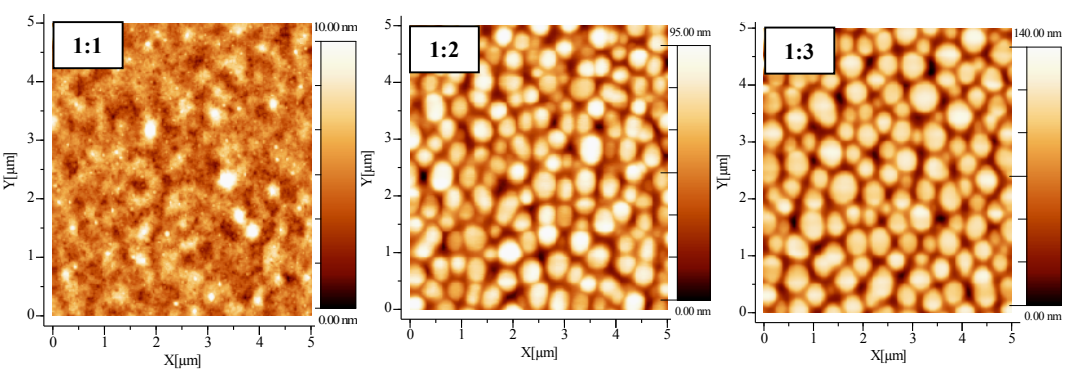

Figure 4.3. 8: *AFM images of **GP1**:PCBM blends 1:1 to 1:3 ratio from left to right.*

Figure 4.3.9 shows the I-V characteristics of the solar cells prepared from **GP2**. The devices with **GP2** show the same trend as observed for the **GP1** system. The nature of the diode in the dark gets better as we go from 1:1 to 1:3 (**GP2**:PCBM) ratios as indicated by improved rectification characteristic. This is due to improved paths and

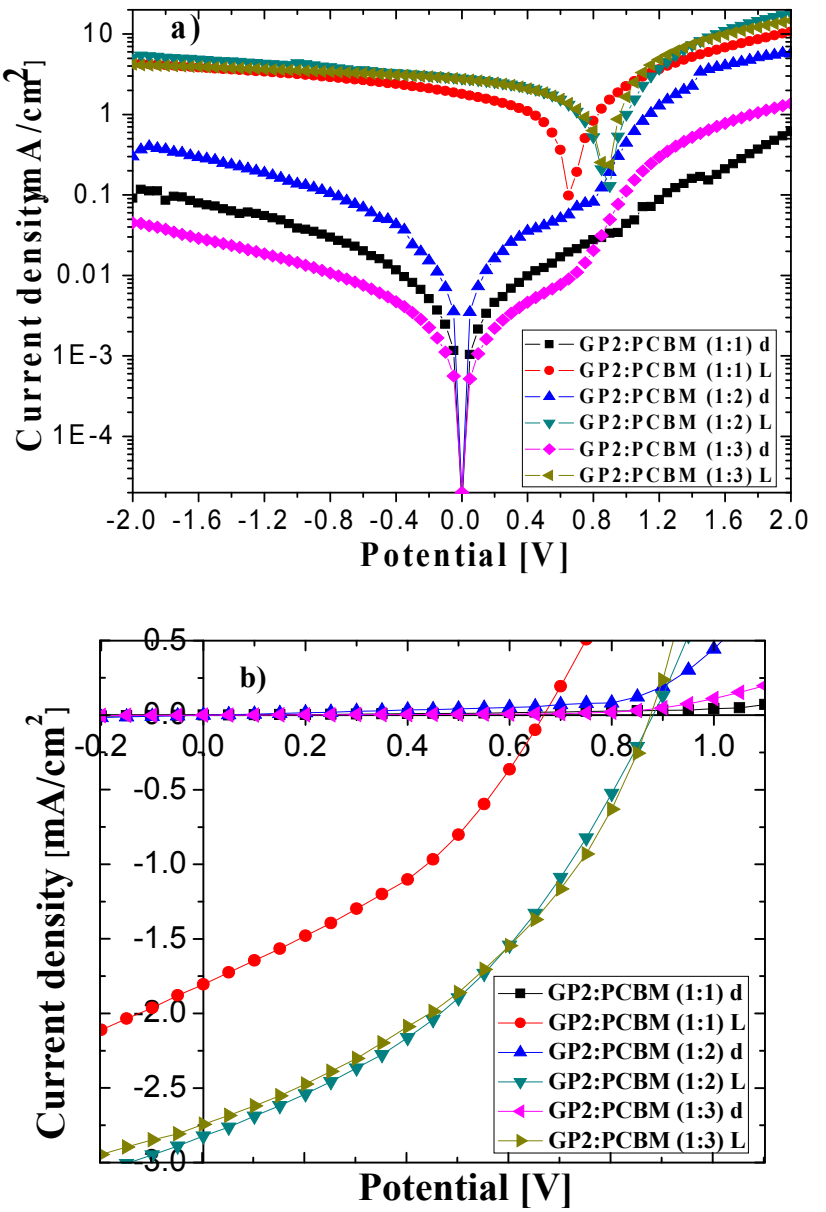

Figure 4.3. 9: *I-V curves of photovoltaic devices in dark (d) and under illumination (L) with different **GP2**:PCBM ratios a) logarithmic scale b) linear scale.*

reduced morphology defects in the diode as a result of phase separated domains of the donor and the acceptor in the active layer of the device.

With an increase in concentration of the acceptor from 1:1 to 1:2, the J_{SC} increased from 1.8 to 2.8 mA/cm^2 with a significant increase in V_{OC} from 670 mV to 890 mV due to the decrease in the serial resistance and an increase of the shunt resistance by better phase separation as shown in the AFM images (Fig 4.3.12) [45, 46, 47, 48]. With 1:3 ratios the current as well as the V_{OC} looks very similar with 1:2 ratio as shown in Figure 4.3.9b and Table 4.3.3.

The fluorescence spectra of the solar cells showed quenching of the polymer fluorescence which is an indication of an efficient photoinduced electron transfer from the polymer to the acceptor PCBM [34] (Figure 4.3.10).

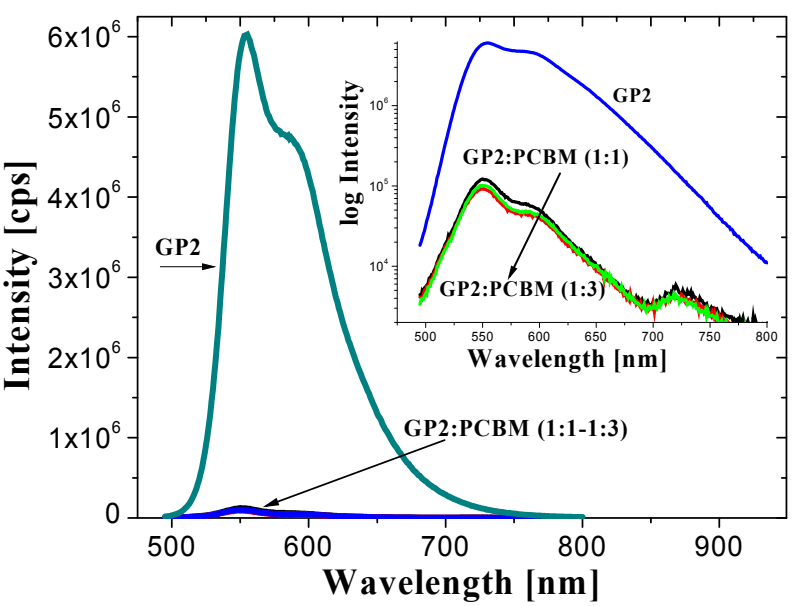

Figure 4.3. 10: *Photoluminescence spectra of the solar cells prepared from varying ratios of **GP1**:PCBM and pure **GP1** films, inset is the logarithmic scale.*

As shown in Figure 4.3.11, the IPCE of the devices made showed maximium (~ 18%) with 1:2 and 1:3 **GP1**:PCBM ratios at the absorption maximum of the pure polymer which is consistent with the highest J_{SC} with these ratio. All the IPCE curves match with the absorption spectrum. The highest short circuit current value (2.8 mA/cm^2) in these groups of polymers was obtained from **GP2**:PCBM with 1:2 ratio as this polymer showed relatively highest carrier mobility and better PDI value of 2.98 which improves the transport.

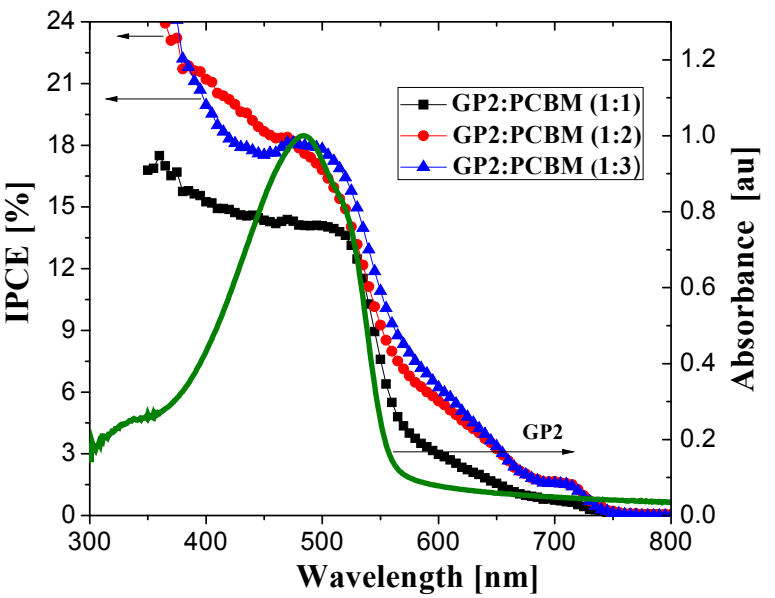

Figure 4.3. 11: *Overlay plot of the IPCE of devices with 1:1, 1:2, 1:3, **GP2**:PCBM ratios and absorption spectra of **GP2** thin film.*

Surface morphology of the solar cell devices measured using AFM in Figure 4.3.12, showed a significant difference in the morphology of the devices with change in concentration of PCBM. With 1:1 (**GP2**:PCBM) ratio the surface showed RMS roughness of 0.8361 with average height 5.0551 indicaing the surface is very smooth with no clear phase separation. As the concentration increased from 1:1 to 1:2 a clear phase separation with RMS roughness of 14.83 nm and average height 58.3879 nm

resulting a significant increase in both J_{SC} and V_{OC} was observed. Further increase in PCBM concentration to 1:3 ratio increased the RMS roughness to 28.53 nm and average height 81.95 nm but both J_{SC} and V_{OC} started to decrease which might be due to extreme phase separation beyond the diffusion length as clearly seen in the images.

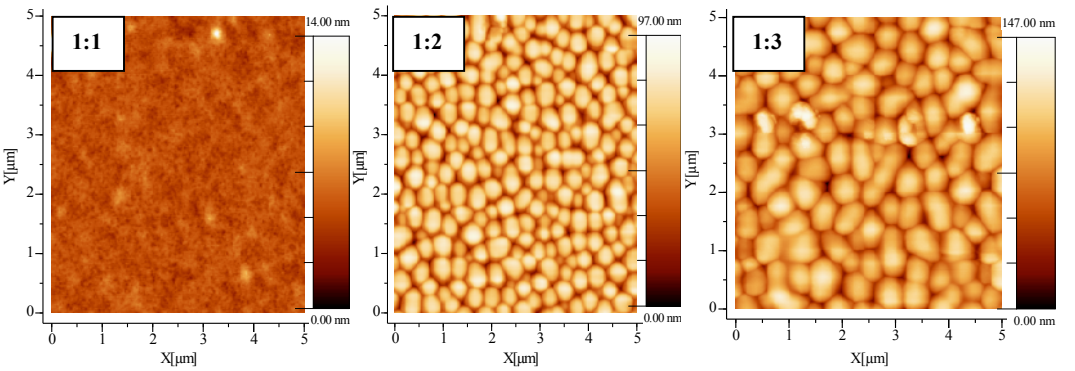

Figure 4.3. 12: *AFM images of **GP2**: PCBM, 1:1 to 1:3 ratios from left to right*

The photovoltaic performance of the solar cells fabricated from **GP3**:PCBM blends is depicted in Figure 4.3.13. The rectifications of the devices in the dark are not as good as the other systems based on polymers **GP1** and **GP2**. Though the diodes rectification in the dark is too small there is a significant photocurrent generation in the devices under illumination.

The amount of the acceptor used in the device also matters for the performance of the solar cell. As it is shown in the overlay plot in Figure 4.3.13b, increasing the amount of PCBM from 1:1 to 1:3 (**GP3**:PCBM) ratio changes the V_{OC} from 600 mV to 815 mV as well as the J_{SC} from 1.17 to 1.45 mA/cm^2. With 1:3 (**GP3**: PCBM) ratio the highest J_{SC} of 1.45 mA/cm^2 and the highest V_{OC} of 815 mV was obtained from this polymer as shown in Table 4.3.3.

The photoluminescence spectra of the solar cells made in Figure 4.3.14 showed quenching of fluorescence of the polymer which is an indication of an efficient photoinduced electron transfer from the polymer to the acceptor PCBM [34]. With increasing the PCBM ratio the degree of quenching slightly increases as shown in the inset.

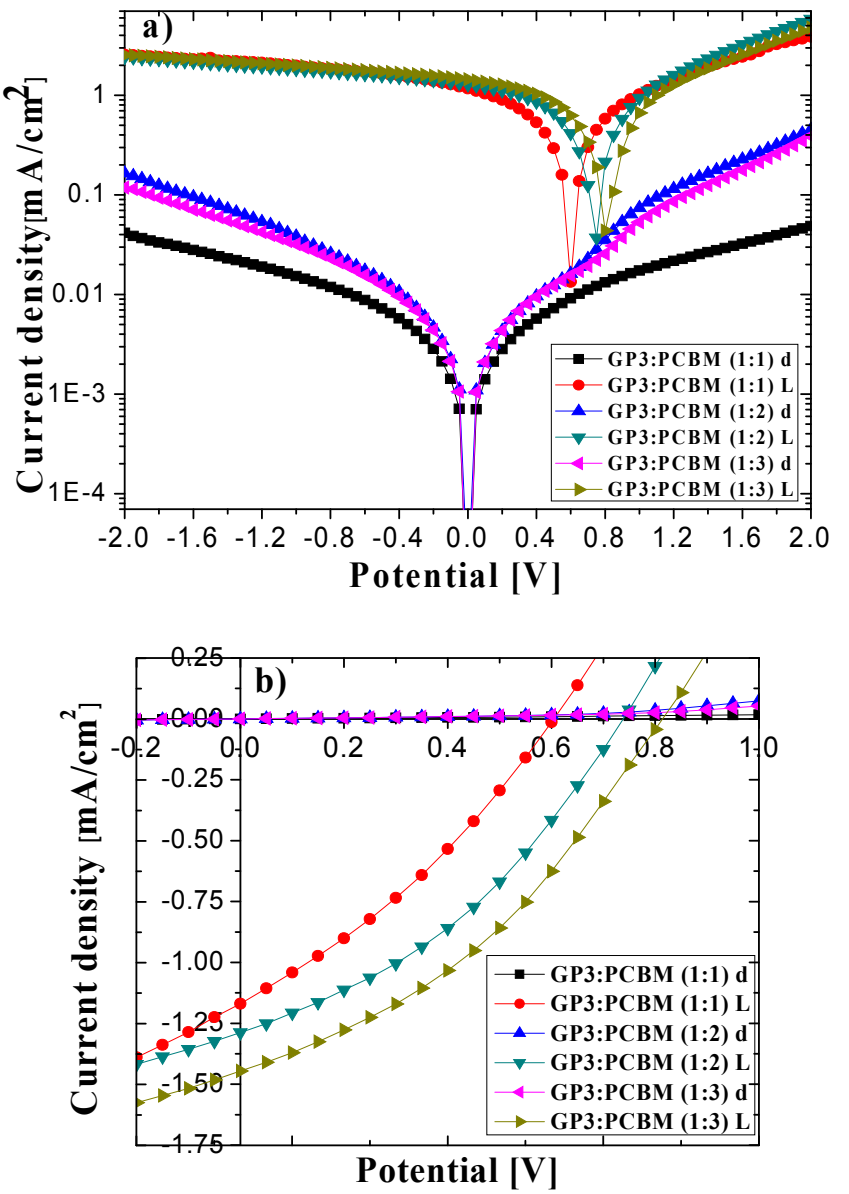

Figure 4.3. 13: *I-V curves of **GP3**:PCBM at different ratios a) logarithmic scale b) linear scale in dark (d) and under illumination (L).*

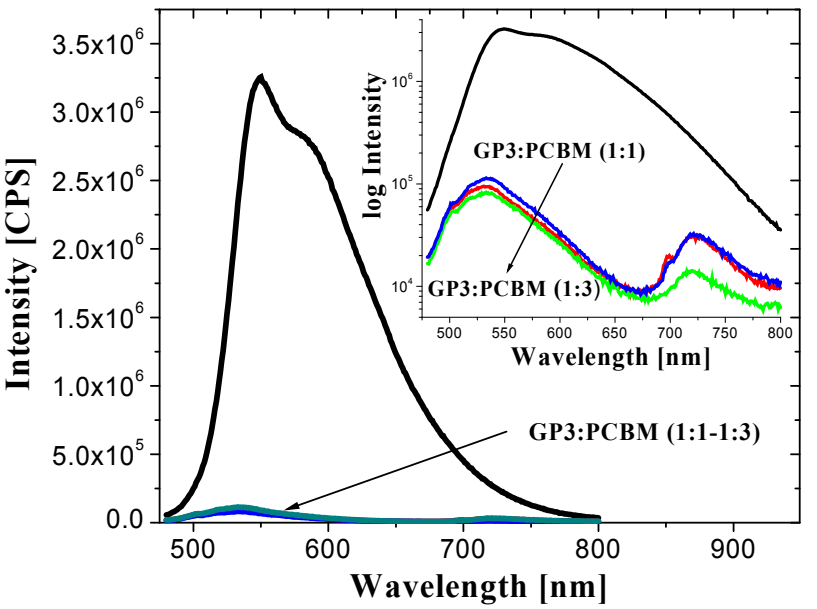

Figure 4.3. 14: *Photoluminescence spectra of the solar cells prepared from varying ratios of **GP1**:PCBM and pure **GP1** films, inset is the logarithmic scale.*

As shown in Figure 4.3.15 IPCE of the devices made showed (~10.4%) with 1:3 **GP3** to PCBM ratio with a slight blue shift from the absorption maximum. All the IPCE curves match with the absorption spectrum with slight blue shift of the maximum. The contribution of PCBM to the photocurrent were clearly reflected in the IPCE curve .

The surface morphology of the solar cell devices made showed an increase in phase separation with an increase in the concentration of PCBM. As it can be seen from the AFM images (Figure 4.3.16) with **GP3**:PCBM of 1:1 ratio the surface roughness is lower with RMS roughness of 3.11 nm, average height of 7.3083 nm. In the same way for the other two polymers **GP1** and **GP2** an increasment in phase separation was observed with increasing PCBM amount to 1:2 showing RMS roughness of 13.23 nm with average height of 42.22 nm. The best performing ratio 1:3 of **GP3** to PCBM showed RMS roughness of 16.43 nm and average height of 64.76 nm.

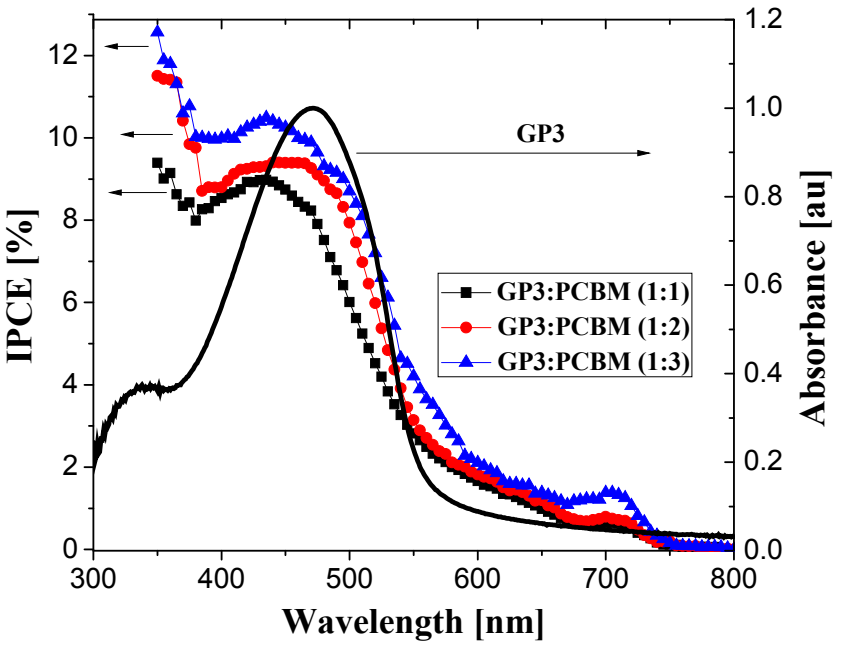

Figure 4.3. 15: *Overlay plot of the IPCE of devices with 1:1, 1:2, 1:3,* ***GP3****:PCBM ratios and absorption spectra of* ***GP3*** *thin film.*

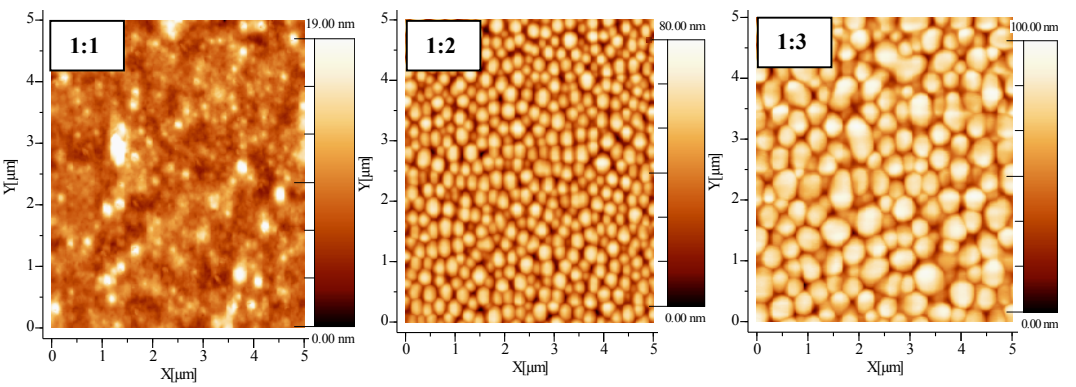

Figure 4.3. 16: *AFM images of* ***GP3****:PCBM solar cells from 1:1 to 1:3 ratios from left to right*

As compared to the other two polymers **GP1** and **GP2** with the same 1:1 ratio with PCBM **GP3** looks slightly immiscible with PCBM because its roughness at this ratio is relatively higher. This might be the reason why this polymer is less efficient than **GP1** and **GP2**. Eventhough optimum phase separation is a key factor for better

performance there should be some degree of miscibility of the acceptor and the donor materials [227]. In case of **GP3**, the very smooth nature of the pure polymer lead to early phase separation at 1:1 ratio as compared to the **GP1** and **GP2**. The highest PDI value of 6.74 that also humpers the transport and reduced the carrier mobility observed in the CELIV experiment might be the reason for its lowest I_{SC} values.

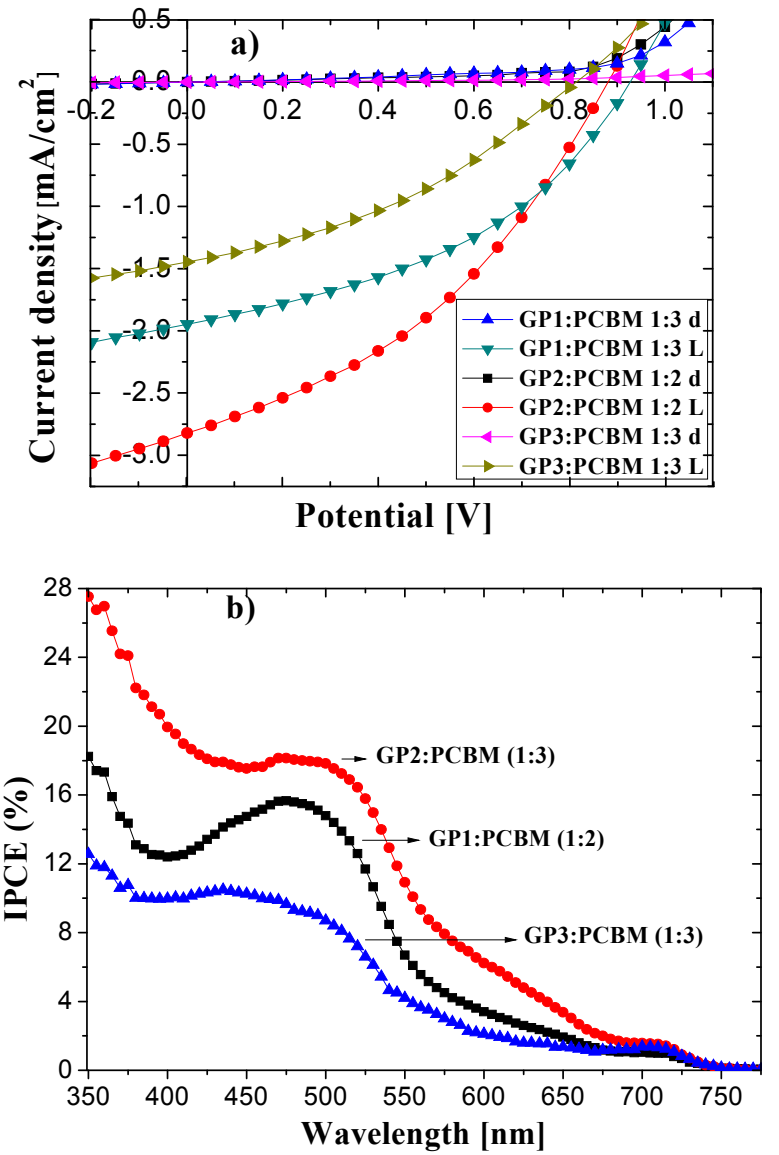

Figure 4.3. 17: *Overlay plots of a) I-V characteristics in dark (d) and under illumination (L) b) IPCE of **GP1**, **GP2** and **GP3** with PCBM at their best performance ratios.*

Overlay plot of the I-V curves with their corresponding IPCE of the solar cells fabricated from three polymers with their best performance ratio with PCBM are shown in Figure 4.3.17. From the figures we can see the photocurrents generated from the devices made, **GP2**:PCBM (1:2) gives the highest short-circuit current density and highest IPCE value among the three polymers which is consistent with its highest charge carrier mobility. Interms of $V_{OC,}$ **GP1**:PCBM (1:3) generates the highest open circuit potential value of 930 mV resulted from its higher HOMO level compared to the **GP2** and **GP3**. In general all the polymers showed higher V_{OC} values as compaired to the well studied P3HT and other thiohene based polymers.

The summery of the best photovoltaic performance of the devices made at different polymer PCBM ratios of the three polymers is shown in Table 4.3.3 to see the similarities and differences.

Table 4.3. 3: *Summary of the I-V characteristic of the best bulk heterojunction solar cell devices fabricated from **GP1**, **GP2** and **GP3** blended with PCBM in three different ratios.*

Polymer:PCBM (Ratio)	**GP1**:PCBM (1:1)	**GP1**:PCBM (1:2)	**GP1**:PCBM (1:3)	**GP2**:PCBM (1:1)	**GP2**:PCBM (1:2)	**GP2**:PCBM (1:3)	**GP3**:PCBM (1:1)	**GP3**:PCBM (1:2)	**GP3**:PCBM (1:3)
V_{OC} [mV]	750	900	930	670	890	880	600	750	815
J_{SC} [mA/cm^2]	1.28	1.81	1.95	1.8	2.8	2.75	1.17	1.29	1.45
FF [%]	35	42	40	38	36	38	32	36	37
η [%]	0.34	0.68	0.74	0.46	0.96	0.92	0.22	0.35	0.43

4.3.3. Conclusion

Copolymers **GP1**, **GP2** and **GP3** were synthesized with the general backbone (Ph-C≡C-**X**-C≡C-Ph-CH=CH-Ph-CH=CH-) with identical alkoxy side chain distribution at the phenylene ring and various moieties at the **X** position thiophene, bithiophene and 3,4-ethylene dioxythiophene, respectively. GPC investigations, photophysical, electrochemical and charge carrier transport characterization and comparison were made and bulk heterojunction solar cell devices were fabricated and characterized.

It was found that polymers **GP1** and **GP3** have very close similarity interms of their optical as well as electrochemical bandgaps where as **GP2** has lower bandgap as compared to the two. Interms of charge carrier mobilites (μ), **GP1** and **GP2** were found to have higher values $\mu = 1.32 \times 10^{-4}$ and $\mu = 1.53 \times 10^{-4}$ compared to $\mu = 8.61 \times 10^{-5}$ for **GP3**. Bulk heterojunction solar cells prepared from each polymer exhibited improved performance at higher PCBM:polymer ratio of 3:1.for **GP1** and **GP3** and 2:1 ratio for **GP2**. Comparing the photovoltaic performance it was found that the system based on **GP1** was the best in terms of V_{OC} (~930 mV) which is consistent with its higher HOMO level where as **GP2** is the best among the three interms of J_{SC} which might be associated with its higher mobility. The performance of **GP3** was found to be the least which might be associated with its high PDI value of 6.74 which makes its charge transport bad as indicated by its low mobility value and its lower miscibility nature with PCBM.

4.4. Effect of chemical doping on photophysical and photovoltaic performance of P3HT/PCBM Bulk heterojunction solar cells

4.4.1. Background

Research on conducting polymers have been started extensively since 1977 when polyacetylene was demonstrated as the simplest conjugated polymer that can be made electrically conductive through a chemical doping (redox doping) reaction. It involves partial reduction or oxidation (n-type or p-type doping) of its spatially extended π-bonding system [313, 334 - 336]. This discovery induced motivations for further research in the areas of chemical and electrochemical synthesis, spectroscopic, spectroelectrochemical, structural and electrical characterization of conducting polymers. Conducting polymers such as polypyrrole, polyaniline, polythiophene, polyparaphenylene, and their copolymers, composites or blends, etc were among the most investigated ones. Because of their interesting properties conducting polymers were used in wide spread technological applications such as batteries, capacitors, sensors, field effect transistors, light emitting diodes, organic solar cells etc [314].

Among the above mentioned group of conducting polymers, polythiophenes are attracting the interest of researchers because of their good environmental stability, easy processability, and easy modification of the properties by varying the synthesis parameters [97]. They can be synthesized by both electrochemical and chemical polymerization techniques. Particularly poly(3-alkylthiophenes) are soluble in common organic solvents as well as melt processable, having excellent electronic, optical, and photonic properties suitable for various device applications [97]. Regioregular poly(3-alkylthiophene)s (P3ATs) have been found to be among the most promising conjugated polymers. They can be used as photoactive materials and hole

transporters in bulk heterojunction polymer solar cells [337, 338]. Power conversion efficiencies (PCE) exceeding 4% under 100 mW/cm^2, AM1.5 white light illumination from a solar simulator have been reported for poly (3-hexylthiophene)/PCBM systems [37, 222, 241].

To increase this efficiency further a lot of research works have been undergoing to minimize the efficiency limiting factors by widening light absorption spectrum, going for efficient exciton diffusion and dissociation and improved charge transport to the respective electrodes [206, 207, 339]. An optimum bicontinous interpenetrating nanoscale network blend morphology of both donor and acceptor materials that leads to efficient exciton diffusion, dissociation, and the charge transport is the main requirement in organic bulk heterojunction solar cells [227, 229, 340]. Among the undergoing efforts are 1) choosing the appropriate processing solvent for best pefromnace attributed to solvation-induced blend morphology and better absorption [230, 231], 2) Solvent additives to the host solvent, such as alkyldithioles, alkylhalides have been used for a better morphology by modifying the degree of intermolecular interaction in order to achieve phase segregation with the ideal domain size for optimal exciton dissociation and improved transport (charge carrier mobility) of the solar cell blend [233 - 235, 296, 341, 342]. The other approach is dopant additives for doping induced increasing in dielectric constant and conductivity. This resulted in decreased series resistance, efficient exciton dissociation, changes in the electric-field distribution, and built-in voltage which also increases the charge carrier mobility of the blend for better photovoltaic performance [343 - 345].

Doping induces changes in the electronic properties of the polymer and its structure or morphology due to the incorporation of the dopant ions [73,76]. In this work 1:1 ratio

of P3HT:PCBM solutions have been prepared by dissolving in chlorobenzene containing four different molar concentrations ($1 \times 10^{-3}\ M$, $5 \times 10^{-4}\ M$, $2 \times 10^{-4}\ M$ and $2 \times 10^{-5}\ M$) of ferric chloride ($FeCl_3$) for doping of P3HT chemically at different levels. The bulk heterojunction solar cell devices prepared from these solutions were characterized to study the effect of doping on photovoltaic performance. Scheme 4.1.1 shows the expected electronic and structural changes in the chemical doping reaction between P3HT and $FeCl_3$.

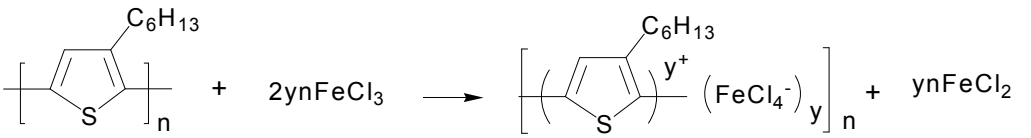

Scheme 4.4.1: *Oxidative doping reaction of P3HT with $FeCl_3$ to P3HT-$FeCl_4^-$ charge transfer complex.*

4.4.2. Results and discussions

Photophysics

The photophysical characterization of P3HT films as well as its solution is shown in Figure 4.4.1. A well structured broader spectra with significant red shift in both absorption and emission are observed as we go from solution to films. This is attributed to the interchain stacking and ordering of P3HT films in the solid state which has a significant effect on absorption of light as compared to the solution [143, 345]. The smaller Stokes shift in P3HT films as compared to the solution spectra showed less conformational changes of the film from the ground state to the first excited states due to planarization of the backbone and high interchain ordering.

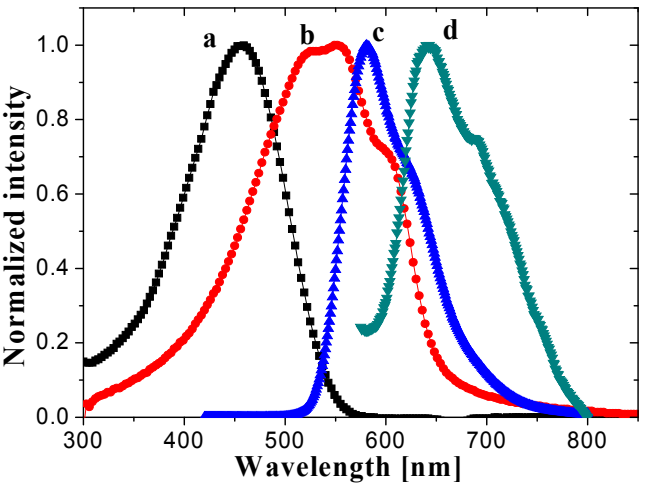

Figure 4.4. 1: *Normalized Uv-Vis absorption spectra of a) P3HT solution b) P3HT film, and fluorescence spectra of c) P3HT solution d) P3HT film.*

Electrochemistry and spectroelectrochemistry

The electrochemical and spectroelectrochemical property of pure polymer was characterized. Pt sheet electrode was used for cyclic voltammetry experiments and transparent indium tin oxide (ITO) coated glass electrode was used for *insitu* spectroelectrochemistry. The cyclic voltammogram in Figure 4.4.2a shows a quasi reversible peak with an oxidation onset of ~ 0.65 V vs quasi Ag/AgCl reference electrode which gives a HOMO level of ~ 5.1 eV consistent with literature value [325, 346]. With increasing scan rate a linear increase in both oxidation and reduction current peaks were observed as shown in Figure 4.4.2b which is a classic response for an electroactive film localized on the electrode surface in the absence of concentration gradient [347 - 349]

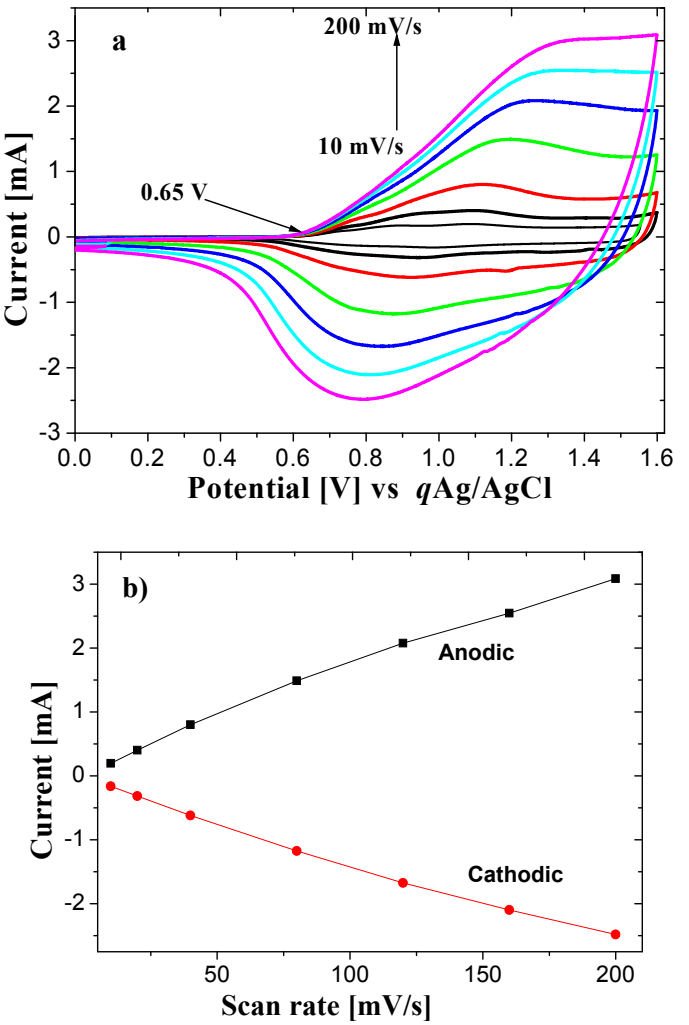

Figure 4.4. 2: *a) Cyclic voltammogram of P3HT at different scan rates 10 , 20, 40 , 80, 120, 160, and 200 mV/s, b) Corresponding scan rate dependence of anodic and cathodic peak currents.*

Thin films of P3HT were deposited on indium tin oxide (ITO) coated glass substrates by drop casting the polymer solution. Figure 4.4.3 presents the spectroelectro chemistry of P3HT showing that absorptions of the polymer at different applied constant potentials in 0.1 M $(C_4H_9)_4NPF_6/CH_3CN$ solution between polymer neutral and fully oxidized states. The absorbance of the $\pi-\pi*$ transition in the neutral state (below 0.65 V) is displaying a maximum at 515 nm. The electronic band gap

calculated from the onset of the $\pi-\pi*$ transition is 1.91 eV. With increasing the applied potential the polymer film was electrochemically oxidized (doped) as a result its absorption at the $\pi-\pi*$ transition was depleted with appearance of new absorption band peaks at about 770 nm corresponding to the charge carriers (polarons), and at about 1100 nm which is in the near-infrared region (NIR) corresponding to the low-energy charge carriers (bipolarons) as clearly observed. Figure 4.4.3 shows nineteen different absorption spectra associated with different oxidation states obtained upon stepwise switching of the polymer in small voltage increments from 0.6 V to 1.5 V. The shift in absorption spectra maxima in the visible region shows the polymer is supposed to have different colors at different oxidation (doping) levels.

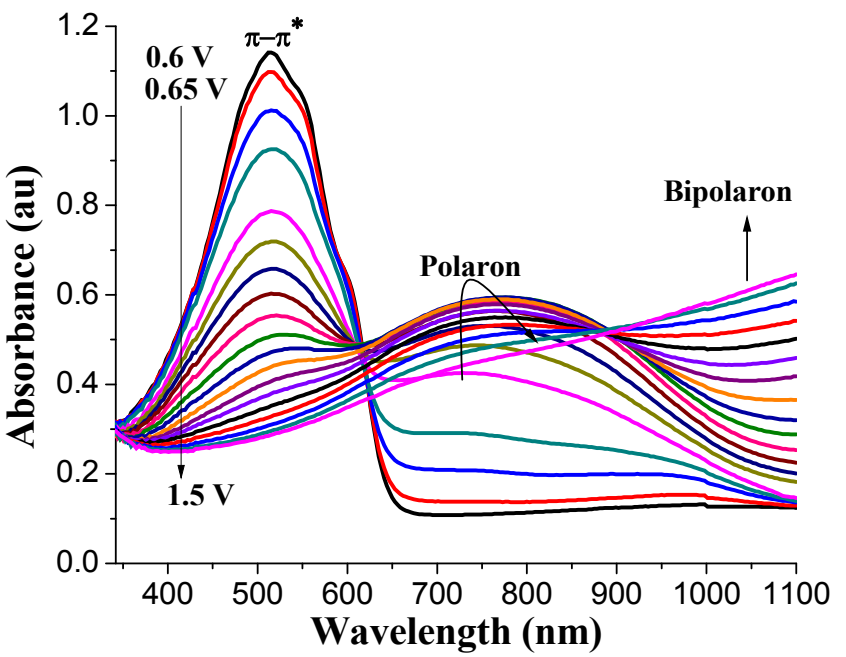

Figure 4.4. 3: *Insitu UV-Vis absorption spectra of P3HT obtained upon stepwise switching of the polymer in small voltage increments.*

Bulk heterojunction photovoltaic performance

Solutions were prepared with 1:1 mixture ratios of P3HT to the acceptor [6,6]-phenyl-C_{61}-butyric acid methyl ester (PCBM) in pure chlorobenzene and in a solution of chlorobenzene containing four different concentrations ($1 \times 10^{-3} M$, $5 \times 10^{-4} M$, $2 \times 10^{-4} M$ $2 \times 10^{-5} M$) of ferric chloride ($FeCl_3$) with a concentration of 20 mg/ml P3HT:PCBM stirred overnight. These solution were then filtered and spin-coated on top of PEDOT:PSS film with 800 rpm. The current voltage (I-V) characteristic of the solar cells fabricated is shown in Figure 4.4.4. The I-V curves in Figure 4.4.4a showed that at the lowest doping level ($2 \times 10^{-5} M$ $FeCl_3$) in these experimental condition, the device showed an improved performance interms of both the short circuit current density and open circuit voltage as compared to the undoped device. But as the concentration of $FeCl_3$ increased by one order of magnitude to $2 \times 10^{-4} M$. The device showed a decrease in open circuit voltage keeping the short circuit current still higher up to a concentration of $5 \times 10^{-4} M$ $FeCl_3$. Further increase to higher concentration $1 \times 10^{-3} M$ of $FeCl_3$ reduced the photovoltaic performance of the device with decrease in short circuit current and open circuit voltage.

Both undoped and doped devices were annealed at a temperature of 140^0C for 5 minutes . In general the I-V characteristics measured after annealing (Figure 4.4.4b) showed the usual behavior of P3HT:PCBM blend system with an increase in short circuit current in all doped and undoped devices [37, 284, 352], but unlike undoped devices, doped devices showed a significant increase in fill factor and open circuit voltage. As compared to undoped devices all doped devices showed higher short circuit current density after annealing but the open circuit voltage is still higher for undoped devices and at lowest concentration of the dopant ($2 \times 10^{-5} M$ $FeCl_3$). The

lower V_{OC} value observed in doped devices before annealing showed a significant improvement with annealing. The effect of doping with different concentrations of $FeCl_3$ showed consistent trend in both annealed devices and devices measured as prepared. In all cases doped devices showed an increase in short circuit current because of an increase in conductivity and charge carrier mobility of P3HT [143, 345].

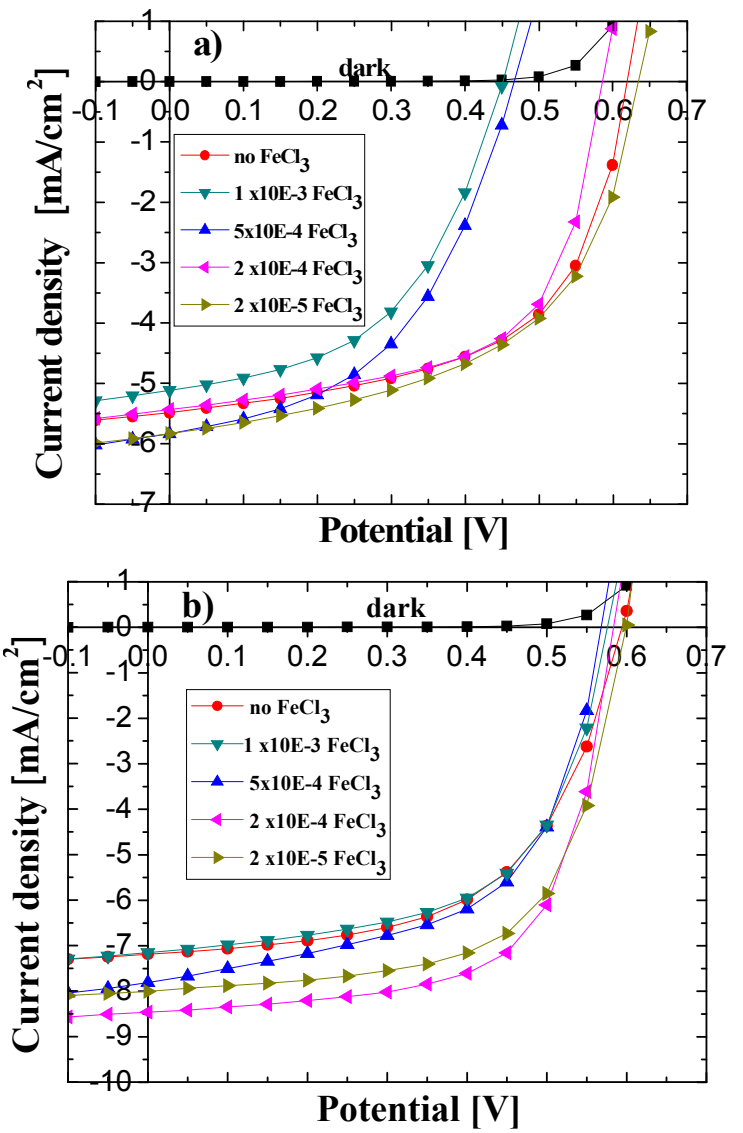

Figure 4.4. 4: *I-V characteristic curves of P3HT:PCBM (1:1) solar cells with varying concentration of $FeCl_3$ a) before annealing b) after annealing at 140^0C for 5 minutes.*

Table 4.4. 1: *Photovoltaic performances of representative solar cell devices fabricated.*

P3HT:PCBM solar cell	Sample No	V_{OC} (mV)		J_{SC} (mA/cm^2)		FF		η (%)	
		before	after	before	after	before	after	before	after
With out $FeCl_3$	1	600	600	5.49	7.19	58.9	56	1.93	2.42
	2	600	600	5.87	7.85	58.6	57	2.07	2.68
	3	600	600	5.47	7.13	58	52	1.90	2.25
doped with 2×10^{-5} M $FeCl_3$	1	650	600	5.84	8.0	52	63	1.96	3.03
	2	650	600	5.42	7.67	54	61	1.78	2.85
	3	650	600	5.56	7.71	52	61	1.88	2.85
doped with 2×10^{-4} M $FeCl_3$	1	600	600	5.50	8.35	54.2	56	1.79	2.79
	2	550	600	6.28	7.74	59	59	2.05	2.77
	3	550	550	6.84	7.97	61	63	2.2	2.75
doped with 5×10^{-4} M $FeCl_3$	1	500	550	5.95	7.80	50	58	1.5	2.49
	2	450	550	5.73	7.43	52	59	1.36	2.40
	3	450	550	6.01	7.88	44	60	1.20	2.64
doped with 1×10^{-3} M $FeCl_3$	1	516	550	6.07	7.36	51	50	1.57	2.03
	2	450	550	6.13	7.81	50	58	1.38	2.52
	3	450	550	5.95	7.46	50.9	58	1.36	2.37

Higher concentration of dopant reduced the open circuit voltage because of the increase in charge carrier mobility of the system due to doping that increases the short circuit current and reduce the ionization potential (uplift the HOMO level) [353]. But at some optimum doping level it is possible to increase the short circuit current with out sacrifying the V_{OC} of the blend. The reproducibility of the results are shown in Table 4.4.1. As shown in the table the highest V_{OC} of 650 mV before annealing were observed for the devices doped with 2×10^{-5} M $FeCl_3$. As the concentration of

$FeCl_3$ increases the V_{OC} reduced down to 450 mV. The efficiencies of solar cells indicated in the table show that relatively better power conversion efficiencies from 2.7 - 3.0% were observed at lower doping levels for 2×10^{-5} *M* and 2×10^{-4} *M* $FeCl_3$ as compared to 2.2 - 2.6% eficiencies for undoped devices.

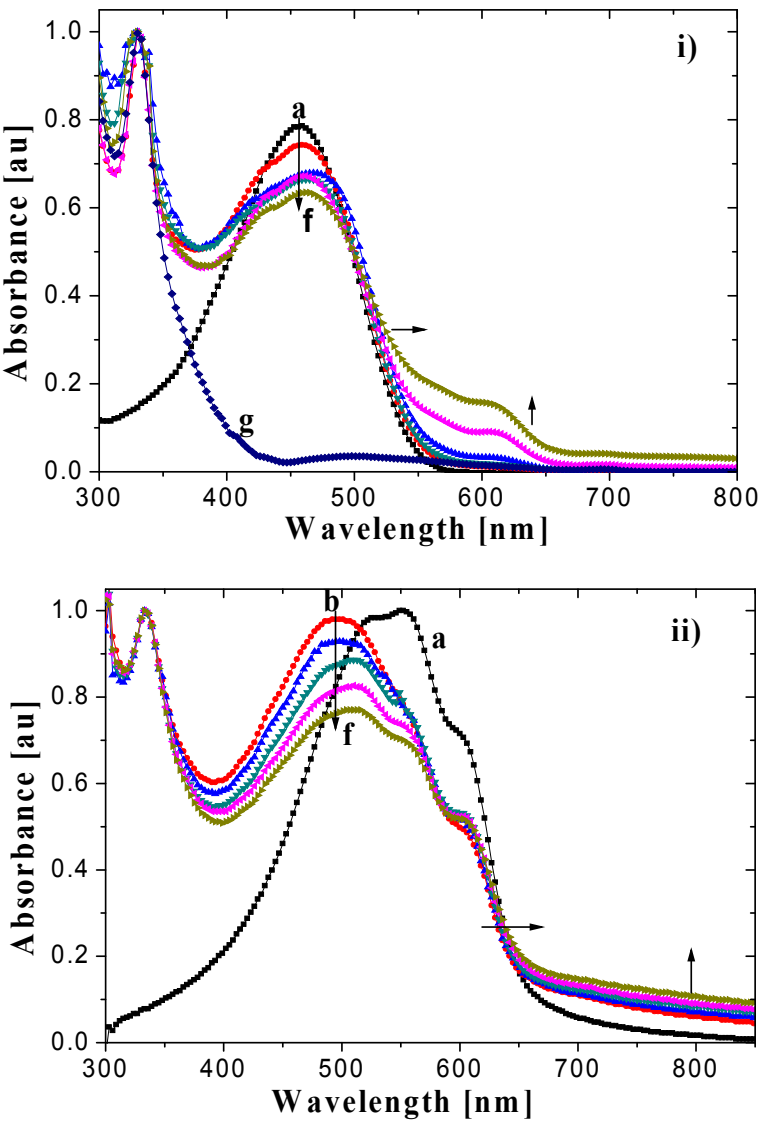

Figure 4.4.5: *Uv-Vis absorption spectra of i) dilute solutions ii) Spin coated films of, a) P3HT b) P3HT:PCBM c) P3HT:PCBM with* 2×10^{-5} *M* $FeCl_3$ *d) P3HT:PCBM with* 2×10^{-4} *M* $FeCl_3$ *e) P3HT:PCBM with* 5×10^{-4} *M* $FeCl_3$ *f) P3HT :PCBM with* 1×10^{-3} *M* $FeCl_3$ *g) PCBM ,all in in chlorobenzene solution.*

UV-Vis optical absorption of blend solutions as well as their corresponding films (prepared with the same RPM as that of the solar cell devices) were measured to see the effect of doping as shown in Figure 4.4.5. As can be seen in Figure 4.4.5a, the spectra of the solutions showed a red shifted new absorption bands with an increasing intensity at the new band and a decrease in intensity at the absorption maximum as the concentration of the dopant increases. The trend of appearance of these red shifted new bands and a decrease in absorption maxima is consistent with the *insitu* spectroelectrochemical result in Figure 4.4.3 which is an evidence for chemical doping of P3HT with in the blend [345]. The solar cell films absorption spectra shown in Figure 4.4.5b is a bit different from the solution spectra since the polymer undergo strong interchain ordering resulting in band broadening as compared to the solution [350, 351]. A similar phenomenon is observed in the film spectra though the intensity and the degree of red shift is low as compared to absorption bands observed in dilute solutions which is also an evidence of doping of the polymer in the blend.

The monochromatic photocurrent spectra in Figure 4.4.6i, showed that as the concentration of the dopant increases the onset of photocurrent generation shows a red shift to longer wavelength as a result of new absorption bands due to doping which is consistent with the red shift in optical absorption in Figure 4.4.5. This is an evidence for increment of photocurrent as the dopant concentration increases. After annealing the device the same doping induced red shift in the monochromatic photocurrent spectra of the devices were observed as shown 4.4.6ii.

As can be seen from the IPCE curve in Figure 4.4.7 the intensity of the current response decrease down with increasing dopant concentration at its absorption maximum and red shifted to longer wavelengths which is consistent with the *insitu*

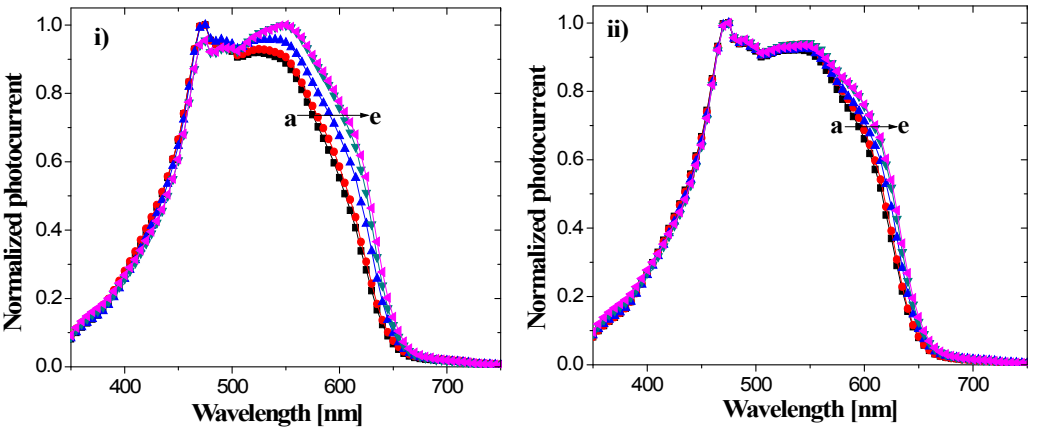

Figure 4.4. 6: *Normalized monochromatic photocurrent spectra of solar cell devices i) before annealing ii) after annealing made from a) P3HT:PCBM b) P3HT: PCBM with* $2 \times 10^{-5} M$ *$FeCl_3$ c) P3HT:PCBM with* $2 \times 10^{-4} M$ *$FeCl_3$ d) P3HT:PCBM with* $5 \times 10^{-4} M$ *$FeCl_3$ e) P3HT:PCBM with* $1 \times 10^{-3} M$ *$FeCl_3$.*

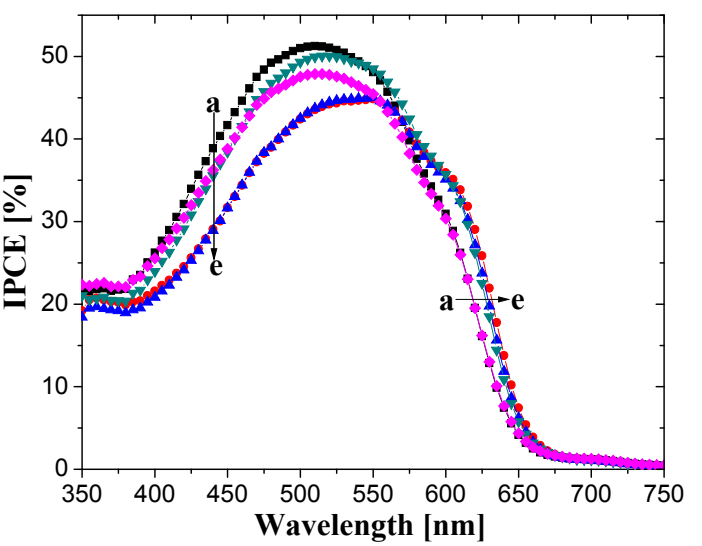

Figure 4.4. 7: *IPCE spectra of annealed devices a) P3HT: PCBM b) P3HT: PCBM with* $2 \times 10^{-5} M$ *$FeCl_3$ c) P3HT: PCBM with* $2 \times 10^{-4} M$ *$FeCl_3$ d) P3HT: PCBM with* $5 \times 10^{-4} M$ *$FeCl_3$ e) P3HT: PCBM with* $1 \times 10^{-3} M$ *$FeCl_3$.*

spectroelectrochemical measurements and optical absorption measured at the corresponding doping concentrations of ferric chloride. This shows that the

electrochemical doping as well as the chemical doping characteristics of the polymer can also be clearly reflected in the device photocurrent response though the solar cell incorporates other materials along with P3HT.

4.4.3. Conclusion

In this work the consistency of chemical doping with electrochemical doping by using *instu* spectroelelectrochemistry of P3HT films dip coated on transparent ITO coated glass electrode was shown. From the photovoltaic performance of the devices made at different concentration of the dopant $FeCl_3$. It was observed that at lower concentration of the dopant in our experimental condition the solar cells showed an improvement in both open circuit voltage and short circuit current as compared to the undoped one. As the concentration of the dopant increase the short circuit current increases further but a decrease in open circuit voltage of the device were observed at very high concentrations. It was also observed that the effect of chemical doping of the polymer is reflected on the absorption spectra, photocurrent spectra, and IPCE of the bulk heterojunction solar cell device made from the polymer.

4.5. Bulk heterojunction solar cells from ternary blend of two donor polymers with complementary absorption with PCBM

4.5.1. Background

Researchers around the world are putting in tremendous efforts to push the efficiencies of polymer solar cells to a value that is competent with their inorganic counterparts. Various strategies have been applied to enhance the efficiencies of organic photovoltaic cells that include morphology control of the active layer [37, 197, 354] utilizing low band gap polymers to enhance the short circuit current (J_{SC}) [295, 355, 356] and increasing the open circuit voltage (V_{OC}) by structural modifications [244, 357]. Due to these efforts, organic solar cells have been showing steadily increasing performances during the last ten years, reaching certified efficiencies of 7 - 10% [40 ,41, 357 - 359] nowadays. With widely investigated bulk hetrojunction solar cells based on a blend of P3HT and PCBM a maximum external quantum efficiencies (EQEs) of about 70% and power conversion efficiencies (PCE) 4 - 6% have been reported [37 - 39, 237].

Still intrinsic limiting properties of organic conjugated polymers, such as their relatively low charge carrier mobility and the short lifetime of the charge carriers [179] limit the maximum thickness of the active layer and hence the number of photons that can be absorbed and photocurrent collected. Apart from their transport properties, organic semiconductors also show limited photovoltaic properties because of their insufficient absorption of the solar spectrum which requires the synthesis of new low bandgap donor materials specifically designed for extended absorption towards longer wavelengths [209, 360 - 364]. However, for the low bandgap organic materials a red shift of the main absorption band can often lead to the sacrifice of

some absorption in the visible region as well as to a reduction of the open circuit voltage [209, 221, 365].

Various new approaches made as possible solution of this problem consists of; the broadening of the absorption band of conjugated polymers by attachment of conjugated side chains [366], using mixtures of homologous dyes absorbing different parts of the solar spectrum which are complementary leads to synergistic effects [367, 368], tandem solar cells, and cascade multilayer device structures where two or more single cells absorbing in a complementary wavelength range are stacked together either in series or parallel [369 - 372]. Tandem solar cells which can have the aformentioned two possible connections have become an increasingly explored alternatives to simple BHJ solar cells cells. In the case of serial connection of the subcells, the Voc of the tandem device can approach the sum of the Voc values of the individual sub cells [369,373] while the Jsc can at best approach the highest Jsc of the subcells [370, 373, 374]. On the other hand, with parallel connection of the subcells, the Jsc approaches the sum of those for the individual subcells [370] but the Voc is limited to the minimum Voc of the individual subcells [370]. Thus, it is clear that tandem cells also do not allow independent and concurrent optimization of both Jsc and Voc beyond that of the individual subcells.

Nevertheless, most of these multilayer devices have been fabricated using complicated and time-consuming thermal evaporation processes with increased complexity of cell design and fabrication [369, 370] which is in contrast to the attractive simple one step solution processing of the active layer in BHJ solar cells. So the other best strategy is forming thin films from two or more dissimilar soluble materials by mixing them together like ternary blends [303, 375, 376]. When

attempting to prepare efficient BHJ solar cells incorporating three blended organic semiconductors, three criteria must be considered for the third organic semiconductor: (i) its energy levels must have the correct offset with respect to those of its blend counterparts; (ii) it should operate as either an electron acceptor and transport or an electron donor and hole transport; and (iii) it should have high absorption coefficients in complementary absorption ranges with respect to those of its counterparts [375].

Here in this work a (1:1) ratio of two donor polymers poly[4,4-bis(2-ethylhexyl)-4*H*-cyclopenta[2,1-*b*:3,4-*b*2]dithiophene-2,6-diyl-*alt*-4,7-bis(2-thienyl)-2,1,3-benzothia-diazole-5',5''-diyl] (PCPDTTBTT) and poly(3-hexylthiophene) (P3HT) having complementary absorption and an acceptor [6,6]-phenyl C_{61}-butyric acid methyl ester (PCBM) were mixed to form a ternary blend bulk heterojunction solar cells. In either P3HT or PCPDTTBTT the absorption range of polymer is narrow and covers only a fraction of the solar spectrum. The ternary blend enables harvesting of light in a relatively wider spectral range. This synergetic effect is attributed to a more efficient photon harvesting of the ternary blend with mixed polymer cells compared to either of the single donor device binary blends. PCPDTTBTT is known in literature where its synthesis and as well as its bulk heterojunction solar cell device characterizations were made [377, 378]. Structures of the donor polymers and the acceptor PCBM used are given in Figure 3.1.1d of experimental section.

4.5.2. Results and discussion

4.5.2.1. Photophyics

For photophysical measurements, the pure polymers P3HT, PCPDTTBTT, their 1:1 mixture and the corresponding blend films and solutions with PCBM in a 1:1 ratio

were prepared from their solution 10 mg/ml polymer in chlorobenzene by spin coating on glass. After the films were allowed to dry in air for 24 h, optical absorption and photoluminescence measurements were carried out. The absorption and photoluminscence spectra of P3HT and PCPDTTBTT are shown in Figure 4.5.1a and b in both solutions and their corresponding films.

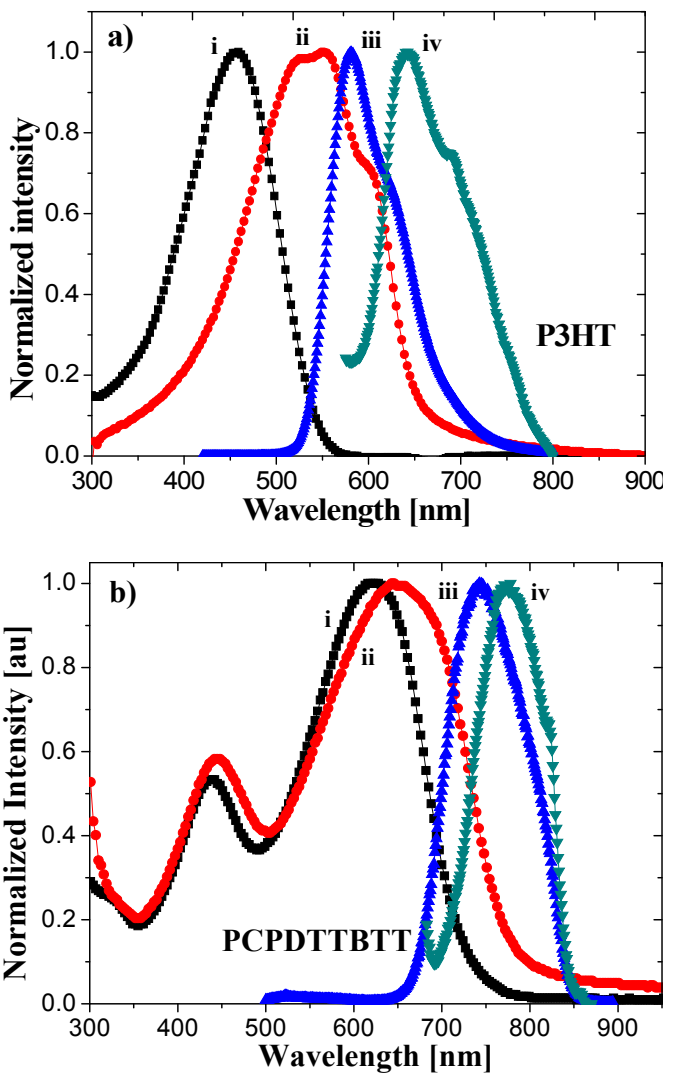

Figure 4.5. 1: *Absorbance and corresponding fluorescence spectra of a) P3HT and b) PCPDTTBTT i) and iii) in solution, ii) and iv) are films spin coated on glass.*

The solid state (film) spectra of P3HT (Figure 4.5.1a) is completely different from its solution with a significant red shifted and well structured spectra in both absorptions and emission due to enhanced planarization of the conjugated backbones and ordering due to π-π stacking from the solutions to the compact bulk materials in solid state [379, 380]. Where as in case of PCPDTTBTT the red shift in film spectra is less significant and no differences in the structure of the two specta are observed which might be due to its branched side chains which inhibit planarization and ordering [380, 251, 252]. Unlike P3HT the non structured spectra in films of PCPDTTBTT showed the vibronic character that can be seen in the solid-state UV/vis absorption spectrum is very little. This indicates that this polymer does not form extended crystalline domains. As shown in the spectra and the corresponding photophysical data calculations in Table 4.5.1, PCPDTTBTT is a lower band gap polymer which have absorbtion onset at 800 nm as compared to P3HT. The relatively smaller Stokes shift in both solution and thin film specra of PCPDTTBTT is an indication of comparatively less conformational changes from the ground to the first excited state as compared to P3HT.

P3HT and PCPDTTBTT are mixed in 1:1 weight ratio and dissolved in the same chlorobenzene solution, the binary mixture solution as well as their corresponding film absorption specta are shown in Figure 4.5.2. In both cases the mixture covers a wider range of solar spectrum as compared to the absorption of individual polymers. In the solution spectra a smooth stucturless spectra of the binary mixture solution was observed (Figure 4.5.2a). The binary mixture film absorption showed a well structured specta covering a wider range of the visible solar spectrum from 800 nm to 350 nm which is an interesting improvement in light harvesting efficiency using devices made from this mixture. The standard spectral irradiance spectra overlayed to

the film spectra in Figure 4.5.2b clearly showed to what extent the photon collecting efficiency of the binary mixture was increased as compared to the individual polymers absorption. Particularly regions of high spectral irradiance have been covered with the binary mixture film absorption spectrum.

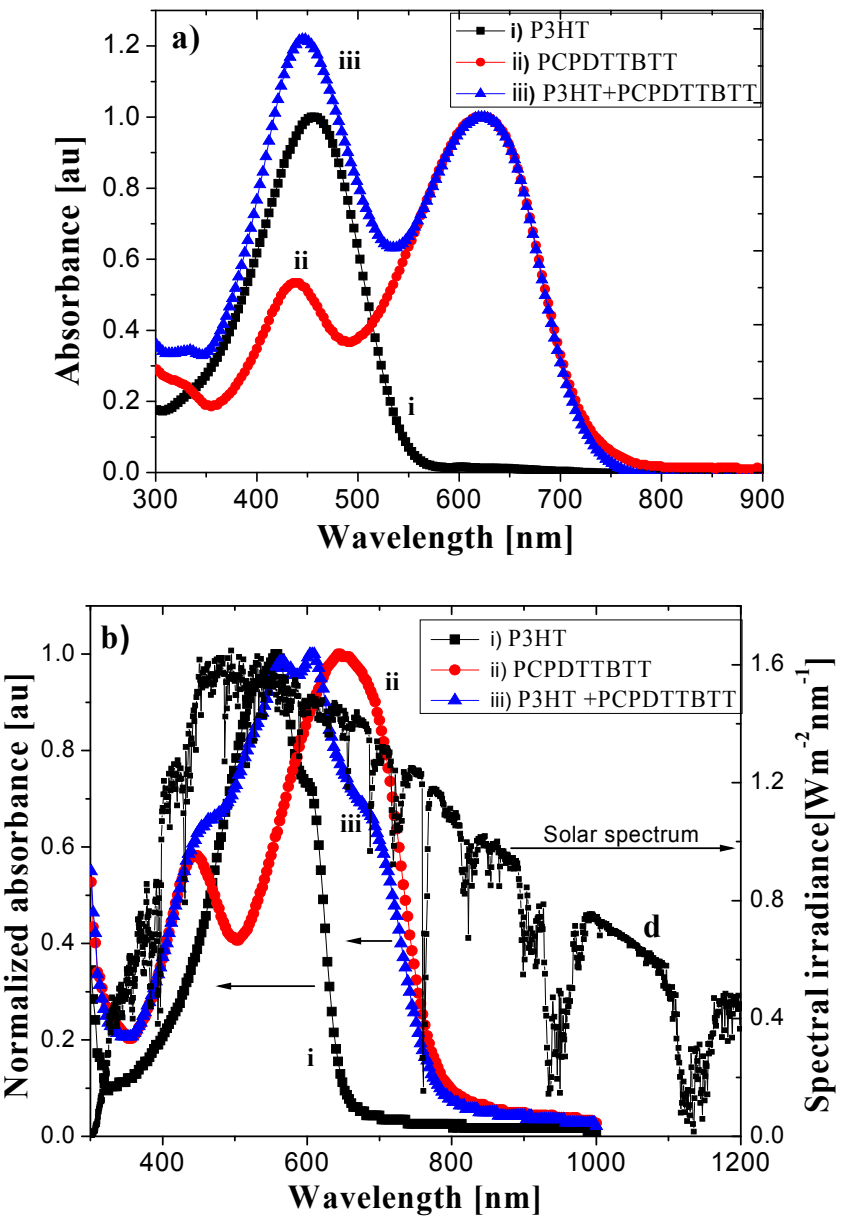

Figure 4.5. 2: *Absorbance of P3HT, PCPDTTBTT, and a 1:1 mixture of P3HT with PCPDTTBTT a) in solution b) thin films compared to the solar spectrum.*

Table 4.5. 1: *Photophysical properties of P3HT and PCPDTTBTT in thin film [f] and in chlorobenzene [s].*

Polymer	Abs. onset (nm)	Abs. max. (nm)	Emis. Max.(nm)	stock shift (cm^{-1})	Optical band gap, (eV)
P3HT [f]	670	551	642	2572	1.88
P3HT [s]	542	457	580	4640	2.29
PCPDTTBTT [f]	800	652	776	2451	1.57
PCPDTTBTT [s]	740	623	744	2611	1.68

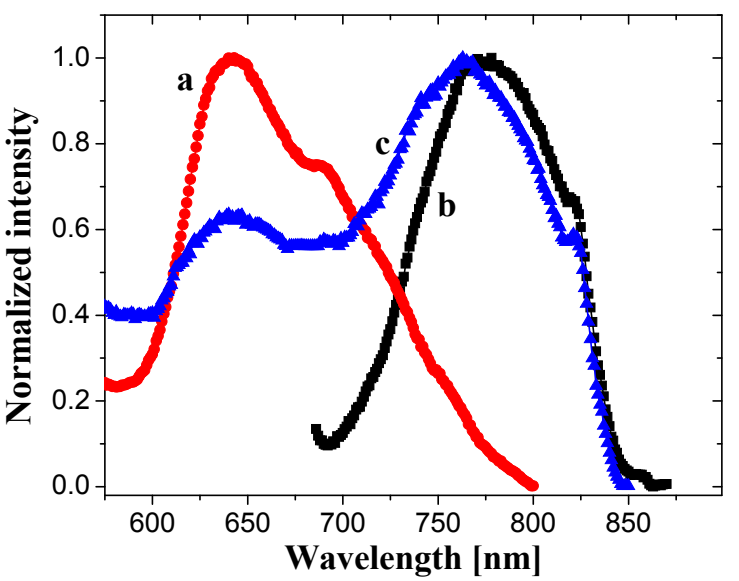

Figure 4.5. 3: *Photoluminscence spectra of thin films of a) P3HT b) PCPDTTBTT c) P3HT: PCPDTTBTT*

The fluorescence spectra of thin films of the two polymers and their mixture displayed in Figure 4.5.3 showed quenching of fluorescence of P3HT upon mixing the two polymers in 1:1 ratio which confirm that there is ultrafast photoiduced charge transfer from P3HT to PCPDTTBTT. This process indicates that PCPDTTBTT acts

as both donor (*p*-type) and acceptor (*n*-type) polymer as it is also evidenced from its electrochemical properties in Figures 4.5.4.

4.5.2.2. Electrochemistry

To see the energy level match between the two donor polymers electrochemical and *insitu* spectroelectrochemical studies were made for both polymers. As can be seen in Figure 4.5.4, the electrochemical oxidation behavior of both polymers (P3HT and PCPDTTBTT) showed similar oxidation onset which confirms that the highest occupied molecular orbital (HOMO) level of both polymers is almost the same at around 5.1 eV calculated using the Equation 2.5 (E_{onset} (Fc/Fc^{+}) Vs (qusi Ag/AgCl) in this experiment was 400 mV). LUMO value of P3HT was estimated to be 3.22 eV from the obtained HOMO and the optical absorption onset (optical bandgap) which is consistent with literature value [209, 243]. So the energy level difference between the two polymers is in their LUMO values since they differ in bandgap.

The LUMO value of PCPDTTBTT was also determined to be 3.57 eV from its electrochemical reduction (*n*-doping) onset potential of - 0.83 V vs quasi Ag/AgCl shown by the cyclic voltammogram in Figure 4.5.4. This voltammogram confirms that PCPDTTBTT is both *p*-and *n*-type polymer which can act either as an electron donor polymer or an acceptor. The lower LUMO level of PCPDTTBTT as compared to PCBM also indicates that the electron transfer from PCPDTTBTT to PCBM is energetically possible.

Both P3HT and PCPDTTBTT are conducting polymers which undergo electrochemical doping by application of potentials to form the oxidized or reduced (*p* or *n*) doped forms of the polymers as observed in the cyclic voltammograms (Figure 4.5.4).

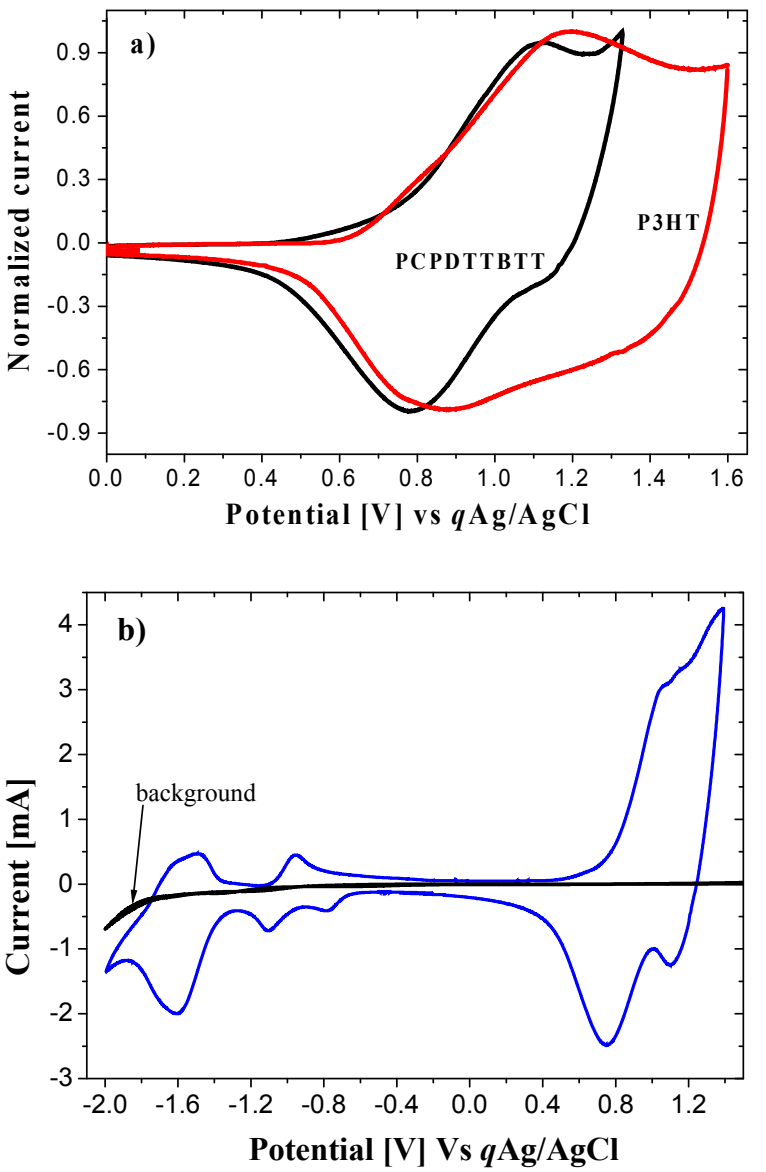

Figure 4.5. 4: *Cyclic voltammogram of a) Anodic oxidation of PCPDTTBTT and P3HT films b) anodic oxidation (p-type) and cathodic reduction (n type) of PCPDTTBTT films on Pt sheet electrode in 0.1 M* $(C_4H_9)_4NPF_6/CH_3CN$ *at a scan rate of 80 mV/s.*

During electrochemical oxidative doping it is known that new absorption bands will appear as a result of formation of polarons and bipolarons. This phenomnenon is clearly observed in the *insitu* spectroelectrochemical spectrum of PCPDTTBTT in

Figure 4.5.5 and in Figure 4.4.3 of section 4.4 for P3HT. In these result doping induced new spectral signals were observed in such a away that the main absorption, $\pi - \pi^*$ band, depleted with appearance of new absorption band peaks at about 900 nm corresponding to the charge carriers (polarons), and at about 1100 nm which is in the near-infrared region (NIR) corresponding to the low-energy charge carriers (bipolarons).

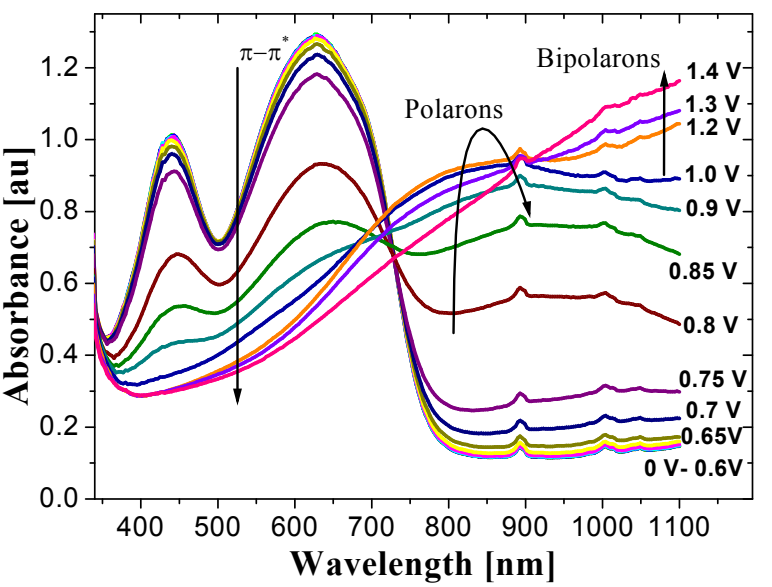

Figure 4.5. 5: *insitu Uv-vis spectroelectrochemistry of PCPDTTBTT drop casted film on ITO coated glass in 0.1 M $(C_4H_9)_4 N PF_6$ in acetonitrile solution.*

By this *insitu* experiment we have double checked where exactly the oxidation onset of the polymers is by looking at changes in the main absorption spectrum. ~ 0.65 V vs quasi Ag/AgCl was the oxidation onset in the cyclic voltammograms in Figure 4.5.4 and it was confirmed in the *insitu* experiment in Figure 4.5.5 that the main absorption $\pi - \pi^*$ band, starts to decrease significantly at that potential..

4.5.2.3. Photovoltaic devices

For the fabrication of bulk heterojunction solar cells, solutions were prepared with mixing ratio of 1:1 polymer to the acceptor (PCBM) in chlorobenzene with a concentration of 20mg/ml Polymer:PCBM stirred overnight. For ternary blend the mixture of the two polymers by 1:1 weight ratio were used. PEDOT:PSS stirred overnight and filtered was spin coated from aqueous solution on top of ITO with 3000 rpm and dried over a hot plate at 140^0C for 10 minutes in open air. The polymer:PCBM solutions were then spin coated on top of PEDOT/PSS film with 800 RPM and dried in air

The calculated HOMO and LUMO energy levels of the two donor polymers with respect to PCBM and with the corresponding work function of the electrodes are shown in Figure 4.5.6. The Energy levels indicate that, PCPDTTBTT has the same LUMO level with P3HT. PCPDTTBTT possesses intermediate energy band edges between PCBM and P3HT having sufficiently large band edge offsets with P3HT and PCBM. This suggesed that photoexcited excitons might be dissociated efficiently at P3HT/PCPDTTBTT, P3HT/PCBM, and PCPDTTBTT/PCBM junctions and that the carriers can be efficiently driven forward until reaching their respective electrodes. In addition to this the common thiophene moiety in both polymers facilitates the miscibility of the two polymers as observed in the homogenous nature of the films in the ternary blend for good charge transport.

The photoluminescence (PL) spectra of the pristine (P3HT and PCPDTTBTT) and blended P3HT:PCPDTTBTT films (Figure 4.5.3) also support the phenomena that PL of the pristine P3HT film were quenched significantly upon the addition of 50% (wt/wt) PCPDTTBTT. This PL quenching arose as a consequence of ultra fast

photoinduced charge transfer from P3HT to PCPDTTBTT. Thus, PCPDTTBTT acts as both an electron acceptor and electron donor when blended with P3HT and PCBM. Moreover, the step wise structure can accelerate the carrier transfer [381 - 383], resulting in an increased extraction of the charge carriers. Furthermore, the appearance of LUMO level of PCPDTTBTT between the LUMO levels of P3HT and PCBM creates wider energy differences between the LUMO energy level of the acceptor and the HOMO energy level of the donor at the P3HT/PCPDTTBTT and PCPDTTBTT/PCBM junctions that would lead to larger open-circuit voltages (V_{OC}) [384].

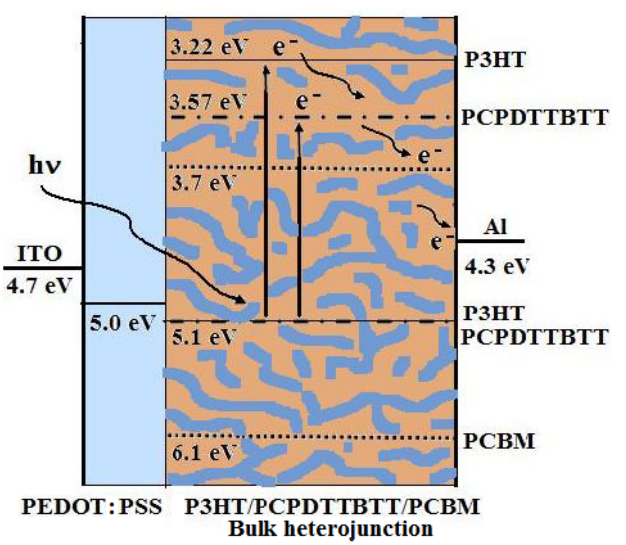

Figure 4.5. 6: *Energy level diagram of the BHJ solar cell from ternary blend showing the HOMO and LUMO levels of each material.*

The dark current voltage (I-V) characteristics of (P3HT:PCPDTTBTT):PCBM ternary blend device as well as the binary blend with each polymer and PCBM is displayed in Figure 4.5.7. In all three devices a rectifying diode behavior is observed. From the magnitude of the dark current in the negative voltage (reverse bias) the device with P3HT:PCBM looks less conductive while PCPDTTBTT:PCBM showed

highest dark current, the ternary blend which consisted equal weight ratio of both polymers showed intermediate conductivity confirming that the ternary blend showed average conductivity of the two binary blends. On the lower positive voltage bias binary blends showed similar plateau due to shunt resistance before rectification starts which is a function of the built in potential. Where as the ternary blend showed extended plateau (higher parallel resistance) confirming that it has higher built in potential to generate higher open circuit voltage as compared to the binary blends. This late turn-on of the device in the dark is known to lead to a high V_{OC}. The turn-on occurs when recombination of injected electrons and holes prevails in the forward bias. Hence a device with diminished charge recombination rate (*i.e.*, device that can build up a larger quantity of separated charges) would yield a high V_{OC} [385, 386]. The appearance of the other plateau (current saturation) after rectification which is a function of the serial resistance appear at lower voltages in case of the blend with P3HT where as in PCPDTTBTT blend it goes to higher voltages and the ternary blend takes the average.

Figure 4.5.7 a-c displays the current-voltage (I-V) curves of solar cell devices made from P3HT:PCBM, PCPDTTBTT:PCBM and (PCPDTTBTT:P3HT):PCBM under simulated irradiation of 80 mW/cm^2 measured in open air. The P3HT:PCBM (1:1) device exhibited a short circuit current density of 3.7 mA/cm^2 and V_{OC} of 625 mV with 0.40 fill factor. The device made with PCPDTTBTT:PCBM (1:1) showed similar V_{OC} value of 625 mV which is consistent with their similarity of HOMO level, lower short circuit current of 3.4 mA/cm^2 with 0.34 fill factor. The FF, $J_{SC,}$ and V_{OC} value obtained for PCPDTTBTT:PCBM (1:1) is consistent with the value obtained in the previous work [377, 378]. The lower short circuit current as compared to P3HT might

be due to its weak absorption at the higher spectral irradiance region where the absorption maximum of P3HT is there.

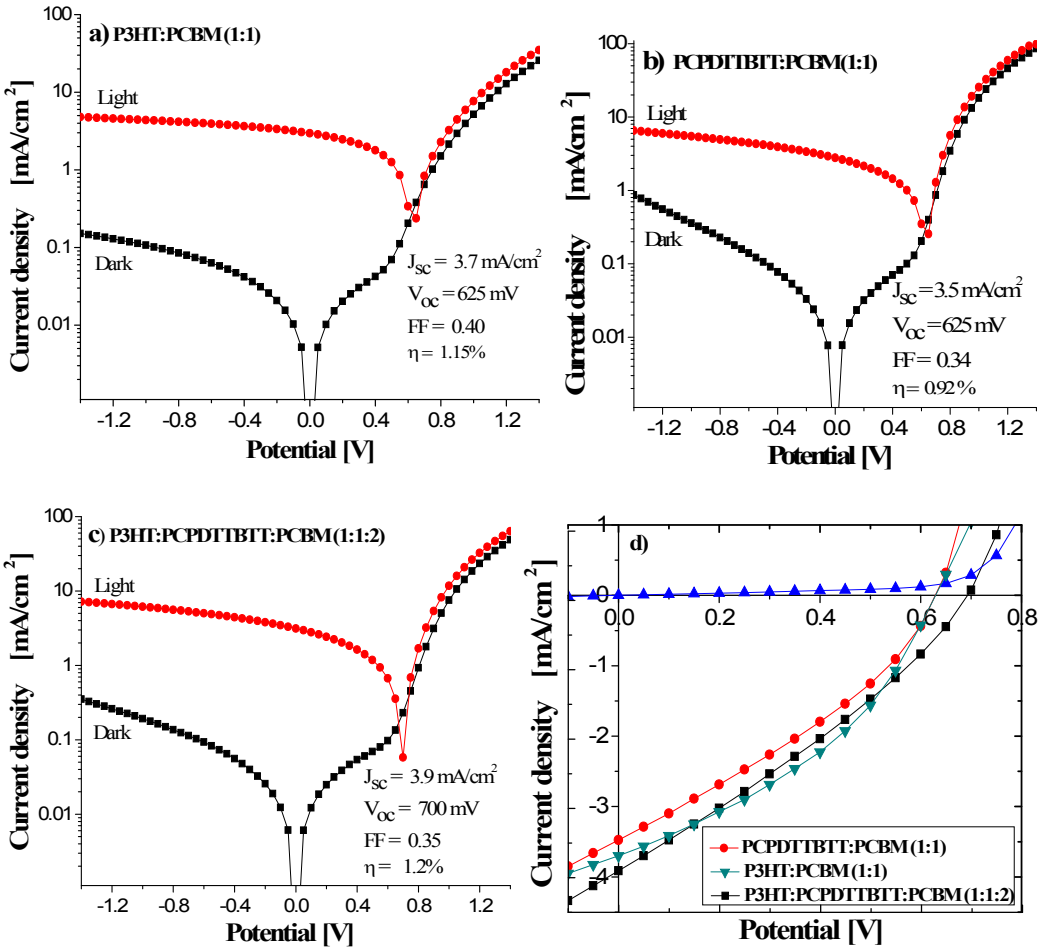

Figure 4.5. 7: *Dark and illumination I-V characteristics of the solar cell devices a) P3HT: PCBM b) PCPDTTBTT:PCBM c) (PCPDTTBTT:P3HT):PCBM d) overlay plots.*

The device which is fabricated by using equal weight ratio of P3HT and PCPDTTBTT to make a ternary blend with PCBM showed the highest short circuit current density of 3.9 mA/cm^2 as well as the highest open circuit voltage of 700 mV with a fill factor of 0.35. Though the binary devices showed the same V_{OC} value the ternary blend showed a significant improvement of V_{OC}. It is true that in organic

tandem solar cell devices the V_{OC} takes the sum of V_{OC} s' of individual devices [30, 38] but here the active layer is a single ternary bulk heterojunction layer is different from tandem devices. So this increment in V_{OC} of this ternary blend is due to the dual behavior of PCPDTTBTT to act as donor and acceptor polymer where its LUMO level with respect to P3HT as well as PCBM induce a significant increase in V_{OC} which is consistent with literature where a ternary blend with two acceptors have shown enhanced V_{OC} [376].

In contrary to the increased device performance of P3HT:PCBM solar cell devices by post production thermal annealing, devices with PCPDTTBTT:PCBM showed a reduced performance (reduced Voc and Jsc) with these treatments when annealed at a temperature of 140^0C for 10 minutes. This result is also similar with the previous results of PCPDTTBTT:PCBM BHJ solar cells where they have confirmed that thermal annealing induces high phase sepatation of ~500 nm with PCBM was observed with AFM studies [377]. This is because thermal tratements further increase the phase separation beyond the diffusion length of excitons that reduce the device efficiency. Due to the large domain size of PCPDTTBTT as well as increased phase separation between the two polymers thermal treatement didn't show an improvement in the ternary device too; rather it reduced the performance of the blend.

Figure 4.5.8a reveals the optical absorption spectra of the solar cell devices fabricated. The binary blends P3HT:PCBM and PCPDTTBTT:PCBM have limited absorption in the visible range. Enhanced absorption was observed by the ternary blend up on blending P3HT and PCPDTTBTT with PCBM which absorbs the entire spectrum from 800 nm up to 300 by the complementary absorption effect of the two polymers and that of PCBM which strongly absorbs in the UV region. The highest short-circuit

current density obtained from the ternary blend is due to this broad absorption spectrum that generate larger number of excitons and thus a larger photocurrent.

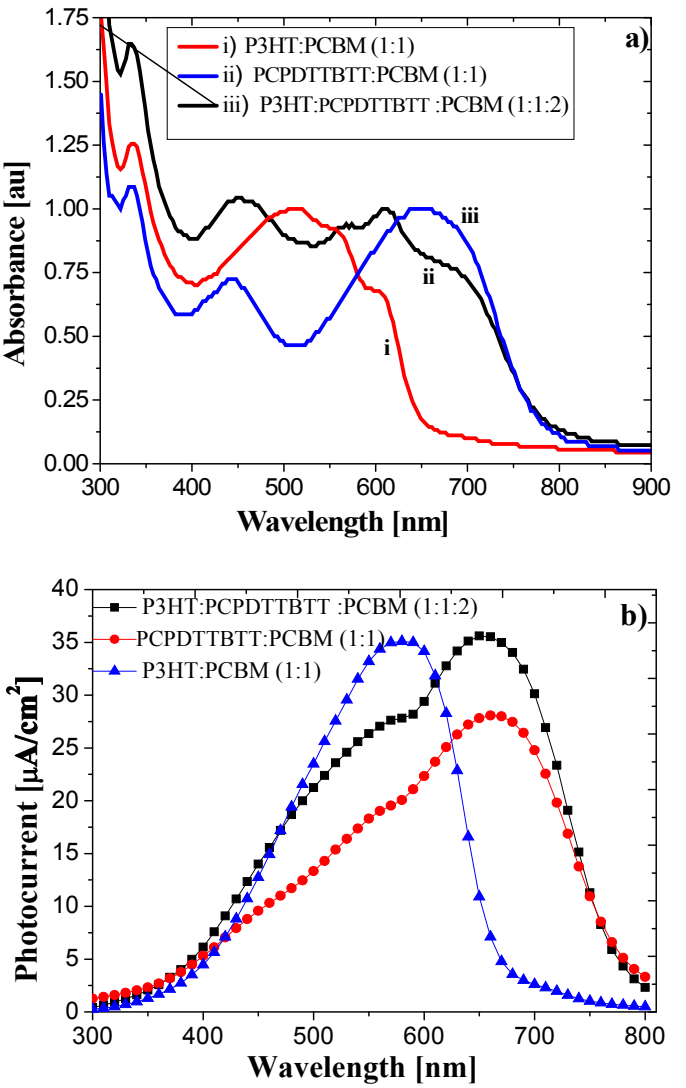

Figure 4.5. 8: *a) Uv-vis optical absorption spectra and b) the corresponding monochromatic photocurrent action spectra of the binary blends and the ternary blend solar cell devices.*

Figure 4.5.8b illustrates the monochromatic photocurrent spectra of the solar cell devices. The photocurrent generated from the binary blends P3HT:PCBM and PCPDTTBTT:PCBM covers narrow range of the spectrum which is consistent with

their corresponding absorption in Figure 4.5.8a, where as the ternary blend generated a photocurrent over the whole visible spectrum in range of 800 nm to 350 nm because of the complementary absorption of P3HT and PCPDTTBTT. The higher short circuit current density for the ternary blend is due to this effect.

IPCE spectra in Figure 4.5.9 reveal that devices based on P3HT:PCBM exhibited their maximum IPCE of 40% at wavelength of 486 nm and devices with PCPDTTBTT:PCBM showed their maxium IPCE of 35%) at 400 nm where as the ternary device which consist of both polymers and PCBM achieved the highest IPCE with its maximium of 43% at 430 nm with a broader range from 800 nm to 300 nm. This IPCE profile is similar to that of the absorption spectrum where wavelength range and the complementary absorption action of the two polymers in the ternary blend is clearly observed. Thus, incorporating two solution processed polymers with complementary absorption in polymer based solar cell device appears to be a good method for improving the solar spectral coverage and device performance.

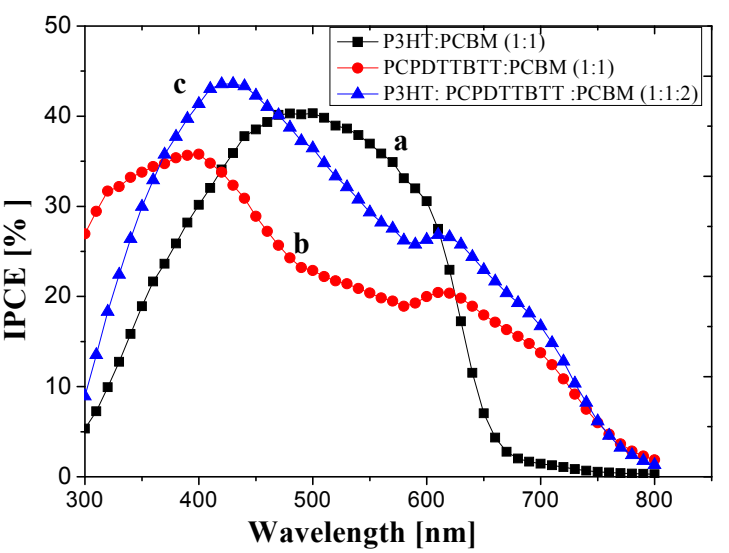

Figure 4.5. 9: *IPCE of the solar cells a) P3HT:PCBM b) P3HT:PCBM, c) (PCPDTTBTT:P3HT): PCBM.*

4.5.3. Conclusion

We have fabricated ternary blend bulk heterojunction solar cells containing P3HT as the donor, PCPDTTBTT as both donor and acceptor and PCBM as an acceptor. These devices were tested and compared with the corresponding binary blends of P3HT and PCPDTTBTT with PCBM. An improvement in both Jsc and V_{OC} values were observed by using the ternary blend due to the increased photon harvesting efficiency and the favorable energy levels as the low bandgap polymer served as an absorber in the longer wavelengths and as an acceptor from the larger bandgap polymer to accelerate the exciton dissociation and charge transfer to the main acceptor PCBM. The result suggests that ternary blends provide a potentially effective route toward maximizing the attainable Jsc and Voc product which is directly proportional to the solar cell efficiency in BHJ solar cells. By carful selection of appropriate donors and acceptors for ternary blend, efficiencies observed in binary blends can be improved without losing the simplicity of a single active layer bulk heterojunction processing step.

REFERENCES

1. *Basic Energy Sciences Workshop on Solar Energy Utilization*, Office of Science, U.S. Department of Energy, April 18-21, (2005). http://www.er.doe.gov/bes/ reports/les /SEU_rpt.pdf.
2. N. S. Lewis; *MRS Bull.* 32 (2007) 808.
3. R. E. Smalley; *MRS Bull*. 30(2005) 412.
4. A. E. Becquerel; *C.R. Acad. Sci.* 9 (1839) 561.
5. A. K. Jana; *J .Photochem. and Photobio. A: Chem*. 132 (2000) 1.
6. M. A. Green; *Physica E* 14 (2002) 11.
7. D. M. Chapin, C. S. Fuller, G. L. Pearson; *J. Appl. Phys.* 25 (1954**)** 676.
8. J. Zao, A. Wang, M. Green, F. N. Forrazza; *App. Phys. Lett.* 73 (1998) 1991.
9. A. Slaoui, R. T. Collins; *MRS Bull*. 32 (2007) 211.
10. K. Ramanathan, M. A. Contreras, C. L. Perkins, S. Asher, F.S. Hasoon, J. Keane, D. Young, M. Romero, W. Metzer, R. Noufi, J. Ward, A. Duda; *Prog. Photovolt. Res. Appl.* 11 (2003) 225.
11. I. Repins, M. A. Contreras, B. Egaas, C. D. Hart, J. Scharf, C. L. Perkins, B. To, R. Noufi; *Prog. Photovolt. Res. Appl*. 16 (2008) 235.
12. T. Aramoto, S. Kumazawa, H. Higuchi, T. Arita, S. Shibutani, T. Nishio, J. Nakajima, M. Tsuji, A. Hanafusa, T. Hibino, K. Omura, H. Ohyama, M. Murozono; *Jpn. J. Appl. Phys. Part 1* 36 (1997) 6304.
13. M. Gratzel; *Nature* 414 (2001) 338.
14. M. K. Nazeeruddin, A. Key, I. Rodicio, R. H-Baker, E. Muller, P. Liska, N.Vlachopoulos, M. Gratzel; *J. Am. Chem. Soc*. 115 (1993) 6382.
15. A.F. Nogueira, C. Longo, M.A. De Paoli; *Coord. Chem. Rev*. 248 (2004) 1455.
16. M. Gratzel; *Inorg. Chem*. 44 (2005) 20.

17. M. Gratzel; *J. Photochem. Photobio. A* 164 (2004) 3.

18. O. Reagan, D. T. Schwartz, S. M. Zakeeruddin, M. Gratzel; *Adv.matter*. 12 (2000) 1263.

19. K. Murakoshi, R. Kogure, Y. Wada, S. Yanagida; *Sol. Energy mater. Sol. Cells* 55 (1998) 113.

20. D. Gebeyehu, N. Vlachopoulos, F. Kienberger, H. Schindler, N. S. Sariciftci; *Synth. Met*. 121 (2001) 1549.

21. T. Yohannes, T. Solomon, O. Inganäs; *Synth. Met*. 82 (1996) 215.

22. T. Yohannes, O. Inganäs; *Sol.Energy mater*. *Sol. Cells* 51 (1998) 193.

23. W. U. Huynh, J. J. Dittmer, A. P. Alivisatos; *Science* 295 (2002) 2425.

24. S. Gunes, N.S. Sariciftci; *Inorg. Chimi. Acta* 361 (2008) 581.

25. P. A. V. Hal, M. M. Wienk, J. M. Kroon, W. J. H. Verhees, L. H. Sloff, W. J. H. V. Gennip, P. Jonkhejm, R. A. J. Janssen; *Adv. Mater.* 15 (2003) 118.

26. W. J. E. Beek, M. M. Wienk, R. A. J. Janssen; *Adv. Funct. Mater*. 16 (2006) 1112.

27. E. Arici, N. S. Sariciftci, D. Meissner; *Adv. Funct. Mater*. 2 (2003) 13.

28. E. Arici, D. Meissner, N.S. Sariciftci, H. S. Nalwa (Ed.); *Encyc.Nanosci. Nanotec.* 1 (2004).

29. K. M. Coakley, Y. X. Liu, M. D. McGehee, K. L. Frindell, G. D. Stucky; *Adv. Funct. Mater.* 13 (2003) 301.

30. H. Hoppe, N. S. Sariciftci; J. *Mater. Res.* 19 (2004) 1924.

31. S. Guenes, H. Neugebauer, N. S. Sariciftci; *Chem. Rev.* 107 (2007) 1324.

32. G. Dennler, N. S. Sariciftci, C. J. Brabec; *semiconducting Polymers: Chemistry, Physics and Engineering,*V1, 2nd Edn, 2007, p 455, G. Hadziioannou & G. G. Malliaras (Ed).

33. A. J. Mozer, N. S. Sariciftci; *C.R. Chimie*. 9 (2006) 568.

34. N. S. Sariciftci, L. Smilowitz, A. J. Heeger, F. Wudl; *Science* 258 (1992) 1474.

35. C. W. Tang, A. C. Albrecht; *J. Chem. Phys.* 62 (1975) 2139.

36. C. W. Tang; *Appl. Phys. Lett*, 48 (1986) 183.

37. G. Li, V. Shrotriya, J. S. Huang, Y. Yao, T. Moriarty, K. Emery, Y. Yang; *Nat. Mater*. 4 (2005) 864.

38. W. L. Ma, C. Y. Yang, X. Gong, K. H. Lee, A. J. Heeger; *Adv. Funct. Mater*. 15 (2005) 1617.

39. S. H. Park, A. Roy, S. Beaupre, S. Cho, N. Coates, J. S. Moon, D.Moses, M. Leclerc, K. Lee, A. J. Heeger; *Nat. Photonics* 3 (2009) 297.

40. Y. Liang, Z. Xu, J. Xia, S. T. Tsai, Y. Wu, G. Li, C. Ray, L. Yu; *Adv. Mater*. 22 (2010) E135.

41. M. A. Green, K. Emery, Y. Hishikawa, W. Warta, E. D. Dunlop; *Prog. Photovolt: Res. Appl.* 20 (2012)12.

42. F. C. Krebs; *Sol. Energy Mater. Sol. Cells* 93 (2009) 394.

43. D. Gupta, S. Mukhopadhyay, K. S. Narayan; *Sol. Energy mater. Sol. Cells* 94 (2010) 1309.

44. R. Koeppe, O. Bossartb, G. Calzaferrib, N. S. Sariciftci; *Sol. Energy mater. Sol. Cells* 91 (2007) 986.

45. Y. J. Cheng, S. H. Yang, C. S. Hsu; *Chem. Rev*. 109 (2009) 5868.

46. B. A. Gregg, M. C. Hanna; *J. Appl.Phys.* 93 (2003) 3605.

47. S. Karg, W. Riess, V. Dyakonov, M. Schwoerer; *Synth. Met.* 54 (1993) 427.

48. L. A. A. Pettersson, L. S. Roman, O. Inganas; *J. Appl. Phys.* 86 (1999) 487.

49. J. Rostalski, D. Meissner; *Sol. Energy mater. Sol.Cells* 63 (2000) 37.

50. P. Peumanns, S. R. Forrest; *Appl. Phys. Lett.* 79 (2001) 126.

51. J. Xue, S. Uchida, B. P. Rand, S. R. Forrest; *Appl Phys.Lett.* 84 (2004) 3013.

52. G. Yu, J. Gao, J. C. Hummelen, F. Wudl, A. J. Heeger; *Science* 270 (1995) 1789.

53. H. Hoppe, D. A. M. Egbe, D. Muhlbacherc, N. S. Sariciftci; *J. Mater.Chem.* 14 (2004) 3462.

54. N. Blouin, A. Michaud, D. Gendron, S. Wakim, E. Blair, R. N. Plesu, M. Belletete, G. Durocher, Y. Tao, M. Leclerc; *J. Am. Chem. Soc*. 130 (2008) 732.

55. J. H. Tsai, C. C. Chueh, M. H. Lai, C. F. Wang, W. C. Chen, B. T. Ko, C. Ting; *Macromolecules* 42 (2009) 1897.

56. D. A .M. Egbe, B. Carbonnier, E. Birckner, U. W. Grummt*; Prog. Polym. Sci.* 34 (2009) 1023.

57. D. A. M. Egbe, L. H. Nguyen, K. Schmidtke, A. Wild, C. Sieber, S. Guenes, N. S. Saricifti; *J. Poly. Sci. Part A: Poly. Chem.* 45 (2007) 1619.

58. J. Chen, Y. Cao; *Acc. Chem. Res. 42* (2009) 1709.

59. P. Troshin, H. Hoppe, J. Renz, M. Egginger, J. Mayorova, A. Goryachev, A. Pereguov, R. Lyubovskaya, G. Gobsch, N. S. Sariciftci, V. Razumov; *Adv. Func. Mater.* 19 (2009) 779.

60. H. Hoppe, N. Arnold, N. S. Sariciftci, D. Meissner; *Sol. Ener. Mat. Sol. Cells.* 80 (2003) 105.

61. R. Schueppel, K. Schmidt, C. Uhrich, K. Schulze, D. Wynands, J. L. Bredas, E. Brier, E. Reinold, H. B. Bu, P. Baeuerle, B. Maennig, M. Pfeiffer, K. Leo; *Phys. Rev. B* 77 (2008) 085311.

62. I. W. Hwang, D. Moses, A. J. Heeger; *J. Phys. Chem. C,* 112 (2008) 4350.

63. M. Breselge, I. V. Severen, L. Lutsen, P. Adriaensens, J. Manca, D. Vanderzande, T. Cleij; *Thin solid films* 511 (2006) 328.

64. L. M. Chen, Z. Hong, G. Li, Y. Yang; *Adv. Mater*. 21 (2009) 1434.

65. A. J. Mozer, N. S. Sariciftci, A. Pivrikas, R. Osterbacka, G. G. Juska, L. Brassat, H. Bassler; *Phys. Rev. B* 71 (2005) 035214.

66. A. Moliton, R. C. Hiorns; *Polym Int.* 53 (2004) 1397.

67. A. J. Heeger, S. Kevelson, J. R. Schrieffer, W. P Su; *Rev. Mod. Phys* 78 (1988) 160.

68. A. J. Heeger; *Chem. Soc. Rev*. 39 (2010) 2354.

69. P. J. Philips; *Rep. Prog. Phys.* 53 (1990) 549.

70. I. H. Campbell, D. L. Smith; *Semiconducting Polymers: Chemistry, Physics and Engineering*,1999, p365 ,G. Hadziioannou, and P. F. Hutten (ed), (Weinheim: Wiley-VCH).

71. A. B. Walker, A. Kambili, S. J. Martin; *J. Phys.Cond. Mat*. 14 (2002) 9825.

72. C. K. Chiang, C. R. Fincher, Y. W. Park, A. J. Heeger, H. Shirakawa, E. J. Louis, S. C. Gau, A. G. MacDiarmid; *Phys. Rev. Lett*. 39 (1977) 1098.

73. A. G. MacDiarmid; *Angew. Chem. Int. Ed*. 40 (2001) 2581.

74. S. Roth, H. Bleier , W. Pukacki; *Faraday Discuss. Chem. Soc.* 88 (1989) 223.

75. A. W. Bott; *Current Separations* 17 (1998) 87.

76. A. J. Heeger; *Rev. Mod. Phys*.73 (2001) 681.

77. M. Skompska, J. Mieczkowski, R. Holze, J. Heinze; *J. Electroana. Chem*. 577 (2005) 9.

78. C. Kvarnstrom, H. Neugebauer, A. Ivaska, N. S. Sariciftci; *J. Molec. Struct.* 521 (2000) 271.

79. N. S. Sariciftci; *Curr. Opin. Solid State. Mater. Sci*. 4 (1999) 373.

80. C. V. Hoven, R. Yang, A. Garcia, V. Crockett, A. J. Heeger, G. C. Bazan, T. Q. Nguyen; *PNAS* 105 (2008) 12730.

81. N. Gospodinova, L. Terlemezyan; *Prog. Polym. Sci.* 23 (1998) 1443.

82. E. S. Matyeeva; *Synth. Met.* 83 (1996) 89.

83. O. Guven; *Rad. Phys. & Chem.* 76 (2007) 1302.

84. S. Roth, D. Carroll; *One-Dimensional Metals*, 2nd Edition, (2004) 1-85, WILEY-VCH Verlag GmbH & Co. KGaA, Weinheim.

85. W. P. Su, J. R. Schrieffer, A. J. Heeger; *Phys. Rev. Lett.* 42 (1979) 1698.

86. J. P. Sethna, S. Kivelson; *Phys. Rev. B* 26 (1982) 3513.

87. S. Kuroda, H. Shirakawa; *Synth.Met*. 17 (1987) 423.

88. R. H.Friend, D. C. Bott, D. D. C. Bradley, C. K. Chai, W. J. Feast, P. J. S. Foot, J. R. M. Giles, M. E. Horton, C. M. Pereira, P. D. Townsend; *Phil. Trans. R. Soc. Lond*. A 314 (1985) 37.

89. J. L. Bredas, G. B. Street; *Acc. Chem. Res.*18 (1985) 309.

90. W. R. Salaneck, R. H. Friend, J. L. Bredas; *Physics Reports* 319 (1999) 231.

91. Y. Onodera; *Phys. Rev*. *B* 30 (1984) 301.

92. T. A. Skotheim, R. L. Elsenbaumer, J. R. Reynolds; *Handbook of Conducting Polymers*, 2nd edn,1998, Marcel Dekker, New York.

93. W. J. Feast, J. Tsibouklis, K. L. Pouwer, L. Groenendaal, E. W. Meijer; *Polymer* 37 (1996) 5017.

94. S. Sadki, P.Schottland, N. Brodie, G.Sabouraud; *Chem. Soc. Rev.* 29 (2000) 283.

95. H. S. Sharma, S. M. Park; *J. Electrochem. Soc.* 151 (2004) 61.

96. G. Sonmez, H. Meng, Q. Zhang, F. Wudl; *Adv. Funct*. *Mater*.13 (2003) 726.

97. R. D. McCullough; *Adv. mater*. 10 (1998) 93.

98. S. W. Feldberg; *J. Am. Chem. Soc* 106 (1984) 4671.

99. A. L. Dyer, J. R. Reynolds; *Handbook of conducting polymers 3rd ed. Conjugated polymers: theory, synthesis, properties and characterization, 2007,* p 860, T.A. Skotheim (ed), Taylor & Francis Group, Boca Raton London, New York.

100. G. Zotti; *Synth. Met*. 97 (1998) 267.

101. C. Deibel, T. Strobel, V. Dyakonov; *Adv. Mater.* 22 (2010) 4097.

102. T. Johansson, W. Mammo, M. Svensson, M. R. Andersson, O. Inganas; *J. Mater. Chem.*13 (2003) 1316.

103. L. Bredas, R. Silbey, D. S. Boudreaux, R. R. Chance; *J. Am. Chem. Soc.* 105 (1983) 6555.

104. C. M. Cardona, W. Li, A. E. Kaifer, D. Stockdale, G. C. Bazan; *Adv. Mater.* 23 (2011) 2367.

105. Y. Liang, Z. Xu, J. Xia, S. T. Tsai, Y. Wu, G. Li, C. Ray, L. Yu; *Adv.Mater.* 22 (2010) E135.

106. L. J. Huo, J. H. Hou, S. Q. Zhang, H. Y. Chen, Y. Yang; *Angew. Chem. Int. Ed.* 49 (2010) 1500.

107. Y. Liang, D. Feng, Y. Wu, S. T. Tsai, G. Li, C. Ray, L. Yu; *J. Am. Chem. Soc.* 31 (2009) 7792.

108. Y. Liang, Y. Wu, D. Feng, S. T. Tsai, H. J. Son, G. Li, L. Yu; *J. Am.Chem. Soc.* 131 (2009) 56.

109. L. Huo, J. Hou, H. Y. Chen, S. Zhang, Y. Jiang, T.L. Chen, Y.Yang, *Macromolecules* 42 (2009) 6564.

110. J. Pommerehne, H. Vestweber, W. Guss, R. F. Mahrt, H. Bässler, M. Porsch, J. Daub; *Adv. Mater.* 7 (1995) 551.

111. A. J. Bard, L. R. Faulkner; *Electrochemical Methods: Fundamentals and Applications,* 2001, Wiley, New York.

112. D. M. Leeuw, M. Simenon, R. Brown, R. Einerhnd; *Synth. Met.* 87 (1997) 53.

113. L. Micaroni, F. C. Nart, I. A. Hummelgen; *J. Solid State Electrochem* . 7 (2002) 55.

114. *http://webbook.nist.gov/,* National Institute of Standards and Technology.

115. A. J. Bard, L. R. Faulkner; *Electrochemical methods- fundamentals and applications,* 2nd Edn, 2000, p 53, Wiley, New York.

116. G. Gritzner, J. Kuta; *Pure Appl. Chem*. 56 (1984) 461.

117. M. S. Liu, X. Jiang, S. Liu, P. Herguth, A.K.Y. Jen; *Macromolecules* 35 (2002) 3532.

118. Y. Liu, M. S. Liu, A. K. Y. Jen; *Acta Polym.* 50 (1999) 105.

119. C. Y. Yu, C. P. Chen, S. H. Chan, G. W. Hwang, C. Ting; *Chem. Mater*. 21 (2009) 3262.

120. D. A. M. Egbe, B. Cornelia, J. Nowotny, W. Gunther, E. Klemm; *Macromolecules* 36 (2003) 5459.

121. M. Al-Ibrahima, H. K. Rotha, U. Zhokhavetsb, G. Gobschb, S. Sensfussa; *Sol. Ener. Mater. Sol. Cells* 85 (2005) 13.

122. L. B. Groenendaal, G. Zotti, P. H. Aubert, S. M. Waybright, J. R. Raynolds; *Adv. matter*. 15 (2003) 855.

123. H. S. Nalwa; *Advanced Functional Molecules and Polymers, V2, Processing and Spectroscopy*, 2001, p 139, OPA, Overseas Publishers Association N.V.

124. C. Kvarnstrom, H. Neugebauer, S. Blomquist, H. J. Ahonenc, J. Kankarec, A. Ivasaka; *Electrochimica Acta* 44 (1999) 2739.

125. H. Neugebauer, C. Kvarnstroem, A. Cravino, T. Yohannes, N. S. Sariciftci; *Synth. Met.* 116 (2001) 115.

126. M. Zagorska, A. Pron, S. Lefrant; *Hand book of organic conductive molecules, V3, Conductive polymers spectroscopy and physical properties*, 1997, p 203, H. S. Nalwa (ed), John Wiley & Sons New York.

127. P. Damlin, C. Kvarnstrom, A. Petr, P. Ek, L. Dunsch, A. Ivaska; *J Solid State*

Electrochem. 6 (2002) 291.

128. M. J. L. Santos, A. G. Brolo, E. M. Girotto; *Electrochimica Acta* 52 (2007) 6141.

129. S. Brazovskii, N. Kirova; *Chem. Soc. Rev.* 39 (2010) 2453.

130. R. Farchioni, G. Grosso; *Organic electronic materials: conjugated polymers and low molecular weight organic solids,* 2001, p127 Springer-Verlag berlin Heidelberg NewYork.

131. M. S. A, Abdou, S. Holdcroft; *Hand book of organic conductive molecules, conductive polymers: Transport, Photophysics and application*, *V4*, 1997, p174, H. S. Nalwa (ed), John Wiley & Sons New York.

132. I. B. Martini, A. D.Smith, B. J. Schwartz; *Phys. Rev. B* 69 (2004) 035204-1.

133. S. A. Jenekhe, J. A. Osaheni; *Science* 265 (1994) 765.

134. N. F. Colaneri, D. D. C.Bradley, R. H. Friend, P. L. Burn, A. B. Holmes, C. W. Spangler; *Phys. Rev.B* 42 (1990) 11670.

135. C. J. Brabace, V. Dyakonov, J. Parisi, N. S. Saricifici; *Organic photovoltaics: concepts and realizations* 2003, p15, Springer-Verlag.

136. E. Frankevich, A. Zakhidov, K. Yoshino, Y. Maruyama, K. Yakushi; *Phys. Rev. B* 53 (1996) 4498.

137. V. Dyakonov, E. Frankevich; *Chemical physics* 227 (1998) 203.

138. A. J.Heeger, S. Kevelson, J. R. Schrieffer, W. P Su; *Rev. Mod. Phys* 60 (1988) 781.

139. H. A. M. van Mullekom, J. A. J. M. Vekemans, E. E. Havinga, E. W. Meijer; *Mater. Sci. and Eng*. 32 (2001) 1.

140. H. Huang, Q. He, H. Lin, F. Bai, Z. Sun, Q. Li; *Polym. Adv. Technol*. 15 (2004) 84.

141. X. M. jiang, R. Osterbacka, O. Korovyanko, C. P. An, B. Horovitz, R. A. J, Janssen, Z. Vardeny; *Adv. Funct. mater*. 12 (2002) 587.

142. J. R. Lakowicz; *Principles of fluorescence spectroscopy*, 2006, 3rd Edn. Springer, New York, NY 10013 ,USA,

143. J. Gruber, R. W.C. Li, L.H.J M.C. Aguiar, T. L. Garcia, H. P.M. De Oliveira, T. D.Z. Atvars, A. F. Nogueira; *Synt. Met.,* 156 (2006) 104

144. Y. Kunugi, Y. Harima, K. Yamashita, N. Ohta, S. Ito; *J. Mater. Chem*. 10 (2000) 2673.

145. Y. Harima, T. Eguchi, K. Yamashita; *Synth. Met*. 95 (1998) 69.

146. A. J. Heeger; *Phil. Trans. R. Soc. Lond. A* 314 (1985) 17.

147. V. I. Arkhipov, E. V. Emelianova, P. Heremans, H. Bässler; *Phys. Rev. B* 72 (2005) 235202.

148. M. Jaiswal, R. Menon; *Polym. Int.* 55 (2006) 1371.

149. S. Stafstrom; *Chem. Soc. Rev*. 39 (2010) 2484.

150. A. J. Heeger; *Faraday Discuss. Chem. Soc.* 88 (1989) 203.

151. V. Coropceanu, J. Cornil, D. A. daSilva Filho, Y. Olivier, R. Silbey, J. L. Bredas; *Chem. Rev*. 107 (2007) 926.

152. L. Zuppiroli, M. N. Bussac, S. Paschen, O. Chauvet, L. Forro; *Physical Rev. B* 50 (1994) 5196.

153. J. Kline, M. D. M. Gehee; *J.Macromol. Sci. Part C: Polym. Rev.* 46 (2006) 27.

154. D. M. Pai, R. C. Enck; *Physical Rev. B* 11 (1975) 5163.

155. A. Pivrikas, N. S. Sariciftci, G. Juska, R. Osterbacka; *Prog. Photovolt: Res. Appl.* 15 (2007) 677.

156. H. Bässler; *Polym. Adv. Technol*. 9 (1998) 402.

157. M. Scheidler, B. Cleve, H. Bässler, P. Thomas; *Chem. Phys.Lett*. 225 (1994)

431.

158. L. J. A. Koster, V. D. Mihailetchi, P. W. M. Blom; *Appl. Phys. Lett*. 88 (2006) 052104.

159. V.I. Arkhipov, E.V. Emelianova, S. Barth, H. Bassler; *Physical Rev. B* 61 (2000) 8207.

160. L. J. A. Koster, V. D. Mihailetchi, R. Ramaker, P. W. M. Blom; *Appl. Phys. Lett*. 86 (2005) 123509.

161. V. I. Arkhipov, P. Heremans, E. V. Emelianova, G. J. Adriaenssens, H. Bässler; *J. Phys. Condens. Matter* 14 (2002) 9899.

162. S. S. Pandey, W. Takashima, S. Nagamatsu, T. Endo, M. Rikukawa, K. Kaneto; *Jpn. J. Appl. Phys*. *Part 1* 39 (2000) 94.

163. A. J. Campbell, D. D. C. Bradley, H. Antoniadis; *Appl. Phys. Lett*. 79 (2001) 2133.

164. A. J. Mozer, N. S. Sariciftci; *Chem. Phys. Lett*. 389 (2004) 438.

165. R. Österbacka, K. Genevicius, A. Pivrikas, G. Juška, K. Arlauskas, T. Kreouzis, D. D. C. Bradley, H. Stub; *Synth. Met.* 139 (2003) 811.

166. A. Pivrikas, G. Juska, A. J. Mozer, M. Scharber, K. Arlauskas, N. S. Sariciftci, H. Stubb, R. Osterbacka; *PRL* 94 (2005) 76806.

167. G. Juška, K. Genevičius, G. Sliaužys, A. Pivrikas, M. Scharber, R.Osterbacka; *J. Appl. Phys.* 101 (2007) 114505.

168. G. Juška, K. Arlauskas, G. Sliaužys, A. J. Mozer, N. S. Sariciftci, M. Scharber, R. Osterbacka; *App. Phys. Lett*. 87 (2005) 222110.

169. J. F. Rubinson, Y. P. Kayinamura; *Chem. Soc. Rev*. 38 (2009) 3339.

170. G. Juska, K. Arlauskas, R. Osterbacka, H. Stubb; *Synth.Met*. 109 (2000) 173.

171. G. Juska, K. Arlauskas, M. Viliunas, J. Kocka; *Phys. Rev. let.* 84 (2000) 4946.

172. G. Juska, K. Arlauskas, M. Viliunas, K. Genevicius, R. Osterbacka, H. Stubb; *Phys. Rev. let. B* 62 (2000) R16325.

173. R. Osterbacka , A. Pivrikas ,G.Juska , K. Genevicius , K. Arlauskas, H. Stubb; *Current App. Phys.* 4 (2004) 534.

174. G.Dennler, A.J.Mozer, G. Juška, A. Pivrikas, R. Österbacka, A. Fuchsbauer, N.S. Sariciftci; *Org. Electronics* 7 (2006) 229.

175. D. A. M. Egbe, E. Tekin, E. Birckner, A. Pivrikas, N.S. Sariciftci, U.S. Schubert; *Macromolecules* 40 (2007) 7786.

176. A. Palmaerts, L. Lutsen, J. T. Cleij, D. Vanderzande, A. Pivrikas, H. Neugebauer, N. S. Sariciftci; *Polymer* 50 (2009) 5007.

177. A. Pivrikas; Charge transport and recombination in bulk-heterojunction solar cells, Doctoral Thesis, Åbo Akademi University, 2006. ISBN 952-12-1786-3.

178. C. Vijila, A. Pivrikas, H. Chun, C. Zhikuan, R. Osterbacka, C. S. Jin; *Org. Electronics* 8 (2007) 8.

179. A.J.Mozer, D. Dennler, N. S. Sariciftci, M. Westerling, A. Pivrikas, R. Österbacka, G. Juška; *Phys. Rev. B* 72 (2005) 035217.

180. A. Pivrikas, R. Osterbacka, G. Juska , K. Arlauskas , H. Stubb; *Synth. Met*. 155 (2005) 242.

181. A. Pivrikas, G. Juska, K. Arlauskas, M. Scharber, A. Mozer, N.S. Sariciftci, H. Stubb, R. Osterbacka; *Proc. of SPIE* 5938 (2005) 59380.

182. R. Osterbacka , A. Pivrikas, G. Juska, K. Genevicius, K. Arlauskas , H. Stubb; *Curr. App. Phys*. 4 (2004) 534.

183. M. Ullah, I. I. Fishchuk, A. Kadshchuk, P. Stadler, A. Pivrikas, C. Simbrunner ,V. N. Poroshin, N. S. Sariciftci, H. Sitter; *Appl. Phys. Lett*. 96 (2010) 213306.

184. J. Heinze, B. A. F. Uribe, S. Ludwigs; *Chem. Rev*. 110 (2010) 4724.

185. N. Toshima, S. Hara; *Prog. Polym. Sci*. 20 (1995) 155.

186. F. A. Carey, R. J. Sundberg; *Adavaced organic chemistry, Part B reactions and synthesis 5th Edn*. 2007 ,Springer Science+Business Media, LLC, 233 Spring Street, New York, NY 10013, USA,P675.

187. J. K. Stille; *Angew. Chem. Int. Ed*. 25 (1986) 508.

188. N. Miyaura, A. Suzuki; *Chem. ReV*. 95 (1995) 2457.

189. K. Sonogashira; *J. Organomet. Chem*. 653 (2002) 46.

190. U. H. F. Bunz; *Chem. Rev*. 100 (2000) 1605.

191. Q. Pei, G. Zuccarello, M. Ahlskog, O. Inganas; *Polymer* 35 (1994) 1347.

192. Q. T. Zhang, J. M. Tour; *J. Am. Chem. Soc*. 120 (1998) 5355.

193. C. Kitamura, S.Tanaka; Y.Yamashita; *Chem. Mater*. 8 (1996) 570.

194. A. Berlin, G. Zotti, S. Zecchin, G. Schiavon, B. Vercelli, A. Zanelli; *Chem. Mater.* 16 (2004) 3667.

195. F. Cacialli, P. Samori, C. Silva; *Mater Today* 7 (2004) 24.

196. Z. Bao, W. K. Chan, L. Yu; *J. Am. Chem. Soc* 117 (1995) 12426.

197. F. Padinger, R. S. Rittberger, N. S. Sariciftci; *Adv Funct Mater* 13 (2003) 85.

198. N. Drolet, J. F. Morin, N. Leclerc, S. Wakim, Y. Tao, M. Leclerc; *Adv Funct Mater* 15 (2005) 1671.

199. C. Waldauf, M. C. Scharber, P. Schilinsky, J. A. Hauch, C. J. Brabec; *J. Appl. Phys*. 99 (2006) 104503-1.

200. C. Waldauf, P. Schilinsky, J. Hauch, C. J. Brabec; *Thin Solid Films* 451 – 452 (2004) 503.

201. V. Dyakonov; *Physica E 14* (2002) 53.

202. B. A. Gregg; *J. Phys. Chem. B* 107 (2003) 4688.

203. W. J. Potscavage, J. A. sharma, B. Kippelen; *Acc. Chem. Res* 42 (2009) 1758.

204. J. L. Bredas, J. E. Norton, J. Cornil, V. Coropceanu; *Acc. Chem. Res* 42 (2009) 1691.

205. T. L. Benanti, D. Venkataraman; *Photosynthesis research* 87 (2006) 73.

206. P. Heremans, D. Cheyns, B. P. Rand; *Acc. Chem. Research* 42 (2009) 1740.

207. B. Kippelen, J. L. Bredas; *Energy Environ. Sci.* 2 (2009) 251.

208. C. Deibel, V. Dyakonov; *Rep. Prog. Phys*. 73 (2010) 096401.

209. M. C. Scharber, D. Muhlbacher, M. Koppe, P. Denk, C. Waldauf, A. J. Heeger, C. J. Brabec; *Adv. Mater.* 18 (2006) 789.

210. B. C. Thompson, J. M. J. Frechet; *Angew. Chem. Int. Ed*. 47 (2008) 58.

211. J. M. Kroona, M. M. Wienk, W. J. H. Verhees, J. C. Hummelen; *Thin Solid Films* 403 – 404 (2002) 223.

212. V. Shrotriya, G. Li, Y. Yao, T. Moriarty, K. Emery, Y. Yang; *Adv. Funct. Mater.* 16 (2006) 2016.

213. H. Hoppe, N. S. Sariciftci; *Adv. Polym. Sci*. 214 (2008) 1.

214. Y. Liang, Y. Wu, D. Feng, S.T. Tsai, H. J. Son, G. Li, L.Yu; *J. Am. Chem. Soc*.131 (2009) 56.

215. S. Barth, H. Bassler; *Phys. Rev. Lett*. 79 (1997) 4445.

216. C.J. Brabec, G. Zerza, G. Cerullo, S.D. Silvestri, S. Luzzati, J.C. Hummelen, N. S. Sariciftci; *Chem. Phys. Lett.* 340 (2001) 232.

217. V. D. Mihailetchi, J. Wildeman, P. W. M. Blom; *Phys. Rev. Lett*. 94 (2005) 126602.

218. V. D. Mihailetchi, P. W. M. Blom, J. C. Hummelen, M. T. Rispens; *J. Appl. Phys*. 94 (2003) 6849.

219. V. D. Mihailetchi, L. J. A. Koster, P. W. M. Blom; *Appl. Phys. Lett*. 85 (2004) 970.

220. ISO 9845-1 (1992), ASTME 892-87 (1992)

221. C. J. Brabec, A. Cravino, D. Meissner, N. S. Sariciftci, T. Fromherz, M. T. Rispens, L. Sanchez, J. C. Hummelen; *Adv. Funct. Mater*. 11 (2001) 374.

222. G. Dennler, M. C. Scharber, C. J. Brabec; *Adv. Mater*. 21 (2009) 1323.

223. J. C. Bernede; J. Chil. *Chem. Soc*. 53 (2008) 1549.

224. T. Aernouts, W. Geens, J. Poortmans, P. Heremans, S. Borghs, T. Mertens; *Thin Solid Films*, 403–404 (2002) 297.

225. I. Riedel, J. Parisi, V. Dyakonov, L. Lutsen, D. Vanderzande, J. C. Hummelen; *Adv. Funct. Mater*. 14 (2004) 38.

226. M. Hallermann, I. Kriegel, E. Da Como, J. M. Berger, E. von Hauff, J. Feldmann; *Adv. Funct. Mater*. 19 (2009) 3662.

227. H. Hoppe, N. S. Sariciftci; *J. Mater. Chem*. 16 (2006) 45.

228. C. R. McNeill, H. Frohne, J. L. Holdsworth, P. C. Dastoor; *Synth. Met.* 147 (2004) 101.

229. X. Yang, J. Loos; *Macromolecules* 40 (2007) 1353.

230. S. Cook, A. Furub, R. Katohj; *J. Appl. Phys.* 47 (2008) 1238.

231. J. Liu, Y. Shi, Y. Yang; *Adv. Funct. Mater*. 11 (2001) 420.

232. M. T. Rispens, A. Meetsma, R. Rittberger, C. J. Brabec, N. S. Sariciftci, J. C. Hummelen; *Chem. Commun.* 17 (2003) 2116.

233. T. Salim, L. H. Wong, B. Brauer, R. Kukreja, Y. L. Foo, Z. Baod, Y. M. Lam; *J. Mater. Chem*. 21 (2011) 242.

234. L. Chang, H. W. A. Lademann, J. B. Bonekamp, K. Meerholz, A. J. Moule; *Adv. Funct. Mater.* 21 (2011) 1779.

235. M. S. Su, C. Y. Kuo, M. C. Yuan, U. S. Jeng, C. J. Su, K. H. Wei; *Adv. Mater.* 23 (2011) 3315.

236. H. Hoppe, M. Niggemann, C. Winder, J. Kraut, J. R. Hiesgen, A. Hinsch, D. Meissner, N. S. Sariciftci; *Adv. Funct. Mater.* 14 (2004) 1005.

237. C. J. Ko, J. K. Lin, F. C. Chen; *Adv. Mater*. 19 (2007) 3520.

238. H. Hoppe, N.S. Saricifitci; *Adv. Polym. Sci.* 241 (2008) 1.

239. G. Dennler, C. Lungenschmied, H. Neugebauer, N.S. Sariciftci, A. Labouret; *J. Mater. Res*. 20 (2005) 3224.

240. C. J. Brabec, J. A.Hauch, P. Schilinsky, C. Waldauf; *MRS Bull*. 30 (2005) 50.

241. M. R. Reyes, K. Kim, D. L. Carolla; *Appl. Phys. Lett*. 87 (2005) 083506.

242. I. McCulloch, M. Heeney, M. L. Chabinyc, D. DeLongchamp, R. J. Kline, M. Cölle, W. Duffy, D. Fischer, D. Gundlach, B. Hamadani, R. Hamilton, L. Richter, A. Salleo, M. Shkunov, D. Sparrowe, S.Tierney, W. Zhang; *Adv. Mater*. 21 (2009) 1091.

243. J. Y. Kim, K. Lee, N. S. Coates, D. Moses, T. Q. Nguyen, M. Dante, A. J. Heeger; *Science* 317 (2007) 222.

244. H. Y. Chen, J. Hou, S. Zhang, Y. Liang, G. Yang, Y. Yang, L. Yu, Y. Wu, G. Li; *Nature Photonics* 3 (2009) 649.

245. http://www.neubers.de/Solar-Taschen.

246. H. Hoppe, N. S. Sariciftci; *Nanostructure and Nanomorphology Engineering in Polymer Solar Cells in Nanstructured Materials for Solar Energy Conversion*, 2006, p. 277, Eds: T. Soga, Elsevier Amsterdam.

247. H. Hoppe, N. S. Sariciftci; *Polymer Solar Cells* in Photoresponsive Polymers II, Eds.: S. R. Marder, K. S. Lee; *Advances in Polymer Science,* 2008, p1-86, *Springer, Berlin-Heidelberg*.

248. Y. Yao, J. Hou, Z. Xu, G. Li, Y. Yang; *Adv. Funct. Mater.* 18 (2008) 178.

249. D. A. M. Egbe, B. Carbonnier, E. Birckner, U. W. Grummt; *Prog. Polym. Sci*.

34 (2009) 1023.

250. R. Jadhav, S. Türk, F. Kühnlenz, V. Cimrova, S. Rathgeber, D. A. M. Egbe, H. Hoppe; *Phys. Status Solidi A* 12 (2009) 2695.

251. D. A. M. Egbe, S.Türk, S. Rathgeber, F. Kühnlenz, R. Jadhav, A. Wild, E. Birckner, G. Adam, A. Pivrikas, V. Cimrova, G. Knor, N. S. Sariciftci, H. Hoppe, *Macromolecules* 43 (2010) 1261.

252. S. Rathgeber, D. B. de Toledo, E. Birckner, H. Hoppe, D. A. M. Egbe; *Macromolecules* 43 (2010) 306.

253. D. T. McQuade, A. E. Pullen, T.M. Swager; *Chem. Rev*. 100 (2000) 2537.

254. A. Wild, D. A. M. Egbe, E. Birckner, V. Cimrova, R. Baumann, U. W. Grummt, U.S. Schubert ; *J. Polym. Sci: Part A: Polym. Chem.* 47 (2009) 2243.

255. M. D. McGehee, A. J. Heeger; *Adv. Mater.* 12 (2000) 1655.

256. T. Nguyen, V. Doan, B. J. Schwartz; *J. Chem. Phys.* 110 (1999) 4068.

257. A. Pivrikas, P. Stadler, H. Neugebauer, N. S. Sariciftci; *Org. Electronics* 9 (2008) 775.

258. G. Juska, K. Genevicius, K. Arlauskas, R. Österbacka, H. Stubb; *Phys. Rev. B* 65 (2002) 233208.

259. H. Bässler; *Phys. Status Solidi B* 175 (1993) 15.

260. G. Yu, A. J. Heeger; *J. Appl. Phys*. 78 (1995) 4510.

261. T. Kietzke, D. A. M.Egbe, H. H. Hörhold, D. Neher; *Macromolecules* 39 (2006**)** 4018.

262. T. Kietzke; *Advances in Opto Electronics*, V2007 (2007) 1.

263. V. D. Mihailetchi, J. K. J.van Duren, P. W. M. Blom, J. C. Hummelen, R. A. J. Janssen, J. M. Kroon, M. T. Rispens, W. J. H. Verhees, M. M. Wienk; *Adv. Funct. Mater.*13 (2003) 43.

264. M. Gaetzel, A. J. McEvoy; *Asian J. Ener. & Environ*. 5 (2004) 197.

265. K. Tennakone, V. P. S. Perera, I. R. M. Kottegoda, G. Kumara; *J. Phys. D Appl. Phys*. 32 (1999) 374.

266. M. Matsumoto, Y. Wada, T. Kitamura, K. Shigaki, T. Inoue, M. Ikeda, S. Yanagida; *Bull. Chem. Soc. Japan* 74 (2001) 387.

267. D. Gebeyehu, C. J. Brabec, N. S. Sariciftci; *Thin Solid Films* 403 (2002) 271.

268. H. Paulsson, A. Hagfeldt, L. Kloo; *J. Phys. Chem. B* 107 (2003) 13665.

269. E. Stathatos, P. Lianos, A. S. Vuk, B. Orel; *Adv. Funct. Mater*. 14 (2004) 45.

270. M. Nekoomanesh, H. S. Nagae, C. Booth, J. R. Owen; *J. Electrochem. Soc.* 139 (1992) 3046.

271. M. Adi, T.Yohannes, T.Solomon; *Sol. Ener. Mater. Sol. Cells* 83 (2004) 301.

272. A. Sergawi; *PHD thesis*, 2007 p73-89, Addis Ababa University, Ethiopia

273. S. Tadesse, T. Yohannes; *Bull. Chem. Soc. Ethiop.* 26-2 (2012) 1.

274. U. Mengeshaa, T. Yohannes; *Sol. Ener. Mater. Sol. Cells* 90 (2006) 3508.

275. S. M. Sze, K. K. Ng; *Physics of Semiconductor Devices 3rd edn* ,2007, John Wiley & Sons, Inc., Hoboken, New Jersey.

276. T. A. Skotheim, S. W. Feldberg, M. B. Armand; *J. Phys. Paris Colloq.* C 3 (1983**)** 615.

277. A. Hagfeldt, M. Gratzel; *Acc. Chem. Res*. 33 (2000) 269.

278. S. Nagae, H. M. Nekoomanesh, C. Booth, J. R. Owen; *Solid State Ionics* 53–56 (1992) 1118.

279. J. N. Freitas, A. Pivrikas, B. F.Nowackic, L. C. Akcelrud, N. S. Sariciftci, A. F. Nogueira; *Synth. Met* 160 (2010) 1654.

280. A. Palmaerts, L. Lutsen, T. J. Cleij, D. Vanderzande, A. Pivrikas, H. Neugebauer, N. S. Sariciftci; *Polymer* 50 (2009) 5007.

281. H. Hoppe, T. Glatzel , M. Niggemann, W. Schwinger, F. Schaeffler, A. Hinsch, M. C. Lux-Steiner, N. S. Sariciftci; *Thin Solid Films* 511 (2006) 587.

282. C. Y. Yang, A. J. Heeger; *Synth. Met.* 83 (1996) 85.

283. J. Peet, M. L. Senatore, A. J. Heeger, G. C. Bazan; *Adv. Mater*. 21 (2009) 1521.

284. G. Li, V. Shrotriya, Y. Yao, Y. Yang; *J. Appl. Phys.* 98 (2005) 043704.

285. N. Y. Canli, S. Günes, A. Pivrikas, A. Fuchsbauer, D. Sinwel, N. S. Sariciftci, O. Yasa, B. B. Eran; *Sol. Energy mater. Sol. Cells* 94 (2010) 1089.

286. Y. Kim, S. cook, S. M. Tuladhar, S. A. Choulis, J. Nelson, J. R. Durrant, D. D. C. Bradley, M. Giles, I. Mcculloch, C. S. Ha, M. Ree; *Nat. Mater* 5 (2006) 197.

287. A. J. Moule, K. Meerholz; *Adv. Mater.* 20 (2008) 240.

288. F. L. Zhang, K. G. Jespersen, C. Bjorstrom, M. Svensson, M. R. Andersson, V. Sundstrom, K. Magnusson, E. Moons, A. Yartsev, O. Inganas; *Adv. Funct. Mater.*16 (2006) 667.

289. V. Shrotriya, Y. Yao, G. Li, Y. Yang; *Appl. Phys. Lett*. 89 (2006) 063505.

290. P. Vanlaeke, G. Vanhoyland, T. Aernouts, D. Cheyns, C. Deibel, J. Manca, P. Heremans, J. Poortmans; *Thin Solid Films* 511 (2006) 358.

291. V. D. Mihailetchi, H. Xie, B. de Boer, L. M. Popescu, J. C. Hummelen, P. W. M. Blom, L. J. A. Koster; *Appl. Phys. Lett.* 89 (2006) 012107.

292. Y. Kim, S. A. Choulis, J. Nelson, D. D. C. Bradley, S. Cook, R. Durrant; *Appl. Phys. Lett.* 86 (2005) 063502.

293. S. E. Shaheen, C. J. Brabec, N.S. Sariciftci; *Appl. Phys. Lett.* 78 (2001) 841.

294. J. Ouyang, Y. Xia; *Sol. Energy Mater. Sol. Cells* 93 (2009) 1592.

295. J. Peet, J. Y. Kim, N. E. Coates, W. L. Ma, D. Moses, A. J. Heeger , G. C.

Bazan; *Nature Mater.* 6 (2007) 496.

296. J. Peet, C. Soci, R. C. Coffin, T. Q. Nguyen, A. Mikhailovsky, D. Moses G. C. Bazan; *App. Phys.Letters.* 89 (2006) 252105.

297. C. H. Yang, J. Qiao, Q. J. Sun, K. J. J. Jiang, Y. L. Li, Y.F. Li; *Synth.Met.* 137 (2003) 1521.

298. F. C. Chen, Q. Xu, Y. Yang; *Appl. Phys. Lett*. 84 (2004) 3181.

299. R. Bechara, N. Leclerc, P. Lévêque, F. Richard, T. Heiser, G. Hadziioannou; *Appl. Phys. Lett.* 93 (2008) 013306.

300. Y. Kim, S. Cook, S. A Choulis, J Nelson, J. R Durrant, D. D. C Bradley; *Synth. Met.* 152 (2005) 105.

301. H. Kim, M. Shin, Y. Kim; *J. Phys. Chem.C* 113 (2009) 1620.

302. Y. Kim, M .Shin, H. Kim, Y. Ha, C. S. Ha; *J. Phys. D: Appl.Phys.* 41 (2008) 225101.

303. C. H. Chen, C. H. Hsieh, M. Dubosc, Y. J. Cheng, C. S. Hsu; *Macromolecules* 43 (2010) 697.

304. S. Günes, A.Wild, E. Cevik, A. Pivrikas, U. S. Schubert, D. A. M. Egbe; *Sol. Energy mater. Sol. Cells* 94 (2010) 484.

305. C. J. Brabec, A. Cravino, G. Zerza, N. S. Sariciftci, R. Kiebooms, D. Vanderzande, J. C. Hummelen; *J. Phys. Chem. B* 105 (2001) 1528.

306. R. J. Kline, D. M. DeLongchamp, D. A. Fischer, E. K. Lin, L. J. Richter, M. L. Chabinyc, M. F. Toney, M. Heeney, I. McCulloch; *Macromolecules* 40 (2007) 7960.

307. L. S.Yu, S. A. Chen; *Adv.Mater*. 16 (2004) 744.

308. E. Tekin, D. A. M. Egbe, J M. Kranenburg, C. Ulbricht, S. Rathgeber, E. Birckner, N. Rehmann, K. Meerholz, U. S. Schubert; *Chem. Mater.* 20 (2008)

2727.

309. D. A. M. Egbe, C. Ulbricht, T. Orgis, B. Carbonnier, T. Kietzke, M. Peip, M. Metzner, M. Gericke, E. Birckner, T. Pakula, D. Neher, U.W. Grummt; *Chem. Mater.* 17 (2005) 6022,

310. D. A. M. Egbe, C. P. Roll, E. Birckner, U.W. Grummt, R. Stockmann, E. Klemm; *Macromolecules* 35 (2002) 3825.

311. G. Juška, G. Sliauzys, K. Genevičius, K. Arlauskas, A. Pivrikas, M. Scharber, G. Dennler, N. S. Sariciftci, R. Österbacka; *Physics Review B* 74 (2006) 115314.

312. A. Pivrikas, G. Juška, R. Österbacka, M. Westerling, M. Viliunas, K. Arlauskas, H. Stubb; *Phys. Rev. B* 71 (2005) 125205.

313. H. Shirakawa; *Rev. Mod. Phys*. 73 (2001) 713.

314. T. A. Skotheim, J. R. Reynolds; (eds) , *Hand book of Conducting Polymers 3rd Edn*, Boca Raton, New York (2007).

315. C. J. Brabec, N. S. Sariciftci, J. C. Hummelen; *Adv. Funct. Mater*. 11(2001) 15.

316. R. D. McCullough, S. P. Williams; *J. Am. Chem. Soc.* 115 (1993) 11608.

317. J. H. Burroughes, D. D. C. Bradley, A. R. Brown, R. N. Marks, K. MacKays, R. H. Friend, P. L. Burn, A. B. Holmes; *Nature* 347 (1990) 539.

318. A. J. Mozer, P. Denk, M. C. Scharber, H. Neugebauer, N. S. Sariciftci, P. Wagner, L. Lutsen, D. Vanderzande; *J. Phys. Chem. B* 108 (2004) 5235.

319. X. Yang, J. K. J. vanDuren, R. A. J. Janssen, M. A. J. Michels, J. Loos; *Macromolecules* 37 (2004) 2151.

320. S. Pfeiffer, H. H. Hörhold; *Macromol. Chem. Phys.* 200 (1999) 1870.

321. S. Pfeiffer, H. H. Hörhold; *Macromol. Chem. Phys.* 200 (1999) 2471.

322. M. Moroni, J. Le. Moigne, S. Luzzati; *Macromolecules* 27 (1994) 562.

323. H. Hoppe, N. S. Sariciftci , D. A. M. Egbe, D. Mühlbacher , M. Koppe; *Mol. Cryst. Liq. Cryst*. 426 (2005) 255.

324. C. V. G. Weder; *Adv Polym Sci.* 177 (2005) 209.

325. X. Zhan, D. Zhu; *Polym. Chem*. 1 (2010) 409.

326. D. A. M. Egbe, T. Kietzke, B. Carbonnier, D. Mühlbacher, H. H. Hörhold, D.Neher; *Macromolecules* 37 (2004) 8863.

327. D. A. M. Egbe, L. H. Nguyen, D. Mühlbacher, H. Hoppe, K. Schmidtke, N. S. Sariciftci; *Thin Solid Films.* 511– 512 (2006) 486.

328. D. A. M. Egbe, L. H. Nguyen, B. Carbonnier, D. Mühlbacher, N.S. Sariciftci; *Polymer* 46 (2005) 9585.

329. G. Adam, A. Pivrikas, A. M. Ramil, S. Tadesse, T.Yohannes, N. S. Sariciftci D. A. M. Egbe; *J. Mater. Chem*. 21 (2011) 2594.

330. D. A. M. Egbe, H. Tillmann, E. Birckner, E. Klemm; *Macromol. Chem. Phys.* 202 (2001) 2712.

331. Y. Zhu, M. O. Wolf; *J.Am. Chem. Soc*. 122 (2000) 10121.

332. D. A. M. Egbe, C. P. Roll, E. Birckner, U. W. Grummt, R. Stockmann, E. Klemm; *Macromolecules* 35 (2002) 3825.

333. B. Valeur; *Molecular Fluorescence Principles and Applications*, WILEY-VCH Verlag GmbH, 69469 Weinheim ,Germany 2002.

334. A. G. MacDiarmid; *Phys. Rev. letters* 39 (1977) 1098.

335. C. K. Chiang, M. A. Druy, S. C. Gau, A. J. Heeger, E. J. Louis, A .G. MacDiarmid, Y. W. Park, H .Shirakawa; *J. Am. Chem. Soc.* 100 **(**1978) 1013.

336. C. K. Chiang, Y. W. Park, A .J. Heeger, H. Shirakawa, E. J. Louis , A. G. MacDiarmid; *J. Chem. Phys* .69 **(**1978) 5098.

337. M. A. Ibrahim, H.K Roth, M. Schroedner, A. Konkin, U. Zhokhavets, G. Gobsch, P. Scharff, S. Sensfuss; *Org. Electron*. 6 (2005) 65.

338. L. H. Nguyen, H. Hoppe, T. Erb, S. Günes, G. Gobsch, N. S. Sariciftci; *Adv.func. mat.* 17 (2007) 1071.

339. G. Chidichimo, L. Filippelli; *Int. J. Photoenergy* V 2010 (2010) 1.

340. T. L. Benanti, D. Venkataraman; *Photosynthesis research* 87 (2006) 73.

341. J. K. Lee, W. L. Ma, C. J. Brabec, J. Yuen, J. S. Moon, J. Y. Kim, K. Lee, G. C. Bazan, A. J. Heeger; *J.Am.Chem. Soc*. 130 (2008) 3619.

342. J. T. Rogers , K. Schmidt , M. F. Toney, E. J. Kramer, G. C. Bazan; *Adv. Mater*. 23 (2011) 2284.

343. C. K. Chan, W. Zhao, A. Kahn, I. G. Hill; *Appl.Phys. Lett*. 94 (2009) 203306.

344. R. Singh, R. K. Singh, J. Kumar, R. Kant, V. Kumar; *J.Polym. Sci: Part B: Polym. Phys.* 48 (2010) 1047.

345. R. K. Singh, J. Kumar, R. Singh, R. Kant, R. C. Rastogi, S. Chand, V. Kumar; *New; J. Phys.* 8 (2006) 112.

346. J. H. Huang, M. Velusamy, K. C. Ho, J. T. Lin, C. W. Chu; *J. Mater. Chem*. 20 (2010) 2820.

347. B. Scrosati; *Application of electroactive polymers*, 1st edn, 1993 p46 Chapman and Hall,2-6 Boundary Raw,London SE1 8HN.

348. P. Chandrasekhar; *Conducting Polymers, Fundamentals and Applications: A Practical Approach*, (1999) p. 83, Kluwer Academic, Boston.

349. O. Atwani, C. Baristiran, A. Erden, G. Sonmez; *Synth. Met.* 158 (2008) 83.

350. J. Clark, C. Silva, R. H. Friend, F. Spano; *Phys. Rev. Lett*. 98 (2007) 206406.

351. C. R. McNeill, A. Abrusci, I. Hwang, M. A. Ruderer, P. M. Buschbaum, N. C. Greenham; *Adv. Funct. Mater*. 19 (2009) 3103.

352. Y.C. Huang , Y.C. Liao, S. S. Li, M. C. Wu, C. W. Chen, W. F. Su; *Sol. Energ. Mater. Sol. Cells* 93 (2009) 888.

353. J. T. Shieh, C. H. Liu, H. F. Meng, S. R. Tseng, Y. C. Chao, S. F. Horng ; *J. App. Phys*. 107 (2010) 084503-1.

354. G. Li, V. Shrotriya, Y. Yao, J. S. Huang, Y. Yang; *J. Mater.Chem*. 17 (2007) 3126.

355. Y. Y. Liang, D. Q. Feng, Y. Wu, S. T. Tsai, G. Li, C. Ray, L. P. Yu; *J. Am. Chem. Soc*. 131 (2009) 7792.

356. J. H. Hou, H. Y. Chen, S. Q. Zhang, G. Li ,Y. Yang; *J. Am. Chem.Soc*. 130 (2008) 16144.

357. M. H. Chen, J. Hou, Z. Hong, G. Yang, S. Sista, L. M. Chen, Y. Yang; *Adv. Mater*. 21 (2009) 4238.

358. 'Solarmer Energy Inc. breaks psychological barrier with 8.13% OPV efficiency', http://www.solarmer.com/news.php.

359. 'Heliatek and IAPP achieve production-relevant efficiency record for organic photovoltaic cells', http://www.heliatek.com/index.php? page¼news.

360. C. Winder, N. S. Sariciftci; *J. Mater. Chem*. 14 (2004) 1077.

361. J. Roncali; *Macromol. Rapid Comm*. 28 (2007) 1761.

362. J. Hou, H. Y. Chen, S. Zhang, G. Li, Y. Yang; *J. Am. Chem. Soc*. 130 (2008) 16144.

363. N. Blouin, A. Michaud, M. Leclerc; *Adv. Mater.* 19 (2007) 2295.

364. Y. Liang, Y. Wu, D. Feng, S. T. Tsai, H. J. Son, G. Li, L. Yu; *J.Am. Chem. Soc*. 131 (2009) 56.

365. A. Gadisa, M. Svensson, M. R. Andersson, O.Inganas; *Appl. Phys. Lett*. 84 (2004) 1609.

366. Y. Li, Y. Zhou; *Adv. Mater*. 20 (2008) 2952.

367. T. Rousseau, A. Cravino, T. Bura, G. Ulrich, R. Ziessel, J. Roncali; *J. Mater. Chem*. 19 (2009) 2298.

368. A. Ojala, H. Bürckstümmer , M. Stolte, R.Sens, H. Reichelt, P. Erk, J. Hwang, D. Hertel, K. Meerholz, F. Würthner; *Adv. Mater.* 23 (2011) 5398.

369. S. Sista, Z. Hong, L. M. Chenx, Y. Yang; *Ener. Envir. Sci*. 4 (2011)1606.

370. M. K. Siddiki, J. Li, D. Galipeau, Q. Qiao; *Ener. Envir. Sci*. 3 (2010) 867.

371. S. Sista, Y. Yao, Y. Yang, M. L. Tang, Z. Bao; *Appl. Phys. Lett*. 91 (2007) 223508.

372. C. Zhang, S. W. Tong, C. Jiang, E. T. Kang, D. S. H. Chan, C. Zhu; *Appl. Phys. Lett*. 92 (2008) 083310.

373. T. Ameri, G. Dennler, C. Lungenschmied, C. J. Brabec; *Ener. Envir. Sci*. 2 (2009) 347.

374. A. Hadipour, B. de Boer, P. W. M. Blom; *Adv. Funct. Mater*.18 (2008) 169.

375. J. H. Huang, M. Velusamy, K. C. Ho, J. T. Lin, C.W. Chu; *J. Mater. Chem*. 20 (2010) 2820.

376. P. P. Khlyabich, B. Burkhart, B.C.Thompson; *J. Am. Chem. Soc*. 133 (2011) 14534.

377. J. Moule, A. Tsami, T. W. Bünnagel, M. Forster, N. M. Kronenberg, M. Scharber, M. Koppe, M. Morana, C. J. Brabec, K.Meerholz, U.Scherf; *Chem. Mater.* 20 (2008) 4045.

378. P. A. Troshin, D. K. Susarova, Y. L. Moskvin, I. E. Kuznetsov, S. A. Ponomarenko, E. N. Myshkovskaya, K. A. Zakharcheva, A. A. Balakai, S.D. Babenko, V. F. Razumov; *Adv. Funct. Mater.* 20 (2010) 4351.

379. B. Carbonnier, D. A. M. Egbe, E. Birckner, U.W. Grummt, T. Pakula;

M*acromolecules* 38 (2005) 7546.

380. T. Yamamoto, D. Komarudin, M. Arai, B. L. Lee, H. Suganuma, N. Asakawa, Y. Inoue, K. Kubota, S. Sasaki, T. Fukuda, H. Matsuda; *J. Am. Chem. Soc.* 120 (1998) 2047.

381. T. Tominaga, K. Hayashi, N. Toshima; *Appl. Phys. Lett*. 70 (1997) 762.

382. B. C. Thompson, J. M. J. Frechet; *Angew. Chem. Int. Ed*. 47 (2008) 58.

383. J. Dai, X. Jiang, H. Wang, D. Yan; *Appl. Phys. Lett*. 91 (2007) 253503.

384. J. H. Huang, C. Y. Yang, Z. Y. Ho, D. Kekuda, M. C. Wu, F. C. Chien, P. Chen, C. W. Chu, K. C. Ho; *Org. Electron*. 10 (2000) 27.

385. N. Zhao, T.P. Osedach, L.Y. Chang, S. M. Geyer, D. Wanger, M.T. Binda, A. C. Arango, M. G. Bawendi, V. Bulovic; *ACS Nano* 4 (2010) 3743.

386. X. Lei, F. Zhang, T. Song, B. Sun; *Appl. Phys. Lett*. 99 (2011) 233305.

Appendix A

Synthesis and general characterization of AnE-PVstat

Poly-{1,4-[2,5-dioctyloxy-or***-di(2-ethylhexyloxy)]phenylene-ethynylene-9,10-anthracenylene-ethynylene-1,4-[2,5-dioctyloxy-***or***-di(2-ethylhexyloxy)]phenylene-vinylene-1,4-[2,5-dioctyloxy-***or***-di(2-ethylhexyloxy)]phenylene-vinylene}***

(AnE-Vstat)

9,10-Bis{[2,5-di(2-ethylhexyloxy)-4-formyl]phenyl]-ethynyl}anthracene (**6a**) (100 mg, 0.1055 mmol) and 9,10-Bis{[2,5-di(2-ethylhexyloxy)-4-formyl]phenyl]-ethynyl} anthracene (**6b**) (100 g, 0.1055 mmol), 2,5-dioctyloxy-*p*-xylylene-bis (diethyl phosphonate) (**14a**) (67 mg, 0.1055 mmol), 2,5-di(2-ethyl)-hexyloxy-*p*-xylylene-bis (diethylphopsphonate) (**14b**) (67 mg, 0.1055 mmol) [251] were dissolved in dry toluene (20 mL). The mixture was heated under reflux and an excess potassium-*tert*-butoxide (96 mg, 0.856 mmol) was added in small portions. After 1.5 h reaction time, more toluene was added and the reaction was quenched after pouring 5% aqueous HCl (20 mL) into the mixture. The organic phase was separated and washed six times with deionized water until the aqueous phase became nearly neutral (pH = ~ 7). The remaining water was removed by heating using a Dean-Stark apparatus. The resulting toluene solution was filtered and evaporated under vacuum to a small rest, which was subsequently precipitated into cold methanol. The polymer was filtered off, dried and extracted for 1.5 h with a 1:1 mixture of methanol:diethylether. Yield: 240 mg (89.24%). GPC (THF as eluent, polystyrene standards): UV detector: M_n = 27,500 g/mol, M_w = 56,900 g/mol, M_z = 97,000 g/mol, M_p = 49,700 g/mol. PDI = 2.0, P_n = 22, IR detector: M_n = 28,100 g/mol, M_w = 58,000 g/mol, M_z = 104,400 g/mol, M_p = 50,700 g/mol. PDI = 2.0, P_n = 22. ^{1}H NMR ($CDCl_3$, 200 MHz): δ/ppm = 8.90 - 8.70,

7.58 - 7.53 and 6.86 - 6.80 (18H, arylene and vinylene H´s); 4.47 - 3.62 (12H, -CH_2O-); 2.20 - 0.79 (90H, $CH_3(CH_2)_6$- and $CH_3(CH_2)_3CH(CH_2CH_3)$-). FTIR: 3058 (w, C_{aryl}-H), 2955, 2923 and 2856 (s, -CH_2- and -CH_3), 2185 (w, disubst.-C≡C-), 1620 and 1598 (w, aryl -C=C-), 200 (vs, C_{phenyl}-OR), 968 (s, trans –CH=CH-) cm^{-1}. Anal. calculated for $(C_{88}H_{120}O_6)_n$ is $(1273.91)_n$: C, 82.97; H, 9.49. Found: C, 81.56; H, 9.86.

Appendix B

Synthesis and general characterization of thiophene containing PPE-PPV conjugated copolymers

1, 4-Dibromohydroquinone (2)

To a suspension of hydroquinone (1) (50 g, 0.454 mol) in glacial acetic acid (200 ml) a solution of bromine (47 ml) in acetic acid (100 ml) was added drop wise. The mixture was then allowed to stired overnight. 1,4-dibromohydroquinone precipitated as grey white product was filtered off, extensively washed with water and dried under vacuum (98.51g, 82% yield) (Scheme 1).

1, 4-Dibromo-2, 5-dioctyloxybenzene (3)

A suspension of KOH powder (24.0 g, 428 mmol) in dried DMSO (120 ml) was stirred and degassed for 1 hr. The addition of 2,5-dibromohydroquinone (**2**) (12.16 g, 45.4.mmol) led to colour changes to a yellowish green and a rise in temperature. After 15 minutes bromooctane (30 ml, 160 mmol) was added which led again to an increase in temperature. The stirring was continued for 4 h. The colur of the mixture fads which showed the progress of the reaction. Finally the reaction mixture was a suspension of yellowish white semicrystalline precipitate. The mixture was poured on an excess of ice. The precipitate was filtered off, washed with distilled water (4 times) and dried. The raw product 1,4-dibromo-2,5-dioctyloxybenzene was recrystalized from acetone filtered out and dried in vacuum to yield white crystal (20.24 g, 45.4 mmol 90% yield) (Scheme 1).

4-Bromo-2,5-dioctyloxybenzaldehyde (4)

To a solution of 1,4-dibromo-2,5-dioctyloxybenzene (**3**), (9.8 g, 20 mmol) in diethyl ether (150 ml), cooled at -5°C and kept under argon, a solution of butyllithium (2.7 M in heptane, 3.75 ml, 10 mmol) was added. After 15 min, DMF (0.96 ml, 12.5 mmol) was added to the mixture, while the temperature was allowed to rise to 15°C. The clear solution was kept between 10 and 15°C and was stirred for 1.5 h. Subsequently hydrochloric acid (10%, 50 ml) was added and the phases were separated. The organic phase was washed with a $NaHCO_3$ solution and dried over sodium sulfate (Na_2SO_4). Diethyl ether was distilled off, and the residue was chromatographed on silica gel using a mixture of toluene/hexane (2/1) as eluent.

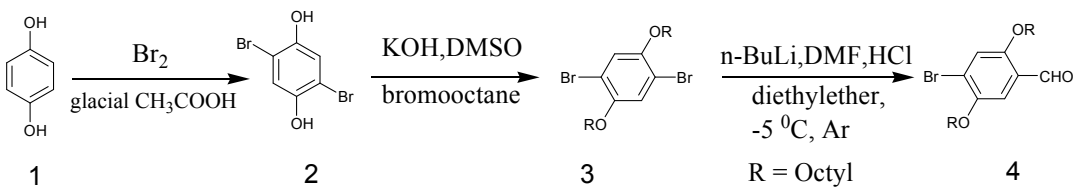

Scheme 1

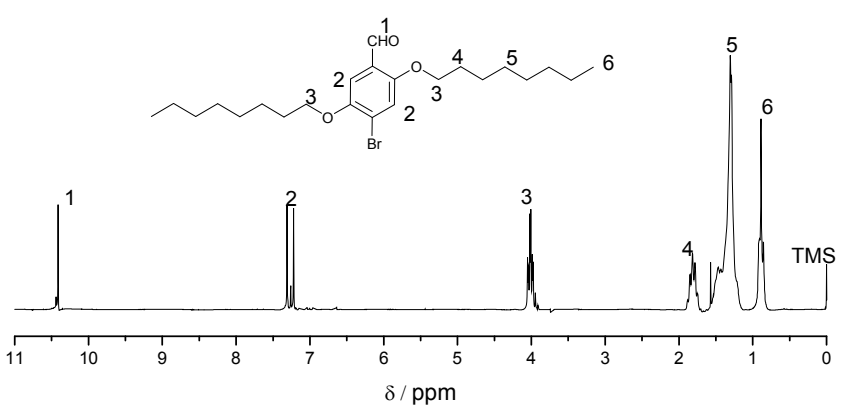

Figure. 1 : *^{1}H NMR of 4-Bromo-2,5-dioctyloxybenzaldehyde*

4-bromo-2,5-dioctyloxybenzaldehyde was obtained as light yellow crystals (Scheme 1). (7.5 g, 85.4% yield), 1H NMR ((500 MHz, $CDCl_3$): δ/ppm) = 0.83 - 1.86 (m, $-CH_3$, $-(CH_2)_6-$), 3.82 - 4.03 (m, $-CH_2O-$), 7.29 (s,C_{aryl}-H), 10.42 (s, -CHO) (Figure 1).

2, 5-Dioctyloxy-4-trimethylsilylethynylbenzaldehyde (5)

4-bromo-2,5-dioctyloxybenzaldehyde (**4**) (4 g, 9.06 mmol), Pd-$(PPh_3)_2Cl_2$ (140 mg, 0.199 mmol), and CuI (43.5 mg, 0.213 mmol) were added to a degassed solution of diisopropylamine (110 mL). Trimethylsilylacetylene (893 mg (1.3 ml), 9.09 mmol) was added slowly and dropwise to the vigorously stirred suspension. The mixture was stired at reflux for 8 hr. After cooling to room temperature, precipitated white diisopropyl ammonium bromide was filtered off. The solvents were removed under reduced pressure, and the residue was chromatographed over a silica gel column with toluene as eluent. A dark yellow solid (3.97 g, 8.65 mmol, 95% yield) was obtained (Scheme 2).

4-Ethynyl-2,5-dioctyloxybenzaldehyde (6)

Methanol (30 ml) and aqueous KF (1.48 g, 25.438 mmol) were added at room temperature to a stirred solution of 2, 5-dioctyloxy-4-trimethylsilylethynylbenzal-dehyde **(5)** (3.89 g, 8.47 mmol) in 40 ml of THF. The mixture was then stirred for 3h at room temperature under nitrogen atmosphere. Afterwards the solution was washed with water (three times) and the solvent was removed on a rotatory evaporator, and the residue was chromatographed on a silica gel column using toluene as eluent. A 2.5 g (76.46% yield) yellow solid substance was obtained (Scheme 2). 1H NMR (500 MHz, $CDCl_3$): δ/ppm) = 0.89 - 1.87 (m, 30H, $-CH_3$, $-CH_2-$), 3.48 (s, 1H, -C≡C-H), 4.08 (m, 4H, O-CH_2), 7.09, 7.31 (s, s, 1H, 1H, C_{aryl}-H), 10.45 (s, 1H, -CHO) (Fig. 2).

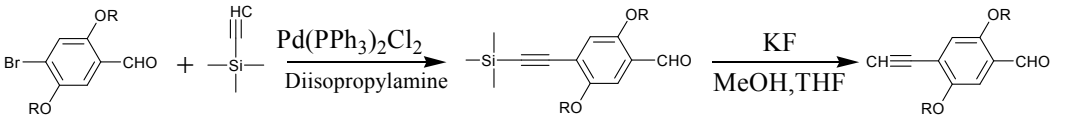

Scheme 2

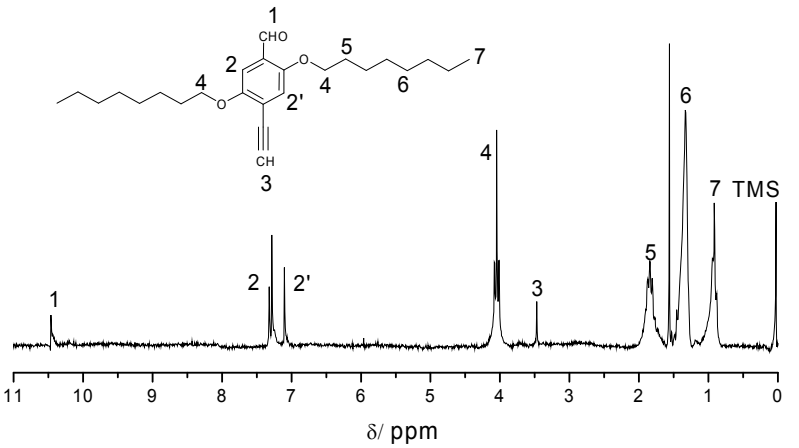

Figure 2: *^{1}H NMR of 4-Ethynyl-2, 5-dioctyloxybenzaldehyde*

2,5-Bis (4-formyl-2,5-dioctyloxyphenylethynyl) thiophene (GD1)

The dialdehyde **GD1** was prepared by Sonogashira reaction [189,190]. A mixture of 4-ethynyl-2,5-dioctyloxybenzaldehyde **(6)** (2.0 g, 5.17 mmol), 2,5-dibromothiophene (625 mg, 2.58 mmol), diisopropylamine (46 ml) and toluene (80 ml) was degassed for 2 h. Pd $(PPh_3)_4$ (128 mg, 0.134 mmol) and CuI (25.5 mg, 0.134 mmol) were added and the reaction mixture was heated to 70-80 ^{0}C for 24 h. Precipitated diisopropyl ammonium bromide salt was filtered off and the solvents were removed under vacuum. The residue was purified by column chromatography (silica, n-hexane: toluene (1:3) as eluent). The desired product 2,5-Bis(4-formyl-2,5-dioctyloxyphenyl ethynyl) thiophene was obtained as a yellow crystalline substance (2.34 g, 53% yield) (Scheme 3). 1H NMR (500 MHz, $CDCl_3$): δ (ppm) = 0.84 - 1.85 (m, 60H, -CH_3, -CH_2-), 3.98 - 4.07 (m, 8H, –CH_2O–), 7.13, 7.25 (s, s, 2H, 2H, phenylene H's), 7.38

(s, 2H, thiophene H's), 10.42 (s, 2H, –CHO) (Figure 3).

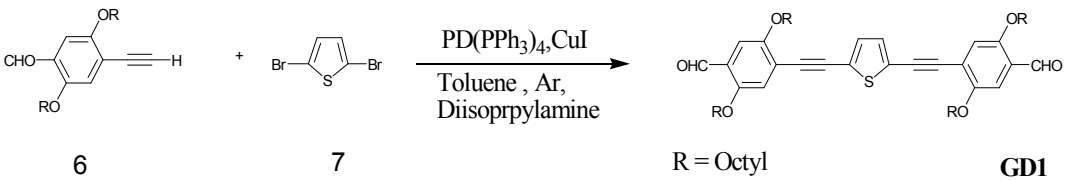

6 7 R = Octyl **GD1**

Scheme 3

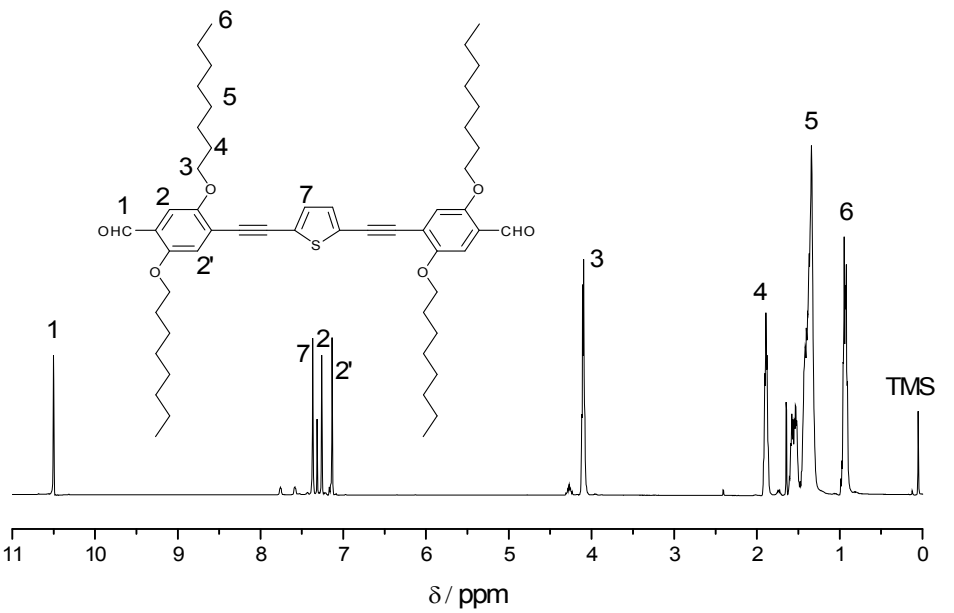

Figure 3: *^{1}H NMR of 2,5-Bis (4-formyl-2,5-dioctyloxyphenylethynyl) thiophene*

5', 5'-Bis (4-formyl-2, 5-dioctyloxyphenylethynyl) bithiophene (GD2)

A mixture of 4-formyl-2,5-dioctyloxyphenylacetylene (**5**) (2.4 g, 6.17 mmol), and 5,5'-dibromobithiophene (1 g, 3.08 mmol), diisopropylamine (40 ml) and toluene (100 ml) was degassed for 2 h. Pd $(PPh_3)_4$ (145 mg, 0.123 mmol) and CuI (25.15 mg, 0.123 mmol) were added and the reaction mixture was heated to 70 – 80^{0}C for 24 h [189,190]. After filtration and removal of the solvents, the residue was purified by column chromatography (silica, n-hexane/toluene (1:3) as eluent. The desired product

2, 5-bis(4-formyl-2,5-dioctyloxyphenylethynyl) bithiophene was obtained as a pale yellow crystal (3.04 g, 49% yield) (Scheme 4). ^{1}H NMR (500 MHz, $CDCl_3$): δ/(ppm) = 0.86 - 1.83 (m, 60H, -CH_3, -CH_2-), 3.96 - 4.12 (8H, -CH_2O-), 5.26 (s, 2H, bithiophene H's), 7.06 and 7.17 (s, s, 2H, 2H, phenylene H's), 7.31 (s, 2H, bithiophene 's), 10.43 (s, 2H, –CHO) (Figure 4).

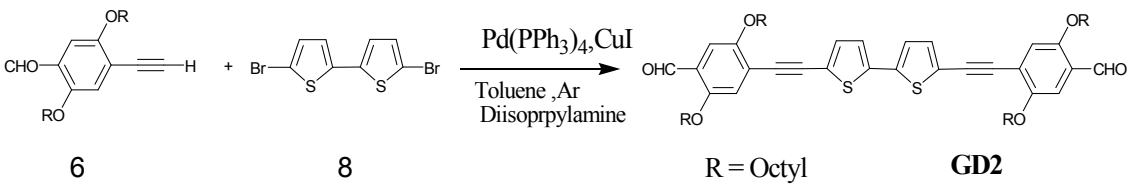

Scheme 4

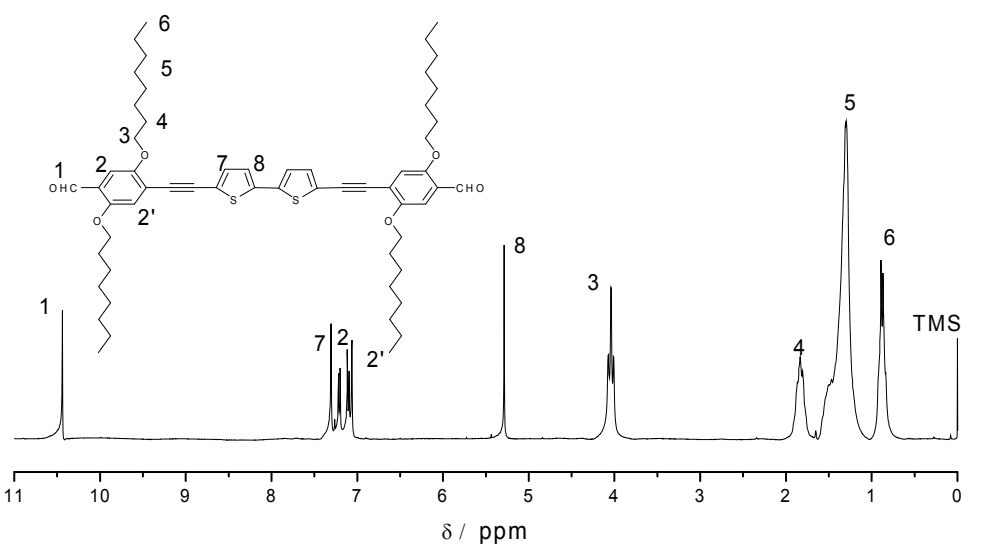

Figure 4: *^{1}H NMR of 5', 5'-Bis (4-formyl-2, 5-dioctyloxyphenylethynyl) bithiophene*

2, 5-dibromo-3, 4-ethylenedioxythiophene (10)

This compound was synthesized according to literature [331]. 3,4-Ethylenedioxy thiophene (9) (3.193 ml, 4.26 g, 30.0 mmol) was dissolved in a mixture of tetrahydrofuran (THF) and acetic acid (120ml, 1:1 by volume), N-Bromosuccinmide (NBS) (11.22 g, 63 mmol) was added. After stirring for 2 hr at room temperature,

distilled water (300 ml) was added resulting in the precipitation of silver white crystalline precipitate which was filtered off and dried over P_2O_5 (8.04 g, 89.3% yield) (Scheme 5).

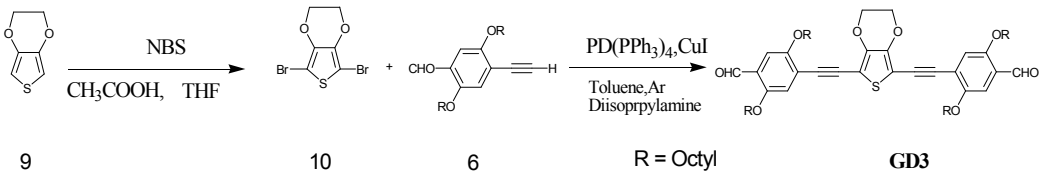

Scheme 5

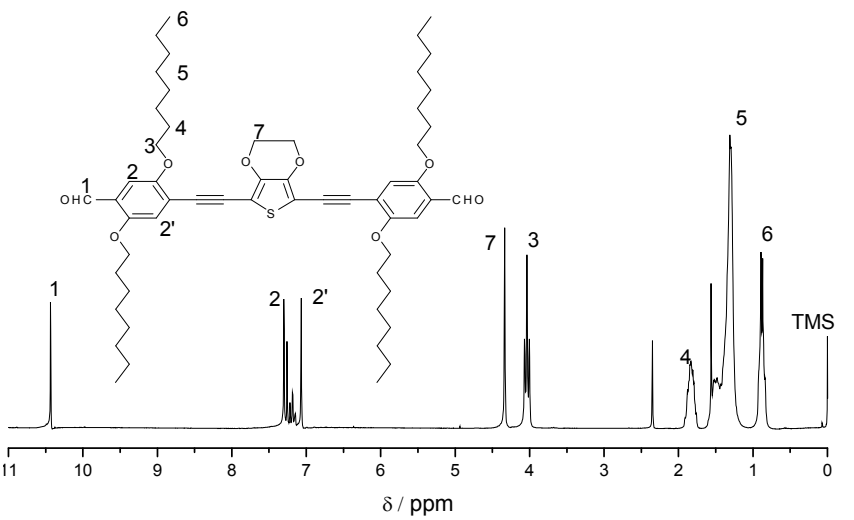

Figure 5: *^{1}H NMR of 2,5-Bis (4-formyl-2,5-dioctyloxyphenylethynyl) 3,4-ethylene dioxythiophene*

2,5-Bis(4-formyl-2,5-dioctyloxyphenylethynyl)3,4-ethylenedioxythiophene (GD3)

A mixture of 4-formyl-2, 5-dioctyloxyphenylacetylene (2.7 g, 7.00 mmol), 2, 5-dibromo-3,4-ethylenedioxythiophene (**10**) (1.0 gm, 3.33 mmol), diisopropylamine (40 ml) and toluene (100 ml) and was degassed for 2 h. Pd $(PPh_3)_4$ (154 mg, 0.133 mmol) and CuI (25.45 mg, 0.133 mmol) were added to the reaction mixture and heated to 70 – 80^0C for 24 h [189,190]. After filtration and removal of the solvents the residue was

purified by column chromatography (silica, n-hexane/tolune (1:3)) as eluent. The desired product 2,5-bis(4-formyl-2,5-dioctyloxyphenylethynyl)3,4-ethylenedioxy thiophene was obtained as a radish yellow crystals (3.25 g , 51% yield) (scheme 5). ^{1}H NMR (500 MHz, $CDCl_3$): δ (ppm) = 0.76 - 1.90 (m,60H, -CH_3, -CH_2-), 3.98 - 4.07 (m, 8H, –CH_2O–), 4.35 (s,4H,-O-CH_2-CH_2-O-), 7.03 and 7.25 (s, s, 2H, 2H phenylene H's), 10.42 (s, 2H, –CHO) (Figure 5).

Poly{1,4-(2,5-dioctyloxy)phenylene-ethynylene-2,5-thiophene-ethylene-1,4-(2,5-dioctyloxyphenylene)vinylene-1,4-[2,5-bis-(2-ethyl)hexyloxy]phenylene-vinylene}(GP1)

The synthesis of GP1 followed a well-established protocol using Horner-Wadsworth-Emmons olefination reaction [332]. 2,5-Bis(4-formyl-2,5-dioctyloxyphenylethynyl) thiophene (**GD1**) (850 mg, 0.9961 mmol) and 2,5-bis(2-ethylhexyloxy)-p-xylylene-bis(diethylphosphonate) (puchesed from Jena polymers) (11) (632 mg, 0.9961 mmol) were dissolved in toluene (50 ml) while stirring vigorously under argon and heating to reflux. Potassium tert-butoxide (560 mg, 4.9 mmol) was added and the reaction mixture was heated at reflux for 1h. Additional toluene (10 ml) was added in small portions due to the fast increase of viscosity of the reaction mixture. After 1hr , benzaldehyde (2 ml) was added and the reaction was further stirred for 10 minutes. Finally the heating is switched off and the reaction is quenched by the addition of hyderochloric acid (5%, 10 ml). The organic phase was separated and extracted several times with distilled water until the water phase became neutral. The organic layer was dried in a Dean–Stark apparatus. The resulting toluene suspension was filtered, the filtrate was concentrated and precipitated in cold methanol (300 ml). The polymer was filtered off and transferred in to a soxhlet extractor. A mixture of

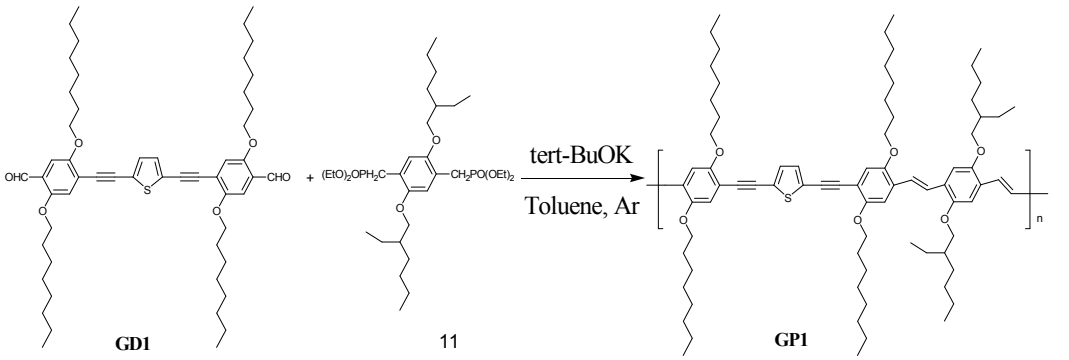

Scheme 6

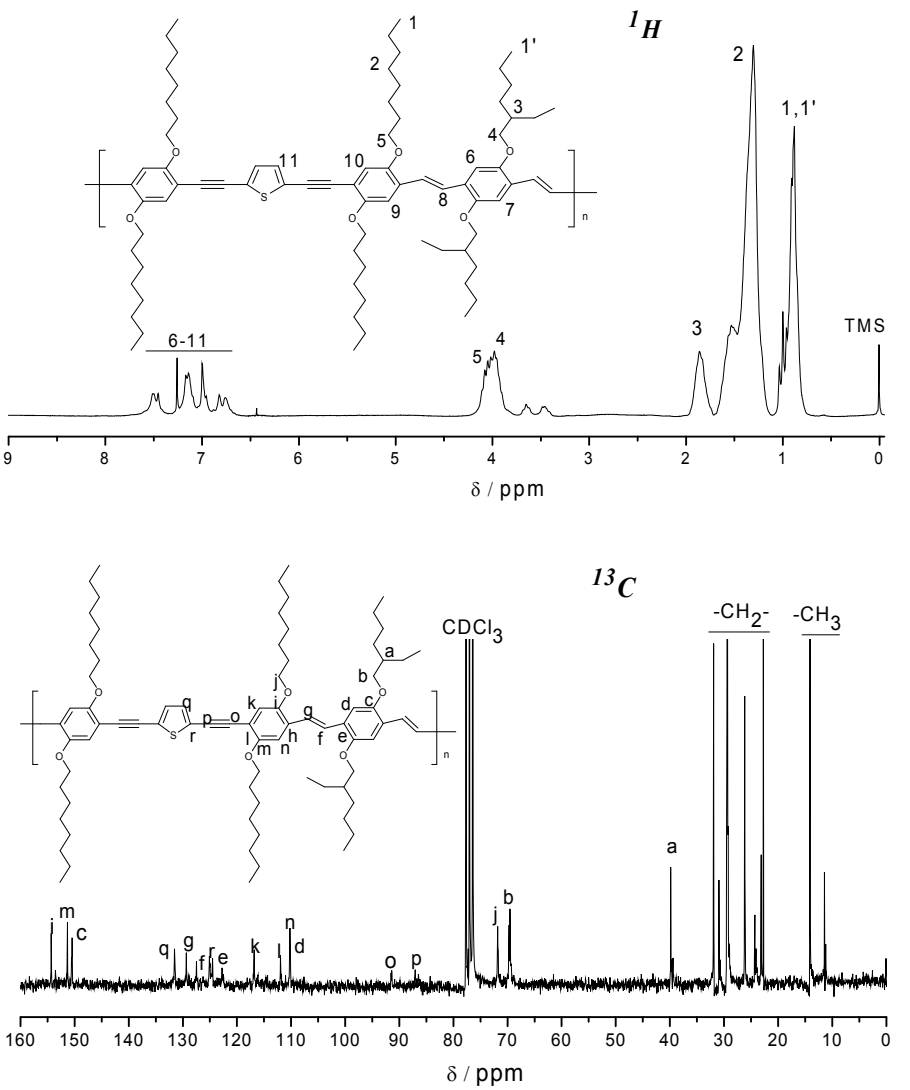

Figure 6: *^{1}H and ^{13}C NMR of GP1*

methanol/diethylether (1:1,400ml) was applied to remove the low molecular weight fractions and soluble impurities. The dark red polymeric material was dried under vacuum (900 mg ,77% yield) (Scheme 6).

GPC (THF, PS standard): Mw = 54534 g/mol, Mn = 18,300 g/mol, PDI = 2.98. 1H NMR (500 MHz, $CDCl_3$): δ/(ppm) = 0.75 - 1.90 (m, $-CH_3$, $-CH_2-$), 3.33 - 4.12 (m, $–CH_2O–$), 6.75 - 7.60 (m, 10H, arylene and vinylene H's). 13C NMR (125 MHz, $CDCl_3$): δ/(ppm) = 11.1, 14.1 ($-CH_3$), 22.5 - 31.8 ($-(CH_2)-$), 39.9 (-CH-), 69.4, 69.7, 71.7 ($-CH_2-O-$), 87.5, 92.1 (–C≡C–), 110.2 - 154.9 (arylene, vinylene C's) (Figure 6).

Poly{1,4-(2,5-dioctyloxy)phenylene-ethynylene-5,5'-bithiophene-ethylene-1,4-(2,5-dioctyloxyphenylene)vinylene-1,4-[2,5-bis-(2-ethyl)hexyloxy]phenylene-vinylene} (**GP2**)

5,5'-Bis(4-formyl-2,5-dioctyloxyphenylethynyl)bithiophene (**GD2**) (932 mg, 0.996 mmol) and 2,5-bis(2-ethylhexyloxy)-p-xylylene-bis(diethylphosphonate) (11) (632 mg, 0.9961 mmol) were dissolved in toluene (50 ml) while stirring vigorously under argon and heating under reflux. Potassium tert-butoxide (560 mg, 4.9 mmol) was added and the reaction mixture was refluxed for 1 h. Additional toluene (10 ml) was added in small portions to compensate the fast increase of viscosity. After 1 h, benzaldehyde (2ml) was added. After further 10 minutes the heating was turned off and the reaction was quenched by the addition of hydrochloric acid (5%, 10 ml). The organic phase was separated and extracted several times with distilled water until the water phase became neutral. The organic layer was dried in a Dean–Stark apparatus. The resulting toluene suspension was filtered and the filtrate was concentrated and precipitated in a cold methanol (300 ml). The polymer was filtered off and transferred in to a soxhlet extractor. A mixture of methanol/diethyl ether (1:1, 400 ml) was

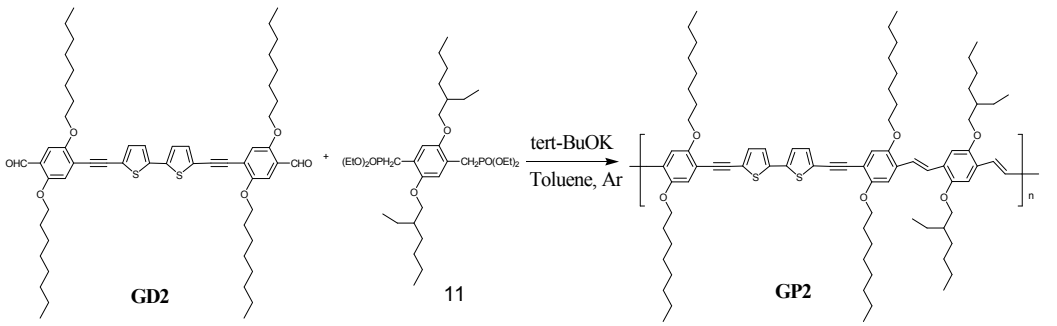

Scheme 7

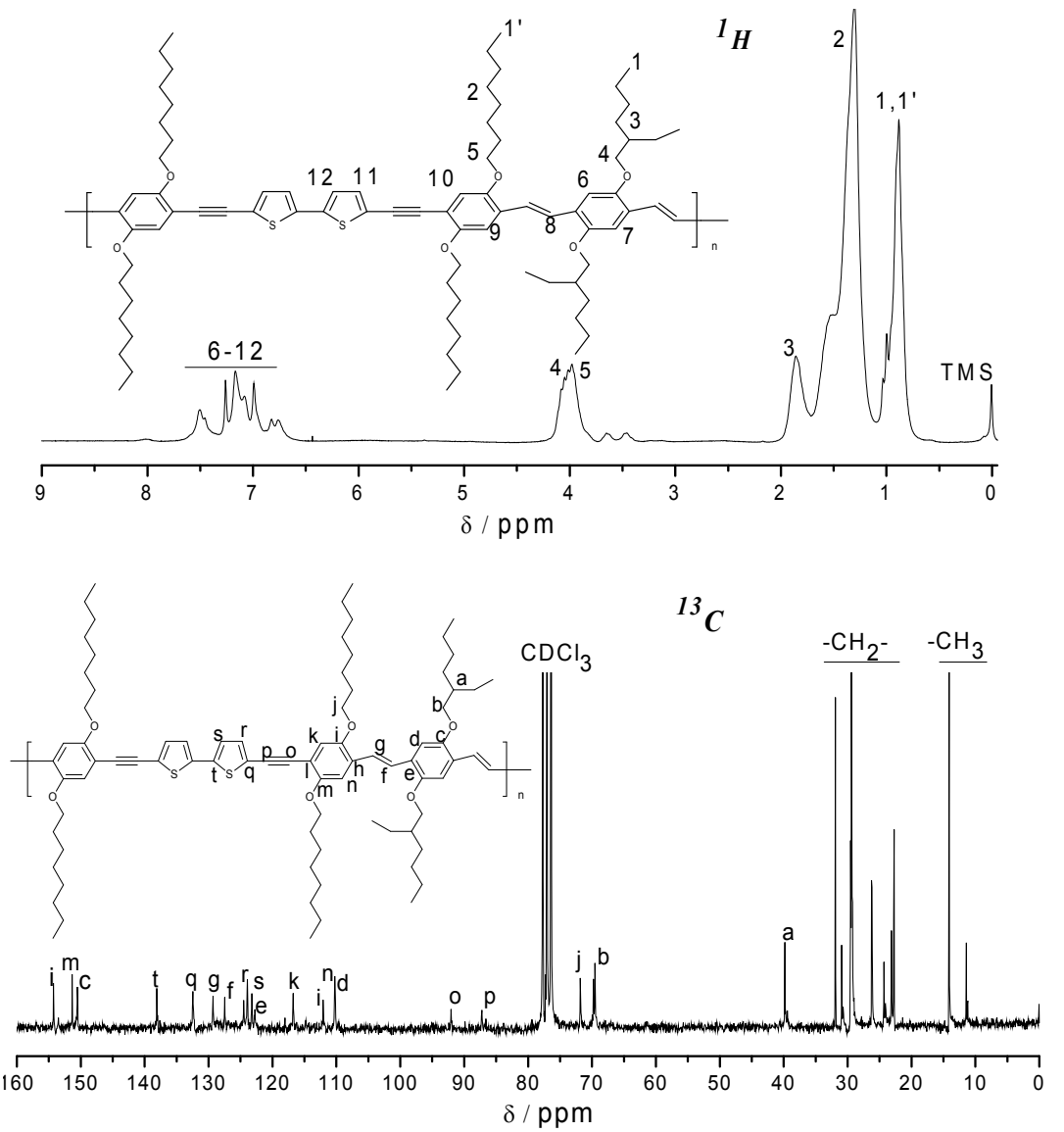

Figure 7: *^{1}H and ^{13}C NMR of GP2*

applied to remove low molecular weight fractions and soluble impurities. The dark red polymeric material was dried under vacuum (850 mg , 68% yield) (Scheme 7).

GPC (PS standard ,THF): Mw = 33700 g/mol, Mn = 8000 g/mol, PDI = 4.20. 1H NMR (500 MHz, $CDCl_3$): δ/(ppm) = 0.75 - 1.90 (m, $-CH_3$ $-CH_2-$), 3.35 - 4.12 (m, $–CH_2-O–$), 6.75 - 7.60 (m, 10H, arylene and vinylene H's). 13C NMR (125 MHz, $CDCl_3$): δ/(ppm) = 11.1 and 14.1 ($-CH_3$), 22.5 - 31.8 ($–(CH_2)–$), 39.9 (–CH–), 69.4, 69.7, 71.7 ($–CH_2-O–$), 87.5, 92.1 (–C≡C–), 110.2 - 154.9 (arylene and vinylene C's) (Figure 7).

Poly{1,4-(2,5-dioctyloxy)phenylene-ethynylene-2,5-(3,4-ethylenedioxythiophene) ethylene-1,4-(2,5-dioctyloxyphenylene)vinylene-1,4-[2,5-bis-(2-ethyl)hexyloxy] phenylene-vinylene} (GP 3)

2,5-Bis(4-formyl-2,5-dioctyloxyphenylethynyl)-3,4-ethylenedioxythiophene (GD3) (1 gm, 1.097 mmol) and 2,5-bis(2-ethylhexyloxy)-p-xylylene-bis(diethylphosphonate) (11) (696 mg, 1.097 mmol) were dissolved in toluene (60 ml) while stirring vigorously under argon and heating under reflux. Potassium tert-butoxide (615 mg, 5.48 mmol) was added to this solution; and the reaction mixture was heated at reflux for 1hr. Additional toluene (10 ml) was added in small portions to compensate the fast increase of viscosity of the olefination reaction mixture. After 35 minutes, benzaldehyde (2 ml) was added and the reaction was further stirred for 10 minutes and finally the heat is turned off and the reaction is quenched by adding hydrochloric acid (5%, 10 ml). The organic phase was separated and extracted several times with distilled water until the water phase became neutral. The organic layer was dried in a Dean–Stark apparatus.The resulting toluene suspension was filtered and evaporated under vacuum to the minimum (30 ml) and precipitated in cooled methanol (300 ml).

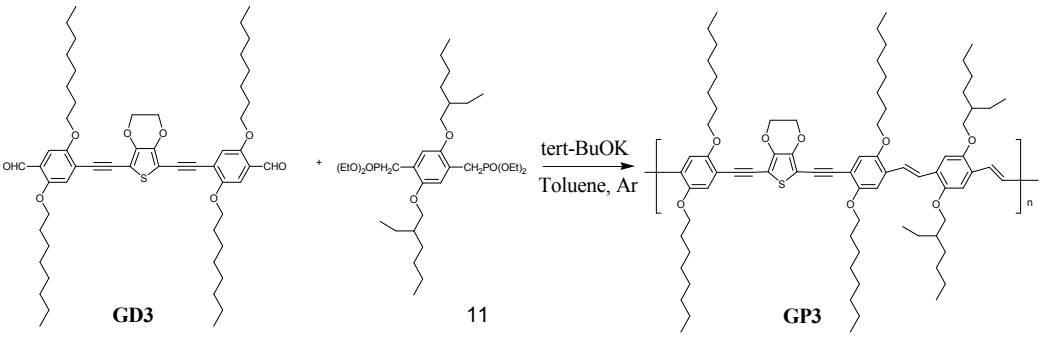

Scheme 8

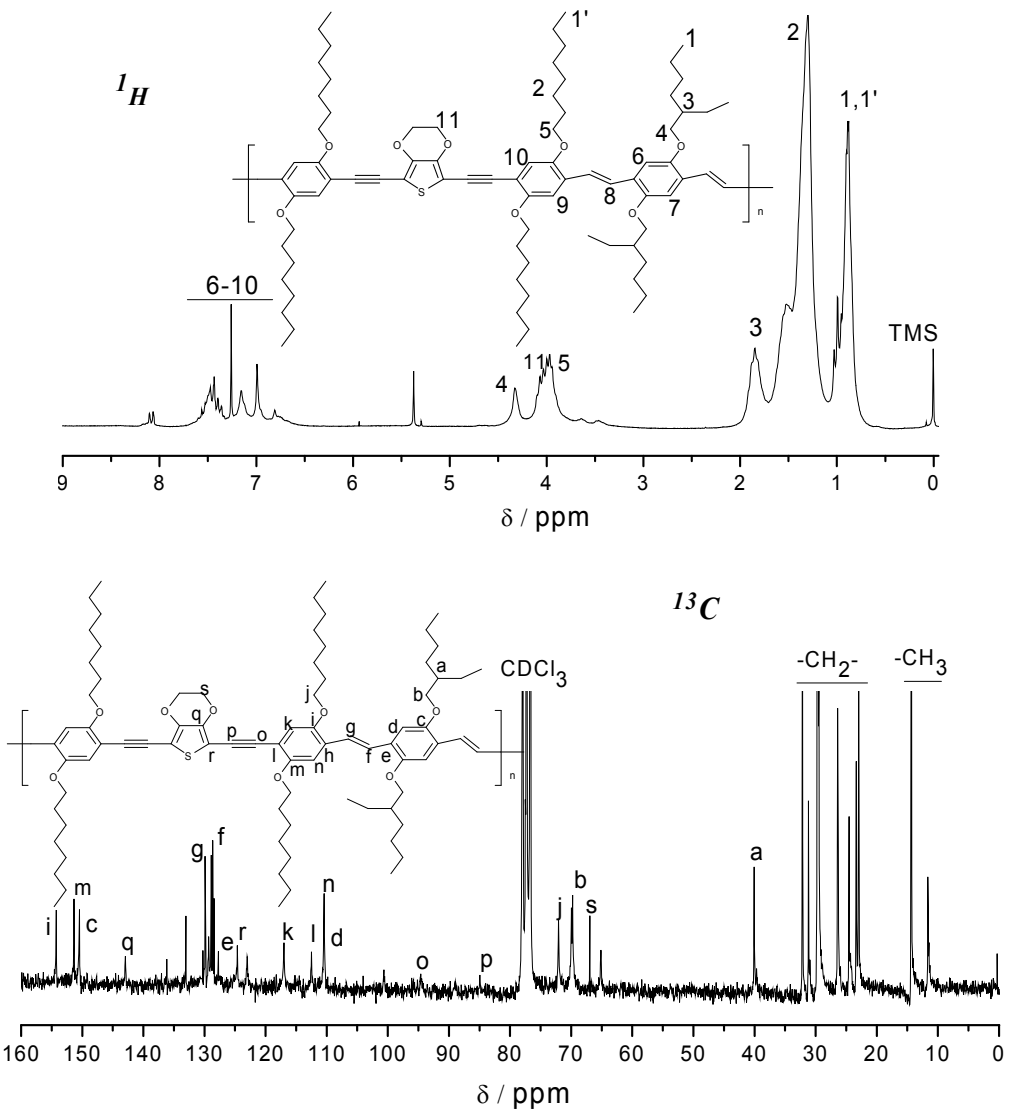

Figure 8: *^{1}H and ^{13}C NMR of GP3*

The dark blue polymeric material was filtered off and dried, purified with soxhlet extraction using methanol/diethyl ether mixture (1:1, 400 ml) to remove the low molecular weight and soluble impurities (1.00 g, 74% yield) (scheme 8).

GPC (PS standard, THF): Mw = 84250 g/mol, Mn = 12,500 g/mol, PDI = 6.74. ^{1}H NMR (500 MHz, $CDCl_3$): δ/(ppm) = 0.78 - 1.97 (m, -CH_3 -CH_2-), 3.31- 4.51 (–CH_2-O-, -O-CH_2-CH_2O-), 6.79 - 7.64 (arylene and vinylene H's). ^{13}C NMR (125 MHz, $CDCl_3$): δ/(ppm) = 11.1 and 14.1 (CH_3), 22.5 - 32.0 (–(CH_2–) , 40.0 (-CH-), 67.1, 69.7, 71.7 (–CH_2O–), 86.1, 94.5 (–C≡C–), 111.0-154.9 (arylene and vinylene C's) (Figure 8).

Schemes 1-8 illustrates the synthetic path with multistep synthesis of the dialdehydes **GD1**, **GD2** and **GD3** bearing octyloxy side chains which are reacted with the 2-ethylhexyloxy equipped biphosphonate (**11)** following the Horner-Wadsworth-Emmons protocol to form the three corresponding copolymers **GP1**, **GP2** and **GP3.** The copolymers **GP1**, **GP2** and **GP3** contain thiophene, bithiophene and 3, 4-ethylenedioxythiophene moity in the X position of the backbone Ph-C≡C-**X**-C≡C-Ph-CH=CH-Ph-CH=CH- respectively with identical alkoxy side chains at the phenyl rings.